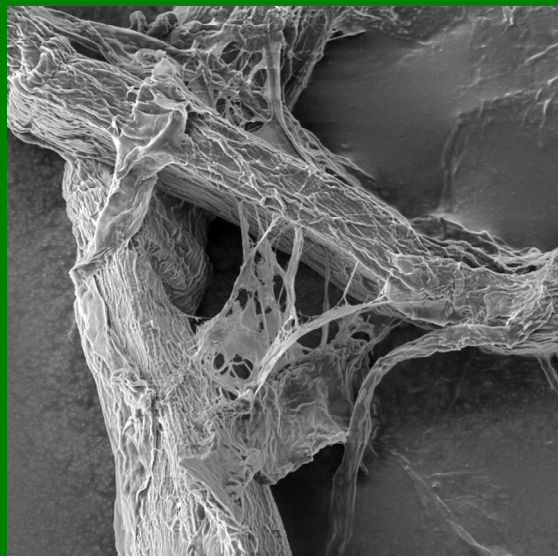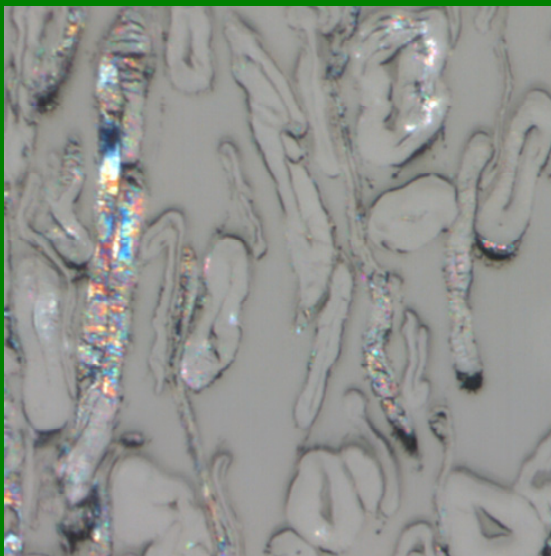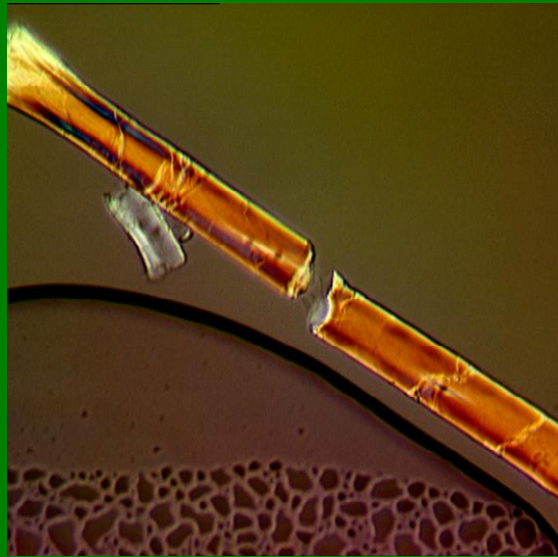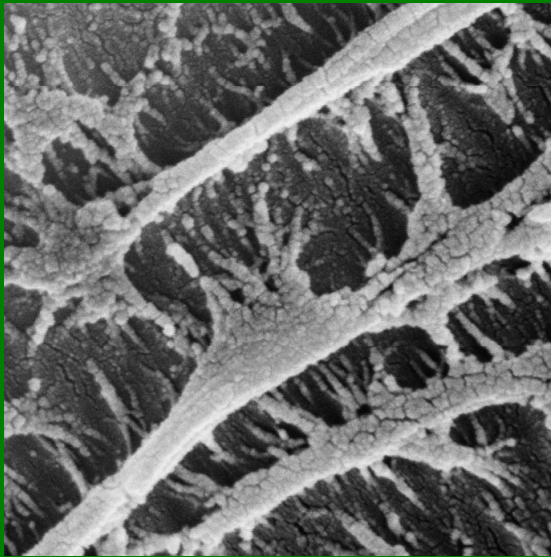# Fine Structure of Papermaking Fibres

The Final Report of COST Action E54

Fine Structure of Papermaking Fibres

COST Action E54 "Characterisation of the fine structure and properties of papermaking fibres using new technologies"

Edited by:
P. Ander, W. Bauer, S. Heinemann,
P. Kallio, R. Passas, A. Treimanis

COST- the acronym for European Cooperation in Science and Technology - is the oldest and widest European intergovernmental network for cooperation in research. Established by the Ministerial Conference in November 1971, COST is presently used by the scientific communities of 36 European countries to cooperate in common research projects supported by national funds.

The funds provided by COST - less than 1% of the total value of the projects - support the COST cooperation networks (COST Actions) through which, with EUR 30 million per year, more than 30 000 European scientists are involved in research having a total value which exceeds EUR 2 billion per year. This is the financial worth of the European added value which COST achieves.

A "bottom up approach" (the initiative of launching a COST Action comes from the European scientists themselves), "à la carte participation" (only countries interested in the Action participate), "equality of access" (participation is open also to the scientific communities of countries not belonging to the European Union) and "flexible structure" (easy implementation and light management of the research initiatives) are the main characteristics of COST.

As precursor of advanced multidisciplinary research COST has a very important role for the realisation of the European Research Area (ERA) anticipating and complementing the activities of the Framework Programmes, constituting a "bridge" towards the scientific communities of emerging countries, increasing the mobility of researchers across Europe and fostering the establishment of "Networks of Excellence" in many key scientific domains such as: Biomedicine and Molecular Biosciences; Food and Agriculture; Forests, their Products and Services; Materials, Physical and Nanosciences; Chemistry and Molecular Sciences and Technologies; Earth System Science and Environmental Management; Information and Communication Technologies; Transport and Urban Development; Individuals, Societies, Cultures and Health. It covers basic and more applied research and also addresses issues of pre-normative nature or of societal importance.

Web: http://www.cost.eu

PREFACE

This book contains important results of COST Action E54 *"Characterisation of the fine structure and properties of papermaking fibres using new technologies"*. For the COST Book front page the shorter title "Fine Structure of Papermaking Fibres" was also adopted.

The Action started on 18 December 2006, and it has continued for four years.

The main objective of the Action E54 was to generate new knowledge on the micro- and nanostructure of papermaking fibres and relevant properties required for the efficient and sustainable use of fibres in traditional, advanced and future products. I am confident that this objective of the Action has been met, and the contents of the book will serve as evidence for that.

Action E54 comprised three working groups:

WG1: Structure and chemical composition of papermaking fibres after different types of treatment. The objectives of the activities of this WG were to develop methods for the characterisation of pulp fibres, and to generate and accumulate new data on the fine structure of fibres for papermaking, and other important purposes.

WG2: Treatment and characterisation of individual fibres by microsystem technologies. This WG focused on the development of new instruments, namely, microrobotic platforms, by which individual fibres can be treated and investigated. Using these platforms new possibilities for testing of single fibres have been created.

WG3: The impact of the fine structure of fibres on their papermaking properties and their chemical and enzymatic reactivity. The participants of the WG exchanged their experience with respect to the impact of the fine structure of fibres and their modification on the quality parameters of the paper and handsheets produced thereof. The fibre and paper properties were assessed mainly by strength and optical indices as well as interfibre bonding.

Tight links among the three working groups have been established and maintained during the whole lifetime of the Action.

A total of 10 joint Management Committee/Working Groups meetings have been organised in Brussels and other cities. The following seven scientific workshops have been held: Riga (2007), Graz and Budapest (2008), Tampere and Grenoble (2009), Coimbra (2010) as well as in Cambridge (2011). Every time abstracts and/or proceedings were printed. From these meetings pdf-files have also been stored at http://gmail.com and are available by the Action members using a special username and password. The Latvian website www.kki.lv/cost can also be consulted for general information.

More than 100 researchers and industrialists participated in the workshops of COST Action E54, while the "core group" consists of some 40 scientists. They are authors of the articles in this book which is composed of the following three chapters:

The first chapter **"*Advanced analyses of wood pulp fibres*"** is devoted to the analytical methods, both chemical and instrumental ones, which have been largely developed during the four years of the Action. For example, different methods for fibre-fibre bonded area measurement have been elaborated. Several articles reflect the results from newly established networking connections between researchers from Sweden and Austria, Latvia and Austria, France, Germany and Finland, etc. One fascinating paper reports on new insights into the architecture of

wood cell walls, while another one discuss about possibilities for production and application of cellulose nanofibrils.

The second chapter *"New and emerging methods such as microrobotics and microscopic techniques"* contains articles related mostly to the applications of microsystem technologies, which actually for the first time ever are widely used in the area of papermaking fibre research. The chapter discusses novel microrobotic based methods for the manipulation and mechanical characterisation of individual pulp fibres. New results on the application of microscopic techniques for studying fibre cross sections using serial sectioning techniques are also published.

The third chapter is called *"Results of standard pulp and paper tests on Common pulps I and II and other fibre material"*. The participants of the Action agreed to investigate common unbleached and bleached Kraft pulp fibre samples using a great number of standard tests widely applied in the European pulp and paper industry. The data provide extended knowledge on the quality and properties of the investigated Common Pulp samples not obtained before.

Thus, the book is primarily for chemists, physicists, biologists and technologists working with papermaking fibres. I do hope that the book will prove useful also for undergraduate and graduate students. Short Term Scientific Missions are not described separately but included in the respective articles.

Concluding this part of the book, I would like to mention and to thank Vice Chairmen of the Action Pasi Kallio and Raphael Passas, as well as WG leaders Tomas Larsson and Paul Ander (WG1), Jean-Marc Breguet and Sabine Heinemann (WG2), Eero Hiltunen and Wolfgang Bauer (WG3). Thanks a lot to the authors of the scientific papers, active participants of the COST Action E54. Last, but not least, I am very grateful to Drs Paul Ander and Sabine Heinemann who took the overall responsibility for collecting the papers and arranging the printing of the book.

General information on COST is available at http://www.cost.eu while on the COST website: http://www.cost.eu/domains_actions/fps/Actions/Papermaking_Fibres_Using_New_Technologies information on Action E54 is available for all those who are interested.

The Action's participants are grateful to COST Scientific Officer Melae Langbein and Administrative Officer Cassia Azevedo Zezzi for the concern they have shown during the Action's lifetime. I would like to thank also the COST Officers, who had served during the first years of the Action E54, namely Günter Siegel, Nic Standaert and Sylvia Liteanu.

Chairman of COST Action E54

Professor Arnis Treimanis, Riga, December 2010

ACKNOWLEDGEMENTS

ADDRESSES OF THE EDITORS

Paul Ander, CRUW, Dept. of Wood Science, Swedish University of Agricultural Sciences, PO Box 7008, SE- 75007, Uppsala, Sweden. E-mail: paul.ander@slu.se

Wolfgang Bauer, Institute for Paper, Pulp and Fiber Technology, Graz University of Technology, Kopernikusgasse 24/II, 010 Graz, Austria. E-mail: wolfgang.bauer@tugraz.at

Sabine Heinemann, PO Box 1000, 02044 VTT (Espoo), Finland.
E-mail: sabine.heinemann@vtt.fi

Pasi Kallio, Micro- and Nanosystems Research Group of Tampere University of Technology, Korkeakoulunkatu 3, 33720 Tampere, Finland. E-mail: pasi.kallio@tut.fi

Raphael Passas, Laboratory of Pulp and Paper Science and Graphic Arts, Grenoble INP-Pagora, 38400 Saint Martin d'Heres Cedex France. E-mail: raphael.passas@pagora.grenoble-inp.fr

Arnis Treimanis, State Institute of Wood Chemistry, 27 Dzerbenes str., Riga LV 1006, Latvia.
E-mail: arnis.treimanis@edi.lv

TABLE OF CONTENTS

NEW INSIGHTS INTO THE MICRO-FIBRIL ARCHITECTURE OF THE WOOD CELL WALL

Philip Turner[1], Michael Kowalczyk[1] and Alan Reynolds[2]

[1]Forest Products Research Institute, Edinburgh Napier University

[2]Brunel University

ph.turner@napier.ac.uk

Abstract

Recent studies on the microfibril architecture of the wood cell wall using a new sample preparation technique (plasma ashing), in combination with Field Emission Electron Microscopy (FE-SEM), has revealed new, previously unpublished microfibril structures. The work indicates that the crystalline cellulose skeleton of the cell is largely fractal. A review of literature has shown that these fractal structures are not unique to the wood cell or indeed to biological materials, leading to the conclusion that fundamental physical processes drive these fractal structures. In our discussions we consider some key milestones in modern physics and their contribution to the development of a hypothesis of the underlying principles that could drive the fractal structure of matter. Based upon two parallel, complementary areas of research, scale relativity theory and string theory, we set a hypothesis that the fractal geometry of the wood cell wall is driven by the fractal geodesics of space-time.

Introduction

The current model of how cellulose microfibrils are laid down within the different layers of the wood cell wall has been established for a number of decades. The conventional view of their arrangement is illustrated in Figure 1. However, the results of work reported here using a new sample preparation technique combined with Scanning Electron Microscopy (SEM) reveals that the microfibril architecture of the cell wall is largely fractal. The paper goes on to explore why these fractal structures are produced. A number of examples are given of similar structures in other biological and inorganic materials indicating that the mechanisms driving these structures are not biological but physical. A review of recent developments in fundamental physics has led to a radical hypothesis that the fractal structure of the cell, and indeed the whole tree and the majority of biological and inorganic materials in general is driven by the geometric structure of space-time which is fractal.
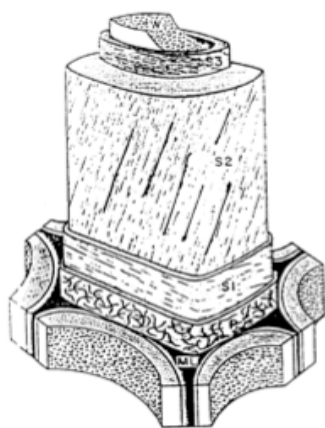
Figure 1. Illustration of the classical model of the orientation of micro-fibrils within the primary wall, S1, S2 and S3 layers within a wood cell (Cŏté 1974)

Methodology

Except where mentioned to the contrary, the bulk of the experimental work was carried out on a single sample of an industrially processed *Eucalyptus grandis* based pulp. A small sample of a few grams of pulp was mixed with deionized water in order to create a dilute suspension of individual fibres. Samples of fibre were prepared by placing drop of the suspension on a number

of electron microscope stubs, which were subsequently dried in an oven to dry at 50 °C. After drying, the fibre samples were placed in a plasma Asher (Emitech K1050X) for a range of exposure times (1 to 5 minutes) at a setting of between 30-60 Watts. Plasma ashing, first reported by Humphries (1979), is a process involving the oxidization of organic matter by oxygen plasma. The resulting carbon oxides and water vapor are volatilized and pumped away under vacuum. When the plasma is applied to wood cells at the correct level of exposure, the more reactive amorphous lignin and polysaccharides are preferentially oxidized, leaving behind the more stable crystalline skeleton, which can be viewed with an Electron Microscope.

After exposure in the plasma Asher, the stubs were gold coated then examined using a Hitachi S4800 Field Emission Scanning Electron Microscope (FE-SEM) at a range of magnifications. A low voltage electron beam was used (<5 kV) to minimize damage to the cellulose structures at high magnification (10 000 to 50 000 x), which typically occurs in conventional electron microscopes operating in the 30 kV range.

At low levels of exposure to the plasma, the microfibril structure of the primary wall is exposed. Using small incremental changes in exposure to the plasma source, it is possible to etch away amorphous polysaccharides and lignin to reveal the microfibril structure of the primary wall. Further incremental exposure to the plasma source reveals the subsequent layers of the cell wall. The process of etching away of the different layers of the cell wall was developed empirically, with a number of replicates at each exposure level. Each sample responds differently to the ashing process, exposing different levels of the cell wall. With care it is possible to get build up a clear picture of the microfibril structure of each layer. Continued exposure to the oxygen plasma eventually removes all the organic material as volatiles. The following images show the different arrangements of microfibrils within the different layers of the cell wall.

Results

With no exposure to the plasma it is possible to see the underlying microfibrils of the primary wall influencing the surface. However, it is not possible to see any detailed structure at 25 000 x magnification (Figure 2).
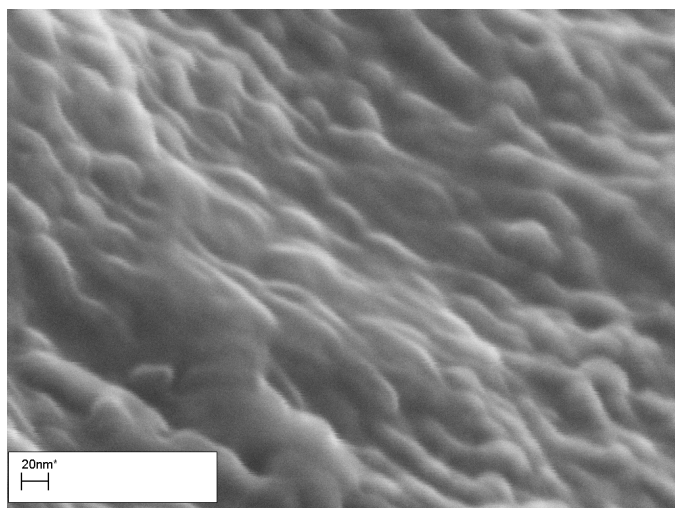
Figure 2. Image of the cell wall surface without exposure to plasma at 10 0000 x magnification. The underlying structure of the primary wall is hidden by amorphous polysaccharides and lignin

Primary wall

The primary wall has traditionally been seen as consisting of a random orientation of micro-fibrils. Figure 3 reveals what appears to be an apparently random structure at low magnification. However, Figure 4 indicates the fibrils are not random but form a dendritic, fractal structure.

T91a_1_30 3.0kV 5.1mm x10.0k SE(U)   5.00um
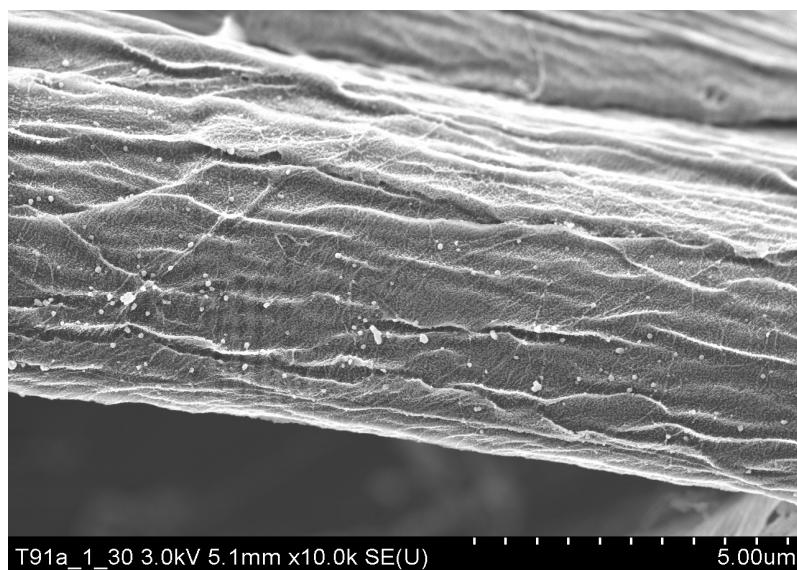
Figure 3. Primary wall at low (10 000 x) magnification

T91a_1_30 3.0kV 5.1mm x50.0k SE(U)   1.00um
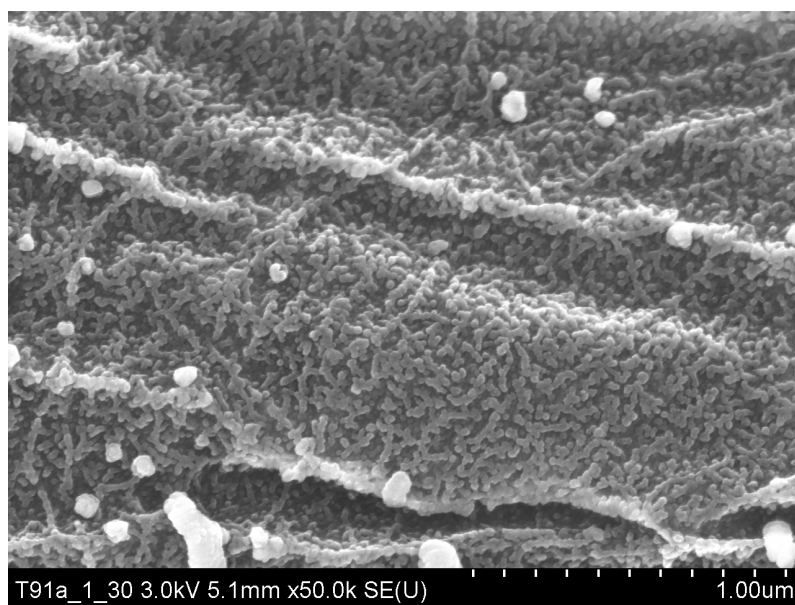
Figure 4. An enlargement of the primary wall illustrated in Figure 3 at 50 000 x magnification. The image reveals the dendritic (fractal) arrangement of the micro-fibrils

The S1 layer

Figure 5 shows an image of the structure just below the primary wall. The predominant structure at this magnification (10 000 x) is an intricately branched fractal scaffold, which is attached to the underlying S1 layer fibrils, which are aligned perpendicular to the cell axis. They can just be seen at this magnification. Figure 6 reveals in more detail how the apparently intermediate fractal scaffold interacts with perpendicular fibrils of the S1 layer. Figure 7 shows yet more detail after further exposure to plasma ashing. It is clear from this figure that the scaffold is an integral part of the S1 layer forming a complex web of interconnections. It should be noted that this combination of fractal web and linear fibrils within the S1 layer was not common to fibres in other eucalyptus pulp samples. Figure 8 shows an image of an alternative industrial eucalyptus pulp fibre at low magnification (5000 x). In this image the fibre has again been stripped of the

primary wall to reveal the underlying S1 layer. Figure 9 shows an enlargement of this same fibre at 25 000 x magnification, showing a neatly arranged set of microfibrils oriented perpendicular to the main fibre axis. A further magnification (50 000 x) of the same structure is illustrated in figure 10. In this set of images the intermediate fractal skeleton found in figures 5-7 is not present. The overall arrangement of the S1 layer in figures 8-10 is comparable to the traditional model seen in Figure 1.

The different structures within the S1 layer suggest some variation between different pulp fibres. It is not possible to say if these variations are due to genetic or environmental influences at this stage.
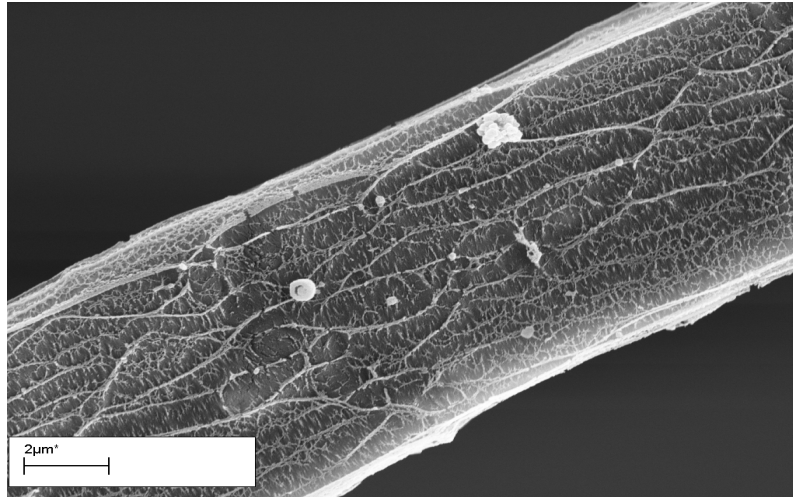
Figure 5. Low magnification image (10 000 x) revealing a fractal scaffold interacting with the under-lying micro-fibrils of the S1 layer which are oriented perpendicular to the main axis of the cell
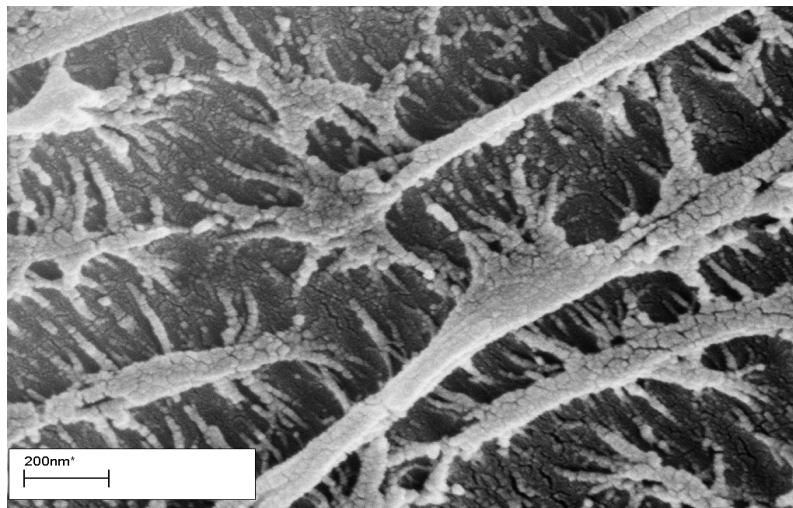
Figure 6. High resolution image (100 000 x) illustrating the complex branching structure that connects the fractal scaffold with the micro-fibrils in the underlying S1 layer which are oriented perpendicular to the main axis of the cell
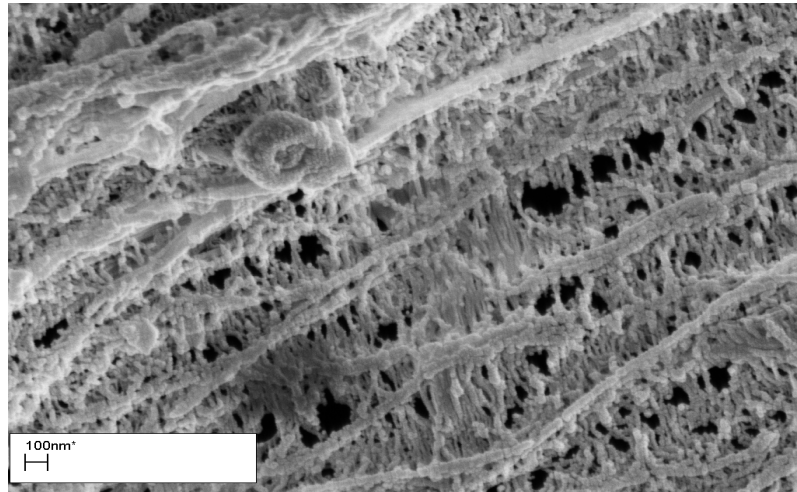
Figure 7. Image showing how the fractal scaffold is an integral part of the structure of the S1 layer in this fibre
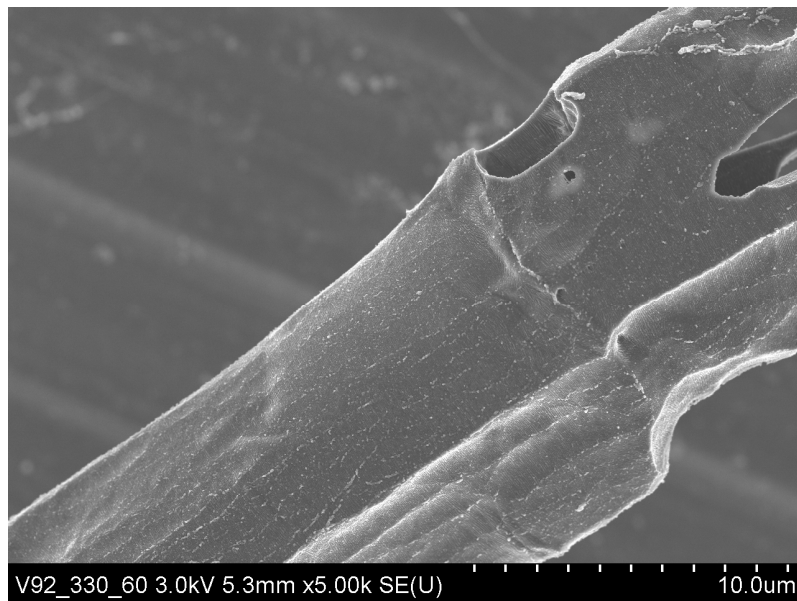
Figure 8. Primary wall of an alternative industrial eucalyptus pulp fibre at low magnification (5000 x). The fine structure of the fibril arrangement cannot be seen at this magnification but is revealed at higher magnifications (Figure 9 and 10)
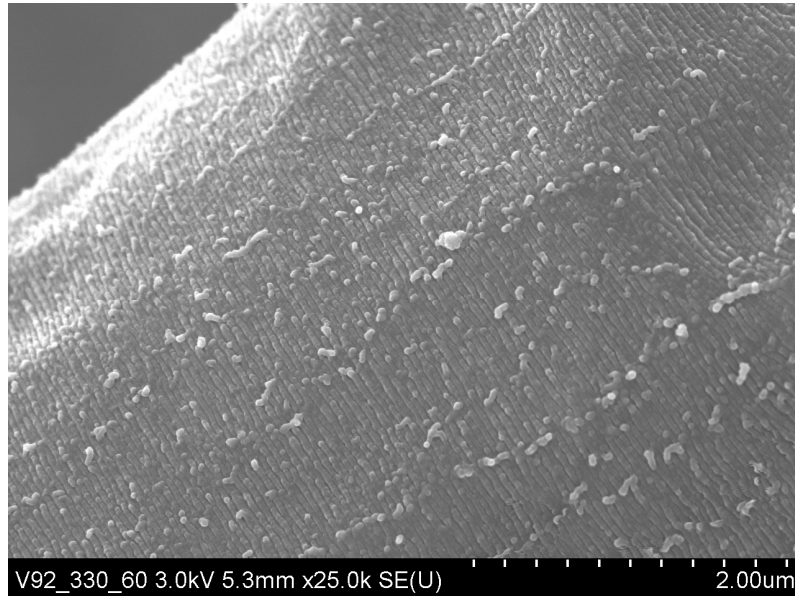
Figure 9. Image of micro-fibrils in the S1 wall layer oriented perpendicular to the main axis of the cell (25 000 x)
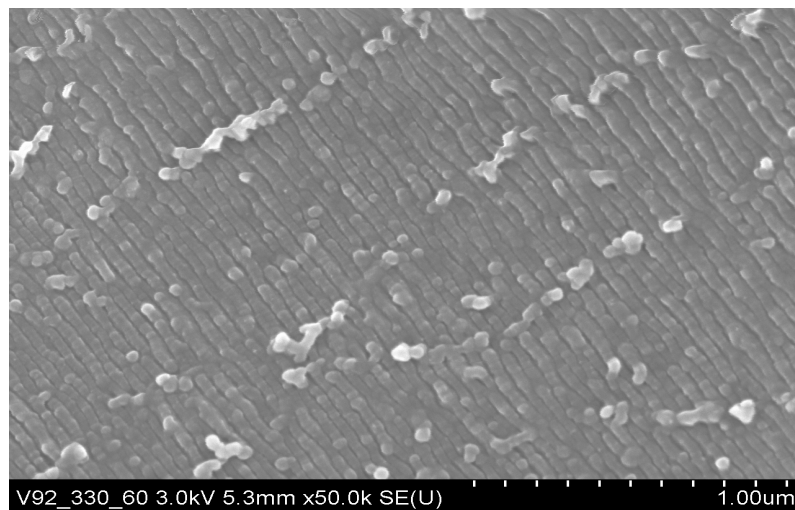
Figure 10. Image of micro-fibrils in the S1 wall layer oriented perpendicular to the main axis of the cell (50 000 x)

The S2 layer

In the established cell wall model the microfibrils in the S2 layer orient parallel to the main axis of the cell. The variation in the micro-fibril angle from the main axis has been extensively reported as impacting on issues such as wood stiffness and shrinkage during drying. Figure 11 shows a low magnification image (10 000 x) of a cell that has been exposed to a relatively high level of plasma ashing. The primary wall and S1 and S3 layers have been completely removed. What remains is the main body of crystalline material within the cell wall, *i. e.* the S2 layer. Imaging of a large portion of the whole cell helps indicate the scale of the crystalline structure relative to the cell.

Figure 12 illustrates the detailed structure of the crystalline fibrils at 100 000 x magnification. Whilst there is a general trend to orientation along the axis of the cell, the micro-fibrils form a

complexed, nodular, "Velcro like" fractal structure. The image of the S2 layer in figure 12 represents the most common structure found to date. However there are some variations on this structure, most of which are related to the level of packing of the fractal structure. To date, no examples of a linear S2 layer have been found to support the traditional model of a linear arrangement of fibrils parallel to the cell axis, despite looking at a range of species including pines, spruce, cedar, eucalyptus and acacia. A wider study may reveal these more classical structures. However, it is proposed that the traditional model of the S2 layer architecture needs to be revisited.

The findings of this work suggest that a rethink is required on the exact role of the S2 layer on the structural characteristics of the cell. It is interesting that Velcro like "slip" properties of wood have been reported in the recent past (Keckes et al. 2003). Our results, revealing a "Velcro like" structure at the fibrilar may offer new insights into how the S2 layer could be influencing these observed characteristics.

One interesting question relates to how this fractal structure is affected by pulping and bleaching processes. Figure 13 shows a highly aggregated structure in a high alpha cellulose pulp. We have not seen this level of aggregation in non-pulped wood samples, suggesting that the aggregation is due to an aggressive pulping and bleaching process which can lead to insoluble structures (and potential problems) in subsequent dissolving pulp processes.
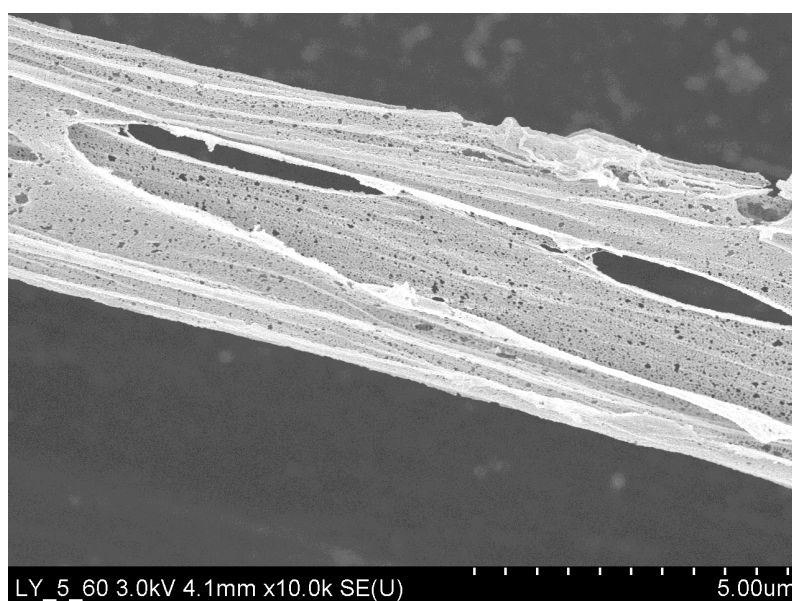
Figure 11. A low magnification image (10 000 x) in which the primary wall and S1 layer have been removed to reveal the S2 skeleton of the cell
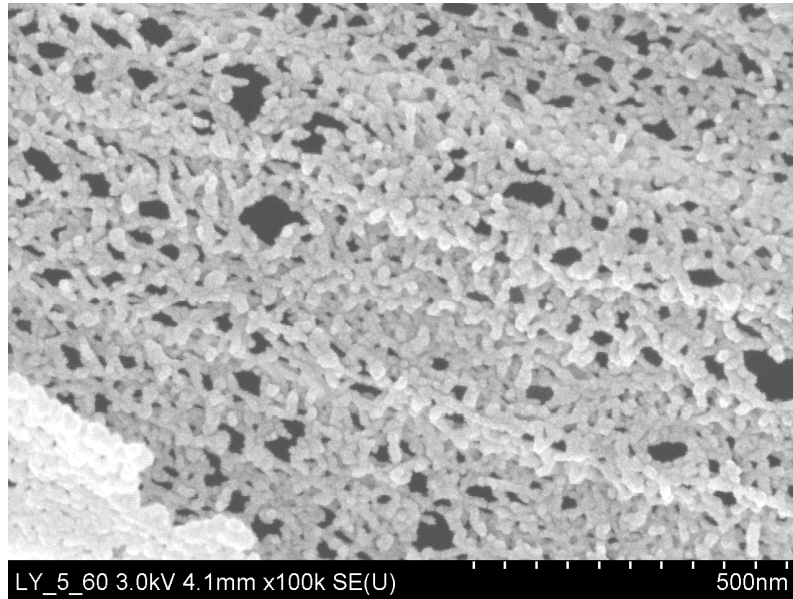
Figure 12. A high-resolution image (100 000 x) of the complex, fractal micro-fibril structure found within the S2 layer
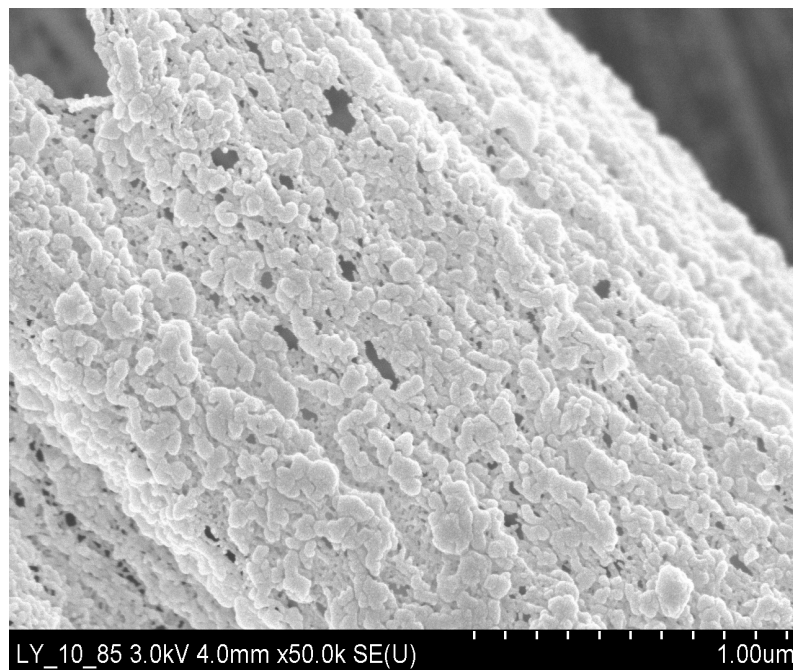
Figure 13. An image of an aggregated S2 layer at 50 000 x magnification, thought to be a result of aggressive pulping and bleaching

The S3 layer

It proved difficult to etch away the S2 layer to reveal the S3 layer. As can be seen from Figure 11, the energy levels required to remove polysaccharides to expose the S2 layer also remove the S3 layer. However, we were able to view the S3 by an alternative mechanism. Figure 14 is a low magnification image of two cells etched to reveal the fractal scaffold that forms part of the S1 layer. The cell on the right has torn during handling, revealing the underside of the S2 layer and exposing the S3 layer, which can be seen in more detail in Figure 15. The S3 layer appears to be fractal in structure, with a similar but not directly comparable structure to that of the primary wall.
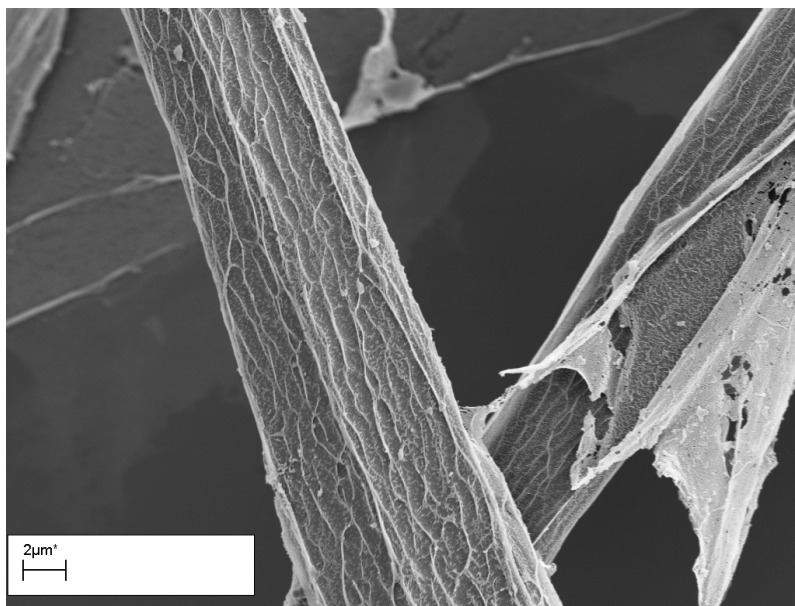
Figure 14. 10 000 x magnification of two cells exposed to plasma to reveal the fractal scaffold of the S1 layer. The right hand cell has torn to reveal the underside of the S2 layer and the S3 layer, which is shown at higher magnification in figure 15
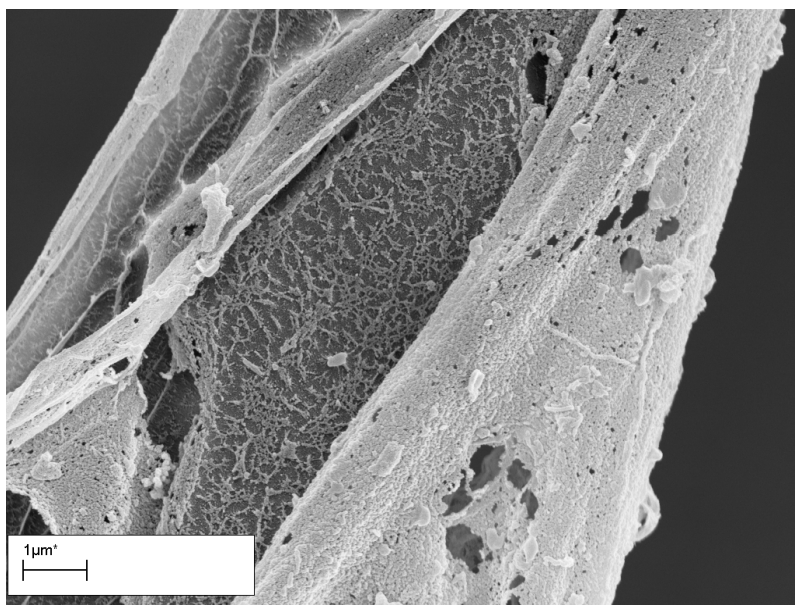
Figure 15. An image showing the fractal structure of the S3 layer exposed by a tear in the S1 and S2 layer which is peeled backwards

Discussion

As part of the process of improving our understanding of microfibril structure we reviewed past literature to see if the fractal cellulose structures reported here (particularly in the S2 layer) had been previously observed. The search was unsuccessful. We concluded that the plasma etching process was, for the first time revealing the true structure of the microfibril architecture. However, we have not ruled out the possibility that some species will have structures similar to the traditional model described in Figure 1.

In order to try and better understand the role that the observed fractal structures might play in the cell and at the level of the tree, we broadened our search to see if comparable structures could be found elsewhere. The result was unexpected. Brune et al. (1994) reported on the formation of fractal structure created by silver atoms, which were almost identical to that shown in the primary wall (Figure 4). A paper by Enculescu and Topa (2006) revealed fractal structures formed by gold atoms in a diffusion limited aggregation process, which were very similar to some of those we found in the S2 layer. A further paper on the fractal structure of brain neurons was published by Hagan et al. (2002). The structures were almost identical to some of our images of the S2 layer.

The overall outcome of our review was a large body of work published over the last 20 years reporting the formation of fractal structures in both organic and inorganic materials. It is clear from the review that fractal structures are ubiquitous in inorganic and biological systems when the structures are allowed to grow in an unconstrained way, normally referred to as diffusion limited aggregation. It is also clear that these fractal structures are not driven by biological processes, but something more fundamental, at the level of atomic structure (or smaller). In order to explain these observations we need a new, higher level hypothesis.

At this stage we refocused our review on historical and current scientific literature in fundamental physics. A full and comprehensive review is beyond the scope of this current paper. For the sake of brevity we have focused on a few key milestones, which form the foundations, upon which we have constructed a new perspective on the fractal structure of materials and biological systems.

We began our search with the hypothesis that the fractal structure of materials must have some sort of foundation in the structure of the atom. In terms of scale, the nucleus is the equivalent of a pinhead in the Albert Hall, i.e., most of the atom is comprised of space though which electrons travel whilst orbiting the nucleus. From this hypothesis, a few key pillars of modern physics emerge.

In 1915 Albert Einstein published the general theory of relativity. His greatest achievement in general relativity was to base the theory of gravity on geometry (Riemannian geometry). The theory generalizes his special theory of relativity and Newton's law of universal gravitation, providing a unified description of gravity as a geometric property of four dimensional space and time (space-time). The theory takes a classical approach using non-linear, partial differential equations to describe smooth changes in the curvature of space-time as opposed to quantum jumps. In that sense, it resembles the 19th century version of electromagnetic theory, not 20th century quantum physics that is used to describe the other three forces known to physics. These forces include electromagnetism plus two additional forces, which operate within the nucleus of an atom. The strong force, holds a nucleus together, in spite of the fact that it contains protons that should repel each other. The weak force is responsible for radioactive decay. Both these forces have only a short range, within an atomic nucleus. A key focus of modern physics is to find a quantum theory of gravity, which can then be combined into one package with the other three quantum fields.

Quantum mechanics was from its origin, fundamentally about wave mechanics, which led to the unification of matter and radiation. In 1905, Einstein introduced the concept of a quantum of light (the photon). He related the frequency of the wave to the energy of the photon and its wavelength to its momentum. In 1923 de Broglie made the same suggestion for matter. De Broglie hypothesized that all particles (e.g. electrons) had similar properties. Assuming that the waves travel roughly along classical paths, he showed that they form standing waves for certain

discrete frequencies. These correspond to discrete energy (or quantum) levels. These proposals by Einstein and de Broglie were the origin of wave mechanics that became quantum mechanics.

Following up on these ideas, Schrödinger developed a wave equation for the electron, which he used to compute the hydrogen spectra series by treating a hydrogen atom's electron as a wave. The solution accurately reproduced the energy levels of the Bohr model.

The Schrödinger equation describes how the quantum state of a physical system changes in time. The most general form is the time-dependant Schrödinger equation, which describes a system evolving with time. A time independent Schrödinger equation can be used for systems in a stationary state. Max Born interpreted the wave as probability amplitude, which became known as the Copenhagen interpretation.

The theory of scale relativity

At this point we come to the work of Laurent Nottale a French astrophysicist. Since 1991, Nottale has published a number of papers on his theory of scale relativity [Nottale (1991, 1993, 1994, 1995a, 1995b, 1997, 2003a, 2003b, 2007), Nottale and Celerier (2009), Nottale et al. (1996)]. The theory of scale relativity is an extension of the theories of relativity. In the general theory of relativity the geodesic curvature of space-time is smooth and differentiable. The scale relativity theory treats space-time as continuous but non-differentiable, (fractal) at all scales from the Planck scale (10^{-33}cm) to infinity.

The length of a non-differentiable (fractal) curve is dependant on the resolution at which it is measured. For example, when measuring the coastline of Norway its length is scale dependant, with smaller scale resolutions leading to an increase in the length of the coastline measured. According to the scale relativity theory, this principle can be applied to space, and more generally to space-time. On a large scale the curvature of space-time approximates to a differentiable curve but as the resolution becomes smaller in scale these curves have an internal fractal structure with an infinite number of possibilities depending upon the scale at which it is observed. In translation, this suggests that a "wave-particle" such as an electron will have the geometric properties of a subset of the fractal geodesics of a non-differentiable space-time i.e. an electron will follow a fractal trajectory in its orbital as it travels through the complex, multidimensional fractal scaffold of space-time. Auffray and Nottale (2008) introduced pure scale laws describing the dependence on scale of fractal paths at a given point of space-time. The paper then goes on to consider the radical consequences on motion of the fractal structure of space-time. The laws of mechanics constructed from the geodesic of fractal space-time become quantum type mechanics. Auffray and Nottale transformed Newton's equations of dynamics into a generalized macroscopic Schrödinger equation, which leads to a profound theory of self-organization.

A Schrödinger-type equation is characterized by the existence of stationary solutions yielding well-defined peaks of probability linked to quantization laws, of the forces applied and of the symmetries of the system. Nottale (1997) interpreted these peaks of probability as a tendency for the system to form structures. The theory doesn't predict precise organization, but rather the most probable structures among the infinity of other close possibilities. This is compatible with the large variability that characterizes living systems.

Traditionally, scientists have viewed growth as a process of "diffusion limited aggregation" while Nottale and Auffray (2008) suggest that growth processes are based upon the laws of quantum mechanics. It should be emphasized that quantum mechanics and diffusion process are

opposite processes. Diffusion laws describe disorganization and entropy increase. Conversely, quantum-type laws are an archetype for laws of self-organization and local entropy decrease.

In living systems, morphologies are acquired through growth processes. According to Auffray and Nottale (2008), following their "Schrödinger process", growth can be described in terms of an infinite family of virtual, fractal and locally irreversible trajectories. However, instead of an infinite number of possible morphologies, only some are possible due to the quantized nature of trajectories and their corresponding morphologies are also quantized. The quantum level (n) can be 0 to infinity. When *n=0* a one–body structure results. If one increases the energy from this value, no stable solution can exist before it reaches the second quantized level when a two-body structure is formed through a process of bifurcation. The passage from the fundamental level to the first excited level provides a rough model of duplication or bifurcation. As the energy levels increase further, bodies of increasing complexity result. The model provides a good hypothesis as to why we see fractal structures at both the macroscopic (tree) level and at the microscopic (within cell) level. This could also explain why we see both relatively simple, almost linear arrangements of micro-fibrils within the S1 layer in combination with increasing levels of complexity in other layers of the cell wall.

To demonstrate the principles behind the theory, Auffray and Nottale (2008) show a simple example of the use of the "Schrödinger process" to "grow" flower-like shapes, with different structures (petals, sepals and stamen) within the flower being derived from the same wave equation.

If space-time is fractal, at all scales then we should see parallel structures both at atomic level and throughout space. It is interesting to note that the fractal structures formed by gold atoms in a diffusion limited aggregation process, referred to earlier are very similar to recent published images of the universe from the Sloan digital sky survey (2007) which are fractal on the scale of billions of light years.

Scale relativity theory provides a fundamental explanation as to how simple through to complex structures (both organic and inorganic) can be influenced by the fundamental structure of space-time through the "Schrödinger process. In theory it should be possible to write a complete system of equations including the effects of fractality and describe the system, the environment and the interaction between them. Nottale (1995, 1996a) suggests it is possible to produce a system of equations that can be integrated in terms of a single, multisystem Schrödinger equation, which could have profound implications for the description of the relations between biological systems and their environment.

String theory

The second area of recent activity of relevance to the fractal character of matter is string theory. According to Edward Witten (Davies and Brown 1998), string theory is essentially a new branch of geometry. Which attempts to unify the four forces of physics into a single, logical framework in a way that is analogous to that of General relativity in which gravity theory is based on geometry.

One of the most developed forms of string theory, Heterotic string theory first developed by Gross et al. (1985) is essentially a theory of gravity in which the particles of matter as well as the other forces of nature emerge in the same way that gravity emerges from geometry. The theory is based on the complex fractal geometry of the E_8 structure illustrated in Figure 16 (Green et al. 1987). This structure, a representation of the Exceptional Lie group E8 was found in a 248 dimensional mathematical puzzle, which was solved in March 2007**.** An international team of

mathematicians produced a complex numerical structure, which was described more than a century ago. Conceptualizing, designing, running the calculations and mapping the 248 dimensional structure, took 18 mathematicians four years. They processed more data than that used to sequence the human genome sequence.

The reason Heterotic string theory has attracted so much interest is that the symmetries of particle physics, which are known about from experiments at energy levels currently accessible, are part of the symmetries of the E_8 structure. This theory combines earlier string theory, which works in twenty-six dimensional space-time with one, which works in ten dimensions. Ten of the twenty-six dimensions are ordinary space-time dimensions, with the string wriggling in ten-dimensional space-time. In addition there are 16 internal dimensions, which lead to extra structure in the theory that ought to describe forces other than gravity.

According to string theory, strings can oscillate and vibrate in different ways – each of these different modes of vibration or oscillation can be thought of as describing a particular type of particle. The electron, graviton, photon, the neutrino and all other particles are different harmonics of a fundamental string i.e. we have one type of string but its pattern of motion (and energy level) defining its nature. It brings a whole new dimension of understanding to Einstein's equation ($E=mc^2$) in which energy and mass have equivalence.
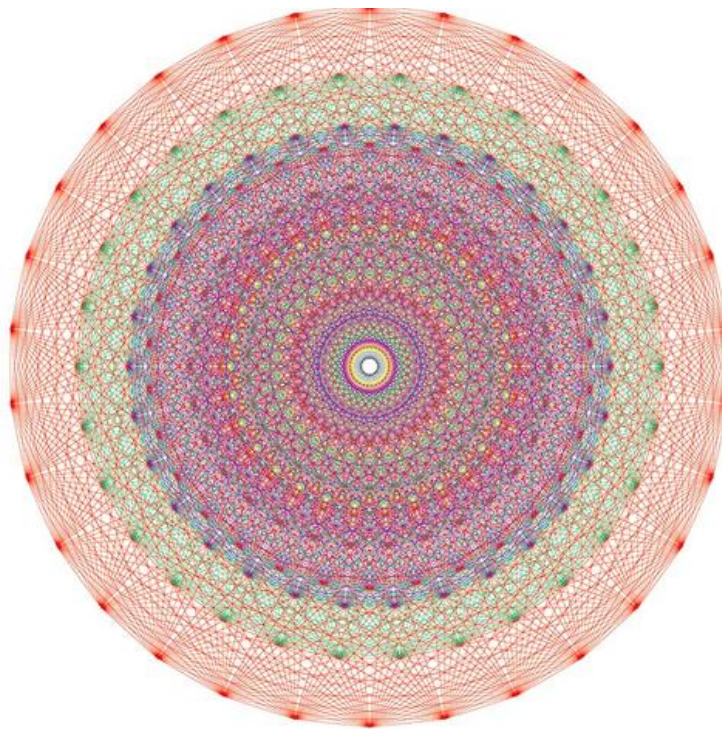
Figure 16. The E8 structure

String theory takes our conceptual understanding of space-time to another level. At the Planck scale (10^{-33}cm), space and time are effectively built of strings rather than strings inhabiting space and time. Conceptually we can consider space-time (and by default all matter) as a complex, multidimensional web like fractal structure made up of strings. The E8 structure forms a good, possibly oversimplified model. This idea has been actively proposed by El Nashie (2006 and 2007). El Nashie's Cantorian E-infinity theory of space-time takes a similar approach to Nottale, describing space-time as an infinitely dimensional fractal structure in which the Exceptional Lie group E8xE8 describes the volume of space-time.

It needs to be emphasized that at this moment in time, string theory is not completely understood with solutions being at best approximations. It is generally accepted that physicists are still looking for the best formulation, which may take years. The radical conclusion to string theory is that all matter is comprised of the vibrating fabric of space-time. If correct, it would certainly explain the ubiquitous fractal character of matter in the natural universe.

Conclusions and the way forward

We have demonstrated a new approach to viewing the internal structure of plant cells that has provided new insights into the architecture of the cell wall and suggests that it has a level of complexity that rivals that of the tree itself (an archetypal fractal structure). The cellulose skeleton is a complex, largely fractal structure that may offer new insights into the possible role of cellulose in wood characteristics. This new understanding may also assist in the development of new models to better predict wood and pulp and paper properties into the future. For example, the classical model of a highly oriented S2 layer and its impact on issues such as wood strength, stability and creep needs a re-think. Work has started to model these structures and to use finite element analysis to assess the role of the different cell layers on structural performance of the cell.

Our high magnification images reveal that the surface of micro fibrils is nodular in appearance, suggesting that the internal arrangement of cellulose chains may not be a simple, linear arrangement of cellulose chains. Sugiyama et al. (1984) showed linear arrangements of cellulose molecules in a straight, bacterial cellulose microfibril so clearly these linear arrangements exist. However, within the context of the discussions highlighted here, it is suggested that the internal structures of the samples we have shown may be fractal. Currently unpublished work indicates that this may well be the case. Work is ongoing to confirm this.

This paper sets the hypothesis that the fractal structure of the tree and the cell itself along with the majority of biological and inorganic materials that are allowed to "grow" is driven by the fundamental fractal structure of space-time. This concept has gained considerable momentum through parallel and independent research programs in fundamental physics.

The macroscopic Schrödinger theory derived from Nottale's theory of scale relativity provides new insights into how biological functions (morphogenesis, duplication, multiscale hierarchy of organization etc) and the ubiquitous fractal structures found in biological systems and the physical world are influenced by quantum mechanics and fundamental geometric structures of space-time.

The development of string theory is still ongoing. The jury is still out on what its final form will take. Meanwhile it provides fundamental insights into the nature of matter and provides an alternative, complementary perspective on the structure and nature of space-time to that proposed by Nottale.

The framework offered by the scale relativity theory opens the opportunity to rethink research in order to better understand the fundamentals of biological systems. This needs to be done taking an integrative systems approach to biology. Such collaboration has already started through the SYSTEMOSCOPE Consortium (Auffray et al. 2003b). The work requires multidisciplinary collaboration between biology, physics, materials science, systems engineering, computer sciences micro and nanotechnologies and modeling and simulation. We need to pull together a diverse range of expertise to establish more profound foundations for a theory of biology

through the integration of the cell, biochemical and evolution-development theories based on first principles. On another level, materials scientists are currently focused on understanding and mimicking biological processes. The ideas discussed in this paper suggest that many biological systems may well turn out to be purely physical processes. Understanding how these systems work could lead to insights into the development of new self assembly processes at molecular and nanometer scales.

References

Auffray C., Imbeaud S., Roux-Rouquie M. and Hood L. (2003a): Self organized living systems: conjunction of a stable organization with chaotic fluctuations in biological space-time. Philos. Trans. Roy. Soc. Math. Phys. Eng. Sci. 361, 1125-1139

Auffrey C., Chen Z., Hood L., Soares B. and Sugano S. (2003b): Foreword: From the transcriptome conferences to the stemoscope International Consortium. C.R Biologies 326, 867-875

Auffrey C. and Nottale L. (2008): Scale relativity theory and integrative systems biology: 1 Founding principles and scale laws. Progress in Biophysics & Molecular Biology 97, 79-114

Brune H., Romainczyk C., Roder H. and Kern K. (1994): Mechanism of the transition from fractal to dendritic growth of surface aggregates. Nature Vol. 369

Côté W.A. (1974): Wood ultrastructure in relation to chemical composition. In: The structure, biosynthesis and degradation of wood. Vol 11, Ch 1. Plenum, New York, 1-44. *Eds*: Loewus, F. and Runeckles, W.C.

Davies P.C.W. and Brown J. (1998): Superstrings. A Theory of Everything? Cambridge University Press

El Naschie M.S. (2007): A review of applications and results of E-infinity theory. Int J Nonlin Sci Simul. 8(1): 11-20

El Naschie M.S. (2006): Elementary prerequisites for E-infinity. Chaos, Solitons and Fractals 30, 579-605

Enculescu M. and Topa V. (2006): Fractal structures of gold obtained by diffusion limited aggregation in alkali halide crystals. Journal of Optoelectronics and Advanced Materials Vol. 8, No. 3, June 2006, p. 1230 – 1233

Green M., Schwarz J. and Witten E. (1987): Superstring Theory, Vols I and II. Cambridge University Press

Hagan S., Hameroff R. and Tuszynski A. (2002): Quantum computation in brain microtubules: Decoherence and biological feasibility. Physical Review E, Volume 65, 061901

Humphries W. J. (1979): Scanning Electron Microscopy of biological specimens surface-etched by an Oxygen plasma. Scanning Electron Microscopy 1979/11

Gross D.J., Harvey J.A., Martinec E. and Rohm R. (1985): Heterotic String theory: (11). The interacting heterotic string. Phys. Rev. Lett. 54, 502-505

Keckes J., Burgert I., Frühmann K., Müller M., Kölln K., Hamilton M., Burghammer M., Roth S. V., Stanzl-Tschegg S. E. and Fratzl P. (2003): The 'molecular Velcro' model of cell-wall recovery after irreversible deformation of wood. Nat. Mater. 2, 810–814

Notalle L. (1991): The theory of scale relativity. Int. J. Modern Physics A, vol. 7, No. 20, 4899-4936

Nottale L. (1993): Fractal space-time and microphysics. Towards a theory of scale relativity. World Scientific. ISBN 9810208782

Nottale L. (1994): Scale relativity, Fractal Space-time and Quantum Mechanics. Chaos, Solitons & Fractals 4(3), 361-388

Nottale L. (1995a): Scale Relativity and Fractal Space-Time: Applications to Quantum Physics, Cosmology and Chaotic Systems. Chaos, Solitons & Fractals 7(6), 877-938

Nottale L. (1995b): Scale Relativity: From Quantum Mechanics to Chaotic Dynamics. Chaos, Solitons & Fractals 6, 399-410

Nottale L. (1997): Scale relativity and quantization of the universe. I. Theoretical framework. Astronomy and Astrophysics 327, 867-889

Nottale L. (2003a): The theory of Scale Relativity: Non- Differentiable Geometry and Fractal Space-Time, Computing Anticipatory Systems. CASYS'03 – Sixth Int. Conf.'' (2003)

Nottale L. (2003b): Scale – relativistic cosmology. Chaos, Solitons & Fractals 16 (2003) 539-564

Nottale L. (2007): Scale Relativity: A Fractal Matrix for Organization in Nature. Electronic Journal of Theoretical Physics 4, No. 16 (II), 187-274

Nottale L. and Auffrey C. (2008): Scale relativity theory and integrative systems biology: 2 Macroscopic quantum-type mechanics. Progress in Biophysics & Molecular Biology 97, 115-157

Nottale L. and Celerier M. (2009): Motion equations for relativistic particles in an external electromagnetic field in scale relativity

Nottale L., Schumacher G. and Gay J. (1997): Scale Relativity and quantization of the solar system. Astronomy and Astrophysics 322, 1018-1025

Sugiyama J., Harada H., Fujiyoshi Y. and Uyeda N. (1984): High resolution observations of cellulose microfibrils. Mokuzai Gakkaishi 30(1), 98-99

CELLULOSIC MATERIALS MODIFICATION BY PHYSICAL AND CHEMICAL METHODS

Marian I. Totolin, Georgeta Cazacu and Cornelia Vasile

"Petru Poni" Institute of Macromolecular Chemistry, 41 A Grigore Ghica Voda Alley, IASI, ROMANIA

E-mail: gcazacu@icmpp.ro

Abstract

It is well-known that paper and cellulosic materials are the best candidates for flexible packaging materials where good barrier properties, water repellence, grease resistance and flame retardance are required. The paper describes several ways of the modification of cellulose substrates by physical methods (such as plasma treatments) and chemical modifications. Evidence for chemical reactions mainly on the surface was obtained.

Introduction

With increasing demand for flexible barrier packaging, the industry has no choice but to continue to innovate and develop new materials and packaging solutions to meet the needs of a growing market. Paper and cellulosic materials hold a good promise of being candidates for flexible packaging materials provided suitable barrier properties such as water repellence and grease resistance are imparted to them. One of the methods to achieve these objectives is surface modification of paper and cellulose by applying thin coatings on the surface.

Cellulose is a complex carbohydrate, $(C_6H_{10}O_5)_n$, composed of glucose units, and forms the main constituent of the cell wall in most plants, and is important in the manufacture of numerous products, such as paper, textiles, pharmaceuticals and composite materials. Cellulose possesses three types of -OH groups, which are quite different in terms of regiochemistry and polarity (Rozmarin 1984; Atalla 1999) (Figure 1).
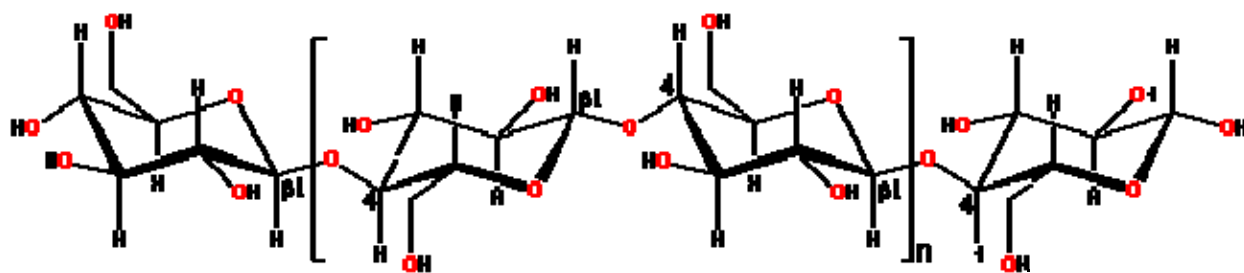
Figure 1. Molecular structure of cellulose (n = polymerization degree)

This difference is considered to be an important factor influencing the physical properties including solubility, crystallinity, reactivity, gelation and liquid crystallinity. Moreover, -OH groups have the capacity to facilitate intra- and intermolecular interactions and to easily react with various reagents allowing the synthesis of derivatives, each of them showing a specific behavior and applications.

Plasma treatment represents a modern technique to modify the wettability of paper surfaces in a controlled manner (Deslandes et al. 1998). Paper is a porous material which can be covered by polymer films in order to make it impermeable to water. Thus, plasma polymerization of

hydrocarbon monomers like cyclohexane (Tu et al. 1994), carbon tetrafluoride (Denes et al. 1995), plasma deposition of the hexamethyldisilazane (Tan et al. 2001), or fluorocarbon films (Vasmawani et al. 2005) have been demonstrated to make cellulose surfaces hydrophobic.

Cellulose and lignocelluloses fibers, the so-called "biofibers", offer several advantages when combined with other polymers, such as giving lighter composites due to their low density; modest abrasivity, ensuring greater longevity of the materials during processing; improved mechanical properties (high modulus, strength and stiffness); little requirements on processing equipment, biodegradability and relatively low price (Joly et al. 1996; Zadorecki and Michell 1989; Klemm et al. 2006; Henriksson and Berglund 2007; Iwamoto et al. 2007; Nisho 1994; Mohanty et al. 2000; Souza et al. 2004). However, cellulosic materials present some limitations since their highly polar and hydrophilic character lead both to poor compatibility (weak interfacial adhesion) with non-polar polymer matrices and to a decrease of mechanical properties due to greater atmospheric moisture adsorption. For these reasons, extensive efforts have been made in the last decades, in order (i) to provide an efficient hydrophobic barrier and (ii) to achieve an optimum interfacial adhesion with the non-polar polymer matrix. With this purpose a wide range of techniques are applied such as: (i) physical adsorption; (ii) chemical modification (etherification, esterification and grafting reactions); and (iii) physical treatments (UV radiation, corona, cold plasma, etc.).

The plasma treatments of the cellulosic substrates (cellulose, lignocellulose and paper materials) by the use of various gases lead to improved surface properties such as mechanical properties (strength, hardness, wear, friction coefficient, abrasion resistance), electrical properties (dielectric coefficient, conductivity) and chemical properties (corrosion, oxidation, wettability and water repellance, flame retardancy, reactive dyeing etc.). These modifications are accompanied by production of barrier layers for chemicals, UV protection, anti-bacterial activity, etc. (Grace and Gerenser 2003).

Different plasma procedures have been used to modify the cellulosic fibers from jute (Sabharwal et al. 1993), wood fibers (Olaru et al. 2005), and cotton fabrics (Almeida and Carneiro 2005). Totolin and co-workers (Totolin et al. 2008) reported the result of the grafting of flax or Spanish broom (*Spartium junceum*, syn. *Genista juncea*) fibers with different kinds of carboxylic acids under action of cold plasma discharges (Vasile et al. 2009).

In case of cold plasma treatment of cellulosic materials (yarns, fibers, fabrics, dust) an increase of specific surface has been observed. For example, treatment of cotton fabrics in hexamethyldisiloxan plasma (HMDSO) was accompanied by an increase in surface roughness associated with increasing of wetting angle of water up to 130 °C, ensuring in this way a strong hydrophobic effect (Hocker 2002). Similarly, using hexafluoroethane plasma, fluorine was bound to the surface giving a waterproof material. Hua et al. (1998) discussed the mechanisms of oxygen and argon-RF-plasma induced surface chemistry of pure cellulose samples and established that the mechanisms involve cleavage of macromolecular chain and pyranose ring and formation of C=O and O-CO-O groups. The external plasma parameters like RF-power and pressure of plasma gas have significant effect on the surface functionalization and these enable the control of substrate modification and characteristics. Totolin et al. (2007) obtained a durable flame retardant treatment on cotton fabrics.

The aim of this paper is to present our trials to modify various cellulose substrates to obtain materials with improved properties both for the paper packaging materials or to increase their compatibility with other polymers.

Materials and Methods

Three types of cellulosic substrates have been used to modify their surfaces by physical treatment: (a) *unbleached* (UBP) *and bleached kraft pulps* (BP) from softwood (supplied by Södra Cell, Sweden for the COST Action E54 project). (b) *cotton cellulose fibers* (supplied by Arshad Enterprises, Pakistan); (b) two paper types: s*tandard printer paper* (80 g/m^2) and *natural degraded old paper* (60 g/m^2, from old documents).

Reagents used for cellulose grafting and chemical modification were: (1) fatty acids: *butyric acid* (B) (Merck, purity > 99%); *oleic acid* (O) (Aldrich, 90 % purity); (2) acrylic polymers like structures: *methyl methacrylate* (MMA)*, methyl acrylate* (MeA), *ethyl acrylate* (EtA), *buthyl acrylate* (BuA), *acrylamide* (AA) (from Merck, purity > 99 %); (3) *poly(amido-ethyl) phosphate* (PAEP) synthesized in our institute according to the literature method (Albright and Wilson (1963). (T_m=60-80°C, P%=23.8%, N%=11%) ; (4) *paraformaldehyde* (PF) (Fluka, 95% purity); (3) solvents: *acetone, chloroform,* e*thyl alcohol, dimethylsulfoxide* (DMSO) grade for synthesis.

Plasma treatments

The cellulose substrates were treated under cold plasma and atmospheric pressure plasma conditions.

The experimental setup for cold plasma grafting of short fibers (horizontal plasma reactor), plane surfaces (paper, cotton fabrics) and for film deposition is presented in Figure 2.
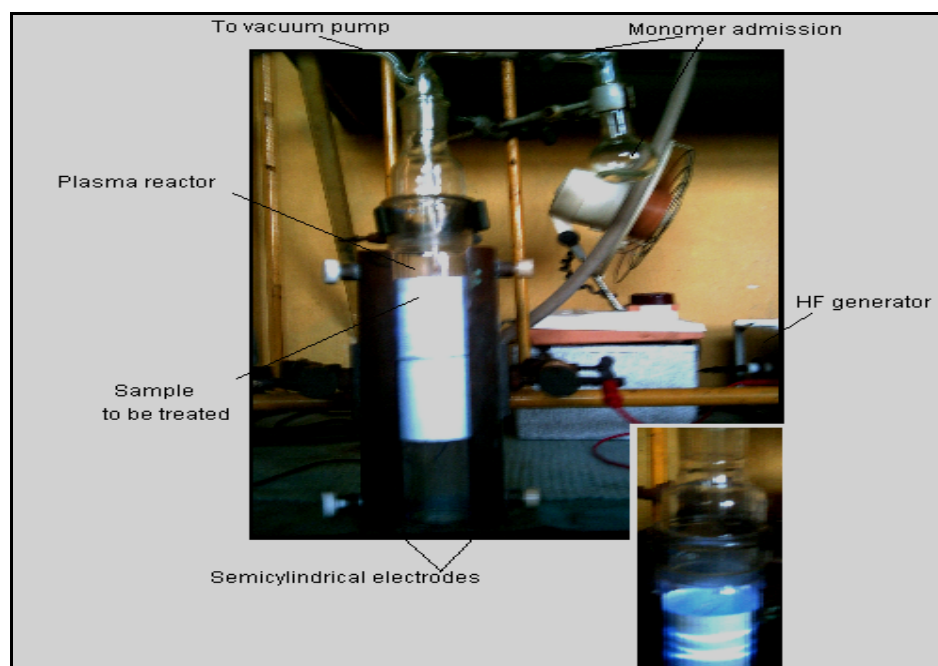
Figure 2. Laboratory experimental equipment for plane surfaces. RF plasma conditions used: 13.5 MHz and 200 W power, monomer pressure 0.3 mm Hg, 35 – 40 °C in purified air, discharge time 600 seconds

Before treatment the fibers substrates (cellulose kraft pulp, cotton fibers, and paper) were impregnated with solutions of reactants. After treatment the cellulosic materials were extracted for 6 h in a Soxhlet extractor and then dried at 105 ºC for 24 hours.

Investigation methods

The following techniques used in this paper to assess the modifications on the fibers surfaces were: ATR FT-IR spectroscopy, scanning electron microscopy (SEM), ESCA (XPS) spectroscopy, AFM surface analysis, thermogravimetry and contact angle measurements, ζ potential measurements (zeta potential) (SurPASS Electrokinetic Analyzer), as well as comparison of physical properties of treated and untreated samples. Other treatments and methods are given in the papers by Totolin et al. (2008) and Vasile et al. (2009)

Results and Discussion

Plasma treatments

Treatment of cellulose substrates in cold plasma conditions

Air-plasma treatments were done on some cellulose materials (cotton, paper) using the plasma device described in Figure 2.

The *FT-IR (ATR) spectra* for untreated and plasma treated cotton samples evidenced that minor chemical changes appeared at the surface of the samples. However, appearance of an additional absorption band (1730 cm^{-1}) in the carbonyl region due to the formation of aldehyde (-CHO) and carboxyl (-COOH) functional groups at the surface was seen (Totolin and Cazacu 2007; Malek and Holme 2003; Fisher 2004; Chen et al. 2004). The absorption at the level of –OH and β-glucosidic groups were not modified; plasma did not affect the macromolecular chain and its degree of polymerization. The changes were not produced in depth but only at the surface; at the nanometric scale no more than a few macromolecular layers (Totolin and Cazacu 2007; Totolin 2007).

The appearance of the new functional groups (-CHO and –COOH) on the surface of the plasma treated cellulose fibers (cotton) was confirmed by the *ESCA (XPS) spectroscopy* (Totolin and Cazacu 2007). These functional groups are responsible for the changes in hydrophilic /hydrophobic balance and roughness of the surface. From data presented in Table 1 it can easily be observed that the peak areas assigned to carboxylic and carbonyl groups increase after plasma treatment. Also, it can be observed a decrease of the C–OH peak surfaces probably due to some cross-linking reactions which take place during plasma treatment. In the case of paper samples XPS gave the same conclusions.

Table 1. Percentage areas of the component signal C 1s for cotton samples

Signal	Area, at% Control cotton fibers	Area, at% Plasma treated cotton fibers
-C-OH	56.30	42.90
-C-O-	29.90	30.40
-C-C-	5.40	5.30
-COOH	8.40	15.30
-CHO	-	6.10

In *X-ray diffractogramms* it can be observed that at $2\theta < 30^{o}$ (higher d spacing) the diffraction peak intensity was higher for plasma treated cotton sample than for untreated ones, whereas for diffraction angles $2\theta > 30^{o}$ (lower d spacing) the peak intensity decreased through plasma treatment (Figure 3a). The differences were not significant and the degree of crystallinity was

little affected by the oxidation and cross-linking processes as a consequence of the action of plasma active species. In the case of the paper samples (Figure 3b) plasma did not affect structural change or crystallinity degree.
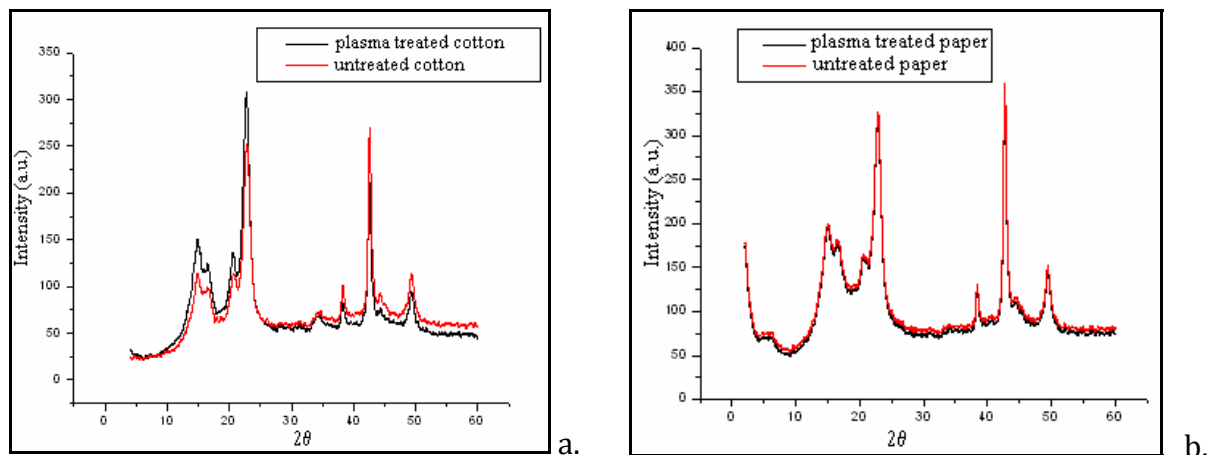
Figure 3. X-ray diffractograms of the: (a). untreated and (b). plasma treated samples

SEM analyses indicated that the topography of the natural fibers is complex and differentiated. Thus, the cotton fiber presents various shapes and cross-sections along a fiber (Figure 4a and b). The SEM micrographs of the treated cotton indicated no significant surface topographic change of the fibers. Both bulk and surface investigation methods were employed and the obtained data show that plasma acts only at the surface level within a depth of a few nanometers without affecting the interior paper structure.

SEM images obtained for paper samples treated indicated that pulp from paper is very stable to the action of cold plasma.
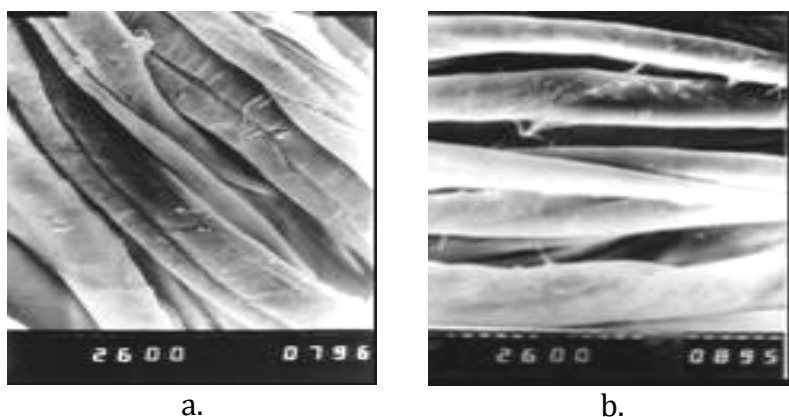
Figure 4. SEM images of cotton fibers: a – control cotton sample; b – cold plasma treated (30 min) cotton sample

Grafting of cellulose substrates in cold plasma conditions

- Plasma grafting cellulose kraft pulp with fatty acids

The pH dependence of the *zeta potential* of cellulose fibers treated with different fatty acids (oleic acid-O; butyric acid-B) is shown in Figure 5.
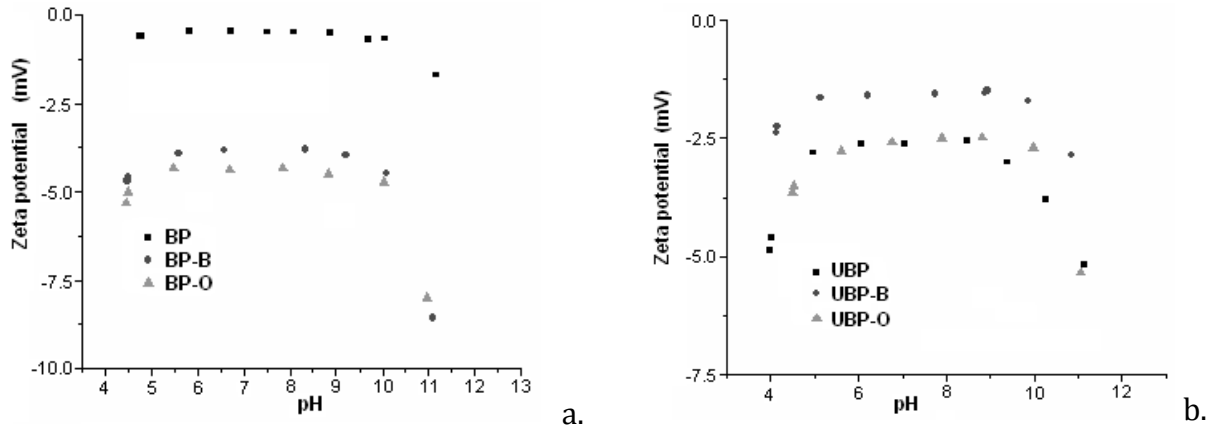
Figure 5. Variation ζ potential vs. pH for bleached and unbleached kraft pulp

One can observe the presence of a zeta potential plateau situated in the pH = 5-10 range. The ζ plateau value of treated bleached pulps was around −3.75 mV in comparison with the ζ plateau of control pulp (−1 mV), due to the distinct reactive groups (especially –COOH groups) introduced by the grafting process during plasma conditions.
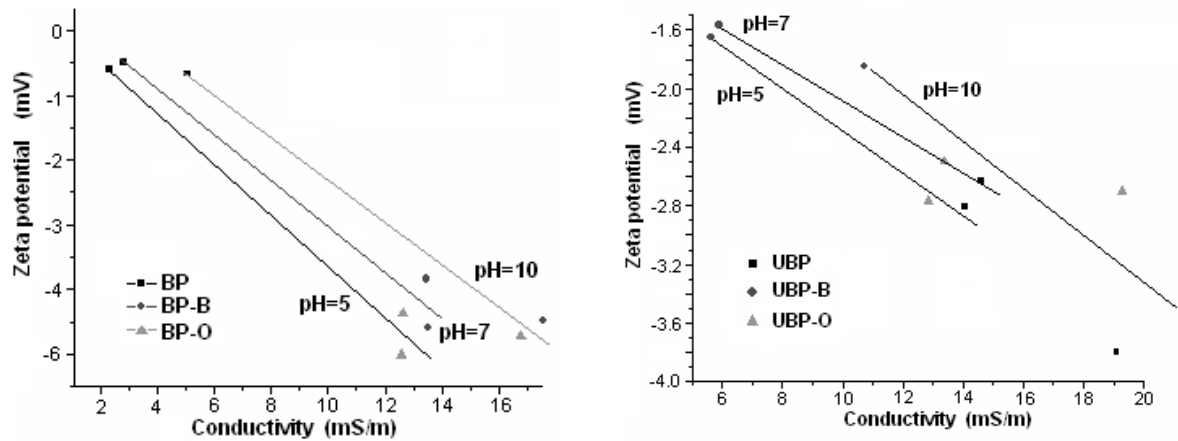
Figure 6. Variation of ζ (zeta) potential vs. conductivity for bleached and unbleached kraft pulp

The unbleached pulp treated with butyric acid (UBP-B) has lower zeta potential plateau (-1.75 mV) than that treated with oleic acid (UBP-O) (-2.6 mV), due to the grafting of short chain fatty acid on the fiber surface. The ζ potential decreased with increase of the conductivity (Figure 6). This suggests that zeta potential may be pH-independent at variable conductivity. The effect of conductivity on ζ potential depends on the nature of the pulp and on treatment conditions.

- Cold plasma grafting of cotton fibers with acrylamide

Grafting reaction of cotton fibers with acrylamide took place in cold plasma installation presented in Figure 2 (Totolin and Cazacu 2007). The experiments were carried out according to a mathematic model of second order: compositional, rotating, centering, factorial, design (Cochran and Cox 1968). The influence of the parameters reaction time, power dissipated to the electrodes and the monomer solution concentration on the process was investigated (Simionescu and Macoveanu 1977). The optimal working parameters for the grafting process were as follows: reaction time 341 s, power dissipated 500W and monomer solution concentration 50%. By a model experiment polymerization of acrylamide on inert surfaces) it was established that the

monomer solution concentration was the most important factor, because it controls the deposited acrylamide layer thickness on the supports.

In addition to the specific absorptions of the cellulose, the *FT-IR spectra* of the acrylamide-grafted cotton fibres also gave vibrations due to the grafted structures: 3182 cm^{-1} (ν CO-NH-CO), 1660 cm^{-1} (ν NH), and 1450 cm^{-1}, 1410 cm^{-1} (ν CO-NHR). Elemental analysis confirmed the presence of 5-9% nitrogen on the cellulose.

The plasma-grafting processes lead to important changes in the physico-mechanical properties of the cellulose fibers as seen in Table 2.

Table 2. Physico-mechanical indices of the grafted cellulose

Sample	Grafting degree, %	Tensile strength, kN/mm²	Elongation at break, %
Cellulose	-	2.40	8.7
Cellulose-g-AAm	33	2.24	8.2
Cellulose-g-AAm	40	2.11	8.0
Cellulose-g-AAm	50	2.09	6.2

It clearly appears that the tensile strength of the grafted fibers diminished noticeably, in comparison with the support polymer, probably due to side destruction reactions and insertion of the polyacrylamide in the volume of the grafted cellulose. Low elongation percentage values of the grafted polymers can be connected to the formation of three-dimensional structures in the case of the high degrees of grafting.

Also, an improved water absorption in various relative humidity conditions was recorded (Figure 7) together with increased wetting heat values (69-79 J/g).
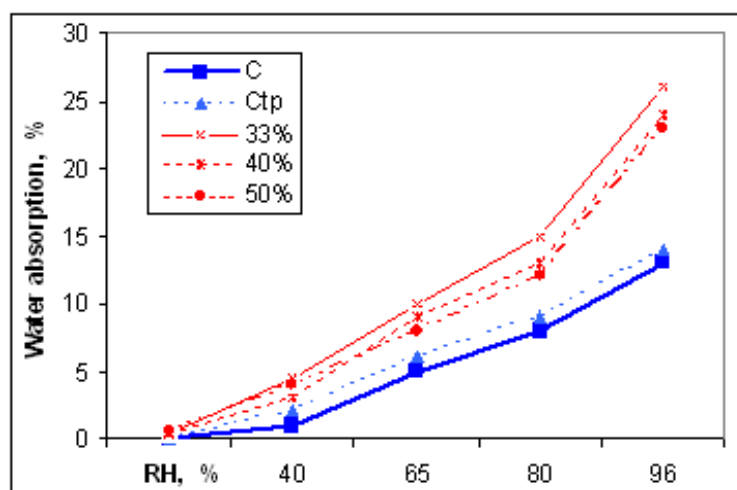
Figure 7. Various relative humidity vs. water absorption data for grafted cellulose

The action of plasma on cellulose (C) is shown by the appearance on the surface of the fibers of –COOH groups in the treated cellulose (Ctp) and of -NH groups in the case of grafted samples; these groups are responsible for water absorption and of wetting properties. The high grafted celluloses (40% and 50%) present the lower water absorption values in respect with the sample with degree of grafting of 33 %, probably because some supplementary cross-linking reactions which took place during plasma treatment.

- Plasma polymer thin films deposition on cellulose supports

After the sample (paper sheet of 15x70 mm - Standard line printer paper of 80 g/m^2) was introduced into the plasma reactor (Fig. 2), the chamber was evacuated to less than 0.3 mm Hg. The pure acrylic monomer from the flask was then introduced at steady flow conditions. After deposition in the plasma reactor, paper sheets coated with films based on poly-methyl methacrylate (PMMA), poly-methyl acrylate (PMeA), poly-ethyl acrylate (PEtA) and poly-buthyl acrylate (PBuA) were kept in the vacuum desiccator before analysis. Figure 8 shows the average quantity of polymer deposited on surface as a function of the reaction time. The average thickness of deposited polymer layer decreased in the order: PMeA > PEtA > PBuA > PMMA.
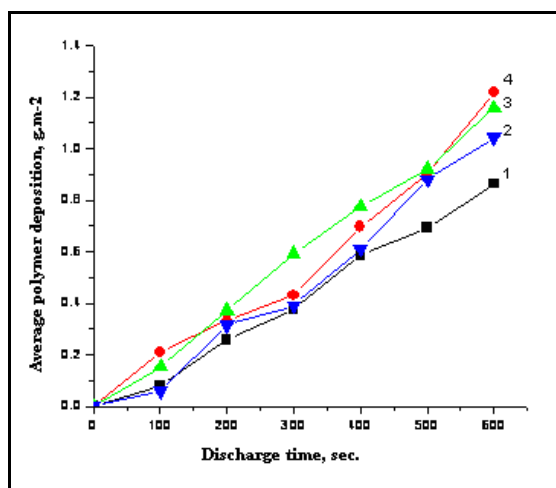
Figure 8. Polymer average deposition vs. discharge time in plasma polymerization:

1 PMMA
2 PBuA
3 PEtA
4 PMeA

The *ATR-FTIR spectra* of the thin films deposited on paper sheet samples revealed a similar structure as with the conventional polymers. The ATR-FTIR spectra of all the samples show a typical broad band in the range of 3330 cm^{-1} corresponding to the OH bending vibration in cellulose (Table 3).

Table 3. Frequencies, relative intensity and assignments of absorption bands for the studied samples

Wave number, cm^{-1}	Relative intensity[x]	Assignments[xx]
~3330	broad	ν (O-H)
~ 2910 - 2970	S	ν (C-H aliphatic)
1731	S	ν (C=O)
~ 1640 - 1660	W	Aldehyde groups in cellulose
~1420 - 1450	S	β(C-H aliphatic)
~1251	W	ν (C-O ester)
~1100 - 1200	S	δ(C-H aliphatic)
~1024	S	ν (C-C ethyl)
850	W	ν (C-C ethyl)

[x] S - strong; W –weak; [xx] ν - stretching; β - bending; δ - bending out-of plane

For all the analyzed samples, the presence of C=O group was confirmed by the characteristic sharp carbonyl stretching peak at 1731 cm^{-1}, while the band at ~1251 cm^{-1} shows the presence of C-O bond (stretching); the band at ~1024 cm^{-1} is assigned to ethyl group (stretching C-C).

The *AFM images* of the reference sample (Figure 9a) showed typical fibrillar morphology of cellulose in paper sheets, while those of the paper sheets coated with (PP) films showed some modifications and differences. Thus, the surface topography imaging of PMMA coated paper (Figure 9b) revealed how the polymer penetrated into the paper substrate and filled the pores, the resulting morphology following the fibrous template cellulose support. An insignificant decrease of RMS value (Table 4 scanned area of 10 µm x10 µm) in comparison with reference paper sheet was obtained.

(a)
(b)
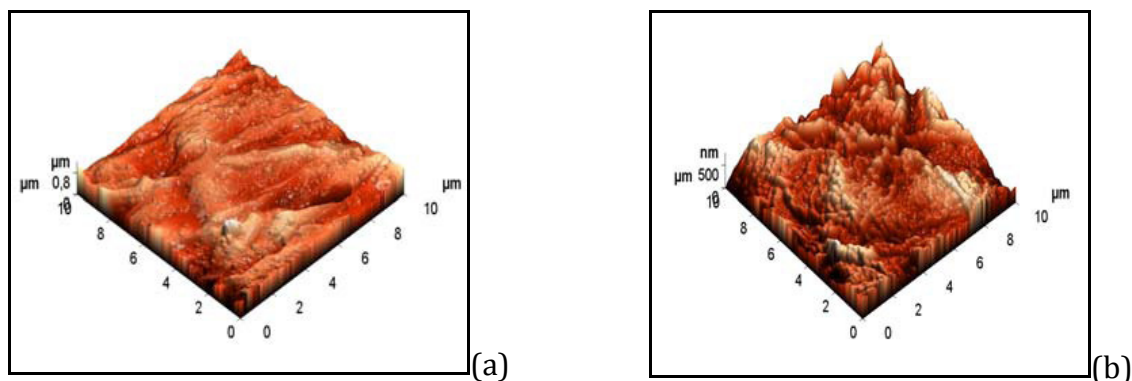
Figure 9. AFM images (3D) of: (a) reference paper sheet; (b) (PP) PMMA coated paper sheet

Table 4. RMS surface roughness and contact angle for the investigated samples

Sample	RMS, nm	Average contact angle, degree
Reference paper sheet	113.8	Instantaneous absorption
PMMA coated paper	112.9	92
PMeA coated paper	125.8	95
PEtA coated paper	171.5	96
PBuA coated paper	125.9	97

In the case of PMeA coated paper sheet it can be noticed that the RMS value slightly increased in comparison with reference sample, accompanied by an evolution of the surface morphology. The result of plasma polymerization with thin film deposition is an isotropic oriented structure.

For PEtA coated paper sheet it can be remarked a more significant increase of the RMS value, while for PBuA sample a small increase of the RMS value was obtained, together with evolution of the surface morphology in relation to the reference sample. Unlike the other studied samples of coated paper, the morphological structure formed in this latter case was branched.

The contact angle with water droplets onto the films deposited on paper sheets was used to estimate the film protective properties against water and water vapors and the result is presented in Table 4. This concept is important not only because it can offer information on the plasma treated surface energies but also on wettability.

For the reference paper sheet the hydrophilicity is relevant, the droplet being instantaneously absorbed by the support, without the capability for optical recording of the contact angle. In the case of PMMA, PMeA, PEtA or PBuA deposited on paper sheets, relative to the reference paper, the average contact angle had increased values, in the range of $92 - 97^o$.

Conclusions

Radio-frequency electrical discharges are suitable for the surface modification of cellulose substrates they leading to the implantation upon the cellulosic substrate surface of the different functionalities at superficial level changing of their quality. The modifications performed are dependent of samples characteristics, type of substrate and the treatment time.

Spectral, physical and chemical analyses show formation of graft-copolymers and the polymeric nature of the grafts. The modifications and grafting processes develop on the material surface only, the bulk properties being unaffected. In the conditions applied, the plasma did not give a degradative effect and the integrity of the substrate was preserved.

The investigations on plasma treated cellulose fibers were focused on obtaining fibers with new or significantly improved properties, with tailored functionalities for special applications, starting from natural fibers.

References

Albright & Wilson Ltd. (1963): Improvements relating to the manufacture of polycondensation products. GB 931146 (A)

Almeida L. and Carneiro N. (2005): Corona treatment, enzyme finishing and application of corona discharge to the pretreatment of cotton fabrics PLASMA COST 628 Meeting, Bucharest, Romania, 17-18th, March 2005

Atalla R. H. (1999): Celluloses, *In* Comprehensive Natural Products Chemistry, D. Barton, K. Nakanishi, O. Meth-Cohn, Eds., Vol. 3, Carbohydrates and Their Derivatives Including Tannins, Cellulose, and Related Lignins, Ed. B. Mario Pinto, Elsevier, Canada, p. 529

Chen Y.Y., Lin H., Ren Y., Wang H.W. and Zhu L. J. (2004): Study on *Bombyx mori* silk treated by oxygen plasma. J. Zhejiang Univ. Sci. 5(8), 918-922

Coats A.W. and Redfern J.T. (1964): Kinetic parameters from thermogravimetric data. Nature (London), 201, 68-69

Cochran W.G. and Cox G.M. (1968): Experimental Designs. Wiley & Sons Inc. New York, p. 335-350

Denes F., Hua Z.Q., Barrios E. and Young R.A. (1995): Influence of RF-cold plasma treatment on the surface properties of paper. J. Macromol. Sci. Pure Appl. Chem. A32, 1405-1443

Deslandes Y., Pleizier G., Poire E., Sapieha S., Wertheimer M.R. and Sacher E. (1998): The surface modification of pure cellulose paper induced by low-pressure nitrogen plasma treatment. Plasmas and Polymers 3, 2, 61-76

Fisher E.R. (2004): A review of plasma-surface interactions during processing of polymeric materials measured using the IRIS technique. Plasma Process. Polym. 1, 13-27

Grace J. M. and Gerenser L. J. (2003): Plasma treatment of polymers. J Dispersion Sci Technol 24 (3-4), 305-341

Henriksson M. and Berglund L.A. (2007): Structure and properties of cellulose nanocomposite films containing melamine formaldehyde. J Appl. Polym. Sci. 106, 2817–2824

Höcker H. (2002): Plasma treatment of textile fibers. Pure Appl. Chem. 74, 3, 423-427

Hua Z.Q., Sitaru R., Denes F. and Young R. A. (1997): Mechanisms of oxygen- and argon-RF-plasma-induced surface chemistry cellulose. Plasmas and Polymers 2(3), 199-224

Iwamoto S., Nakagaito A.N. and Yano H. (2007): Nano-fibrillation of pulp fibers for the processing of transparent nanocomposites. Appl. Phys. A-Mater Sci. Process 89, 461–466

Joly C., Kofman M. and Gauthier R.J. (1996): Polypropylene/cellulose fiber composites chemical treatment of the cellulose assuming compatibilization between the two materials. J. Macromol. Sci.-Pure Appl. Chem. A33 (12), 1981-1996

Klemm D., Schumann D., Kramer F., Hessler N., Hornung M., Schmauder H.P. and Marsch S. (2006): Nanocelluloses as innovative polymers in research and application. Polysaccharides 205, 49–96

Malek R.M.A. and Holme I. (2003): The effect of plasma treatment on some properties of cotton. Iranian Polym. J. 12(4), 271-280

Mohanty A. K., Misra M. and Hinrichsen G. (2000): Biofibres, biodegradable polymers and biocomposites: An overview. Macromolecular Mater. Eng. 276/277, 1-24

Nisho Y. (1994): Hyperfine composites of cellulose with synthetic polymers. *In* Cellulosic Polymers, Blends and Composites. Ed: R.D. Gilberst, Hanser Publishers, New York, p. 95-113

Oehr C., Müller M., Elkin B., Hegemann D. and Vohrer U., (1999): Plasma grafting – a method to obtain monofunctional surfaces. Surf. Coat. Technol. 116-119, 25-35

Olaru N., Olaru L. and Cobiliac G. (2005): Plasma-modified wood fibers as fillers in polymeric materials. Rom. J. Phys. 50(9–10), 1095-1101

Petreus O., Bubulac T., Petreus I. and Cazacu G. (2003): Reactions of some phosphorus compounds with cellulose dissolved in aqueous alkaline solution. J. Appl. Polym. Sci. 90, 327-333

Rozmarin G. (1984): Macromolecular Fundaments of Wood Chemistry. Technical Editure, Bucuresti, pp. 34, 45

Sabharwal H.S., Denes F., Nielsen L. and Young R.A. (1993): Free-radical formation in jute from argon plasma treatment. J. Agric. Food Chem. 41, 2202-2207

Simionescu C.I. and Macoveanu M.M. (1977): The effects of radiofrequency electrical discharge in cotton cellulose. Cell. Chem. Technol. 11, 87-89

Souza Lima M.M. and Borsali R. (2004): Rodlike cellulose microcrystals: structure, properties and applications. Macromol. Rapid Comm. 25, 771-787

Tan I.T., da Silva M.L.P. and Demarquette N.R. (2001): Paper surface modification by plasma deposition layers of organic silicon compounds. J. Mater. Chem. 11, 1019-1025

Totolin M., Macocinschi D., Ioanid G. E., Filip D. and Ioanid A. (2007): Materials supports for cultural heritage objects treated in cold plasma. Optoelectronics and Advanced Materials – Rapid Communications 1 (12), 722-728

Totolin M. I. (2007): Fourier-transformed infrared spectroscopy, *In* Cold Plasma in Material's Treatment. From Fundamental to Applications. Eds: M. I. Totolin, I. Neamtu, G. I. Ioanid. Published by Performantica, Iasi, Romania, p. 145-180

Totolin M.I. and Cazacu G. (2007): Natural polymer modification under radiofrequency electrical discharge conditions. *In* Plasma Chemistry and Natural Polymers, Ed: M. Totolin, p. 77-102

Totolin M. I., Vasile C., Tibirna M. C. and Popescu M. C. (2008): Grafting of Spanish broom (*Spartium junceum*) fibers with fatty acids under cold plasma conditions. Cell. Chem. Technol. 42(7-8), 317-333

Tu X., Young R.A. and Denes F. (1994): Improvement of bonding between cellulose and polypropylene by plasma treatment. Cellulose 1, 87-106

Vasile C., Totolin M.I. and Tibirna M.C. (2009): Grafting of some bio-fibres with carboxylic acids under cold plasma conditions. *In* Chemistry and Biochemistry: From Pure to Applied Science Eds: E. M. Pearce and G. E. Zaikov, New Horizons, vol. 3, Nova Science Publishers, INC, p. 9 – 40

Vaswani S., Koskinen J. and Hess D.W. (2005): Surface modification of paper and cellulose by plasma-assisted deposition of fluorocarbon films. Surface & Coatings Technol. 195, 121-129.

Zadorecki P. and Michell A.J. (1989): Future prospects for wood cellulose as reinforcement in organic polymer composites. Polym. Compos. 10, 69-77

SURFACE ENERGETICS OF SOFTWOOD KRAFT PULPS BY INVERSE GAS CHROMATOGRAPHY

[1*]José A. F. Gamelas, [2]José M. R. C. A. Santos and [1]Paulo J. Ferreira

[1]Departamento de Engenharia Química, Universidade de Coimbra, Pólo II – R. Sílvio Lima, 3030-790 Coimbra, Portugal

[2]CeNTI-Centre for Nanotechnology and Smart Materials, Rua Fernando Mesquita 2785, 4760-034 VN Famalicão, Portugal

*jafgas@eq.uc.pt

Abstract

The results of the analysis of a softwood kraft pulp by inverse gas chromatography (IGC) are presented. The effect of the beating process on the surface energy properties of this pulp was also assessed. The dispersive component of the surface energy, the enthalpy and the entropy of adsorption with apolar and polar probes, and the Lewis acid-base constants, K_a and K_b, were determined. The value of the dispersive component of the surface energy at 40 °C was 41.7 mJ/m^2, and after beating it was 44.7 mJ/m^2. For both unbeaten and beaten pulps, the highest specific component of the entalphy of adsorption, $-\Delta H_a^s$, was obtained with acetone, indicating an amphoteric behaviour of the corresponding surfaces. Nonetheless, the ratios $-\Delta H_a^s(THF)/-\Delta H_a^s(TCM)$ and $W_a^s(THF)/W_a^s(TCM)$ were always higher than 1, suggesting the presence of surfaces with a more acidic than basic character. A decrease of the basicity constant (K_b) with beating was observed, while the acidity constant (K_a) was nearly the same before and after beating. The results presented in this work are comparable with those reported in the literature for other bleached kraft pulps.

Keywords: IGC; pine; spruce; beating; bleached kraft pulps; surface energy; acid-base

Introduction

IGC (inverse gas chromatography) has been widely used to study the thermodynamics of adsorption and the surface properties of organic and inorganic materials (Conder and Young 1979; Santos and Guthrie 2005). This technique is based on the physical adsorption of a well-known probe by a solid surface. From the elution peak, the retention time and the peak shape provide information about the adsorption process. IGC allows the determination of enthalpy, free energy, and entropy of adsorption. The London dispersive component of the surface energy (Kamdem and Riedl 1991; 1992) and the acid-base surface properties (Saint Flour and Papirer 1982; Shultz et al. 1987) of the stationary phase can also be obtained by IGC. It should be noted that the dispersive and polar component of the surface energy can be obtained from classical contact-angle measurements. However, the surface roughness, the presence of pores, and surface energy gradients of some materials make the contact angle method not so adequate for rigorous surface energetics measurements (Riedl and Kamdem 1992). An alternative route for estimating the surface energy and the acid-base surface properties is based on the IGC technique.

Several studies have been reported previously regarding the use of IGC for the study of cellulose, wood fibres from pulping and bleaching processes, paper samples, among other materials (Gurnagul and Gray 1985; Lee and Luner 1989; Kamdem and Riedl 1991; 1992; Felix and Gatenholm 1993; Jacob and Berg 1994; Belgacem et al. 1995, Belgacem et al. 1996; Tshabalala 1997; Shen et al. 1998; Shen and Parker 1999; Belgacem 2000; Santos et al. 2001; Carvalho et al. 2005a; 2005b; Megiatto et al. 2007; Mills et al. 2008). For instance, bleached

Eucalyptus globulus kraft pulps showed values for the dispersive component of the surface energy (γ_s^d) at 40 °C of 35-45 mJ/m^2, and an amphoteric character with more acidic than basic properties (Shen et al. 1998; Carvalho et al. 2005a; 2005b). On the other hand, beating of the fibres lead to an increase of the γ_s^d value as well as the Lewis acidic character of the surface (Carvalho et al. 2005b). The cooking and bleaching processes may also influence the final surface properties of the pulps (Shen and Parker 1999; Carvalho et al. 2005b). The introduction of an oxygen delignification stage prior to bleaching has enhanced the Lewis acidic character of the fibres.

In this paper, the analysis by IGC of a softwood kraft pulp, before and after beating, will be reported. The dispersive component of the surface energy was determined by the measurement of the interaction with a series of *n*-alkanes. The specific component of the enthalpy of adsorption of Lewis acidic probes and of Lewis basic probes on the pulps, together with the acidity (K_a) and basicity (K_b) constants of the surfaces, were also determined.

Experimental

A bleached kraft pulp (Södra Cell, Sweden, Common Pulp II), as dry, containing 81% of spruce fibres and 19% of pine fibres was analysed before (A) and after beating (B). Pulp was refined in a pilot disc refiner at PTS - Papiertechnische Stiftung (Germany), using a cutting angle of 60°, a specific edge load of 2 W.s/m and a cutting length/ per second of 2.85 km/s. Before analysis by IGC, the samples were previously air dried in laboratory and milled in order to obtain a pulp of granular structure with small size.

A DANI GC 1000 digital pressure control (DPC) gas chromatograph, equipped with a hydrogen flame ionization detector (FID), was used for IGC data collection. Stainless steel columns, 0.5 m long and 0.4 cm inside diameter, were degreased, washed and dried before packing. 1.5–2.0 g of sample were packed into the GC columns using a vacuum pump. The columns were shaped in a smooth ''U'' shape to fit the detector/injector geometry of the instrument. The packed columns were conditioned overnight at 105 °C, under a helium flow, before any measurements were made. This procedure was used to remove any volatiles, including water molecules, adsorbed on the stationary phase surface and that, consequently, could affect the retention of the probe molecules.

Experiments were carried out at a column temperature between 40 and 55 °C with increments of 5 °C. The injector and detector were kept at 180 and 200 °C, respectively. Helium was used as carrier gas and its flow was selected to ensure that neither absorption nor diffusion of the probes would occur inside the column stationary phase. Small quantities of probe vapour (<1 µL) were injected into the carrier gas flow to ensure that the experiments took place at infinite dilution.

The probes, methane, n-hexane (C6), n-heptane (C7), n-octane (C8), n-nonane (C9), n-decane (C10), trichloromethane (TCM), dichloromethane (DCM), acetone, tetrahydro-furan (THF) and ethyl acetate (ETA), were of chromatographic grade and were used as received (Sigma–Aldrich). The retention times were the average of at least three injections and were determined at the peak maximum for symmetrical peaks or by the recommended Conder and Young method (Conder and Young 1979; Kamdem and Riedl 1992) for the less symmetrical chromatograms (observed with C9, C10, THF, ETA and acetone). This method is illustrated in Figure 1. The coefficient of variation between runs was no larger than 3%.
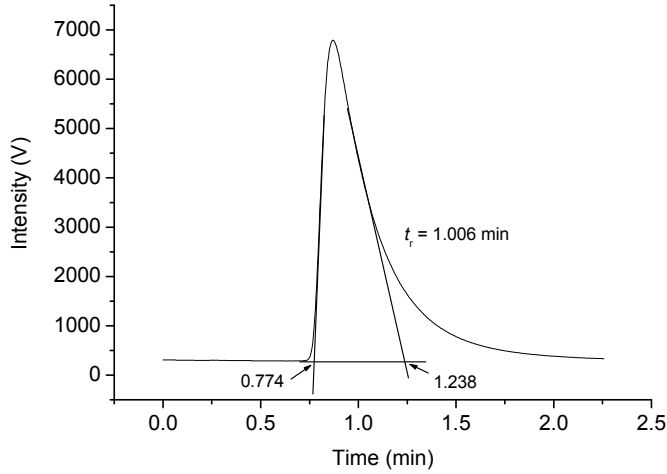
Figure 1. Determination of the retention time using the Conder and Young method for ETA on pulp B at 40 °C

Results and Discussion

IGC data analysis

The net retention volume V_n, which is the volume of inert carrier gas that is necessary to push the probe molecule through the chromatographic column containing the solid sample, depends on the sample–probe interactions and can be calculated from IGC data using Equation 1. Here, t_r is the retention time of the injected probe through the column, t_0 is the retention time of the non-interacting probe (methane), F is the flow rate of the inert carrier gas (measured with a digital flow meter), and J is the James–Martin compression correction factor, determined by Equation 2. Here, P_1 is equal to P_a (atmospheric pressure) plus the pressure drop in the column (Chtourou et al. 1995).

$$V_n = (t_r - t_o)\, F\, J \tag{1}$$

$$J = \frac{3}{2} \frac{[\,1 - (P_1 / P_a)^2\,]}{[\,1 - (P_1 / P_a)^3\,]} \tag{2}$$

Assuming that the experiments take place at infinite dilution, the free energy of adsorption of the probe on the stationary phase surface, per mole, ΔG_a, can be determined from the retention volume, V_n, according to Equation 3. R is the gas constant and T is the column absolute temperature. The constant K is dependent on the chosen reference state (Dorris and Gray 1980; Santos and Guthrie 2005).

$$\Delta G_a = -RT\, ln(V_n) + K \tag{3}$$

On the other hand, the free energy of adsorption can be related to the work of adhesion, W_a, according to Equation 4, where N is the Avogadro number and a is the surface area of the probe (Dorris and Gray 1980; Santos and Guthrie 2005).

$$-\Delta G_a = N.a.W_a \tag{4}$$

If only dispersive interactions occur, the work of adhesion is given by Equation 5, where γ_s^d and γ_l^d are the dispersive components of the surface energy of the interacting solid and probe, respectively.

$$W_a = 2\sqrt{\gamma_s^d . \gamma_l^d} \tag{5}$$

Thus, based on Equations 3, 4 and 5, the net retention volume V_n can be related to the dispersive components, γ_s^d and γ_l^d, by Equation 6.

$$RT\,ln(V_n) = \sqrt{\gamma_s^d}\,2N.a\sqrt{\gamma_l^d} + K \tag{6}$$

According to Equation 6, it is possible to estimate the dispersive component of the surface of the sample, from the slope of the linear fit of $RT\,ln(V_n)$ as a function of $2N \cdot a(\gamma_l^d)^{0.5}$, using the IGC data obtained with the apolar probes. It should be noted that the dispersive component of the surface energy represents the potential of materials to undergo London dispersion interactions.

If a Lewis acid–Lewis base interaction occurs, as is the case with polar probes, there will be a corresponding specific component contribution, ΔG_a^s, in addition to the dispersive component, to the overall free energy of adsorption, ΔG_a (Santos and Guthrie 2005). The overall free energy of adsorption, ΔG_a, is related to the net retention volume by Equation 3. Therefore, the free energy of adsorption that is caused by specific interactions, ΔG_a^s, can be estimated by calculating the difference between the values of $RT\,ln(V_n)$, obtained for the polar probes and the corresponding estimation for the apolar probe. The graphical method is represented in Figure 2.
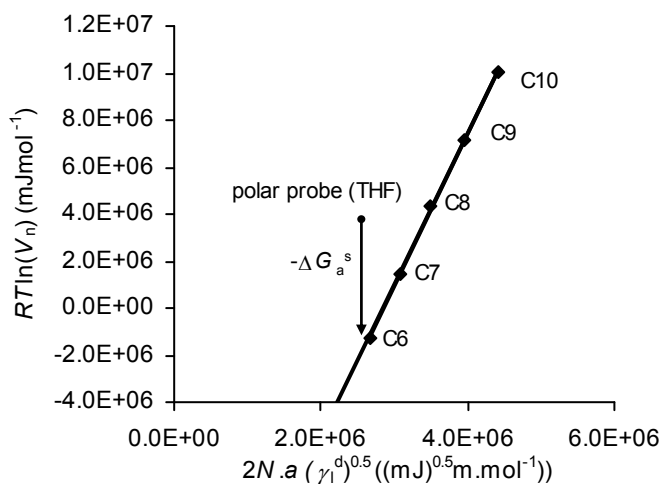
Figure 2. Determination of -ΔG_a^s for the basic probe THF in pulp A at 40 °C

If the experiments take place at different temperatures, it is possible to calculate the specific component of the enthalpy of adsorption, ΔH_a^s, and the specific component of the entropy of adsorption, ΔS_a^s, by plotting ΔG_a^s versus $1/T$ (Equation 7). On the other hand, the enthalpy of adsorption, ΔH_a^s, is related to the electron acceptor and electron donor parameters of the solid surface, K_a and K_b, by Equation 8 (Saint Flour and Papier 1982; Shultz et al. 1987; Chtourou et al. 1995; Santos and Guthrie 2005). K_a is the Lewis acidity constant and K_b is the Lewis basicity constant. *DN* and *AN** are the Gutmann's electron donor and electron acceptor numbers,

respectively, of the acid-base probe (Gutmann 1978; Riddle and Fowkes 1990). Thus, K_a and K_b can be graphically determined by plotting $-\Delta H_a^s/AN^*$ versus DN/AN^*. According to Equation 8, K_a is obtained as the slope of the linear fit, whereas K_b is the origin of such plot.

$$\frac{\Delta G_a^s}{T} = \frac{\Delta H_a^s}{T} - \Delta S_a^s \tag{7}$$

$$-\Delta H_a^s = K_a DN + K_b AN^* \tag{8}$$

The physical properties of the probes used in this work are listed in Table 1 (Riddle and Fowkes 1990; Kamdem et al. 1993; Santos and Guthrie 2005).

Table 1. Properties of the probes used in the calculation of the surface energy parameters by IGC

Probe	a (Å²)	γ_l^d (mJ/m²)	AN^* (KJ/mol)	DN (KJ/mol)
C6	51.5	18.4		
C7	57.0	20.3		
C8	63.0	21.3		
C9	69.0	22.7		
C10	75.0	23.4		
DCM	31.5	27.6	16.4	0
TCM	44.0	25.0	22.7	0
Acetone	42.5	16.5	10.5	71.4
THF	45.0	22.5	2.1	84.4
ETA	48.0	19.6	6.3	71.8

Results of the pulps analysis by IGC

Table 2 presents details of the retention times, for each probe, in each sample (unbeaten pulp A and beaten pulp B) obtained at 40 °C.

The dispersive component of the surface energy was determined at several temperatures, in the range 40-55 °C, based on the retention times obtained for a series of *n*-alkanes (C6, C7, C8, C9, and C10). The values determined at 40 °C were of 41.7 and 44.7 mJ/m² for pulps A and B, respectively. Values of the dispersive component of the surface energy in the range of 38-45 mJ/m² have been reported for bleached *Eucalyptus globulus* kraft pulps (Shen et al. 1998; Carvalho et al. 2005a; 2005b), and for a bleached sulphite pulp, obtained from 60% beech wood and 40% birchwood (Felix and Gatenholm 1993). Moreover, values in the range of 43-48 mJ/m², at similar temperature, have also been obtained for samples of purified α-cellulose fibres (Belgacem et al. 1995; Belgacem et al. 1996; Tshabalala 1997). Therefore, the values obtained in this work for bleached softwood kraft pulps are close to those reported for other cellulosic materials, and confirm the dominant presence of cellulose at the fibre surface. The decrease of the γ_s^d value with beating has been previously observed for bleached *Eucalyptus globulus* kraft pulps (45.0 and 48.2 mJ/m² before and after beating, respectively) (Carvalho et al. 2005b). In addition, γ_s^d was found to decrease with the increase of temperature (up to 55 °C) for both pulps (Figure 3). The $d\gamma_s^d/dT$ values obtained were of -0.33 mJm⁻²K⁻¹ and -0.31 mJm⁻²K⁻¹, for pulps A and B, respectively.

Table 2. Retention times at 40 °C for the different probes in pulps A and B

Retention time (min)	Pulp A	Pulp B
Methane	0.343 ± 0.000	0.263 ± 0.000
C6	0.385 ± 0.002	0.318 ± 0.001
C7	0.462 ± 0.002	0.433 ± 0.000
C8	0.699 ± 0.002	0.792 ± 0.004
C9	1.388 ± 0.004	1.836 ± 0.011
C10	3.525 ± 0.033	5.199 ± 0.005
DCM	0.371 ± 0.002	0.303 ± 0.000
TCM	0.411 ± 0.003	0.357 ± 0.000
Acetone	0.512 ± 0.013	0.589 ± 0.007
THF	0.626 ± 0.017	0.805 ± 0.014
ETA	0.732 ± 0.018	0.991 ± 0.050
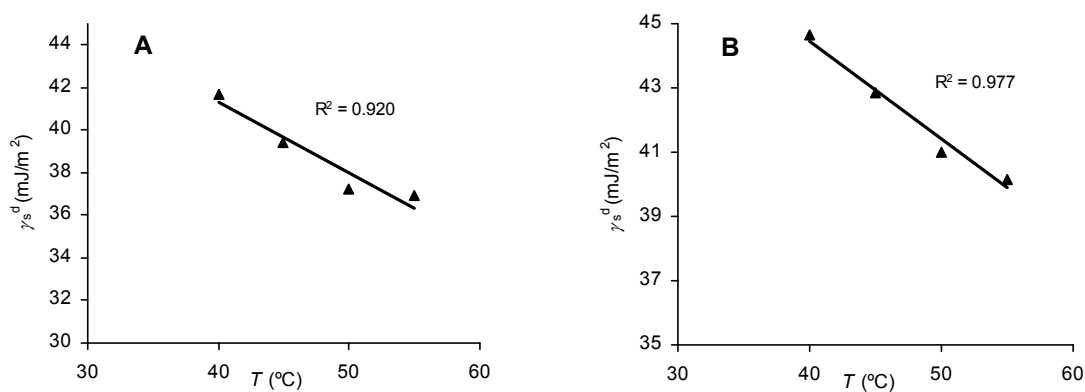
Figure 3. values of γ_s^d at several temperatures for pulps A (A) and B (B)

The enthalpy of adsorption and the entropy of adsorption of the apolar probes were also calculated based on the variations of $-\Delta G_a/T$ *versus* $1/T$ for each *n*-alkane (Figure 4). The results are presented in Table 3. The greater the value of $-\Delta H_a$, the greater is the interaction intensity between the probe molecules and the solid's surface. Therefore, it can be concluded that that the interaction intensity increases in the order: *n*-hexane < *n*-heptane < *n*-octane < *n*-nonane < *n*-decane, as expected. The entropy of adsorption is lower than zero for all the *n*-alkanes, which agrees well with expectation since during adsorption the system goes from a less ordered phase (gas) to a more ordered adsorbed phase.
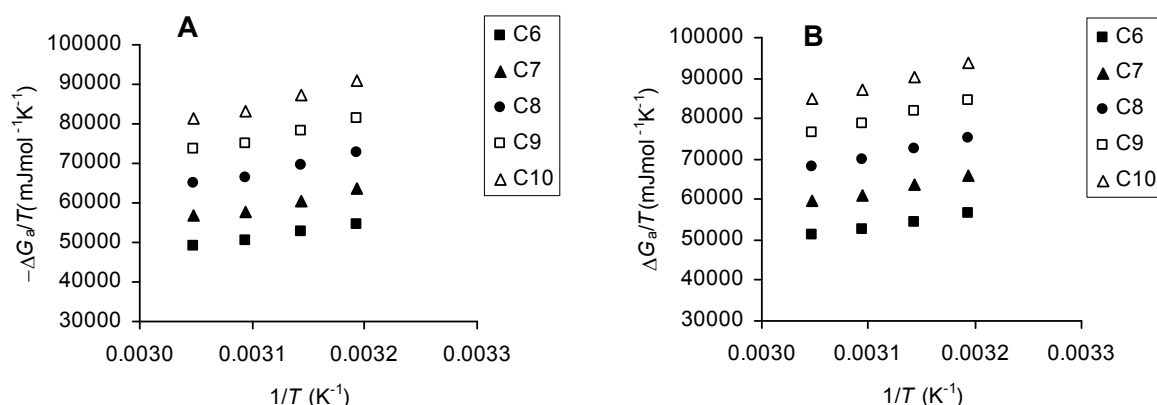
Figure 4. Determination of the enthalpy of adsorption and entropy of adsorption for the n-alkanes on the surface of pulps A (A) and B (B)

Table 3. Enthalpy of adsorption and entropy of adsorption for the n-alkanes on the surface of pulps A and B

Pulp	Probe	$-\Delta H_a$ (mJ/mol)	ΔS_a (mJ/mol K)	Correlation coefficient
A	C6	3.85E+07	-6.82E+04	0.99
A	C7	4.55E+07	-8.22E+04	0.98
A	C8	5.34E+07	-9.82E+04	0.98
A	C9	5.71E+07	-1.01E+05	0.99
A	C10	6.49E+07	-1.17E+05	0.99
B	C6	3.67E+07	-6.09E+04	1.00
B	C7	4.35E+07	-7.33E+04	0.99
B	C8	5.08E+07	-8.70E+04	1.00
B	C9	5.51E+07	-9.16E+04	1.00
B	C10	6.18E+07	-1.04E+05	1.00

For the polar probes, the free energy of adsorption has one component corresponding to dispersive interactions and an additional one due to specific interactions, *i.e.*, that due to Lewis donor-acceptor interactions between the probe and the surface of the material under examination. The determination of the specific component of the free energy of adsorption (ΔG_a^s) may be used to characterize the surface in terms of its acidity and basicity.

The specific components of the enthalpy of adsorption ($-\Delta H_a^s$) and of the entropy of adsorption (ΔS_a^s) for each polar probe were obtained from the plots of $-\Delta G_a^s/T$ *versus* $1/T$ (Figure 5), following Equation 7. The results presented in Table 4 show that, for both pulps, the highest value of $-\Delta H_a^s$ is obtained with acetone, being followed by those with ETA and THF. The higher interaction of the pulps surfaces with amphoteric probes such as acetone and ETA suggests that the materials are of amphoteric nature. The ratio $-\Delta H_a^s(THF)/-\Delta H_a^s(TCM)$ was 2.3 for the unbeaten pulp A and 3.8 for the beaten pulp B. The greater affinity of the pulps surfaces with a basic probe (THF), than with an acidic one (TCM), suggests that both pulps have a more acidic than basic character.

Similar conclusions can be drawn from the determination of the work of adhesion, W_a^s, for each polar probe, by using Equation 4. At 40 °C, the ratio $W_a^s(THF)/W_a^s(TCM)$ was 4.1 for the unbeaten pulp A and 4.6 for the beaten pulp B, confirming the amphoteric, predominantly Lewis acid character of the surface of the bleached pulps. This is in agreement with the studies reported in the literature for other bleached pulps and α-cellulose fibres by using similar methods for the evaluation of the surface acid-base properties (Jacob and Berg 1994; Belgacem et al. 1995; Shen et al. 1998; Carvalho et al. 2005a; 2005b). In addition, the increase of the $-\Delta H_a^s(THF)/-\Delta H_a^s(TCM)$ and $W_a^s(THF)/W_a^s(TCM)$ ratios after beating indicates that there is a larger number of the highest energy acidic sites relative to that of the highest energy basic sites upon the beating operation. This must be due to an increase of the accessibility at the fibres surface of the OH functional groups (acidic) relatively to that of the oxygen atoms (basic) not bound to hydrogen as a consequence of the beating action (Carvalho et al. 2005b).
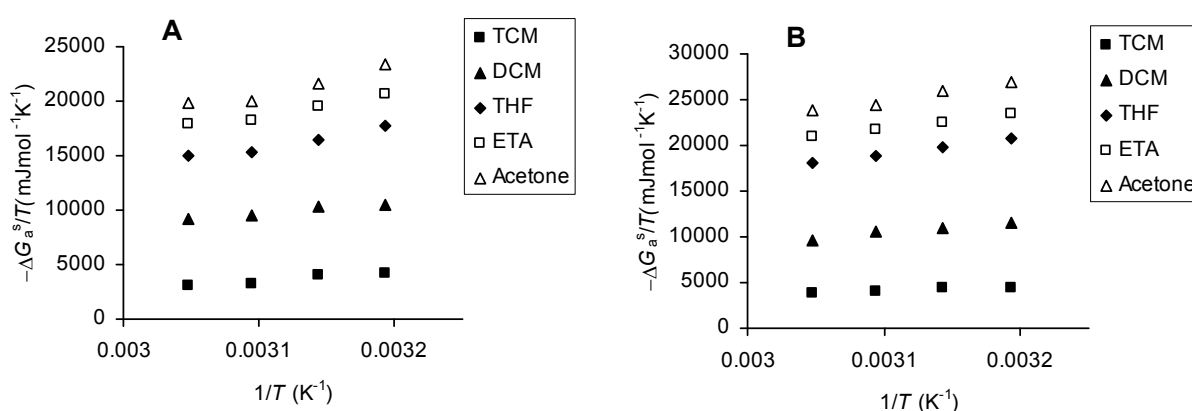
Figure 5. Determination of the specific component of the enthalpy of adsorption and entropy of adsorption for the polar probes on the surface of pulps A (A) and B (B)

Table 4. Values of the specific component of the enthalpy and entropy of adsorption for the polar probes on the surface of pulps A and B

Pulp	Probe	DN/AN^*	$-\Delta H_a^s$ (mJ/mol)	ΔS_a^s (mJ/molK)	Correlation coefficient
A	TCM	0.0	8.46E+06	-2.27E+04	0.94
A	DCM	0.0	9.86E+06	-2.09E+04	0.98
A	Acetone	6.8	2.51E+07	-5.70E+04	0.96
A	ETA	11.4	1.94E+07	-4.17E+04	0.97
A	THF	40.2	1.93E+07	-4.42E+04	0.97
B	TCM	0.0	4.94E+06	-1.13E+04	0.97
B	DCM	0.0	1.17E+07	-2.58E+04	0.98
B	Acetone	6.8	2.20E+07	-4.34E+04	0.99
B	ETA	11.4	1.66E+07	-2.95E+04	1.00
B	THF	40.2	1.87E+07	-3.89E+04	0.99

Based on the variation of $-\Delta H_a^s/AN^*$ with DN/AN^*, shown in Figure 6, K_a and K_b values are obtained as the slope and the intersection at the origin of the linear fit, respectively. For pulp A, a K_a value of 0.215 and a K_b value of 0.621 were determined; the values of K_a and K_b for pulp B were 0.209 and 0.470, respectively. The higher values of K_b with respect to those of K_a for both

pulps could suggest the presence of more basic than acidic surfaces, *i.e.*, a higher propensity of donating electrons, which is in disagreement with the results above for the $-\Delta H_a^s$(THF)/$-\Delta H_a^s$(TCM) and W_a^s(THF)/W_a^s(TCM) ratios. In addition, it is not expected that the surfaces of cellulosic pulp fibres are more basic than acidic, in account for the dominant presence of OH functional groups in the structure of these materials. However, as pointed out previously (Chehimi et al. 1999), it is not possible to compare these scales of acidity (K_a) and basicity (K_b) as they depend on the choice of the reference substances used for their determinations.
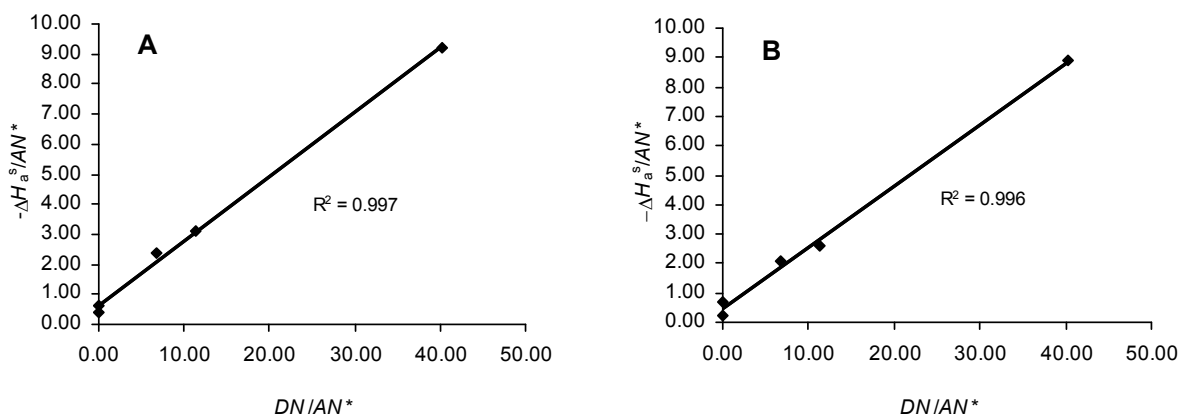
Figure 6. Determination of K_a and K_b for the surface of pulps A (A) and B (B)

It should be reminded that the donor number (*DN*) parameter is defined as the negative enthalpy value for the reaction of the liquid under test with the acceptor SbCl$_5$. The acceptor number (*AN*) parameter is defined as the relative ^{31}P NMR chemical shift of triethylphosphine oxide (Et$_3$P=O), when this donor substance is dissolved in the liquid being evaluated (when the liquid is hexane, *AN* is set to zero) (Gutmann 1978). *AN** is obtained from *AN* after correcting from the London dispersion forces contribution to the chemical shift, in order to obtain the true acid-base contribution (Riddle and Fowkes 1990). The reference species used for the determinations of *DN* and *AN** differ in hardness according to the Hard and Soft Acids and Bases (HSAB) principle of Pearson. While SbCl$_5$ is a soft acid, Et$_3$P=O is known to be a hard base. *DN* is a scale of softness whereas *AN** is a scale of hardness. Thus, for these reasons, the straight comparison of the K_a and K_b values in terms of the prevalence of the acidic or basic properties can not be made. Notwithstanding, the amphoteric characteristic of the pulps surfaces is confirmed by the determination of the acidity and basicity constants.

Conclusions

A bleached softwood kraft pulp (A) and the corresponding beaten pulp (B) were analysed by inverse gas chromatography. The dispersive component of the surface energy increased slightly from 41.7 to 44.7 mJ/m^2 (T=40 °C) after beating. The specific component of the enthalpy of adsorption ($-\Delta H_a^s$) of several acidic, basic and amphoteric polar probes on the pulps surfaces was determined. The highest value for $-\Delta H_a^s$ was obtained with acetone, suggesting a prevailing amphoteric behaviour. The value of the ratio $-\Delta H_a^s$(THF)/$-\Delta H_a^s$(TCM) was higher than 1, as well as that of the ratio W_a^s(THF)/W_a^s(TCM), both values indicating a higher affinity of the pulps surface with THF than with TCM, and, consequently, a surface with a more acidic than basic character. Overall, the results of this study are comparable to those reported for bleached hardwood kraft pulps.

References

Belgacem M.N. (2000): Characterization of polysaccharides, lignin and other woody components by inverse gas chromatography: a review. Cell. Chem. Technol. 34, 357-383

Belgacem M.N., Blayo A. and Gandini A. (1996): Surface characterization of polysaccharides, lignins, printing ink pigments, and ink fillers by inverse gas chromatography. J. Colloid Interf. Sci. 182, 431-436

Belgacem M.N., Czeremuszkin G., Sapieha S. and Gandini A. (1995): Surface characterization of cellulose fibres by XPS and inverse gas chromatography. Cellulose 2, 145-157

Carvalho M.G., Ferreira P.J., Santos J.M.R.C.A., Amaral J.L. and Figueiredo M.M. (2005a): Effect of extended cooking and oxygen prebleaching on the surface energy of *Eucalyptus globulus* kraft pulps. J. Pulp Pap. Sci. 31(2), 90-94

Carvalho M.G., Santos J.M.R.C.A., Martins A.A. and Figueiredo M.M. (2005b): The effects of beating, web forming and sizing on the surface energy of *Eucalyptus globulus* kraft fibres evaluated by inverse gas chromatography. Cellulose 12, 371-383

Chehimi M.M., Abel M., Perruchot C., Delamar M., Lascelles S.F. and Armes S.P. (1999): The determination of the surface energy of conducting polymers by inverse gas chromatography at infinite dilution. Synthetic Methods 104, 51-59

Chtourou H., Riedl B. and Kokta B.V. (1995): Surface Characterizations of modified polyethylene pulp and wood pulps fibres using XPS and inverse gas chromatography. J. Adhes. Sci. Technol. 9, 551-574

Conder J.R. and Young C.L. (1979): Physicochemical measurement by gas chromatography. Wiley-Interscience, New York

Dorris G.M. and Gray D.G. (1980): Adsorption of n-alkanes at zero surface coverage on cellulose paper and wood fibres. J. Colloid Interf. Sci. 77, 353-362

Felix J.M. and Gatenholm P. (1993): Characterization of cellulose fibers using inverse gas chromatography. Nordic Pulp Paper Res. J. 8(1), 200-203

Gurnagul N. and Gray D.G. (1985): An inverse gas chromatographic study of newsprint surface area. J. Pulp Pap. Sci. 11(4), 98-101

Gutmann V. (1978): The donor-acceptor approach to molecular interactions. Plenum Press, New York

Jacob P.N. and Berg J.C. (1994): Acid-base surface energy characterization of microcrystalline cellulose and two wood pulp fiber types using inverse gas chromatography. Langmuir 10, 3086-3093

Kamdem D.P. and Riedl B. (1991): IGC Characterization of PMMA grafted onto CTMP fiber. J. Wood Chem. Technol. 11(1), 57-91

Kamdem D.P. and Riedl B. (1992): Inverse gas chromatography of lignocellulosic fibres coated with a thermosetting polymer: use of peak maximum and Conder and Young methods. J. Colloid Interf. Sci. 150, 507-516

Kamdem D.P., Bose S.K. and Luner P. (1993): Inverse gas chromatography characterization of birch wood meal. Langmuir 9, 3039-3044

Lee H.L. and Luner P. (1989): Characterization of AKD sized papers by inverse gas chromatography. Nordic Pulp Paper Res. J. 4(2), 164-172

Megiatto J.D., Oliveira F.B., Rosa D.S., Gardrat C., Castellan A. and Frollini, E. (2007): Renewable resources as reinforcement of polymeric matrices: composites based on phenolic thermosets and chemically modified sisal fibers. Macromol. Biosci. 7, 1121-1131

Mills R.H., Gardner D.J. and Wimmer R. (2008): Inverse gas chromatography for determining the dispersive surface free energy and acid-base interactions of sheet molding compound-Part II 14 lignocellulosic fiber types for possible composite reinforcement. J. Appl. Polym. Sci. 110, 3880-3888

Riddle F.L. and Fowkes F.M. (1990): Spectral shifts in acid-base chemistry. 1. Van der Waals contributions to acceptor numbers. J. Am. Chem. Soc. 112, 3259-3264

Riedl B. and Kamdem D.P. (1992): Estimation of the dispersive component of surface energy of polymer grafted lignocellulosic fibers with inverse gas chromatography. J. Adhes. Sci. Technol. 9, 1053-1067

Saint Flour C. and Papirer E. (1982): Gas solid chromatography: a method of measuring surface free energy characteristics of short glass fibers. 2. Through retention volumes measured near zero surface coverage. Ind. Eng. Chem. Prod. Res. Dev. 21, 666-669

Santos J.M.R.C.A., Gil M.H., Portugal A. and Guthrie J.T. (2001): Characterization of the surface of a cellulosic multi-purpose office paper by inverse gas chromatography. Cellulose 8, 217-224

Santos J.M.R.C.A. and Guthrie J.T. (2005): Analysis of interactions in multicomponent polymeric systems: The key-role of inverse gas chromatography. Mat. Sci. Eng. R. 50, 79-107

Shen W., Yao W., Li M. and Parker I. (1998): Characterization of eucalypt fibre surface using inverse gas chromatography and X-ray photoelectron spectroscopy. Appita J. 51(2), 147-151

Shen W. and Parker I.H. (1999): Surface composition and surface energetics of various eucalypt pulps. Cellulose 6, 41-55

Shultz J., Lavielle L. and Martin C. (1987): The role of the interface in carbon fibre-epoxy composites. J. Adhesion 23, 45-60

Tshabalala M.A. (1997): Determination of the acid-base characteristics of lignocellulosic surfaces by inverse gas chromatography. J. Appl. Polym. Sci. 65, 1013-1020

CELLULOSE NANOFIBRILS -
PRODUCTION, CHARACTERIZATION AND APPLICATIONS

Gary Chinga-Carrasco and Kristin Syverud

Paper and Fibre Research Institute (PFI AS), Høgskoleringen 6b,

NO-7491 Trondheim, Norway.

gary.chinga.carrasco@pfi.no

Abstract

This works focuses on the production, characterisation and application of cellulose nanofibrils. A short description of cellulose fibres is given. In addition, examples of how mechanical and chemi-mechanical production of nanofibrils affect their properties are presented. The nanofibrillated material can be characterised in detail by applying several complementary microscopy techniques, such as scanners, laser profilometry, x-ray microtomography, scanning electron microscopy and transmission electron microscopy. The various microscopy methods cover a wide range of structure sizes and reveal several characteristic details of fibres and the corresponding nanofibrillated material. Finally, a short overview of various application areas that have been explored and are foreseen for cellulose nanofibrils is given.

Introduction

In the beginning of the 20th century, there was an extensive research on the utilization of the most abundant biopolymer on earth, i.e. cellulose. This resulted in a variety of products, e.g. cellophane, rayon, nitrocellulose (used in gun powder), adhesives and lacquer. During the 20th century, petroleum-based polymers became the focus of research, also resulting in a variety of products, e.g. plastic materials having several superior properties (e.g. water repellence, mouldability). There are however two major drawbacks with petroleum-based polymers, i) oil is not a renewable resource and ii) the products are not bio-degradable. Factors such as increasing oil prices, dwindling oil resources and a high focus on sustainability have motivated a renewed interest for bio-based polymers. There are reasons to believe that with extensive research, novel bio-degradable materials will offer a good alternative to petroleum-based products in the near future.

The structure of cellulose fibres

Cellulose fibres are presently a major area of research for several end-use applications. Fibres can be utilized as reinforcement in bio-degradable composites and as a source of raw materials for bio-energy and biochemicals production. As mentioned above, there is a growing interest in utilization of by-products from agricultural sources and forest industries in order to e.g. develop biodegradable polymers and thus replace synthetic oil-based products (Lucia and Rojas 2009). During the last years, chemical pulp fibres have been applied as the raw material for the production of cellulose nanofibrils, which have enormous potential in several applications (Turbak et al. 1983). However, a successful utilization of cellulose fibres requires the development of energy- and cost-efficient procedures for production of nanofibrils. A comprehensive understanding of cellulose fibres, their structure, their nanocomponents, and how their morphologies are affected by a given production procedure and treatment is thus necessary.

The structure of cellulose fibres has multiscale characteristics, spanning from the millimetre length and micrometer width of fibres to the nanometre diameter of nanofibrils (Chinga-Carrasco 2011). Chemical pulp fibres have a surface, which is characterized by a particular pattern created by wrinkles and nanofibrils in the outer layers of the fibre wall structure. The surface structure of chemical pulp fibres corresponds mainly to the primary and S1 layers of the fibre wall (Figure 1). Such structures are mainly preserved during chemical pulping, where the lignin and hemicellulose are extracted. Contrary to the outer layers of the fibre wall (primary and S1 layers), the S2 layer is characterised by having a structure of fibrils organized in a helical manner. S2 layers are commonly observed in thermo-mechanical pulp fibres where the S2 layer appears due to the mechanical fibrillation of the fibres outer layers. During the years, several microscopy techniques have been applied for visualization and quantification of fibre structures (see e.g. Page and Emerton 1959; Smith 1959; Jang et al. 1991; Moss et al. 1993; Duchesne and Daniel 2000; Reme et al. 2002; Gustafsson et al. 2003; Brändström et al. 2003; Fernando and Daniel 2004; Chinga-Carrasco et al. 2010).
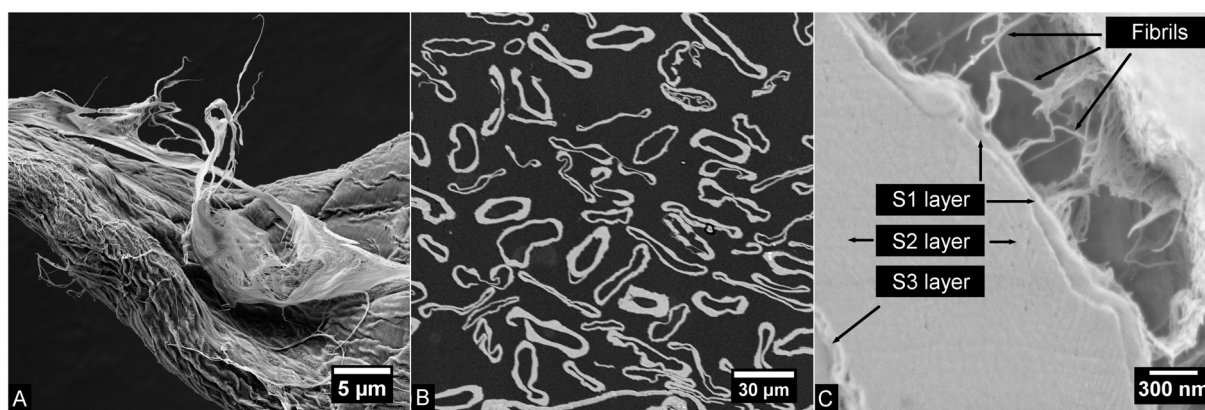
Figure 1. Assessment of Pinus radiata kraft pulp fibres. A) Surface structure. Note the white network of fibrils, which probably correspond to the primary wall layer. B) SEM cross-sectional image, acquired in backscattered electron imaging (BEI) mode. C) Cross-section of a small area of a fibre wall structure. The fibrils, S1, S2 and S3 layers are indicated

Production of cellulose nanofibrils

Production of homogeneous nanofibril qualities require a major amount of energy during production (Figure 2). The less energy that is utilized, the less is the fibrillation of cellulose fibres and the less the amount of produced nanofibrils (Syverud et al. 2011). Several pathways have been proposed for producing cellulose nanofibrils (Turbak et al. 1983; Saito et al. 2006; Pääkkö et al. 2007; Heijnesson-Hultén 2007; Eriksen et al. 2008; Zimmermann et al. 2010). However, the energy consumption during production seems to be the limiting factor for utilizing nanofibrils in industrial applications.
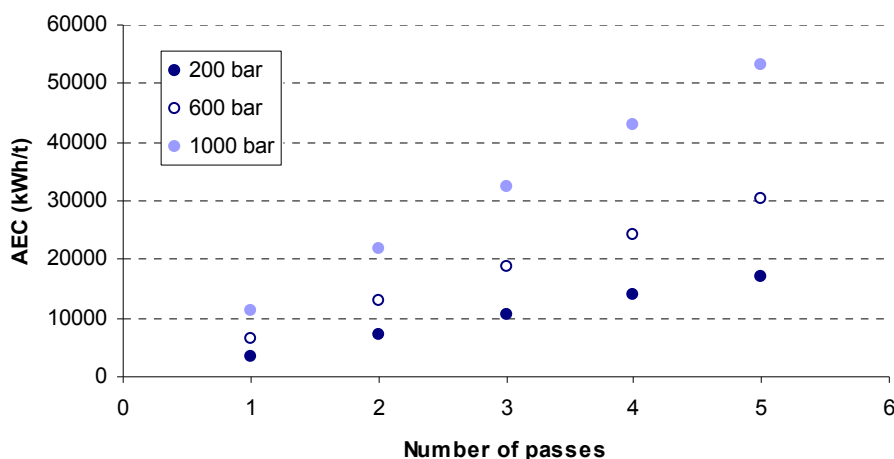
Figure 2. Homogenisation of Pinus radiata kraft pulp fibres. Accumulated energy consumption (AEC) as a function of the number of passes through a homogeniser for 3 different pressures

Conventional homogenization (Turbak et al. 1983) may produce a fibrillated material with an inhomogeneous quality (Figure 6). A chemi-mechanical procedure based on TEMPO-mediated oxidation has been proposed for producing nanofibrils with homogeneous dimensions, *i.e.* diameters of less than approx. 15 nm (Saito et al. 2006). Pääkkö et al. (2007) applied an innovative procedure where a pre-treatment based on enzymatic hydrolysis was introduced. The authors have recently reported a reduction of energy of up to 98%, which is industrially relevant. Presently, new equipment is being installed for upscaling the production of the nanofibrillated material (Ankerfors 2010).

Characterisation of nanofibril structures

Relevant procedures for quantification of nanofibril quality are most desirable. There are several methods, which can be applied for direct quantification of cellulose nanofibril structures (Table 1). In the following, microscopy methods for direct assessment of some characteristics details are shortly reviewed.

Assessment of the fibrillation degree is most interesting. However, the quality of nanofibrils tend to be evaluated with devices covering the nano-range only (e.g. FE-SEM, AFM, TEM). Proper characterisation requires the quantification of the fibrillated material at several scales. Spectrophotometers have been applied for estimating the fibrillation degree (Iwamoto et al. 2008). The higher the fibrillation of the cellulose fibres, the higher the transmittance. A complementary technique is based on desktop scanners. Although such devices are simple, they can yield a good assessment of the fibres that have not been fibrillated completely. As an attempt to demonstrate the suitability of the technique, scanner images have been acquired from films made of three fibril qualities. The fibrils were produced from *Pinus radiata* pulp fibres, applying a TEMPO-mediated oxidation as pre-treatment and three pressures during homogenisation (Syverud et al. 2011). The images were acquired in transmission mode with 2400 DPI (Figure 3). A transparency measure can be estimated based on the ratio between the average grey-level of the acquired samples and the average grey-level of the background (Figure 4). Significant differences were detected between the nanofibrillated materials. However, note that the transparency values differed only by 2% (Figure 4), though the energy consumption differed by roughly 35000 KWh/t (Figure 2). This indicates that depending on the application, the homogenisation may be adjusted to considerably reduce the energy consumption.

Table 1. Some image acquisition devices that are suitable for assessing several scales of nanofibril structures. The resolution is given considering theoretical aspects, resolution values reported in the literature and personal communications. See also Chinga-Carrasco (2009)

Technique	Abbreviation	Approx. res. (µm)	Comments
Desktop scanners		>10	Fast, assessment of large areas. Can be used in transmission and reflective modes
Profilometry		1.0	Fast and automated method, non-destructive, image acquisition of large areas.
X-ray microtomography	X- CT	<1.0	3D assessment, limited resolution
Light microscopy	LM	0.2	Fast, assessment of large areas.
Atomic force microscopy	AFM	0.001-0.02	Suitable for nano-characterization of surface structures
(Field-emission)-scanning electron microscopy	(FE)-SEM	0.001-0.02	High resolution, good contrast between paper components. Relatively flexible image acquisition.
Transmission electron microscopy	TEM	0.0002	Resolution at sub-nanoscale. TEM tomography can yield 3D images of nanostructures.
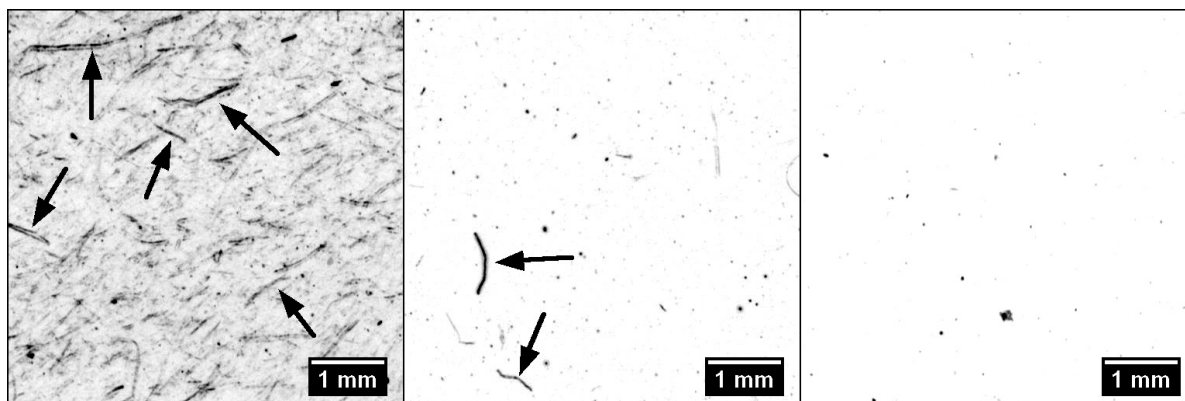
Figure 3. From left to right: TEMPO pre-treated samples, homogenized at 200, 600 and 1000 bar, respectively. The nanofibrils were produced from P. radiata pulp fibres and was collected after 5 passes through the homogeniser. The arrows indicate fibres and fibre fragments. The contrast of the images has been enhanced for better visualization of the fibres and fibre fragments
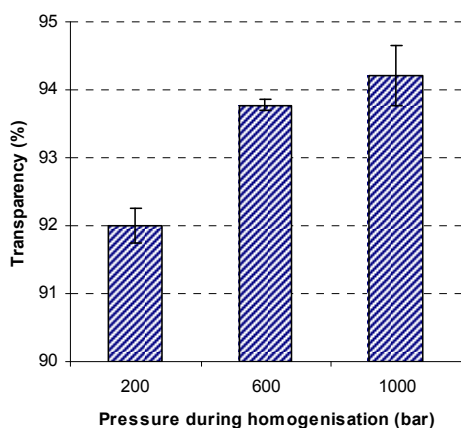
Figure 4. Transmittance levels for films made of nanofibrils homogenized at 200, 600 and 1000 bars

As demonstrated in this study, scanners can be applied for assessing the fibrillation degree based on the assessment of relatively large areas (> 1 cm^2). In addition to the quantification of the fibrillation degree at the macro-scale, the micro-structure can be assessed with laser profilometry. Laser profilometry is a most suitable method for quantification of surface topography at the micro-level (Figure 5). This capability has been applied for measuring the roughness of nanofibril films (Chinga-Carrasco and Syverud 2010). The less the fibrillation of fibres, the rougher the surface of films (Figure 5). It is worth to mention that in order to improve the detection of the surface topography by the laser beam, a thin layer of gold has been applied on films made of cellulose nanofibrils. The method has proved to be adequate and yield a detailed description of the surface topography (Chinga-Carrasco and Syverud 2010).

In addition to the assessment of surface micro-structures, the detailed characterisation of nanofibril-based materials require high-resolution devices, such as the scanning electron microscope (SEM). One of the advantages of SEM is its versatility. Images can rapidly be acquired at low (<1000x) and high magnifications (>50000x). In addition, SEM can be operated in several modes, e.g. secondary electron imaging (SEI), backscatter electron imaging (BEI), in low vacuum and applying modern in-lens detectors. Figure 6 shows the surface and cross-sectional structures of nanofibril films. The surface and cross-sectional images were acquired in SEM-SEI and SEM-BEI mode, respectively. Note that the cross-sectional images acquired in SEM-BEI mode are most suitable for direct quantification of nanofibril film thicknesses, and roughnesses.
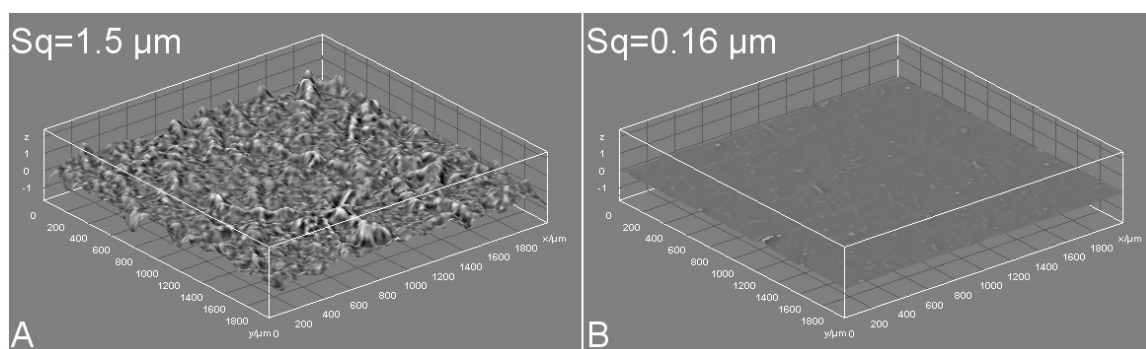
Figure 5. Laser profilometry of films made of nanofibrils from P. radiata. The nanofibrillated material was collected after 5 passes through the homogeniser. A) The fibrillated material was produced without pre-treatment. B) A TEMPO pre-treatment was applied. Size of images 2 x 2 mm^2. Note that the surface roughness (Sq) is considerably lower for the film made of TEMPO-mediated oxidated fibrils (B)

With respect to the morphology of fibril structures, the assessment of fibril diameter has been one of the applied approaches for evaluating a given fibril quality. The estimation of fibril diameter have been based on AFM, FESEM and TEM images. Fukuzumi et al. (2009) compared AFM and FE-SEM for estimating the fibril diameters. FE-SEM seemed to overestimate the fibril diameters. This was probably due to the metallic coating, which was required for making the sample conductive under the electron beam. Chinga-Carrasco and Syverud (2010) demonstrated that it is possible to conduct a FE-SEM analysis of fibril structures without having a metallic conductive layer. Applying a low acceleration voltage (< 1 kV) and short working distance (< 1 mm) makes it possible to visualize nanofibril structures at high magnification (>50000x), as seen in the inset in Figure 6B.
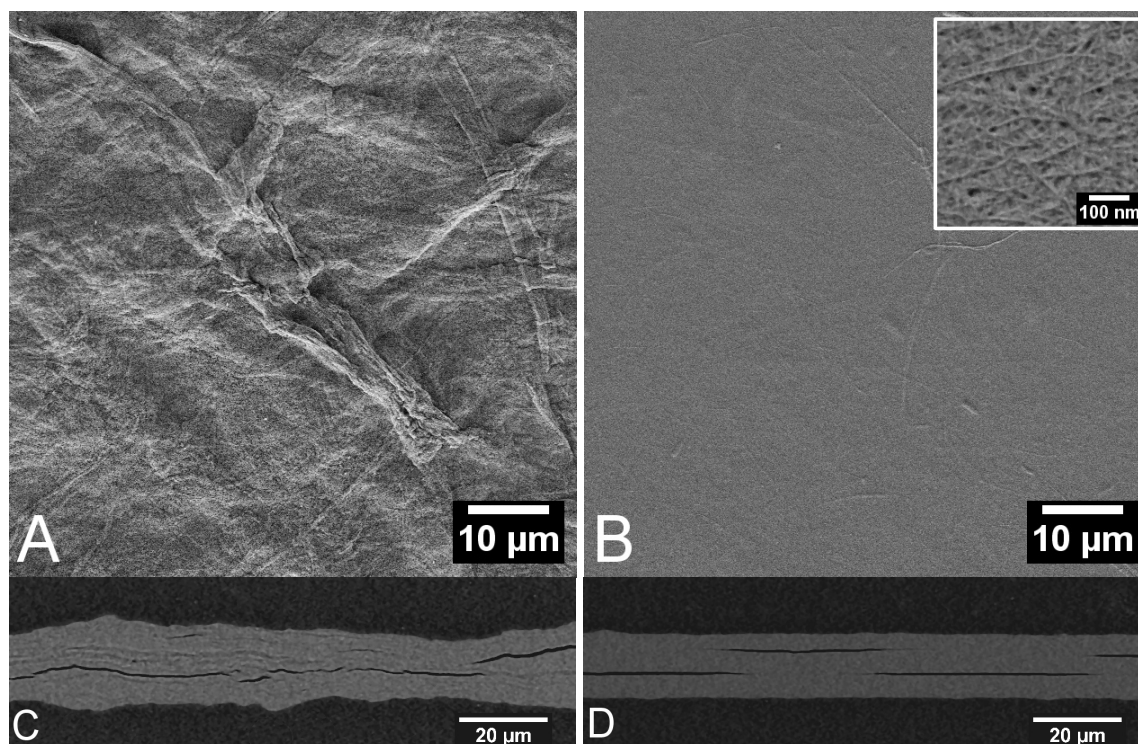
Figure 6. Structures of films made of nanofibrils made of Pinus radiata. A) The nanofibrils have been manufactured by passing the pulp fibres 5 times through the homogeniser. B) The pulp fibres have been pre-treated with TEMPO before passing the pulp fibres 5 times through the homogeniser. Note the homogeneous nanofibril diameters (< 100 nm) exemplified in the inset in B). The corresponding cross-sectional images (acquired in SEM-BEI mode) are given in C and D

(FE)-SEM is thus a valuable method for exploring a given structure, at the micro- and nano-level. However a major limitation is the 2D assessment of 3D structures. Modern methods based on X-ray microtomography seems to yield valuable 3D information and are complementary in structural assessments, though the resolution of such devices is still a limiting factor (Figure 7). It is worth to mention that a relatively new in-situ serial microtoming device can be mounted in a FE-SEM device (Denk and Hortsman 2004). Such approach may expand the assessment of nanofibril structures to 3D and at high-magnification.
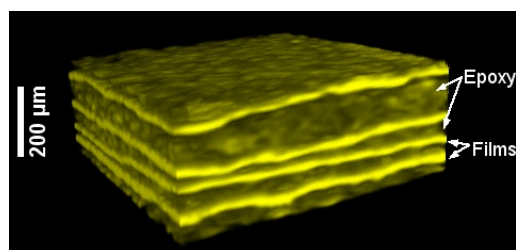
Figure 7. X-μCT of nanofibril films embedded in epoxy resin

TEM is the ultimate tool for assessment of nanofibril morphology (Figure 8). Visualization of fibril structures has been demonstrated by several authors (e.g. Andresen et al. 2006; Wågberg et al. 2008; Syverud et al. 2010). TEM yields images at high-resolution, making it possible to visualize sub-nanometer structures. TEM in high-resolution mode (HRTEM) has even been most useful for visualizing the surface modification of cellulose nanofibrils (Stenstad et al. 2008; Syverud et al. 2010a). In addition, TEM tomography may open new possibilities for assessing nano- and sub-nano structures in 3D, thus introducing a new dimension in the comprehension of a renewable and bio-degradable material, such as cellulose nanofibrils.
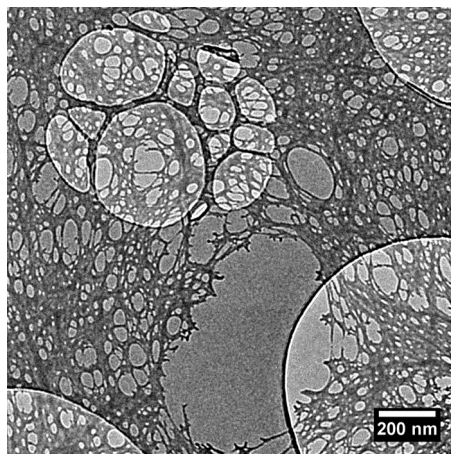
Figure 8. TEM image of a network of cellulose nanofibrils produced from P. radiata

Relevant application areas

A series of application areas have been suggested for cellulose nanofibrils, e.g. for rheology adjustment and as emulsion stabilizer of food, paint and cosmetics (Turbak et al. 1982; 1985). During the last years, some of these applications have been explored in more detail, and additional applications have been added to an expanding list. In the following, a brief description of some relevant applications is given.

Paper

Fibrils adhere, make inter-fibril bonds and form networks in a similar way as fibres do. Due to the small dimensions of single fibrils, the number of bonds in a sheet of fibrils is large compared to e.g. a sheet of paper. This influences the mechanical properties of the material (such as high density and superior strength), as has been demonstrated in several studies (e.g. Taniguchi and Okamura 1998; Henriksson et al. 2008; Syverud and Stenius 2009). In a recent study, the influence of adding 4 % cellulose nanofibrils to TMP handsheets was studied (Eriksen et al. 2008). The tensile strength was increased with up to 34 % depending on the nanofibril quality. The light scattering and opacity were however reduced. Nanofibrils have been applied as a coating layer on handsheets composed of 70 % bleached TMP and 30 % clay (Syverud et al. 2009). The nanofibrils formed a dense and continuous film. Hence, a considerable reduction in surface roughness was quantified. However, the paper gloss did not increase. This was probably due to the coverage of glossy clay particles by the less glossy nanofibrils (Syverud et al. 2009). Despite the lower gloss, the lower roughness of nanofibril coated surfaces may be advantageous for improving the quality of printed surfaces. In addition, the application of cellulose nanofibrils in layered TMP handsheets has been explored by Mörseburg and Chinga-Carrasco (2009). A series of handsheets were made, where the nanofibrils were blended with the middle and surface

layers. It was shown that the appropriate application of nanofibrils counteracts the potential reduction in strength caused by clay particles. Recently, a patent application about using cellulose nanofibrils together with a polysaccharide hydrocolloid (e.g. starch) as a coating of printing paper for reducing linting or dusting has been published (Ankerfors et al. 2009).

Packaging

The ability of cellulose nanofibrils to form dense and continuous films proposes the nanofibrillated material as most suitable for barrier applications in packaging. Superior barrier against oxygen at low relative humidity has been demonstrated (Syverud and Stenius 2009). As the humidity increases the oxygen permeability increases dramatically (Aulin et al. 2010; Minelli et al. 2010). This is probably caused by swelling due to the interaction between water molecules and the hydroxyl groups on the nanofibril surfaces. Cellulose nanofibrils have an hydrophilic nature. Good barrier against water and oxygen thus requires the combination of nanofibrils with complementary materials. As an example, the combination of nanofibrils and shellac has revealed good barrier properties against water and oxygen (Hult et al. 2010).

Membranes

The application of nanofibrils in membranes has been suggested in several studies. It has been demonstrated that a composite membrane of bacterial cellulose and chitosan is able to separate ethanol and water with good selectivity, flux and mechanical properties (Dubey 2005). Nanofibrils have also been applied in loudspeaker membranes, alone and as a composite with melamine formaldehyde. In this respect, the combination of high mechanical dampening and high sound propagation velocity is of technical interest (Henriksson and Berglund 2007).

Composites

Nanofibrillated cellulose applied in composite materials have been summarized in two recent reviews (Hubbe et al. 2008, Siró and Plackett 2010). Superior thermal, mechanical and barrier properties at low reinforcement levels and better recyclability, transparency and low weight are reported as advantages of nano-composites compared to conventional composites (Oksman et al. 2006, Sorrentine et al. 2007; Siró and Plackett 2010). The nanocomposites can be divided into several groups depending on the properties of the matrices (Siró and Plackett 2010) (Table 2).

Table 2. Classification of composite matrices

	Non-biodegradable	Biodegradable
Hydrophilic matrices	acrylic resins, epoxy resins, EVOH, latex	starch, poly(ethylene)oxide (PEO), chitosan
Hydrophobic matrices	polyethylene, polypropylene	polylactide, polycaprolactone

The most frequently mentioned motivation for adding fibrils to polymers and forming a composite is the increase in tensile strength and E-modulus. This has been mentioned by various authors (see e.g. the review of Hubbe et al. 2008). However, due to the hydrophilic nature of cellulose, it is necessary to surface modify the material for increasing its compatibility with hydrophobic matrices. Several approaches are reported, e.g. acetylation (e.g. Kim et al. 2002; Tingaut et al. 2010), silylation (Goussé et al. 2004; Andresen et al. 2006) and grafting (e.g. Stenstad et al. 2008). Many of these methods involve change of solvent and are thus time consuming and will not be easily applicable in an industrial perspective. Simpler methods for surface modification are therefore sought. One approach is to use cationic surfactants that can

adsorb to the surfaces of fibrils produced by TEMPO-mediated oxidation, which have a negatively charged surface (Syverud et al. 2010a).

Emulsions

Since the beginning of the 20th century, it has been known that emulsions can be stabilized by solid particles that are partly wetted by the water phase, and partly by the oil phase; so-called Pickering emulsions (Pickering 1907). Recently, a few studies have demonstrated that hydrophobized nanofibrils can be applied for stabilization of water-in-oil emulsions (Andresen et al. 2007; Xhanari et al. 2010; Lif et al. 2010), which is most interesting for end-use products such as paints and low-emission diesel.

Thickeners

Cellulose nanoparticles have unusual rheological properties. As the cellulose fibres are divided into individual nano-scaled particles the viscosity increases considerably and a high viscous gel-like structure is formed (Ioelovich 2008). The use of nanosized cellulose particles as carrier of enzymes is demonstrated with the intended use in cosmetic applications (Ioelovich and Figovsky 2008). In addition, the water-holding capacity of bacterial cellulose has been utilized in meat balls (Lin and Lin 2004).

Medical applications

An area of research for cellulosic nano-materials is within medical applications. In this respect, bacterial cellulose has mostly been in focus due to its purity and the highly swollen 3D structure of the fibrils. It is especially two applications that are foreseen for the nanofibrillated material, 1) as scaffolds for tissue or bone (see review by Klemm et al. 2006) and 2) for controlled drug delivery. Hydrogel nanoparticles for drug delivery is an area that has been in focus for some time (see e.g. reviews by Soppimath et al. (2001) and Hamidi et al. (2008). The use of cellulose nanofibrils has been suggested as a suitable material for preparing such hydrogels (Johnson et al. 2009).

In addition, it has been shown that it is possible to add functionality to the surface of nanofibrils by binding functional molecules to the surface hydroxyl groups. Non-leaching antimicrobial films have been prepared from nanofibrils. An antimicrobial compound, octadecyldimethyl(3-trimethoxysilylpropyl)-ammonium chloride (ODDMAC) was covalently bonded to the fibril surfaces. The films showed antibacterial activity against both Gram-positive and Gram-negative bacteria (Andresen et al. 2007).

Concluding remarks

Nanofibrillated cellulose is an interesting material for several industry sectors. This study gives a general overview of nanofibril production, how different treatments can affect a given nanofibril quality, how nanofibrils can be efficiently quantified by microscopy methods, and how nanofibrils can be utilized in several applications.

Being produced from cellulose fibres, a promising application will be in paper products. Cellulose nanofibrils give strength and improve the surface properties of printing paper. However, the price of cellulose nanofibrils, not yet commercialized, will determine if the promising results regarding use in paper applications can be set into practice. The challenges in this case are the total production costs of nanofibrils, including energy, chemical costs, investments in production equipments and in upgrading a given paper machine. In addition, runnability is a challenging issue with respect to nanofibril and paper production.

In addition to applying the nanofibrillated material in paper, cellulose nanofibrils have a wide range of applications, including emulsions, thickeners, novel membranes, filters, composite materials and in medicine, to name a few. However, a proper utilization of nanofibrils will require a comprehensive understanding of its morphology, mechanical properties, and how these properties are affected by a given production procedure. In this respect, adequate characterisation and quantification of the various scales of cellulose fibres and nanofibrils will be necessary. Complementary microscopy techniques in combination with effective computerized image analysis will be most suitable for controlling a given nanofibril quality and it properties.

Acknowledgement

References

Andresen M., Johansson L.-S., Tanem B.S. and Stenius P. (2006): Properties and characterization of hydrophobized microfibrillated cellulose. Cellulose 13, 665-667

Andresen M. and Stenius P. (2007): Water-in-oil Emulsions Stabilized by Hydrophobized Microfibrillated Cellulose. J. Dispersion Sci. Technol., 28 (5), 837 – 844

Andresen M., Stenstad P., Møretrø T., Langsrud S., Syverud K., Johansson L.-S. and Stenius P. (2007): Nonleaching Antimicrobial Films Prepared from Surface-Modified Microfibrillated Cellulose. Biomacromolecules, 8 (7), 2149 – 2155

Ankerfors M., Lindström T., Hoc M. and Song H. (2009): Composition for coating of printing paper. WO/2009/123560

Ankerfors M. (2010): Great interest in pilot plant for nanocellulose production. Innventia – Beyond 2/2010

Aulin C., Gällstedt M. and Lindström T. (2010): Oxygen and oil barrier properties of microfibrillated cellulose films and coatings. Cellulose 17, 559-574

Brändström J., Bardage S.L., Daniel G. and Nilsson T. (2003): The structural organisation of the S1 cell wall layer of Norway spruce tracheids. IAWA J. 24 (1), 27-40

Chinga-Carrasco G. (2009): Exploring the multi-scale structure of printing paper - A review of modern technology. J. Microscopy-Oxford 234(3), 211-242

Chinga-Carrasco G. (2011): Microscopy and computerised image analysis of cellulose fibres multiscale structures. In: Microscopy: Science, Technology, Applications and Education. Microscopy Book Series. To appear January 2011

Chinga-Carrasco G. and Syverud K. (2010): Computer-assisted quantification of the multiscale structure of films made of nanofibrillated cellulose. J. Nanop. Res. 12(3), 841-851

Chinga-Carrasco G., Johnsen P.O. and Øyaas K. (2010): Structural quantification of wood fibres surfaces - morphological effects of pulping and enzymatic treatment. Micron 41(6), 648-59

Denk W. and Horstman H. (2004): Serial block-face scanning electron microscopy to reconstruct three-dimensional tissue nanostructure. Plos Biology 2(11), 1900-1909

Dubey V., Pandey L.K. and Saxena C. (2005): Pervaporative separation of ethanol/water azeotrope using a novel chitosan-impregnated bacterial cellulose membrane and chitosan-poly(vinyl alcohol) blends. J. Membrane Science 251, 131-136

Duchesne I. and Daniel G. (2000): Changes in surface ultrastructure of Norway spruce fibres during kraft pulping - visualization by field emission-SEM. Nordic Pulp Paper Res. J. 15(1), 54-61

Eriksen Ø., Gregersen Ø. W. and Syverud K. (2008): The use of microfibrillated cellulose produced from kraft pulp as strength enhancer in TMP paper. Nordic Pulp Paper Res. J. 23(3), 299-304

Fernando D. and Daniel G. (2004): Micro-morphological observations on spruce TMP fibre fractions with emphasis on fibre cell wall fibrillation and splitting. Nordic Pulp Paper Res. J. 19(3), 278-285.

Fukuzumi H., Saito T., Iwata T., Kumamoto Y. and Isogai A. (2009): Transparent and high gas barrier films of cellulose nanofibers prepared by TEMPO-mediated oxidation. Biomacromolecules 10, 162-165

Goussé C., Chanzy H., Cerrada M.L. and Fleury E. (2004): Surface silylation of cellulose microfibrils: preparation and rheological properties. Polymer 45, 1569-1575

Gustafsson J., Ciovica J. and Peltonen J. (2003): The ultrastructure of spruce kraft pulps studied by atomic force microscopy (AFM) and X-ray photoelectron spectroscopy (XPS). Polymer 44, 661-670

Hamidi M., Azadi A. and Rafei P. (2008): Hydrogel nanoparticles in drug delivery. Advanced drug delivery reviews 60, 1638-1649

Heijnesson-Hultén A. (2007): patent no. WO 2007/001229 A1: Method for preparing microfibrillar polysaccharide

Henriksson M. and Berglund L.A. (2007): Structure and properties of cellulose nanocomposite films containing melamine formaldehyde. J. Appl. Polymer Sci. 106, 2817-2824

Henriksson M., Berglund L.A., Lindström T. and Nishino T. (2008): Cellulose Nanopaper structures of high toughness. Biomacromolecules 9, 1579-1585

Hubbe M.A., Rojas O.J., Lucia L.A. and Mohini S. (2008): Cellulosic nanocomposites: a review. BioResources 3 (3), 929-980

Hult E-L., Iotti M. and Lenes M. (2010): Efficient approach to high barrier packaging using microfibrillar cellulose and shellac. Cellulose 17, 575–586

Ioelovich M. (2008): Cellulose as a nanostructures polymer: a short review. BioRes. 3 (4), 1403-1418

Ioelovich M. and Figovsky O. (2008): Nano-cellulose as promising biocarrier. Trans Tech publications, DOI: 10.4028/www.scientific.net/AMR.47-50.1286

Iwamoto S., Abe K. and Yano H. (2008): The effect of hemicelluloses on wood pulp nanofibrillation and nanofiber network characteristics. Biomacromolecules 9, 1022-1026

Jang H.F., Robertson A.G. and Seth R.S. (1991): Optical sectioning of pulp fibres using confocal scanning laser microscopy. Tappi J. 74(10), 217-219

Johnson R.K., Sharp A.Z., Renneckar S.H. and Glasser W.G. (2009): A new bio-based nanocomposite: fibrillated TEMPO-oxidized celluloses in hydroxypropylcellulose matrix. Cellulose 16, 227-238

Kim D.Y., Nishiyama Y. and Kuga S. (2002): Surface acetylation of bacterial cellulose. Cellulose 9, 361-367

Klemm D., Schumann D., Kramer F., Hessler N., Hornung M., Schmauder H.-P. and Marsch S. (2006): Nanocelluloses as innovative polymers in research and application. Adv. Polym. Sci. 205, 49-96

Lif A., Stenstad P., Syverud K., Nydén M. and Holmgren K. (2010): Fischer-Tropsch diesel emulsions stabilised by microfibrillated cellulose. J. Colloid Interface Science, accepted

Lin K.-W. and Lin H.-Y. (2004): Quality characteristics of Chinese-style meatball containing bacterial cellulose (Nata). J. Food Sci. 69 (3), 107-111

Minelli M., Baschetti M.G., Doghieri F., Ankerfors M., Lindström T., Siró I. and Plackett D. (2010): Investigation of mass transport properties of microfibrillated cellulose (MFC) films. J. Memb. Sci. 358, 67-75

Moss P.A., Retulainen E., Paulapuro H. and Aaltonen P. (1993): Taking a new look at pulp and paper: Applications of confocal laser scanning microscopy (CLSM) to pulp and paper research. Paperi Ja Puu 75(1-2), 74-79

Mörseburg K. and Chinga-Carrasco G. (2009): Assessing the combined benefits of clay and nanofibrillated cellulose in layered TMP-based sheets. Cellulose 16(5): 795-806

Oksman K., Mathew A.P., Bondeson D. and Kvien I. (2006): Manufacturing process of cellulose whiskers/polylactic acid nanocomposites. Compos. Sci. Technol. 66, 2776-2784

Page D.H. and Emerton H.W. (1959): The microscopic examination of fibres, paper, board and wood – Improved methods for the study of surfaces. Svensk Papperstidn. 62(9), 318-332

Pickering S.U. (1907): Emulsions. J. Chem. Soc. 91, 2001-2021

Pääkkö M., Ankerfors M., Kosonen H., Nykänen A., Ahola S., Österberg M., Ruokolainen J., Laine J., Larsson P.T., Ikkala O. and Lindström T. (2007): Enzymatic hydrolysis combined with mechanical shearing and high-pressure homogenization for nanoscale cellulose fibrils and strong gels. Biomacromol. 8, 1934-1941

Reme P.A., Johnsen P.O. and Helle T. (2002): Assessment of fibre transverse dimensions using SEM and image analysis. J. Pulp Pap. Sci. 28(4), 122-128

Saito T., Nishiyama Y., Putaux J.L., Vignon M. and Isogai A. (2006): Homogeneous suspensions of individualized microfibrils from TEMPO-catalyzed oxidation of native cellulose. Biomacromol. 7(6), 1687-1691

Smith K.C.A. (1959): Scanning electron microscopy in pulp and paper research. Pulp Paper Can. 60(12), 366-371

Siró I. and Plackett D. (2010): Microfibrillated cellulose and new nanocomposite materials: a review. Cellulose 17, 459-494

Soppimath K.S., Aminabhavi T.M., Kulkarni A.R. and Rudzinski W.E. (2001): Biodegradable polymeric nanoparticles as drug delivery devices. J. Controlled Release 70, 1-20

Sorrentino A., Gorrasi G., Vittoria V. (2007): Potential perspectives of bio-nanocomposites for food packaging applications. Trends Food Sci Technol 18, 84-95

Stenstad P., Andresen M., Tanem B.S. and Stenius P. (2008): Chemical surface modifications of microfibrillated cellulose. Cellulose 15, 35-45

Syverud K. and Stenius P. (2009): Strength and permeability of MFC films. Cellulose 16 (1), 75-85

Syverud K., Gregersen Ø., Chinga-Carrasco G. and Eriksen, Ø. (2009): The influence of microfibrillated cellulose, MFC, on paper strength and surface properties. 14th Fund. Res. Symp., 899-930, Oxford

Syverud K., Xhanari K., Chinga-Carrasco G., Yu Y. and Stenius P. (2010a): Films made of cellulose nanofibrils - surface modification by adsorption of a cationic surfactant and characterisation by computer-assisted electron microscopy. J. Nanoparticle Res. DOI: 10.1007/s11051-010-0077-1

Syverud K., Chinga-Carrasco G., Toledo J. and Toledo P. (2011): Comparison of Eucalyptus and P. radiata pulp fibres as raw materials for production of cellulose nanofibrils. Submitted

Taniguchi T. and Okamura K. (1998): New films produced from microfibrillated natural fibres. Polymer International 47, 291-294

Tingaut P., Zimmermann T. and Lopez-Suevos F. (2010): Synthesis and characterization of bionanocomposites with tunable properties from poly (lactic acid) and acetylated microfibrillated cellulose. Biomacromol. 11, 454-464

Turbak A.F., Snyder F.W. and Sandberg K.R. (1982): Food products containing microfibrillated cellulose. US Patent no. 4,341,807, Jul. 27

Turbak A.F., Snyder F.W. and Sandberg K.R. (1983): Microfibrillated cellulose, a new cellulose product: properties, uses, and commercial potential. J. Appl. Polym. Sci., Appl. Polym. Symp. 37, 815–827

Turbak A.F., Snyder F.W. and Sandberg K.R. (1985): Suspensions containing microfibrillated cellulose. US Patent no. 4,500,546, Feb. 19

Wågberg L., Decher G., Norgren M., Lindström T., Ankerfors M. and Axnäs K. (2008): The build-up of polyelectrolyte multilayers of microfibrillated cellulose and cationic polyelectrolytes. Langmuir 24: 784-795

Xhanari K., Syverud K. and Stenius P. (2010): Emulsions stabilized by microfibrillated cellulose: the effect of hydrophobization, concentration and o/w ratio. J. Disp. Sci. Technol. In press

Zimmermann T., Bordeanu N. and Strub E. (2010): Properties of nanofibrillated cellulose from different raw materials and its reinforcement potential. Carbohydrate Polymers 79(4), 1086-1093

SEC STUDIES ON HCL TREATED SOFTWOOD AND BIRCH KRAFT PULPS

Paul Ander[1], Ute Henniges[2] and Antje Potthast[2]

[1]CRUW, Dept. of Forest Products/Wood Science, SLU, Uppsala, Sweden

[2]BOKU - University of Natural Resources and Life Sciences, Vienna, Department of Chemistry, Christian Doppler Laboratory "Advanced Chemistry and Analytics of Cellulose"

Vienna, Austria. E-mail: paul.ander@slu.se

Abstract

Unbleached and bleached softwood kraft pulps and six birch kraft pulps were treated with hydrochloric acid and evaluated for molecular weight changes using Size Exclusion Chromatography (SEC-MALLS). In addition the distribution of uronic acids in hemicelluloses relative to molecular weight was analysed applying group selective fluorescence labelling. The goal was to evaluate how cellulose and hemicellulose are affected by acid treatment of these softwood and hardwood pulps. The softwood pulp fibres were strongly cleaved by the acid during hemicellulose degradation and an overall molecular weight decrease was observed. The uronic acid content associated with hemicellulose also decreased. The birch fibres were affected only little by HCl. The SEC results clearly reflect the observed cleavage rates of the used softwood and hardwood pulps. While for the bleached and HCl treated softwood pulp a clear decrease of Mw was observed, the effect on birch pulp was smaller.

Introduction

Fibre deformations are already present in small amounts in naturally grown trees and they increase during pulp cooking and bleaching. These irregularities have been defined as dislocations. This term describes the localized change or distortion of the crystalline cellulose microfibrils in either the S1 or both S1 and S2 secondary cell wall layers (Nyholm et al. 2001). While small dislocations are not considered to be significant and are thought to add to fibre flexibility, large dislocations are considered to be a target for chemical, mechanical or enzymatic attack due to their less ordered or more open amorphous cellulose structure.

Several investigations (Ander et al. 2005; 2008) show that all acid conditions partly cleave fibres in dislocations. Thus, dislocations make the cell wall more susceptible to enzymatic and chemical attack allowing for a stronger penetration of cooking and bleaching chemicals during pulping and this leads to inferior strength of the resulting paper.

In this study it was tried to link the enhanced availability of dislocations that were produced by hydrochloric treatment in the fibres to changes in molecular weight and uronic acid content. In order to shed some light on the effects of HCl on the softwood and birch fibres and possible molecular weight changes of hemicellulose and cellulose, SEC was run on the different pulps before and after acid treatment.

Materials and Methods

Pulps

Unbleached (3.9% lignin) and bleached (0.2% lignin) mixed spruce (*Picea abies*) and pine (*Pinus sylvestris*) kraft pulps were obtained from Karin Sjöström, Södra Cell, Sweden (Common pulp samples COST E54). The ratio of spruce to pine was 79:21. The pulps resulted from a batch

cook and were TCF-bleached with the sequence Q - OP - Q+Paa – PO (Q: chelator, Paa: Peraacetic acid). Lignin and carbohydrate composition was determined at Stora Enso, Karlstad, Sweden and given in the paper by Heinemann and Ander (2011) in this book.

Six birch (*Betula verrucosa*) kraft pulps from a pulp bleaching line were obtained from Irina Rauvanto, Lappeenranta, Finland.

HCl-treatment

HCl-treatment was done using 100 mg pulp (dry-weight) and 1M HCl pH 0 at 81 °C according to Ander et al. (2008). The equipment for making HCl treatment is shown in Heinemann and Ander (2011) this book.

Fibre characterisation

Fibre lengths before and after acid treatment were determined using a FibreMaster at Södra Cell for softwood fibres. For birch fibres a Fiber tester from Lorentzen & Wettre was used.

Cellulose characterization

Size exclusion chromatography and fluorescence labelling of oxidized cellulose functionalities before and after HCl treatments were done as described in Bohrn et al. (2006).

Results and Discussion

Softwood pulps and HCl method

The results for unbleached and bleached softwood pulp fibres are shown in Table 1 below.

Table 1. Characterization of bleached and unbleached softwood pulp fibres

Pulp type	LWFL (mm) (L_0)	LWFL (mm) (L)	Cleavage per fibre $(L_0 / L) - 1$	Cleavage per mm fibre
Unbleached pulp	2.73	0.59	3.62	1.33
Bleached pulp	2.60	0.37	6.11	2.35

Cleavage values of 3.6 for the unbleached pulp and of 6.1 for the bleached pulp can be considered typical (Ander et al. 2008). They reflect an increased formation of dislocations and other weak points during pulping and bleaching. HCl releases more xylose than glucose indicating a stronger effect of HCl on hemicellulose. A typical kraft pulp of the same kind as here can give 0.055 g/l of xylose and 0.0075 g/l of glucose for 100 mg pulp (Ander et al. 2008).

Polarized light microscopy (PLM)

Typical appearance of some unbleached and bleached softwood fibres before and after HCl treatment is shown in Figures 1a-d. Some birch fibres and vessels after HCl treatment are shown in Figure 2a-c. The vessels appear to be rather acid stable, and although they appear in only a few percent they may contribute to a seemingly lower acid cleavage of the fibres. See also Table 2.
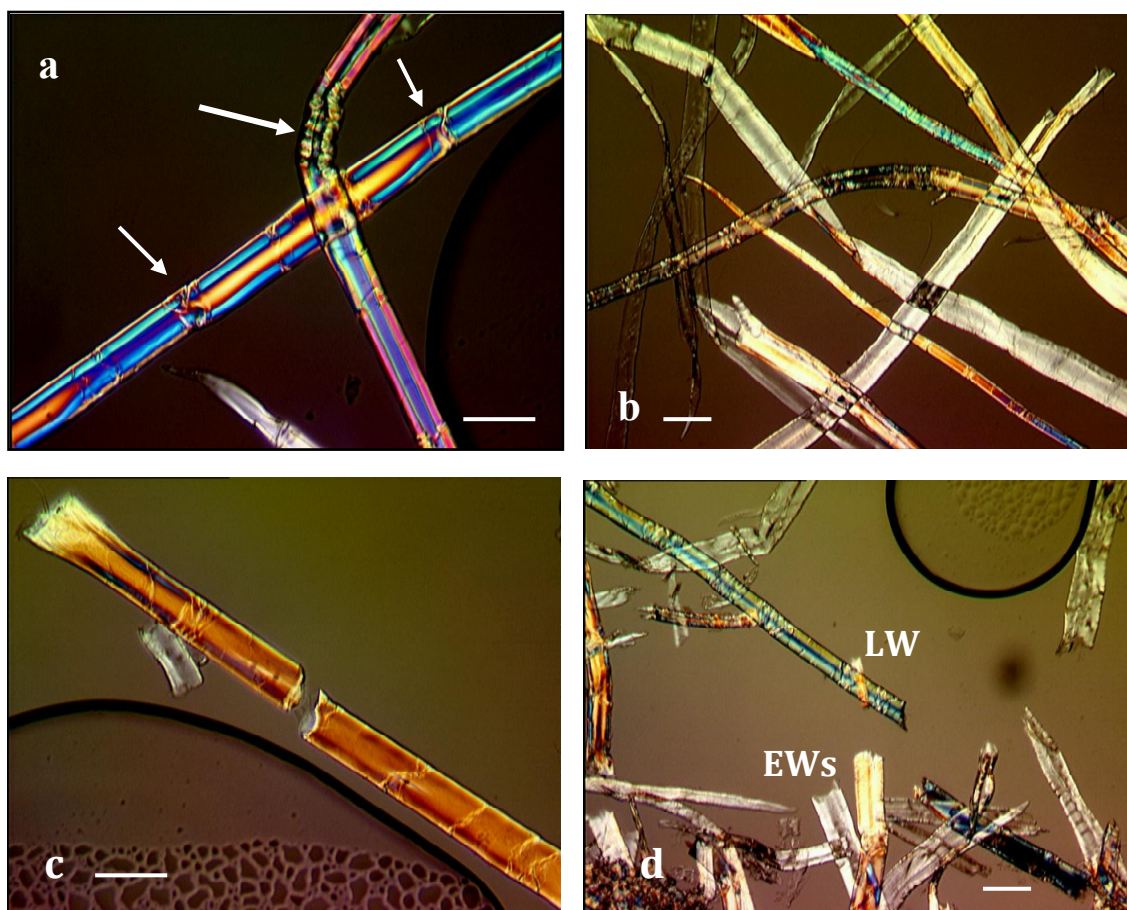
Figure 1a. Latewood (LW) spruce fibres under polarized light microscopy showing dislocations of different sizes. See arrows. Water treated undelignified fibres, 20x

Figure 1b. Grey earlywood (EW) and coloured latewood fibres. Some breakages caused by the industrial pulp bleaching are seen. Bleached fibres water treated controls, 10x

Figure 1c. A latewood spruce fibre after cleavage in a dislocation, 20x. Unbleached and HCl treated fibre

Figure 1d. LW and EW fibres cut by the acid treatment are seen. Bleached fibres, 10x. All bars are 30 μm

HCl treatment of birch fibres and PLM
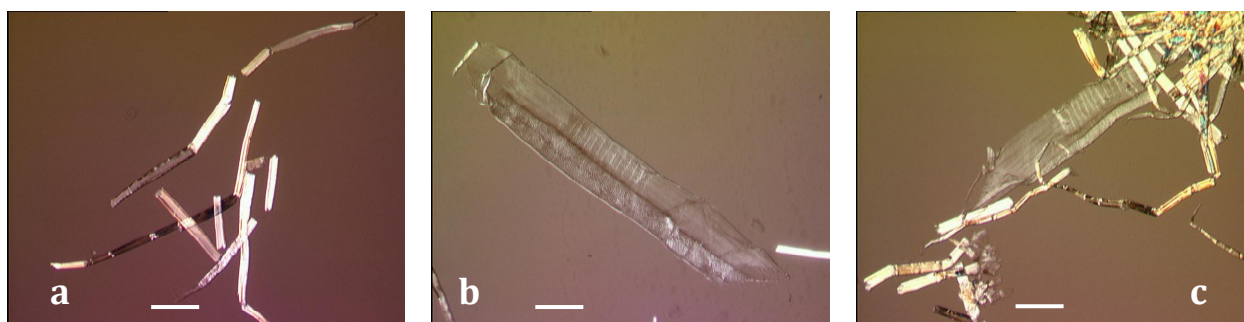
Figure 2a. Birch fibres after HCl cleavage.

Figure 2b with a typical birch vessel. Both figures were photographed at magnification 10x indicating that the width of the vessels are about 7 times larger than the width of normal birch fibres.

Figure 2c with typical difference in size of birch vessels and fibres cut by the acid. The vessels appear to be rather stable against acid cleavage. Figure 2a & b are from fibre line nr 1; 2c from the most bleached part of the fibre line nr 6. Bars are 50 μm

SEC investigations

Figure 3 gives the weighted average molecular weight of the softwood pulp obtained from SEC before and after acid treatment for bleached and unbleached samples.
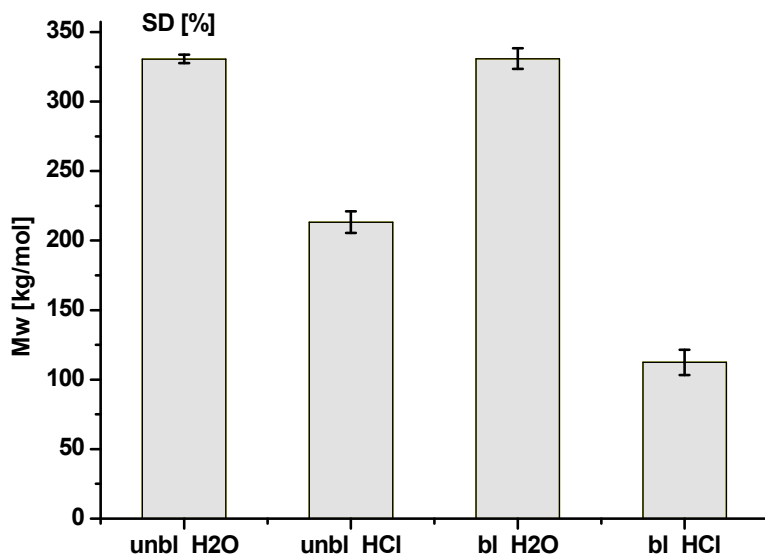
Figure 3. Change in Mw for unbleached and bleached softwood pulps before and after HCl treatment

The observed effect on Mw for the unbleached material was significantly lower compared to the bleached pulp. Bleaching renders the cellulose more accessible, cellulose hydrolysis is more severe. In addition, lignin may serve as a barrier and protects the pulp during the acid treatment.
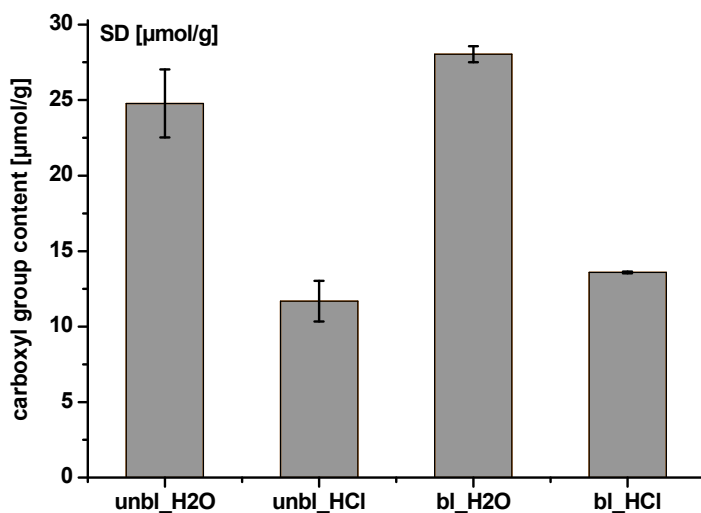
Figure 4. Change in carboxyl group content for unbleached and bleached softwood pulps before and after HCl treatment. Error bars give the standard deviation in μmol/g

The carboxyl group content given in Figure 4 mainly corresponds to the uronic acids, which are not as pronounced in softwoods compared to hardwood. The uronic acids mainly reflect the

xylan content of the material. The differences observed between bleached and unbleached pulp is not very pronounced, slightly lower numbers were found for the unbleached pulp.
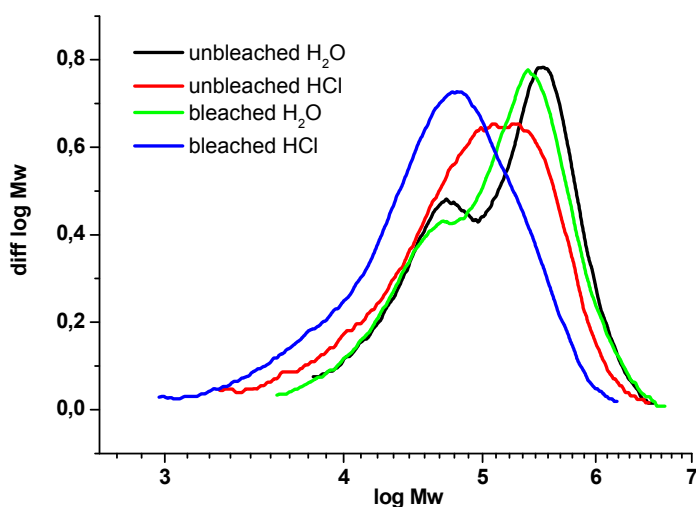
Figure 5. Molecular weight distribution of the unbleached and bleached softwood samples

In Figure 5 it can be observed that the molecular weight distribution of the two starting samples is already different, as one would expect. The water treated samples show a low molecular weight shoulder that was removed by the acid treatment. This low molecular weight shoulder is already affected by the water treatment; even though there is no significant change in Mw, this shoulder is noticeably decreased by the treatment. After HCl-treatment however, the whole MWD shifted towards smaller masses.

Hardwood birch pulp

The results for the HCl test method for the birch pulp fibre line are given in Table 2.

Table 2. Characterization of cleavage of birch pulp fibre

Birch Pulp sample	Cleavage per fibre 80.5°C & 30 min std stirring	Cleavage per fibre 85.5°C & 30 min std stirring	Cleavage per fibre 85.5°C & 45 min long stirring
1	0.35	0.62	0.56
2	0.28	0.76	0.77
3	0.33	--	--
4	0.305	--	--
5	0.33	--	--
6	0.225	0.54	0.635

Cleavage per fibre (0.225 – 0.35) at the standard temperature 80.5 °C was unexpectedly low. At 85.5 °C the detected cleavage increased somewhat to 0.54 – 0.76. Longer stirring time had little effect on the acid degradation. One explanation for this result may be the stability of birch vessels in acidic environments, which result in lower overall cleavage (see Figure 2). Protection by hemicellulose is another possibility (Ander and Daniel 2006). Although, another hardwood fibre, bleached eucalyptus also has vessels it was more HCl sensitive and a larger cleavage

number was obtained for that fibre (0.835 and 1.17; Ander 2008). More research is needed for hardwood fibres.
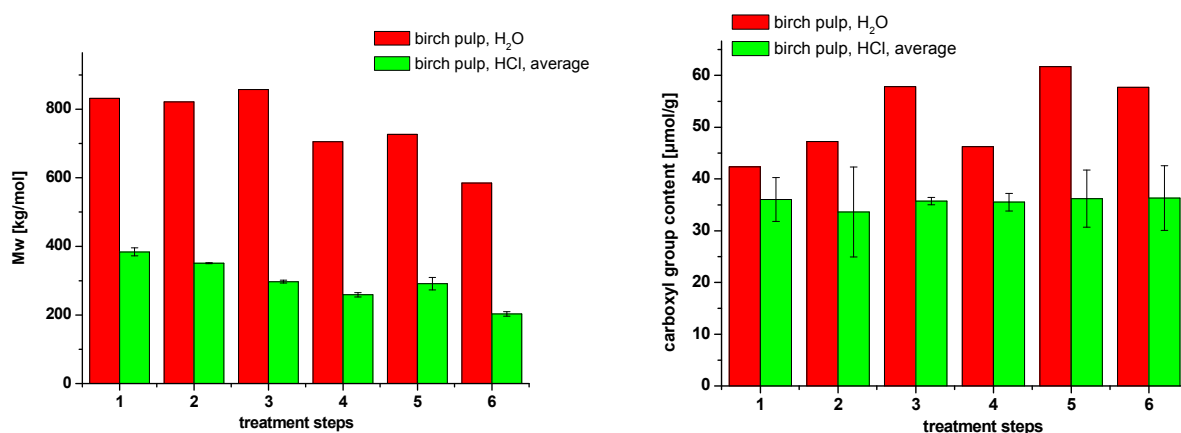
Figure 5. Change in Mw (left) and carboxyl group content (right) for birch pulps before and after HCl treatment

Regarding birch fibres, Figure 5 left shows that high Mw cellulose decreased in the pulp fibre line during bleaching. After HCl treatment, the starting Mw was much lower than for water samples and further decreased for fibre line samples 1 to 4. It appears as if hemicellulose was not degraded so much by HCl in opposite to the softwood fibres. This result is supported by the MWD of the birch samples: the low molecular weight shoulder that reflects the hemicellulose content did not disappear in the course of the bleaching treatment (not shown).

Regarding the uronic acid content (Figure 5 right), the trend was not clear for the water samples. For the HCl-treated samples, the uronic acid groups did not change, which may be due low hemicellulose degradation in birch. That result may fit with the low cleavage induced by HCl of the birch fibres reported here in Table 2. With softwood fibres, however, HCl gave strong fibre cleavage (Table 1). Similarly, Ander et al. (2008) have shown that HCl releases the hemicellulose sugar xylose in large amounts and rather little cellulose sugars.

Conclusion

In short, the molecular weight of softwood pulp decreased by the acid treatment due to degradation. The fibre cleavage corresponds in this case to the molecular weight decrease. Bleaching in combination with HCl treatment gave the strongest degradation, but no further decrease in uronic acid content. This is mainly because the hemicelluloses have been removed by the bleaching already, resulting in a decreased uronic acid content. Noticeable degradation by HCl was obtained in all molecular regions; this was most visible for the bleached pulps.

With birch pulp, less fibre cleavage was observed. Hemicelluloses were not affected in the same way as in softwood pulp. So the lower fibre cleavage observed again reflects the higher stability of the samples as demonstrated by SEC-MALLS. This is mainly explained by more protection of the cellulose fibre due to the hemicelluloses in birch pulp that are not easily attacked and withstand the acid treatment as shown in a generally unchanged uronic acid content.

Acknowledgement

References

Ander P. (2008): COST Action E54 Workshop "Fine fibre", 10-11 April 2008, Graz, Austria

Ander P., Daniel G., Garcia-Lindgren C. and Marklund A. (2005): Characterization of industrial and laboratory pulp fibres using HCl, Cellulase and FiberMaster analyses. Nordic Pulp Paper Res. J. 20(1), 115-120

Ander P., Hildén L. and Daniel G. (2008): Cleavage of softwood kraft pulp fibres by HCl and Cellulases. Bioresources 3(2), 477-490

Ander P. and Daniel G. (2006): Dislocation counting and comparison of pulp fibre properties after HCl-treatment and fibre length determination. Proc. 5th Plant Biomechanics Conference, Stockholm, Vol. I. August 28 – September 1, 2006. *Ed.*: L. Salmén. STFI-Packforsk, Stockholm, Sweden, ISBN 91-86018-12-4, pp. 169-174

Bohrn R., Potthast A., Schiehser S., Rosenau T., Sixta H. and Kosma P. (2006): The FDAM method: Determination of carboxyl profiles in cellulosic materials by combining group-selective fluorescence labeling with GPC. Biomacromolecules 7 (6), 1743-1750

Heinemann S. and Ander P. (2011): Standard pulp and paper tests. *In* COST Action E54 "Characterisation of the fine structure and properties of papermaking fibres using new technologies". *Eds:* Ander P., Bauer W., Heinemann S., Kallio P., Passas R. and Treimanis A. Swedish University of Agricultural Sciences. p. 211-232. ISBN 978-91-576-9007-4

Nyholm K., Ander P., Bardage S. and Daniel G. (2001): Dislocations in pulp fibres – their origin, characteristics and importance – a review. Nordic Pulp Paper Res. J. 16:4, 376-384

ANALYSIS OF THE SURFACE LAYERS OF MECHANICALLY PEELED UNBLEACHED AND BLEACHED EUCALYPTUS KRAFT PULP FIBRES

Arnis Treimanis[2], Antje Potthast[1], Ute Henniges[1], Thomas Rosenau[1],

Uldis Grinfelds[2], Tatjana Bikova[2], Marite Skute[2]

[1]University of Natural Resources and Applied Life Sciences, Muthgasse 18, A-1190, Vienna, Austria, E-mail: antje.potthast@boku.ac.at

[2]State Institute of Wood Chemistry, 27 Dzerbenes str., Riga LV 1006, Latvia,

E-mail: arnis.treimanis@edi.lv

Abstract

The objective of the present work was to separate and to analyse the surface layers of eucalyptus unbleached and bleached kraft pulp fibres. Upgraded hydromechanical peeling techniques were applied to isolate fibre wall morphological layers. UV- spectra revealed that the content of lignin and hexenuronic acids was 3-4 times higher in fibre surface layers as compared to the average values. The content of heteroaromatic compounds (furanoids/furan resins) and oxypoly-saccharides was also estimated to be higher in the surface fibre wall fraction. Fluorescence labelling and GPC-MALLS showed that the molecular weight distribution of the surface fraction differed significantly from that of the bulk fibre, mostly in the low molecular weight fraction. The main fibre secondary wall layer fractions equaled the molecular weight distribution of the bulk fibre. The same held true for molecular weight and carbonyl group content. The impact of bleaching on the fraction obtained from the surface layers was very pronounced in spite of the lower final ISO brigthness value. After bleaching, the molecular weights and carboxyl group contents were found to decrease in all analyzed samples. Again, the surface layer fraction exhibited a different behaviour than bulk sample and main fibre secondary wall fractions.

Introduction

The residual constituents of middle lamella and primary wall of wood cell walls affect the composition of pulp fibre surface layers. It is expected that this translates into the pulp fibres' bleachability. The objective of the present work was to separate the surface layers of eucalyptus unbleached kraft pulp fibres by improved hydromechanical peeling techniques and to proceed with enzyme-aided bleaching of the separated layers according to the sequence peroxide – xylanase treatment – alkaline extraction – peroxide P1-X-E-P2. The composition of both unbleached and bleached fibre wall fractions were analysed by UV/Vis spectroscopy and fluorescence labelling of cellulose functionalities followed by GPC-MALLS.

Hydromechanical (mechanical) method of the separation of fibre wall outer layers was introduced in the 60s (e.g. Krause 1967). It is based on the fact that there are comparatively weaker bonds between the surface of secondary wall layers S1 and S2 due to the different cellulose fibril angles in relation to the fibre axis. An advantage of the *fibre surface layer separation method* is the possibility to isolate chemically unmodified fractions of the fibre wall. At the Latvian State Institute of Wood Chemistry in Riga, the composition of different unbleached and bleached pulp fibre samples has been investigated during a number of years. Both the hydromechanical and the chemical fibre wall peeling (heterogeneous acetylation) methods have been applied. The first one was modified (Gromov et al. 1976) by adding ethanol to the fibre suspension in order to prevent the dissolution of hemicelluloses during the prolonged (30-60 h) mixing procedure in a laboratory disintegrator built according to the ISO

standard 5263:1995. As regards the chemical peeling method, acetylation of fibre substance and subsequent dissolution of esterified matter in methylene dichloride, a decrease of the acetylation time and the amount of catalyst was recommended by Purina et al. (1979). A new parameter – degree of exposure (DE) of the fibre wall S2 layer – was introduced to characterize the openness of the main part of the secondary wall. Later the hydromechanical peeling procedure was upgraded (Treimanis 2006) by using a digital device the "FiberTester" from Lorentzen & Wettre, Sweden (L&W), for evaluation of the quantity of fibre fines (fragments of the surface layers P and S1) created by peeling.

Materials and Methods

Pulp

Eucalyptus unbleached kraft pulp fibres were kindly provided by Portucel Soporcel group. The sample was taken after cooking before the oxygen delignification stage.

Hydromechanical peeling

The unbleached kraft pulp fibre walls were divided in two parts by using the upgraded technique of hydromechanical peeling (Treimanis 2006). This method seen in Figure 1, involves a continuous intense stirring of a 3% fibre-water (plus ethanol) suspension, resulting in a partial removal of the primary wall (P) and the outer (S1) layer of the secondary wall from the central part of the fibre walls. Before peeling, the parenchyma cells, vessel fragments and fibre debris were separated by screening of the fibre suspension. The intact fibres are collected on sieves with 600 and 400 μm holes and then combined. During the peeling process, the fibres are examined using light microscope "Leica DM5500" and fibre dimensions using the digital analysis equipment L&W "FiberTester" to establish the end of the process. It is not possible to peel off 100% of the surface material due to the arising cross-sectional destruction of the fibres. According to the SEM micrographs, certain portion of the fibres remains unpeeled (Figure 2). It means that the fraction containing fibre wall surface material is quite "clean" but the main part of the fibre wall (S2-S3 layers) is "contaminated" with small quantities of the surface material.

After the peeling the fibre surface layer fragments are collected by sedimentation, centrifugation and freeze drying steps. During screening the fraction which passed the sieve with 400 μm holes is accumulated. The yield of the fraction containing fibre surface material, consisting mainly of the residues of the primary wall P and the outer layer S1 of the secondary wall, was determined to be approx. 5% by mass. Chemical composition of the two fibre wall fractions was presented in a previous paper (Treimanis et al. 2008). It is noteworthy to mention that Klason lignin content in the surface fraction exceeded the average number by 4 times (2.6% vs. 0.6%).
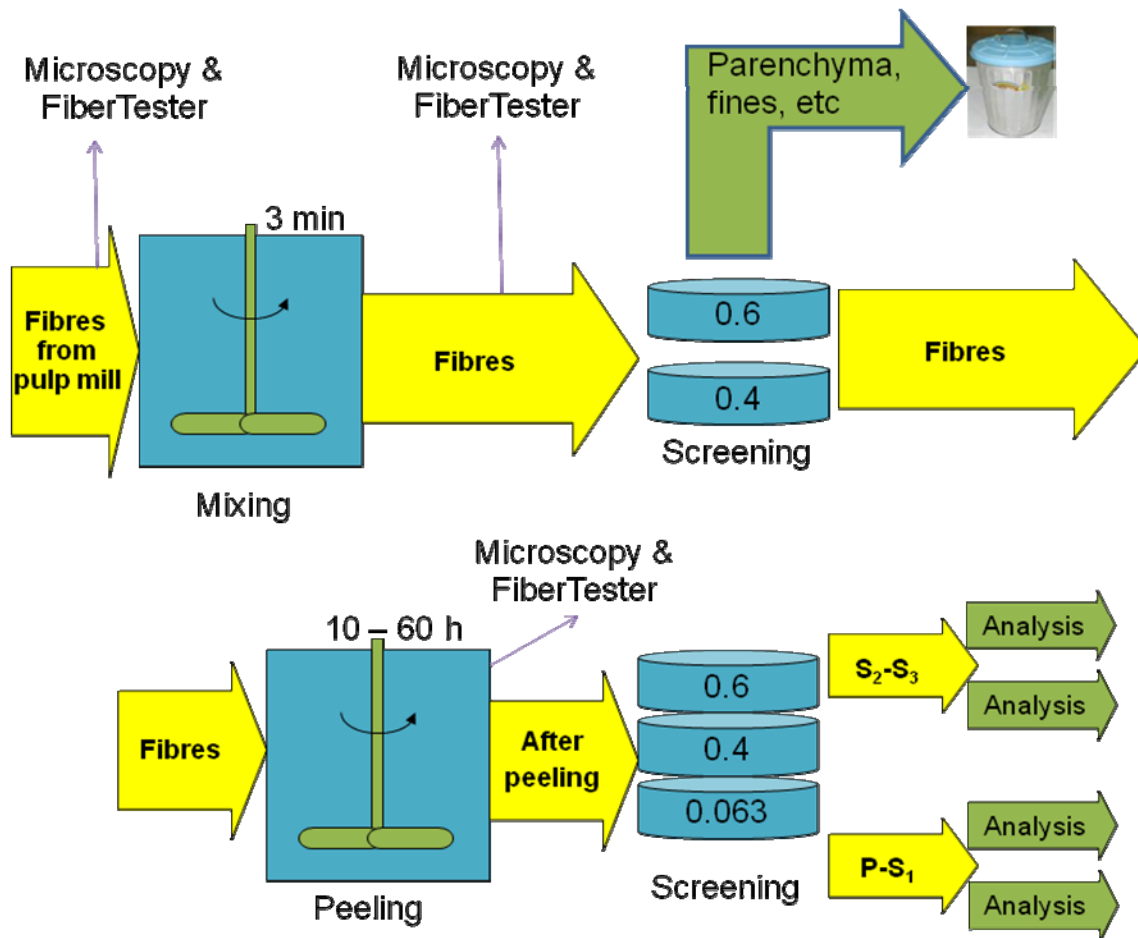
Figure 1. Scheme of the hydromechanical peeling procedure of the selected pulp fibres
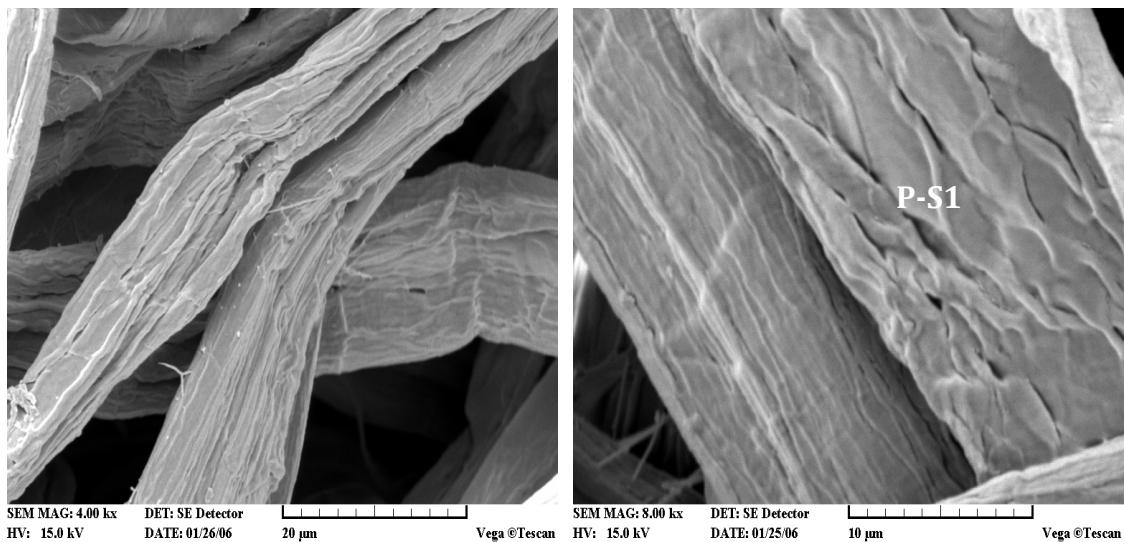
Figure 2. SEM micrographs of eucalyptus unbleached kraft pulp fibres after peeling of the surface layers.
Right-side picture shows the fibre with retained surface layers P-S1

Enzyme aided bleaching

The bleaching of the two separated fibre wall fractions was performed according to the sequence peroxide (P1) – enzyme treatment (X) – alkaline extraction (E) – peroxide (P2). More detailed pulp bleaching conditions has been reported earlier (Treimanis et al. 2009).

UV/ Vis spectroscopy

Perkin Elmer instrument „Lambda 35" was used. In order to differentiate the UV-absorbance derived by residual lignin and oxypolysaccharides, sequential alkaline extraction with 0.5% and 10% NaOH was applied. The total NaOH solubility was 40% by weight for unbleached surface layers and 19% for the residual part of the fibre wall.

Cellulose characterization

Size exclusion chromatography and fluorescence labelling of oxidized cellulose functionalities before and after bleaching treatments were performed as described in Röhrling et al. (2002) for the CCOA-protocol to detect carbonyl groups and in Bohrn et al. (2006) for the FDAM-protocol to determine carboxyl group content.

Results and Discussion

In Table 1 it can be observed that *the analytical data* of the entire fibre equals those of the main fibre wall fraction S2-S3. Mainly, the molecular weights Mw of the two fractions are very similar. The carbonyl group content, however, is more similar between the entire fibre and the surface layer fraction. When calculating the theoretical amount of reducing endgroups in these samples, none of them showed any sign of oxidation; all determined carbonyl groups originate from the reducing ends of the cellulose. Differences between the two values, determined carbonyl groups and calculated reducing end groups, are assumed to be caused by experimental error and uncertainties in the calculation itself. Carboxyl group content was not determined in this case (Table 1).

Table 1. Overview of the main analytical characteristics of the unbleached samples

Abbreviation	Description	Mw [kg/mol]	Mn [kg/mol]	Carboxyl groups [µmol/g]	REG theor. [µmol/g]	Carbonyl groups [µmol/g]
EUK1	Kraft Pulp	534	130	n.d.	7.7	8.3
EUK2	Kraft Pulp, P-S1	406	114	n.d.	8.8	8.2
EUK3	Kraft Pulp, S2-S3	559	109	n.d.	9.2	7.3

n.d.: not determined

Fluorescence labelling and GPC-MALLS showed that the molecular weight distribution of the surface layer fraction differed significantly from that of the whole fibre, mostly in the low molecular weight fraction. The S2-S3 layers fractions equaled the molecular weight distribution of the whole fibre (Figure 3).

This is also true for the carbonyl group distribution profile along the cellulose chains. The S2-S3 layers fraction followed mainly the suggested profile for reducing end groups only, while the two other samples had a different profile that is influenced by a more prominent presence of hemicelluloses.
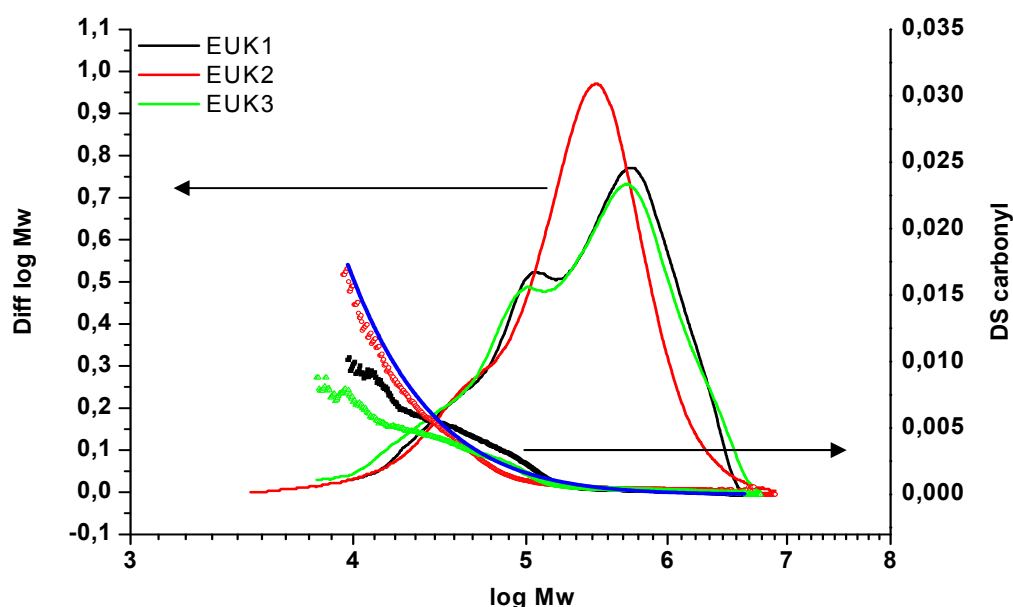
Figure 3. Distribution of carbonyl groups relative to the molecular weight in unbleached eucalyptus samples

In Table 2 the analytical data for the bleached samples are compiled. In general it can be observed that due to the bleaching sequence the Mw decreased while the total carbonyl group content increased considerably as expected (Table 2). The impact of bleaching was most pronounced in the fraction obtained from the surface layers. The carbonyl group content in the surface layer P-S1 increased 3 times compared to only 2 times in the S2-S3 part or in the whole fibre (*cf.* Table 1).

When it comes to the oxidized cellulose functionalities, e.g. carbonyl and carboxyl groups, most similarity can be found between the data of the entire fibre and those of the secondary wall layers S2-S3 of the sample. These values are virtually the same. Also, Mn is very similar between these two samples. For the Mw this observation is not entirely true.

Table 2. Overview of the main analytical characteristics of the bleached samples

Abbreviation	Description	Mw [kg/mol]	Mn [kg/mol]	Carboxyl groups [µmol/g]	REG theor. [µmol/g]	Carbonyl groups [µmol/g]
EUK1-bleached	Kraft Pulp	426	54	60.2	2.4	16.1
EUK2-bleached	Kraft Pulp, P-S1	260	39	30.1	3.9	28.4
EUK3-bleached	Kraft Pulp, S2-S3	283	55	63.8	3.5	16.9

The differences in the Mw are also reflected in the molecular weight distribution (Figure 4). Unlike the unbleached samples, the MWD of the bleached samples differed between the three of them.
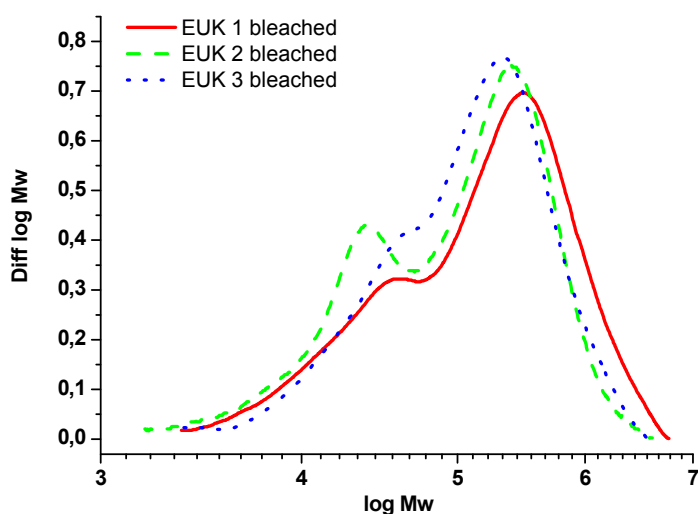
Figure 4. Differential molecular weight distribution of bleached samples

The differences impaired to the single fraction and the entire fibre can be studied more in detail when comparing the two samples, bleached and unbleached, directly to each other. In Figure 5 the molecular weight distribution of the entire fibre shifted rather parallel to lower molecular weight fractions with largest impact in the low molecular weight regions.
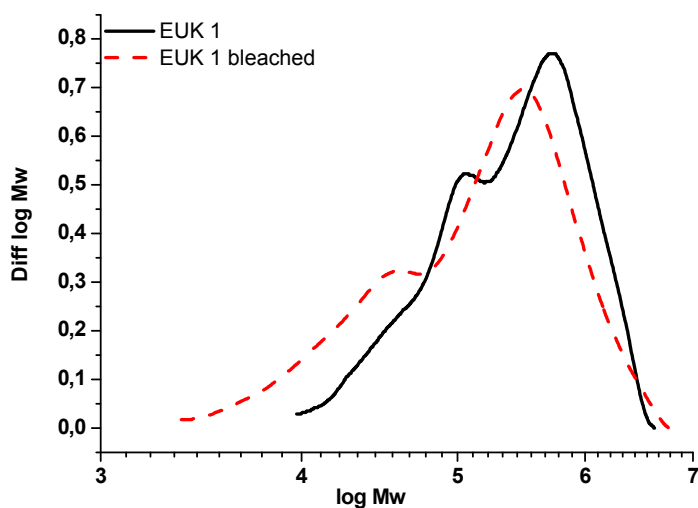
Figure 5. Comparison of differential molecular weight distribution of untreated and bleached sample eucalyptus kraft pulp

Figure 6 shows the impact on the surface layer fraction of the sample before and after bleaching. As new hemicelluloses cannot be generated due to the bleaching treatment it has to be assumed that the increase in the low molecular weight should be caused by cellulose degradation products that accumulate in this area.
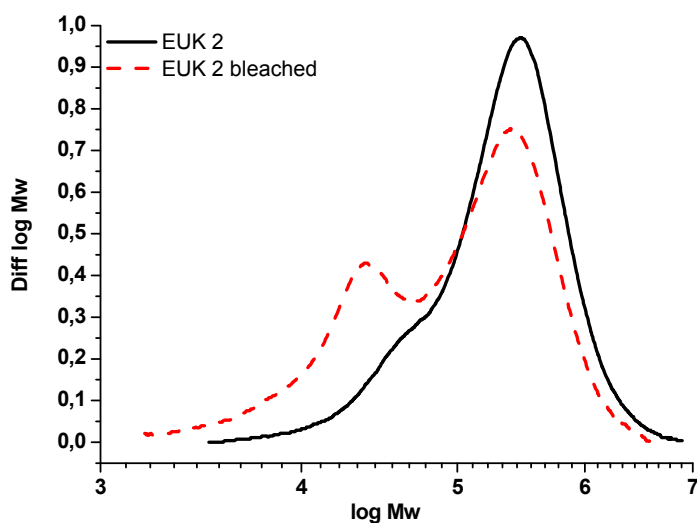
Figure 6. Comparison of differential molecular weight distribution of untreated and bleached eucalyptus kraft pulp surface layers (P- S1)

The changes that occur in the outer layer fraction of the sample caused by bleaching again resemble the changes observed for the entire fibre. However, the high molecular weight fraction was more severely affected in this sample fraction than in the entire fibre (Figure 7).
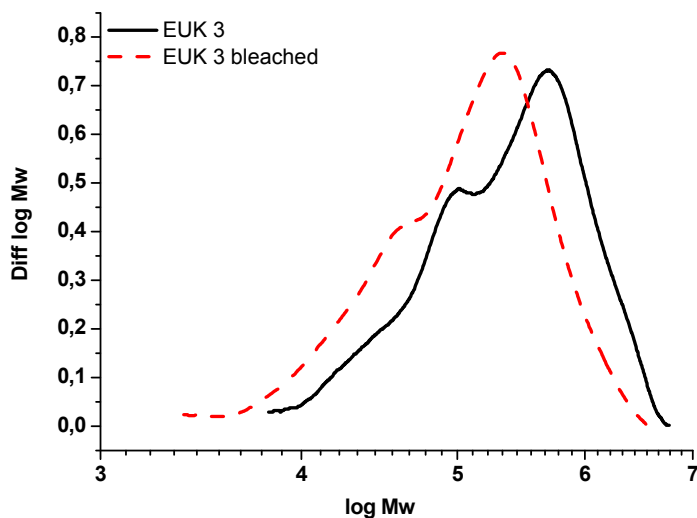
Figure 7. Comparison of differential molecular weight distribution of untreated and bleached eucalyptus pulp fibre wall main layers S2-S3

In spite of the rather exhaustive changes in the chemical composition during the fibre wall fractions, the ISO brightness of the isolated surface layers P-S1 remained much lower as compared to the main part of the fibre wall. P-S1 provided 50% ISO brightness as compared to 67% ISO brightness for the main part of the fibres.

In order to elucidate the distinctions in the chemical composition of the fractions before the bleaching, the *UV-spectra* (Figure 8) and the 1st derivative of the spectra were analysed. With 0.5% NaOH solution, the absorbance values at 218, 290, 330, 350, 386, and 390 nm are attributed to lignin. Strong absorbance of the alkaline extract from fibre surface layers at 245 nm and weaker UV-absorbance at 244, 254, 266, and 276 nm for the alkaline extract of the fraction enriched in S2 and S3 layers indicate the presence of heteroaromatic compounds of the furanoid (pyranoid) type.
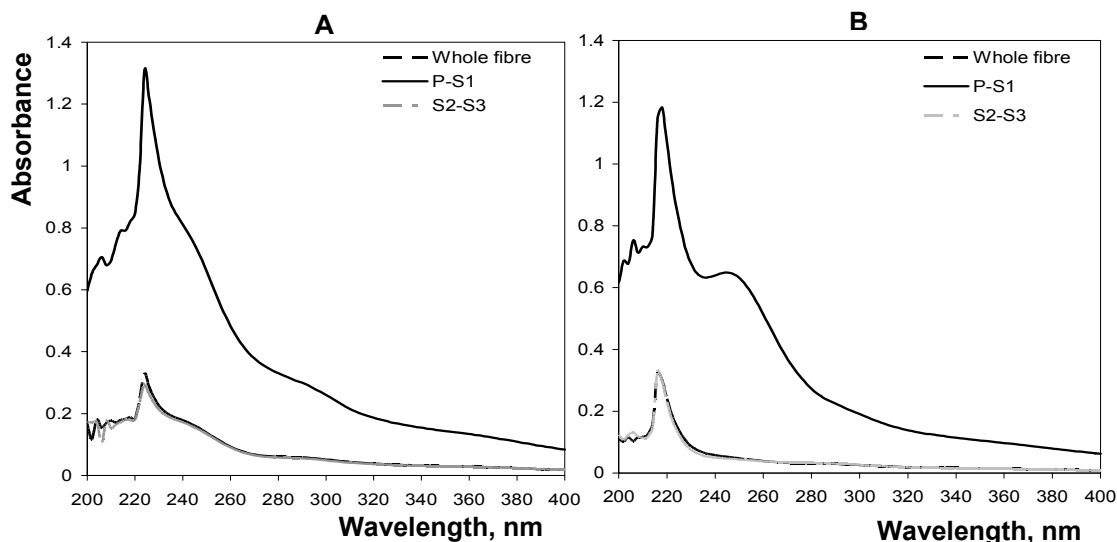
Figure 8. The UV-spectra of the alkaline extracts from unbleached P-S1 (upper curves) and S2-S3 fractions (lower curves); A – 0.5% NaOH; B – 10.0% NaOH

In 10% NaOH extracts, the absorbance at 235 nm is attributed to hexenuronic acids (HexA). From UV-spectra analysis we conclude that the content of lignin and hexenuronic acids are 3-4 times higher in the fibre surface layers as compared to whole pulp values. The content of heteroaromatic compounds (furanoids / furan resins) and oxypolysaccharides was also estimated to be much higher in the surface fraction.

For the bleached fractions the total NaOH solubility decreased and was 25% by mass for the fibre surface layers and 15% for the main part of fibre wall. The decrease of the absorbance of the components from surface fractions occurred over the whole spectral range. The absorbance drop at 218 nm and 250 nm by 45% and 63%, respectively, in the 10% NaOH extract of the surface P-S1 layers indicates the degradation of the heteroaromatic compounds possibly incorporated in the furan resins. The decrease of absorbance at 280-300 nm and around 340-360 nm indicates the elimination of both carbonyl groups and double bond conjugated structures in the fibre walls. The main part of the fibre wall, the S2-S3 layers, had lost most of the easily accessible fractions of hemicelluloses and HexA during the bleaching procedure as indicated by the decrease of the absorbance around 235 nm. At the same time an increase of the absorbance at 235 nm in the case of the polyoses from S2-S3 layers soluble in strong alkali points to some increase of HexA at the bleaching conditions used (no acidic stage applied).

Conclusions

The analysis of the samples shows clearly that the composition of the papermaking fibres (eucalyptus kraft pulp) surface layers differs from that of the main part of the fibre wall. It was shown that in spite of rather exhaustive changes during bleaching, ISO brightness of the isolated surface layers remains much lower.

The molecular data of the entire fibre wall are strongly influenced by the characteristics of the outer layer. This means that in technological processes, for example, during the bleaching, one has to consider not only the composition of the bulk fibre wall but also the properties of the comparatively tiny surface layers.

It is concluded that the upgraded hydromechanical peeling method can provide pulp fibre wall fractions both for analytical procedures and for further treatment and conversion.

Acknowledgements

References

Bohrn R., Potthast A., Schiehser S., Rosenau T., Sixta H. and Kosma P. (2006): The FDAM method: Determination of carboxyl profiles in cellulosic materials by combining group-selective fluorescence labeling with GPC. Biomacromolecules 7 (6), 1743-1750

Gromov V.S., Purina L.T., Treimanis A., Konstantinova L.M. and Kampuse A. (1976): Distribution of hemicelluloses and lignin in fiber walls of birch sulphite pulp. Khimiya Drevesini 5, 3-12

Krause T. (1967): Änderung der morphologischen Struktur und chemischen Zusammensetzung von Zellstoff-Fasern bei mechanischer Abschälung der äusseren Wandschichten. Das Papier 21(7), 385-393

Purina L., Treimanis A. and Timermane G. (1994): Distribution of residual lignin and hemicelluloses in the outer and central layers of organosolv pulp fiber walls. Nordic Pulp Paper Res. J. 9(2), 101-105, 119

Röhrling J., Potthast A., Rosenau T., Lange T., Ebner G., Sixta H. and Kosma P. (2002): A novel method for the determination of carbonyl groups in cellulosics by fluorescence labeling. 1. Method development. Biomacromolecules 3 (5), 959-968

Treimanis A. (2006): Advanced traditional methods of analysis of fiber surface layers – a powerful tool in research of lignocellulosics. La Chimica e l'Industria 88(2), 72-75

Treimanis A., Potthast A., Henniges U., Rosenau T., Grinfelds U., Bikova T. and Skute M. (2008): Analysis of mechanically peeled kraft pulp fibres surface layers. Papíripar 2008, 52, 225-230

Treimanis A., Grinfelds U. and Skute M. (2009): Are the pulp fiber surface layers the most resistant ones toward bleaching. Bioresources 4(2), 554-565

COMPARISON OF TWO DIFFERENT METHODS FOR FIBER-FIBER BONDED AREA MEASUREMENT

[1]Lisbeth Kappel, [1]Ulrich Hirn, [1]Wolfgang Bauer and [2]Robert Schennach

[1]Graz University of Technology, Institute of Paper, Pulp and Fiber Technology, Kopernikusgasse 24/II, 8010 Graz, Austria

[2]Graz University of Technology, Institute of Solid State Physics, Petersgasse 16/II, 8010 Graz, Austria

[1,2]CD-Laboratory for Surface Chemical and Physical Fundamentals of Paper Strength

ulrich.hirn@tugraz.at

Abstract

A method for measuring the bonded area of individual fiber-fiber bonds is presented. It is based on microtome serial sectioning and image analysis. The size and the three-dimensional structure of the bonded area are assessed together with the cross sectional fiber morphology. Additionally holes and unbonded fiber regions can be measured.

Based on the above, polarized light microscopy was used as a non-destructive reference method. Both methods were compared and the results show that the bonded area is over- or underestimated using polarized light microscopy depending on the refining state of the pulp that is used. A factor for this over- and underestimation was determined for unrefined and refined pulp, respectively. The methods presented in this article lead to a deeper understanding of fiber-fiber bonds and provide a basis for specific bonding strength measurements.

Introduction

Paper strength is developed from the strength of single fibers and the strength of the fiber-fiber bonds. Furthermore, the strength of the fiber-fiber bonds depends on the size of the bonded area as well as on the specific bonding strength. Non-destructive measurement of the bonded area in a fiber-fiber bond is a key goal to determine the specific bonding strength (bonding force per unit area) between fibers.

In this study we will demonstrate that polarized light microscopy is a suitable tool for measuring the bonded area of individual fiber-fiber bonds. Polarized light microscopy, as developed by Page (1960), was applied for fiber-fiber bonded area measurement. Page states that under polarized vertical illumination bonded areas appear dark while unbonded areas are bright. In earlier studies it has already been shown that polarized light microscopy shows the bonded area correctly, if one of the fibers in the fiber-fiber bond is dyed black (Kappel et al. 2010b). Still, it is not applicable for undyed fibers (Kappel et al. 2010a). We compare the results from polarized light microscopy to a measurement where the bonded area is determined using a 3D-representation of the fiber-fiber bond obtained with a microtome serial sectioning technique (Kappel et al. 2009).

Materials and Methods

Used Pulp

All experiments were performed with an unbleached Kraft pulp from spruce and pine wood. This pulp is usually used for the production of sack paper. Fiber-fiber bonds were prepared from unbeaten pulp as well as from pulp that was beaten during 9000 revolutions in a PFI mill. Half

of the fibers were dyed with Chlorazol Black and then dyed and undyed fibers were mixed creating bonds between the two types of fibers as given by Forsström and Torgnysdotter (2005).

Measuring the three-dimensional bonded area

The method for measuring the bonded area is based on microtome serial sectioning and image analysis. The size of the bonded area together with the three-dimensional structure of the bonded area and morphological parameters can be obtained from this method. The major steps of the method are shown in Figure 1.
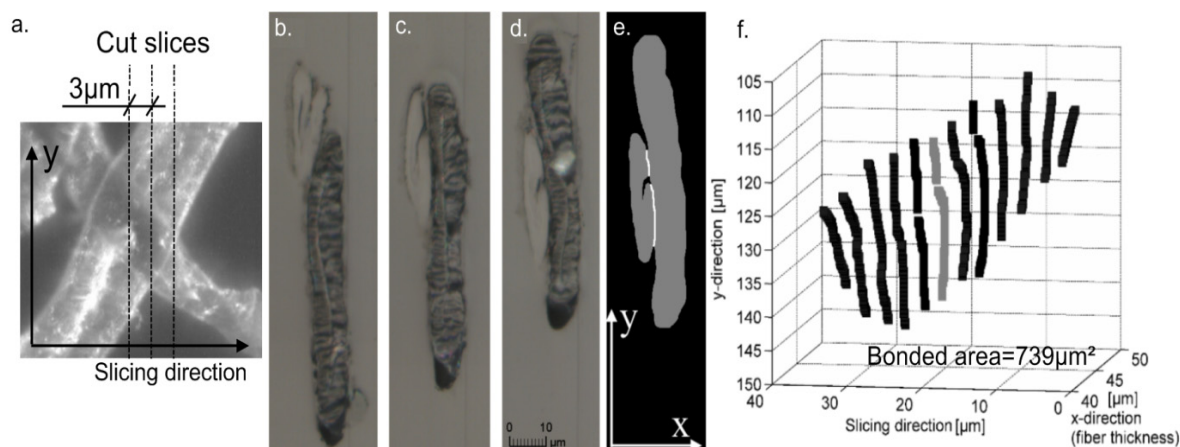
Figure 1. The same fiber-fiber bond under polarized light microscopy (a), in serial sectioning (b-d), after image analysis of one slice (e) and visualization of the 3D bonded area (f)

A single fiber-fiber bond (Figure 1a) is prepared according to Forsström and Torgnysdotter (2005), embedded in resin and clamped in a microtome. Slices with a thickness of 3 μm are cut off the embedded sample and the cutting area is imaged using an automated light microscope with an optical resolution of 0.16 μm/ pixel (Wiltsche et al. 2005). Figure 1b, c and d show images of the bond cross sections at different cutting positions. Fiber-fiber contact was determined by image analysis, yielding a bonding line for every cut, as indicated by the white line in Figure 1e. We are aware that the resolution of the optical microscope is too low to quantify whether the fibers really are in contact on a nanometer scale, we measure optically bonded area. Bonded area is calculated from bond line length and the cut thickness (3 μm). A three dimensional visualization of the bonding region was obtained by plotting these consecutive bonding lines (Figure 1f).

The size and 3-dimensional structure of the optically bonded area is assessed together with cross sectional fiber morphology (fiber cross sectional area, fiber perimeter, fiber wall thickness, fiber collapse and fiber width). Holes and overlapping but unbonded regions of the fiber edges are also identified.

Measuring the bonded area with polarized light

Page (1960) introduced polarized light microscopy for bonded area measurement of fiber-fiber bonds. The phenomenology of the method can be described as follows. Light is linearly polarized, so waves with only one plane of oscillation are directed through the objective and to the surface of the sample, where it is reflected. The second polarizing filter is rotated 90° towards the first one, so that only optically modified light is able to pass it. Light that is reflected at surfaces under vertical illumination does not change its state of polarization. Therefore reflexes at surfaces are of negligible intensity. The geometry of the optical system at the fiber-

fiber bond yields very small reflected over-all intensities, so that the fiber-fiber bonds appear dark, while the inner reflection at the back surface of a single fiber yields reflected light with quite a high intensity and a changed polarization direction. Thus single fibers appear bright.

The polarized light microscopy investigations were performed with a Leica Leitz DMRX microscope, which was equipped with crossed polarizing filters. A 20-fold objective with an optical resolution of 0.25 μm/Pixel was used. The images were taken with a Leica DFC290 camera. The fiber-fiber bonds were imaged in eight different rotary positions, the image with the highest contrast was chosen for further analysis (Kappel et al. 2010b). The bonded area, which appears dark under polarized light microscopy, was drawn manually and the amount of pixels in the dark region was determined using image analysis. Bonded area was calculated by multiplying number of pixels times area per pixel.

The bonded area was measured with polarized light microscopy and with microtomy. The size and shape of the bonded area were compared for the beaten and for the unbeaten pulp.

Explaining the deviations between the methods

Based on the measured morphological parameters several factors that may explain the deviations between the bonded areas measured with the two different methods were investigated. Multiple linear regression was performed to quantify the significance (F*-statistics) and impact (ANOVA) of the predictor variables (Neter et al.1996). The deviation between the measurement results was the response variable, all morphological parameters and the degree of bonding (holes and overlapping but unbonded regions of the fiber edges) were the predictor variables.

Results and Discussion

Comparison of bonded area for unbeaten pulp

Bonded area of 73 fiber-fiber bonds was measured with polarized light microscopy and with the microtome serial sectioning method, the results are compared in Figure 2. The diagonal indicates equal values. In general the values show quite good agreement, although bonded area is overestimated more often by polarized light microscopy. On average the values measured with polarized light microscopy were 12.5 % higher for the investigated bonds.

To explain this overestimation of bonded area a multiple linear regression model was built. Table 1 shows the significance (p-value of the F*-statistics) and the impact (ANOVA) of the variables. The results of the model are interpreted on basis of the stepwise R^2 values, i.e. the ANOVA. Because of redundancies and interactions the R^2 values alone are not really meaningful and are not used for interpretation of the results. The p-value shows the significance on a 95 % confidence level, this is the case if p is smaller than 0.05. Only the significant parameters are given in Table 1. It can be shown that unbonded fiber edges account for 56.7 % of the deviations (the R^2 value is 0.567). By adding the fraction of holes in the bond to the model, the stepwise R^2 value increased from 0.567 to 0.590, indicating that the holes in the bond explain further 2.3 % of the deviations. All other morphological parameters are not significant on a 95 % confidence level (i.e. p>0.05).

Figure 2. Comparison of bonded area measured with polarized light microscopy and with microtomy – unbeaten pulp

Table 1. Results of multiple linear regression and ANOVA with the deviation of bonded area between microtomy and polarized light microscopy as the response variable

Variable	R² stepwise	R² alone	p-Value	Sign of Coeff.
Unbonded fiber edges	0.567	0.567	$<10^{-5}$	- (minus)
Holes in the bond	0.590	0.092	0.03	- (minus)

The model results indicate that unbonded fiber regions cannot always be identified correctly with polarized light microscopy and lead to overestimation of the bonded area. The reason why unbonded fiber regions can only be identified in some cases is still under study.

Figure 3 shows an example where the fiber-fiber bonded area is overestimated with polarized light microscopy. The microtome image (left) shows that the left fiber is folded in the lower part of the bond. Here the fibers are not bonded, a small gap between the fibers is evident (see scale up in Figure 3, left). This unbonded fiber edges do not show under the polarized light microscope. It is rather suggested that the bonded area reaches over the border of the fiber-fiber crossing region, as the fold also appears as bonded fiber (marked with the white arrow, right).
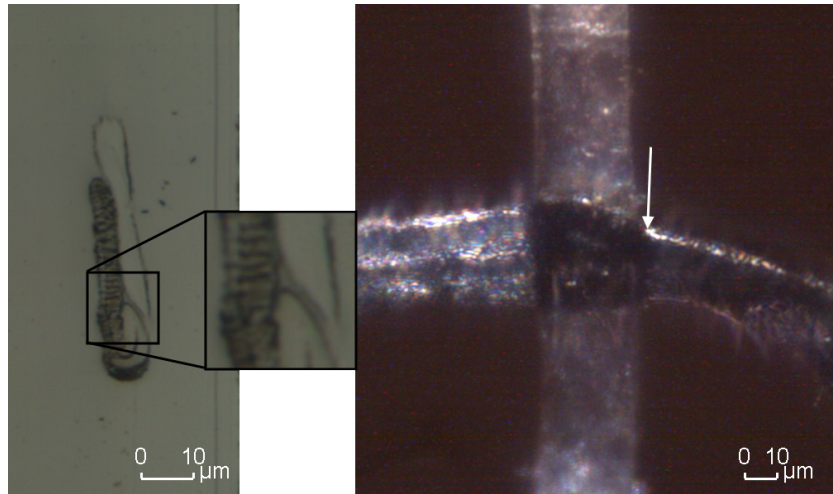
Figure 3. Overestimation of bonded area with polarized light microscopy: the fold appears dark under polarized light, although the fibers are unbonded in this region (marked with white arrow)

Comparison of bonded area for beaten pulp

Fiber-fiber bonds of a highly beaten pulp were analyzed first with the polarized light microscope and then with the microtome. The size and the shape of bonded area of 68 fiber-fiber bonds were compared. In Figure 4 bonded area measured with polarized light microscopy is plotted versus bonded area measured with the microtome. The diagonal indicates equal values. In contrast to the unbeaten case, now bonded area is underestimated by polarized light microscopy in most cases (on average by 15.9 %).
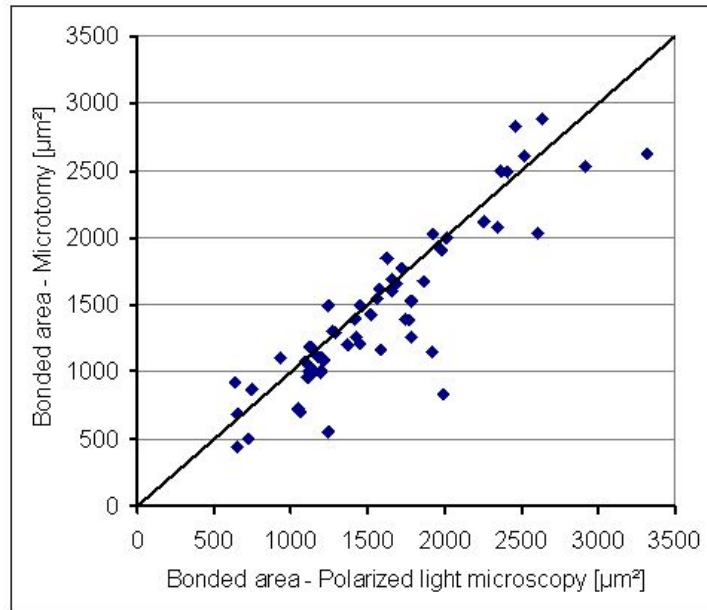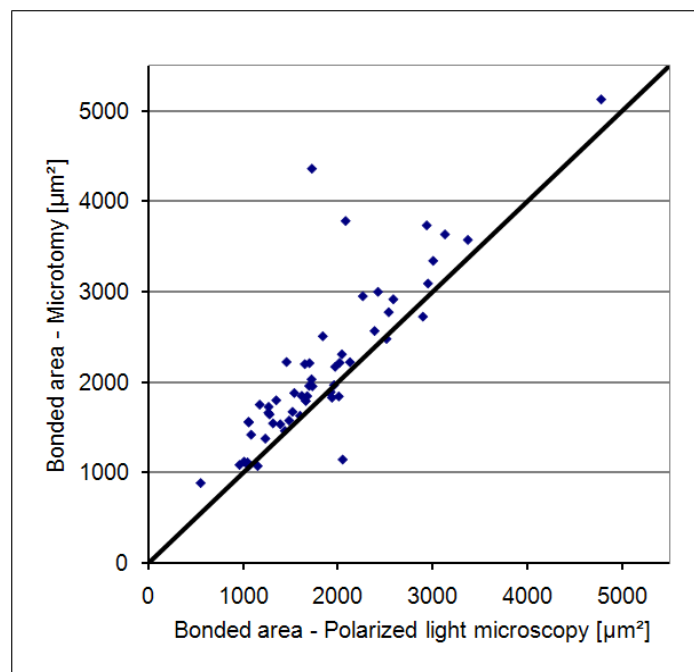

Figure 4. Comparison of bonded area measured with polarized light microscopy and with microtomy – beaten pulp

To explain the deviations between the measurement results again multiple linear regression modeling was performed. The mathematical model showed that none of the morphological parameters has a statistically significant influence on the deviations on a 95 % confidence level.

It seems as if most of the deviations between the measurement results can be explained only with the fibrils on the beaten pulp fiber surfaces, which cannot be reproduced with any of the applied measurement methods. The fibrils cause additional reflections, so that the polarized light microscope images are brighter in total. In the crossing region these bright reflections are evaluated as unbonded fiber edges and holes in the bond.

As an example, comparison of a polarized light microscope image with the fiber-fiber bond cross section is shown in Figure 5. The center of the bond appears brighter under the polarized light microscope (right), suggesting that the fibers are unbonded in this area. Also the fiber edges appear as unbonded under the polarized light. However, the microtome image on the left shows that the fibers are optically bonded over the entire length. This comparison confirms the assumption that additional reflections caused by fibrils are the origin of underestimation of the bonded area in the case of beaten pulp.
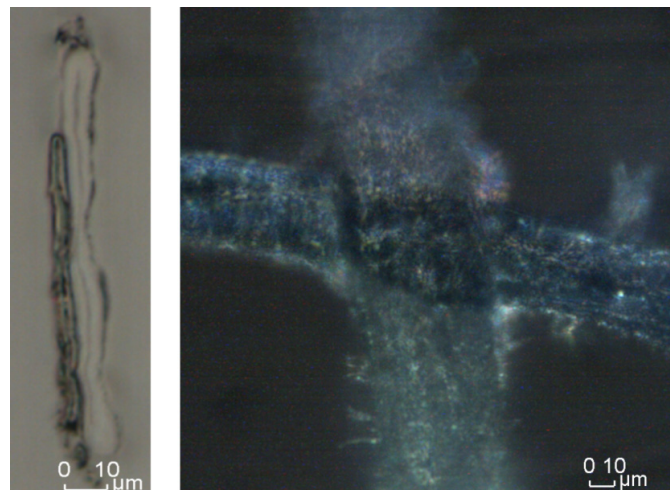
Figure 5. Underestimation of bonded area with polarized light microscopy: fibrils on the fiber surface are evaluated as holes in the bond and as unbonded fiber edges

Conclusions

The comparison of the two different methods showed that polarized light microscopy is an appropriate tool for fiber-fiber bonded area measurement. However, for unbeaten pulp the bonded area is overestimated while it is underestimated for beaten pulp. If these deviations are considered polarized light microscopy provides a non-destructive method for bonded area measurement. It can be applied in combination with micro tensile testing of fiber-fiber bonds in order to determine the specific bonding strength.

Acknowledgement

References

Forsström J. and Torgnysdotter A. (2005): Influence of fibre/ fibre joint strength and fibre flexibility on the strength of papers from unbleached kraft fibers. Nordic Pulp Paper Res. J. 20(2), 186-191

Kappel L., Hirn U., Bauer W. and Schennach R. (2009): A novel method for the determination of bonded area of individual fiber-fiber bonds. Nordic Pulp Paper Res. J. 24(2), 199-205

Kappel L., Hirn U., Gilli E., Bauer W. and Schennach R. (2010a): Revisiting polarized light microscopy for fiber-fiber bond area measurement - Part I: Theoretical Fundamentals. Nordic Pulp Paper Res. J. 25(1), 71-75

Kappel L., Hirn U., Gilli E., Bauer W. and Schennach R. (2010b): Revisiting polarized light microscopy for fiber-fiber bond area measurement - Part II: Proving the applicability. Nordic Pulp Paper Res. J. 25(1), 65-70

Neter J., Kutner M.H., Nachtsheim C.J. and Wassermann W. (1996): Applied Linear Statistical Models, Fourth Edition, Richard D. Irwin. Illinois (USA)

Page D.H. (1960): Fibre-to-fibre bonds Part 1 – A method for their direct observation. Paper Technology 1(4), 407-411

Wiltsche M., Donoser M., Bauer W. and Bischof H. (2005): A New Slice-Based Concept for 3D Paper Structure Analysis Applied to Spatial Coating Layer Formation. In Advances in Paper Science and Technology, Fund. Res. Symp., Cambridge, 853-899

PULP DEWATERING AND REFINING EFFICIENCY IMPROVEMENT BY CELLULASE TREATMENT

Ivo V. Valchev, Petar Y. Bikov

University of Chemical Technology and Metallurgy

8 Kl. Ohridski, 1756 Sofia, Bulgaria

ivoval@uctm.edu

Abstract

Refining and pulp drying are the most energy-intensive processes in the production of paper and boards. The usage of cellulases products is one of the modern methods to improve dewatering and refining efficiency.

The enzyme treatment was performed with the Novozymes AS cellulase product FiberCare[®]D.

The carried out investigation shows the positive effect of enzyme treatment on the secondary fiber dewatering. The obtained results of enzyme action can be interpreted by partial destruction of colloidal substances of secondary fibers.

The effect of enzyme treatment on the pulp strength properties shows insignificant increasing of breaking length, while the tear index and the burst index decrease. Probably the FiberCare[®]D action at low enzyme charge contributes to an improvement of the paper structure independent of fiber degradation processes. Optimal balance between paper qualities and pulp dewatering is reached at low level enzyme charge.

The pre-refining cellulase treatment of Svilocell and eucalyptus bleached pulp significant improves beating efficiency without pulp strength properties loss. The influence of enzyme treatment on the pulp yield and waste water pollution are not significant.

FiberCare[®] D is able to waste paper dewatering improvement and is a prerequisite for dryer steam consumption decreasing, refining energy costs saving and paper machine capacity increasing.

Introduction

Cellulase pulp treatment has been investigated for several years, with the goal of achieving improved refining efficiency and fiber dewatering. There are two methods for enzyme treatment. Addition of enzyme prior to refining has a very different effect compared with a post-refining treatment. Pre-refining application results in improved refining efficiency, while a post-refining treatment results in increased furnish freeness. A combination of the two can provide optimized strength and drainage benefits. This has been reported earlier (Moran 1996). Beating and refining are mechanical processes that enhance fibrillation and inter-fiber bonding. Properly applied, cellulases can enhance or restore fiber strength, reduce beating times, and increase inter-fiber bonding through fibrillation. A correctly applied enzyme treatment provides a tool that can improve recycled paperboard operations. This is accomplished by treating the refined stock with an enzyme blend to recover a portion of the freeness typically lost through refining. A pre-refining enzyme treatment can help the papermaker meet strength tests more readily through improved refining efficiency. Mill experience has shown that a combination of these two methods can provide strength and drainage benefits.

Distinguishing feature of secondary fibers is the breaking down of cell walls, causing liberating fine particles, which grow swollen and change in gel form. They retain water, slow down the dewatering, impede drying, and causing over-consumption of chemicals in the paper production. It is a known fact reported by Moran (1996) and Skartaunm et al. (1995) that cellulase lead to breaking down the gel form structures. They can be applied to improve the drainage by hydrolyzing the most accessible parts of cellulose and hemicellulose present in the fibers, fines and dissolved colloidal substances. This has been reported earlier by Valtschev et al. (2001).

Jackson et al. (1993) suggest that enzymes can either flocculate or hydrolysis fines and remove fibrils from the surface of large fibers. According to these authors, enzyme-aided flocculation occurred when a low enzyme dosage was used. In this case, fines and small fiber particles can aggregate with each other or with the larger fibers, decreasing the amount of small particles in the pulp and consequently improving pulp drainage. For higher enzyme concentration, flocculation became less significant, and fragmentation of the fibers began to predominate. Several authors (Miletzky 1996; Stock et al. 1995) have however observed a decrease in pulp strength properties by increase in enzyme quantities and reaction time.

Surface properties may be modified, not only because of enzymatic hydrolysis of the outer layers of the fiber, but also because of adsorption of enzyme molecules onto the fiber surface. It could be speculated by Pala et al. (2006) that changes in fiber–water interaction, induced by the presence of enzyme molecules, might be the factor responsible for drainage and strength modification.

The purpose of this work was to investigate the effect of the cellulase on refining and dewatering improvement and on pulp strength properties.

Materials and Methods

The investigations were performed with OCC pulp suplied by "Duropak - Trakia-Papir" AD – Pazardjik, deinking pulp provided by "Mayr-Melnhof" AD – Nikopol, bleached pulp supplied by Svilocell AD - Bulgaria and with bleached Brazilian eucalyptus pulp.

The enzyme treatment was performed with the Novozymes AS cellulase product FiberCare[®] D, which is designed to be effective, yet gentle on fibers. This is accomplished because FiberCare[®] D takes advantage of Novozymes' proprietary mono-component cellulase technology, resulting in a product that is highly specific and targeted in its action.

The enzyme treatmant conditions were as follows: pulp consistency 6 and 10 %, temperature 60°C, reaction time 60 min., enzyme charge 0.025 – 0.5 %, and pH 4 – 7.

The reducing sugars were determined according to a DNS method by Miller (1959).

Pulp beating was performed with Jokro mill according to DIN 54360 at duration from 10 to 50 min.

Degree of refining was determined in a Schopper Riegler apparatus according to ISO 5267. Rate of dewatering was determined on the same apparatus.

Pulp strength properties: breaking length, tear index and burst index were determined according to the ISO 1924, ISO 1974 and ISO 2758 respectively.

Results and discussion

The effect of FiberCare® D treatment on the dewatering time and refining degree of Duropak - Trakia-Papir OCC pulp is shown in Figure 1 & 2. The enzyme charge 0.05 – 0.2 % improved pulp dewatering by 20 - 45 % and refining degree up to 25% respectively. In paper production, dryer steam consumption could be reduced by over 4%. The obtained results of enzyme action can be interpreted to be due to partial degradation of colloidal substances of secondary fibers. That gel fraction retains water causing slower dewatering of secondary fibers.
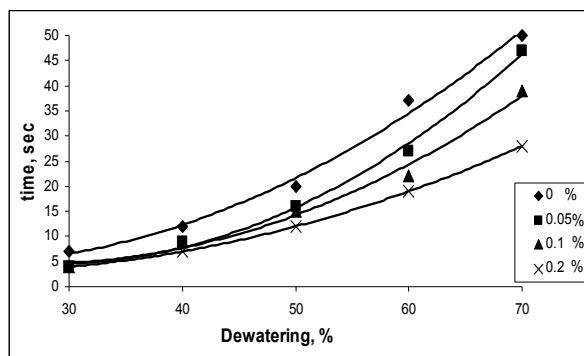
Figure 1. Influence of enzyme charge on the refining pulp dewatering rate, (pH 5, T=60°C and t = 60 min)
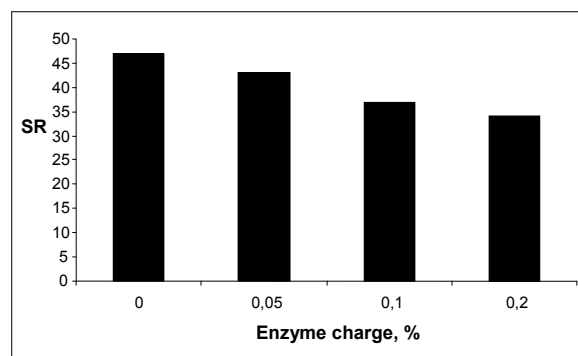
Figure 2. Effect of enzyme charge on the pulp degree (pH 5, T=60°C and t = 60 min)

A similar study of cellulase action on the pulp dewatering was conducted with deinking pulp supplied by "Mayr-Melnhof" AD. Typical feature of that pulp is the present of fillers (basic $CaCO_3$), pulp additives and mechanical fibers. A lower enzyme activity was found for this pulp, which makes it possible to charge a higher amount of FiberCare® D and still obtain the same dewatering.

The effect of enzyme treatment on the pulp strength properties is shown in Table 1. Breaking length slowly increased by the enzyme charge, while tear index and burst index decreased. Probably the FiberCare® D action at low enzyme charge contributed to an improvement in paper structure independent of fiber destruction processes.

Table 1. Effect of FiberCare® D charge on the recovered paper strength properties

Enzyme charge, %	Duropak - Trakia-Papir OCC pulp			Mayr-Melnhof – Nikopol deinking pulp		
	Breaking length, m	Tear index, $mN.m^2/g$	Burst index, $kPa.m^2/g$	Breaking length, m	Tear index, $mN.m^2/g$	Burst index, $kPa.m^2/g$
0	2720	4.5	2.7			
0.05	2740	4.4	2.7			
0.1	3040	3.7	2.5	2790	4.0	2.5
0.2	3000	3.3	2.2	3130	3.6	2.3
0.5				2970	3.2	2.1

Analysis of reduced sugars in the solution showed fiber losses of about 0.4 – 0.5 % which are connected with dissolving of colloidal substances. Optimal balance between paper qualities and pulp dewatering was reached at a low level of enzyme charge.

The effect of cellulase charge in pre-refining of chemical pulp treatment on the pulp beating efficiency was studied. The results obtained for the two types of bleached pulp, presented in Figure 3, show a total refining degree increase with 14 SR and 24 SR for eucalyptus and

Svilocell pulps respectively. The performed investigation on the effect of enzyme charge on the strength properties of the two types of pulp show improvement in the breaking length, while the tear index was not adversely affected by FiberCare[®] D at low dosage (Table 2).
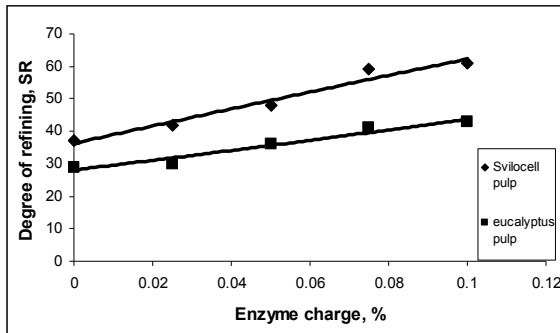
Figure 3. Influence of enzyme charge on the refining efficiency
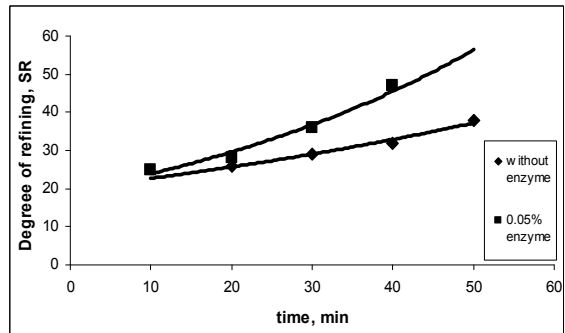
Figure 4. Effect of enzyme treatment (pH 4.5, T=60°C, t=60 min) on the rate of eucalyptus pulp beating

Table 2. Influence of pre-refining cellulase charge on the pulp strength properties

Enzyme charge, %	Svilocell pulp, pH 6.5, T=60°C, t = 60min			Eucalyptus pulp, pH 4.5, T=60°C, t = 60min		
	Breaking length, m	Tear index, mN.m^2/g	Burst index, kPa.m^2/g	Breaking length, m	Tear index, mN.m^2/g	Burst index, kPa.m^2/g
0	5200	5.0	4.2	7800	5.2	5.6
0.025	5300	5.1	4.2	7900	5.2	5.7
0.050	5400	4.9	4.3	8200	5.3	6.4
0.075	5450	4.7	4.3	8200	4.8	6.1
0.1	5600	4.4	4.4	8100	4.6	6.0

The influence of enzyme action on the rate of eucalyptus pulp beating can be seen in Figure 4. It can be observed that pulp refining degree 40 SR was reached 20 min. less in the case of FiberCare[®] D treatment. In the same time the pulp strength properties dependence between tear index and breaking length is common (Figure 5).
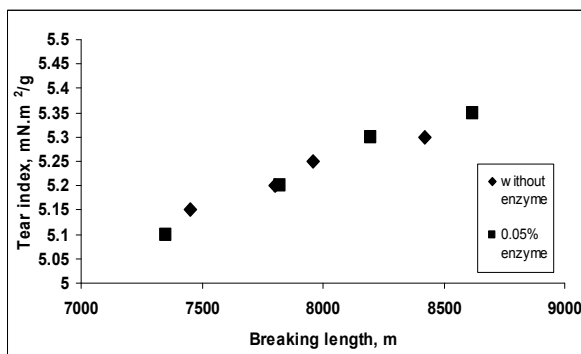
Figure 5. Influence of enzyme treatment on the eucalyptus pulp breaking length - tear index dependence
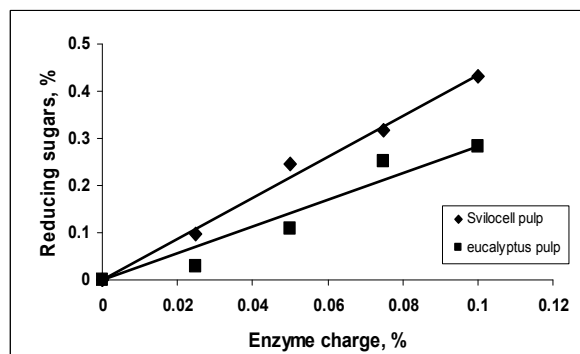
Figure 6. Effect of enzyme charge on reducing sugar formation

Therefore the obtained significant beating improvement to a given refining degree by FiberCare[®] D treatment at low enzyme dosage up to 0.05% did not affect on pulp strength properties, which can be developed with less refining energy requirements.

The obtained reducing sugars as a result of enzyme treatment were in the range up to 0.4 % oven-dry pulp in relation to enzyme charge and type of pulp (Figure 6). At optimal dosage of FiberCare[®] D (0.025% for Svilocell pulp and 0.05% for eucalyptus pulp) the generated sugars were less than 0.2%. Therefore, after enzyme treatment the yield loss and waste water pollution were not significant.

Conclusions

The carried out investigations on cellulase treatment of secondary fiber materials by FiberCare[®] D show an opportunity for significant improvement of pulp dewatering. Breaking length improvement at an optimum enzyme dosage was obtained, and the cellulase affected mainly dissolved colloidal substances and slightly reduced the pulp yield. FiberCare[®] D efficiency depends on the type of secondary fibers and enzyme activity decreases on the presence of fillers and pulp additives. The pre-refining enzyme treatment significantly improved beating efficiency without pulp strength properties deterioration. At optimal FiberCare[®] D dosages 0.025% - 0.05%, the yield loss and waste water pollution were not significant.

The established effect of the enzyme treatment on pulp beating or waste paper dewatering is a prerequisite for decreasing dryer steam consumption, for refining energy cost saving and for paper machine capacity increase.

References

Jackson L., Heitmann J. and Joyce T. (1993): Enzymatic modifications of secondary fibre. Tappi J. 76(3), 147–154

Miletzky F. (1996): Biotechnology in the pulp and paper industry. *In*: Biotechnol. Pulp Paper Ind. Recent Advances in Applied and Fundamental Research. Eds: Srebotnik, E. and Messner, K. Facultas-Universitätsverlag, Wien, 1996, pp. 9-15

Miller G. (1959): Use of Dinitrosalicylic Acid Reagent for Determination of Reducing Sugar. Anal. Chem. 31, 426 -/428

Moran B. (1996): Enzyme treatment improves refining efficiency, recycled fiber freeness. Pulp and Paper 70(9), 119-121

Pala H., Mota M. and Gama F. (2002): Enzymatic Modification of Paper Fibres. Biocatalysis and Biotransformation 20 (5), 353–361

Skartaunm P., Reinhardt B. and Trasser G. (1995): Einfluss der Enzyme als Entwässerungs - und Hilfsmittel bei der Mahlung in der Papierindustrie, PTS - VB 02/95 - PTS-TUD-Symposium "Zellstofftechnik für Papier", 1995, 5, Dresden

Stock G., Pereira H., Wood T. and Dusterhoft E. (1995): Upgrading recycled pulps using enzymatic treatment. Tappi J. 78(2), 79

Valtschev I., Bentscheva S. and Christova E. (2001): Einfluss der Enzyme bei der Veredlung von Sekundärfaserstoffen. Wochenblatt für Papierfabrikation 20, 1348-1351

INFLUENCE OF CELLULASE TREATMENT ON THE INDIVIDUAL FIBER STRUCTURE AND THE PAPERMAKING PROPERTIES

Ivo V. Valchev[1], Ventsislav N. Blyahovski[1], Petar Y. Bikov[1], Sanchi K. Nenkova[1] and

Harald Grossmann[2]

[1] UCTM, Sofia, Bulgaria, e-mail: ivoval@uctm.edu

[2] TU, Dresden, Germany, e-mail: harald.grossmann@tu-dresden.de

Abstract

Traditionally, chemical and mechanical treatments have been used in fiber processing. Such treatments affect the morphology of the fiber-wall structure at micro and nano level. The use of enzyme to modify the fiber surfaces and properties of paper fibres has received increasing interest. Cellulase treatment was observed to give internal fibrillation of the fibres and resulted in defects of the fiber surfaces. The defects were more prevalent at higher enzyme dosage. These results indicate that the enzyme action is local. The existing fiber defect might be the starting point of the enzyme action.

Beating and refining are mechanical processes that enhance fibrillation and inter-fiber bonding. Properly applied, cellulases can enhance or restore fiber strength, reduce beating time, and increase inter-fiber bonding through fibrillation. A pre-refining enzyme treatment can help the papermaker to meet strength tests more readily through improved refining efficiency.

The purpose of this work was to investigate the impact of cellulase treatment on the structure of the individual fibers, as well as on the beating efficiency, the pulp strength properties and the correlations between them.

The research was made with hardwood pulp provided by "Svilocell" AD, Svishov, and Brazilian eucalyptus pulp.

It has been established that the pre-refining cellulase treatment at optimal FiberCare® B dosage significantly improves the beating efficiency. Enzyme treatment reduced Svilocell fiber length and fiber volume and increased the fines fraction, compared to the eucalyptus pulp. In spite of some reduction in the length of individual fibers, the strength properties of the hand-made pulp sheets were not much affected.

The established FiberCare® B effects on the pulp beating is a precondition for refining energy cost saving and for reduced use of paper chemicals.

Introduction

The pulp and paper industry processes large quantities of lignocellulosic biomass every year. The technology for pulp manufacture is highly diverse, and numerous opportunities exist for the application of microbial enzymes. Historically, enzymes have found some uses in the paper industry, but these have been mainly confined to areas such as modifications of raw starch. However, a wide range of applications in the pulp and paper industry have now been identified. The use of enzymes in the pulp and paper industry has grown rapidly since the mid 1980s. While many applications of enzymes in the pulp and paper industry are still in the research and development stage, several applications have found their way into the mills in an unprecedented short period of time. This has been reported earlier (Bajpai 1999).

Jackson et al. (1993) suggested that enzymes can either flocculate or hydrolysis fines and remove fibrils from the surface of large fibers. According to these authors, the enzyme-aided flocculation occurs when a low enzyme dosage is used. In this case, fines and small fiber particles aggregate with each other or with the larger fibers, decreasing the amount of small particles in the pulp and consequently improving pulp drainage. For higher enzyme concentration, flocculation becomes less significant, and fragmentation of the fibers begins to predominate. A numbers of authors (Miletzky 1996; Stock et al. 1995) have observed that pulp strength properties decrease at increase of enzyme quantities and by increased reaction time.

A related strategy is to add cellulase enzymes to papermaking furnish after the refining. The object then is to remove very fine, fibrillar material from the suspension and from fiber surfaces so that water can drain more easily. In principle, better dewatering means that less water has to be evaporated in the dryer section of a paper machine - a major area of energy consumption. More often, however, the faster dewatering rates mean increased machine speeds and higher production rates. The same thing was reported by (King et al. 1998).

The extent of the modification of fiber morphology by the action of cellulases remains unclear. However, if the enzymes could selectively alter the outermost surfaces of pulp fibers, it is possible that inherent characteristics, such as stiffness and collapsibility, could be modified to enhance conformability and inter-fiber bonding. This is given by (Blanco et al. 1998; Mansfield et al.1997). Drying of the fibers results in a hornification phenomenon whose consequences can clearly be observed by the deterioration of fiber properties as reported by Jayme (1994) and Weise (1998).

Our previous investigations on cellulase treatment of secondary fiber materials by FiberCare[®]D indicated an opportunity for significant improvement of pulp dewatering. The pre-refining cellulase treatment significantly improved beating efficiency, without deterioration of pulp strength properties. At optimal dosages, the yield loss and waste-water pollution were low.

The purpose of this work was to investigate the impact of cellulase treatment on the structure of the individual fibers, as well as on beating efficiency, pulp strength properties and correlations between them.

Materials and Methods

The research was made with mixture hardwood kraft pulp provided by "Svilocell" AD, Svishov, and Brazilian eucalyptus pulp.

The cellulase product FiberCare® B by Novozymes AS Denmark was used in the selected conditions; pulp consistence 6 %, temperature 60 °C, reaction time 60 min., enzyme charge 0,0125 % - 0,05 % and pH 5 - 6.

Pulp beating was performed with a Jokro mill according to ISO 5264-3. The degree of refining was determined in a Schopper-Riegler apparatus, according to ISO 5267-1. Pulp strength properties were determined according to ISO 1924-2 and ISO 1974.

The fiber structure was measured on kajaani FiberLab™, according to ISO 16065-1 and SEM on JEOL JSM-5510.

Results and Discussion

Cellulase pre-refining treatment shows that beating efficiency increased by 15 SR and 17 SR for eucalyptus and Svilocell pulp respectively (Figure 1). Higher SR was due to the production of more fines after pulp treatment by FiberCare B. It seems as if the effect of the treatment was more visible in the Svilocell pulp than in the eucalyptus pulp. Enzyme treatment of eucalyptus pulp improved beating efficiency without fiber length reduction at 0.05% dosage (Figure 2).
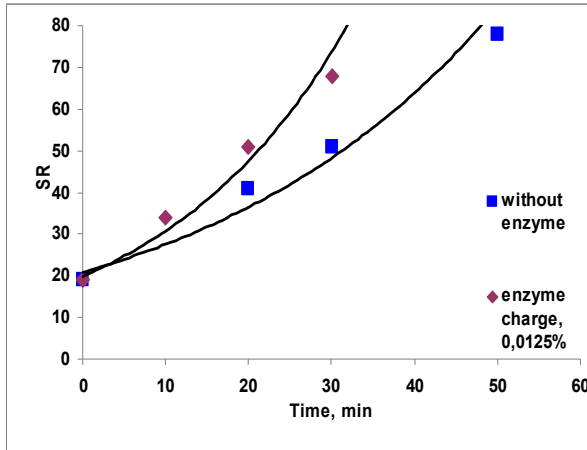
Figure 1. Effect of enzyme treatment on the rate of Svilocell hardwood pulp beating
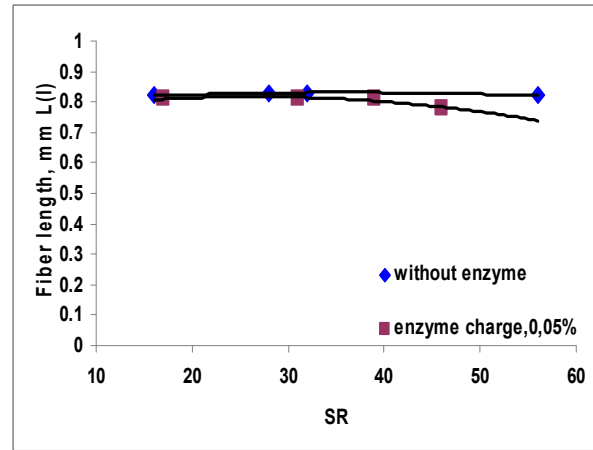
Figure 2. Effect of enzyme treatment on eucalyptus pulp fiber length during beating

Different dosage of FiberCare® B treatment lead to a larger Svilocell fiber length reduction as compared with eucalyptus pulp (Figure 3), giving effects on the pulp strength properties. For the Svilocell pulp it is recommended that the enzyme is dosed at a low amount, in order not to decrease the strength properties. The morphology of Svilocell pulp required lower enzyme dosage (0.0125 %).
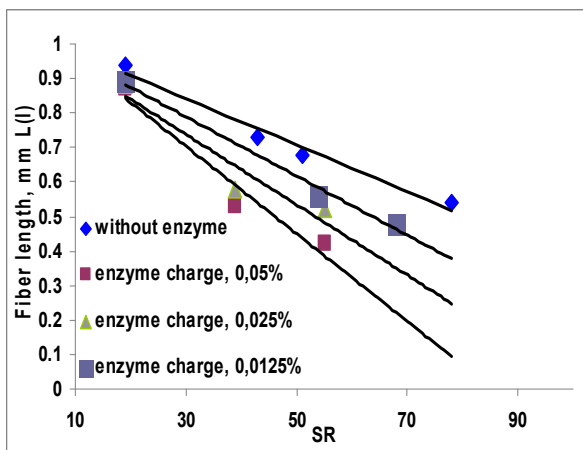
Figure 3. Influence of enzyme treatment on the Svilocell fiber length during beating
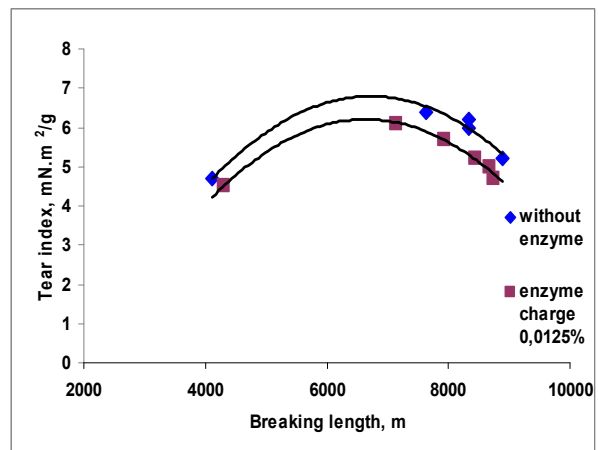
Figure 4. Svilocell pulp breaking length – tear index dependence

FiberCare® B pre-refining treatment reduced the tear index of Svilocell pulp while the eucalyptus pulp was not affected at low dosage (Figure 4 and 5).
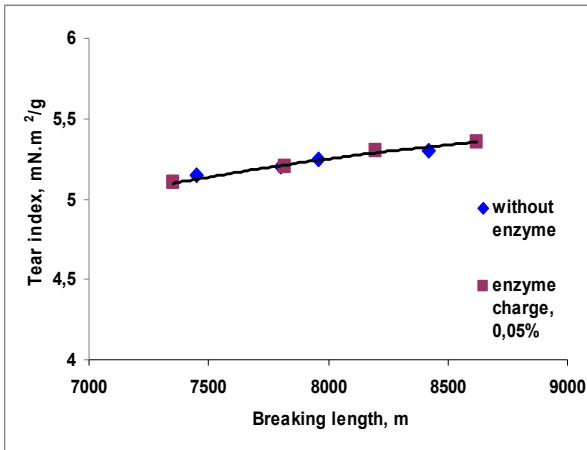
Figure 5. Eucalyptus pulp breaking length tear index dependence
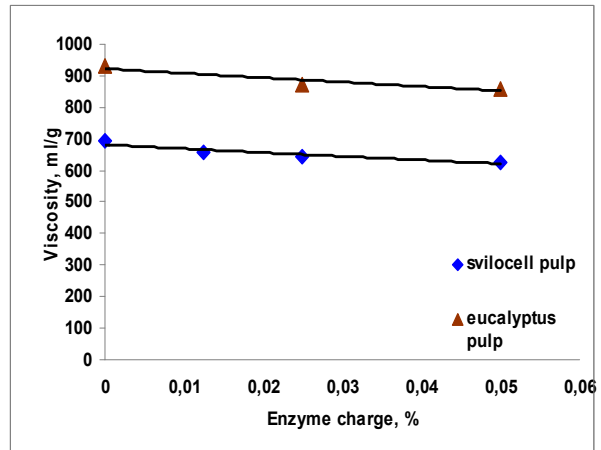
Figure 6. Influence of enzyme charge on Svilocell and eucalyptus pulp viscosity

With increasing of FiberCare® B charge, the pulp viscosity slightly dropped and a correlation between fiber length and viscosity was observed (Figure 6 and 7).
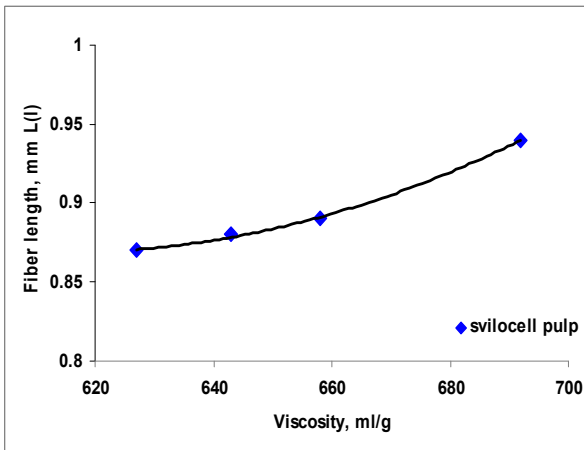
Figure 7. Svilocell pulp fiber length – viscosity dependence as a result of enzyme dosage

FiberCare® B treatment lead to a larger Svilocell fiber volume reduction as compared with the eucalyptus pulp (Figure 8 and 9). With increasing enzyme dosage and SR the fiber volume was reduced with about 50%. This can positively affect paper printing properties. The effect on the eucalyptus pulp was minimal (Figure 9).

The fines fraction of FiberCare® B treated Svilocell pulp was a few times higher as compared with the eucalyptus hardwood pulp. This is probably due to differences in fiber morphology, which varied more in the Svilocell hardwood pulp. The cellulase reacts dominantly on the fiber surface and increased fines, which reflects on the beating efficiency. In the Svilocell pulp the fines fraction increased strongly with about 15 % (Figure 10), while fines fraction in the eucalyptus pulp increased insignificantly at the same enzyme dosage (Figure 11). For both types of pulps, FiberCare® B did not affect the fibrillation index (Figure 12 and 13).

FiberCare® B did not affect cell wall thickness and cross section area (CSA), because the enzyme reacts mostly on the fiber surface for both cellulose pulp types (Figure 14 and 15).
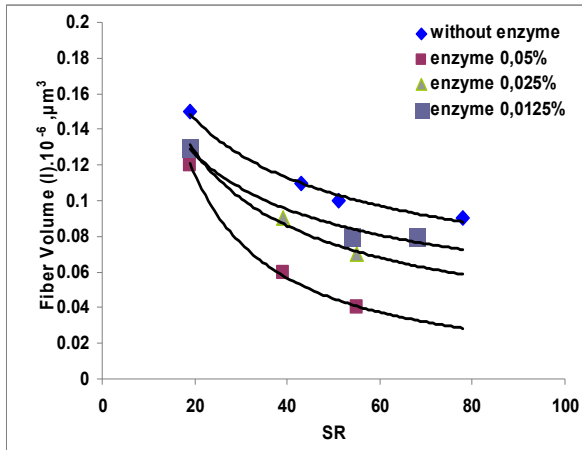
Figure 8. Influence of enzyme treatment on Svilocell fiber volume during beating
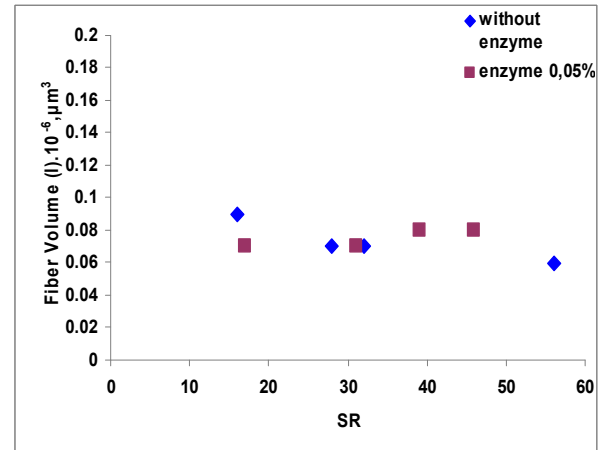
Figure 9. Influence of enzyme treatment on eucalyptus fiber volume during beating
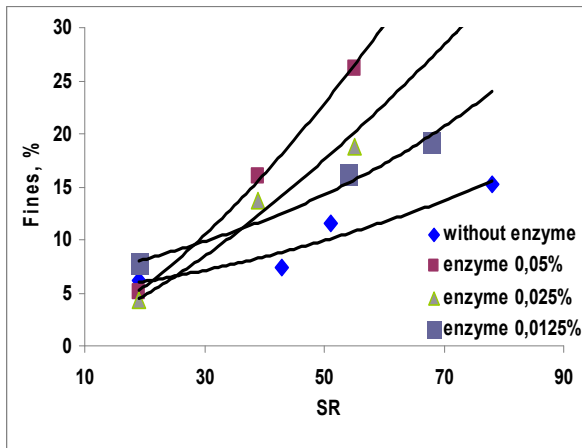
Figure 10. Influence of enzyme treatment on the Svilocell pulp fines fraction during beating
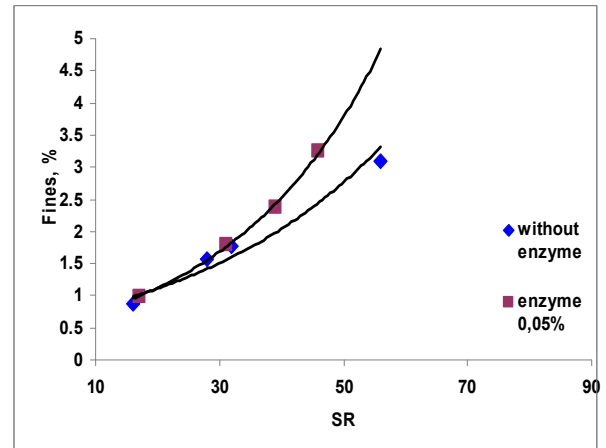
Figure 11. Influence of enzyme treatment on the eucalyptus fines fraction during beating
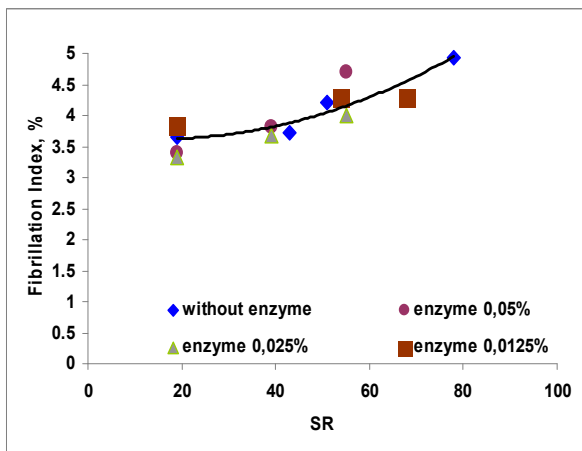
Figure 12. Influence of enzyme treatment on the Svilocell pulp fibrillation index during beating
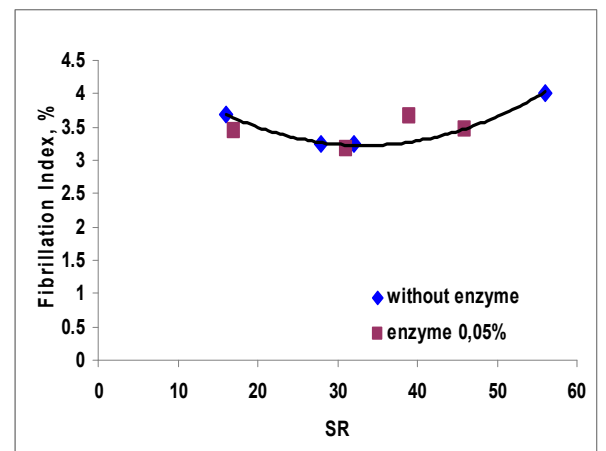
Figure 13. Influence of enzyme treatment on the eucalyptus pulp fibrillation index during beating
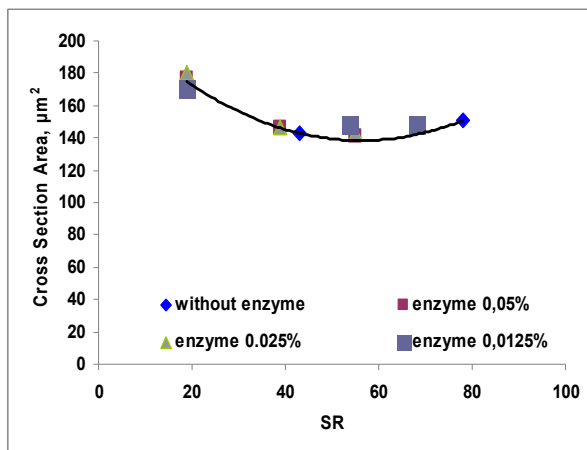
Figure 14. Influence of enzyme treatment on Svilocell CSA during beating
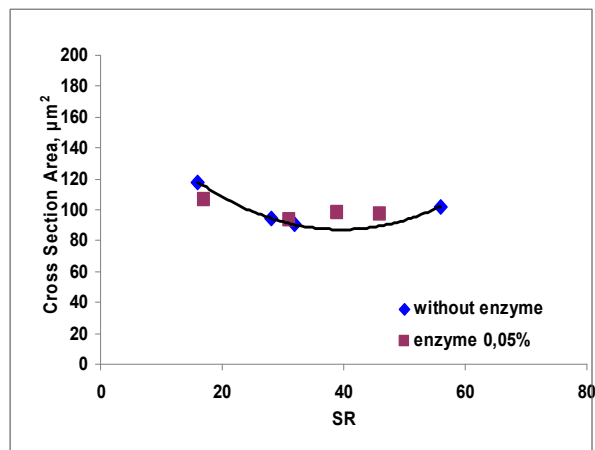
Figure 15. Influence of enzyme treatment on the eucalyptus pulp CSA during beating

Scanning electron microscopy, SEM

SEM was applied to make certain fiber wall characteristics visible. The SEM images of the Svilocell hardwood and the eucalyptus pulps reveal that the enzyme-modified fibers have a cleaner surface (Figures 16-20). That can give reduced chemicals consumption in paper production and open up new possibilities for further fiber processing. Some fibrillation which is due to the enzyme action was observed.
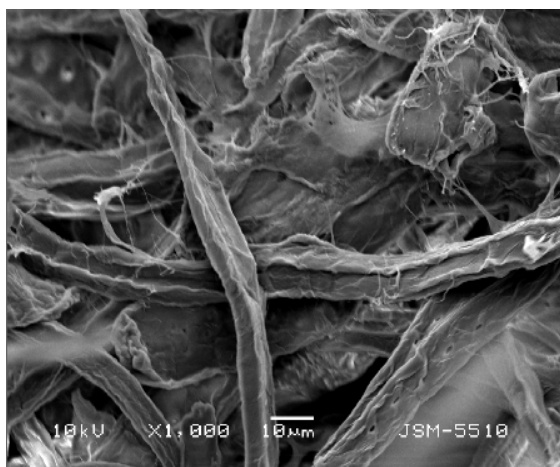
Figure 16. Svilocell pulp without enzyme
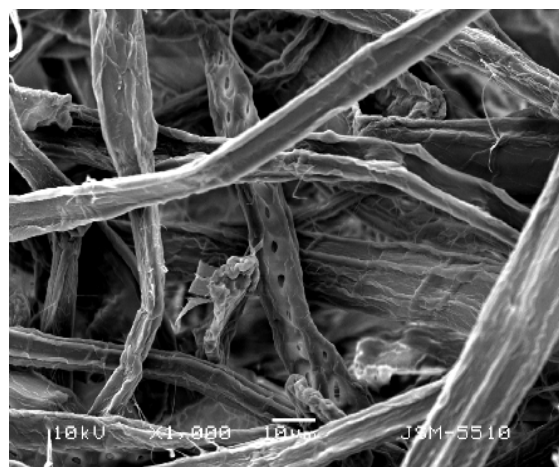
Figure 17. Svilocell pulp treated with 0.0125% FiberCare® B
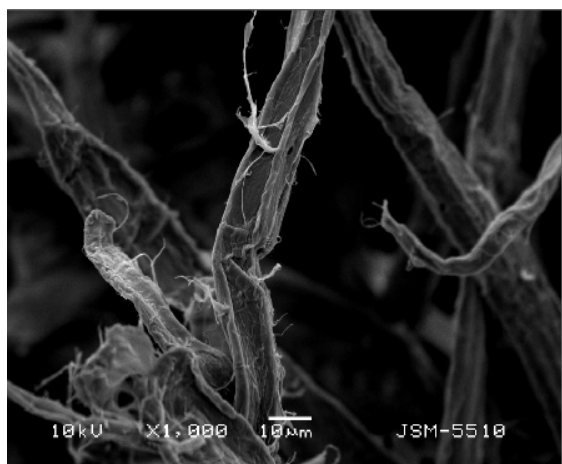
Figure 18. Svilocell pulp treated with 0.05% FiberCare® B
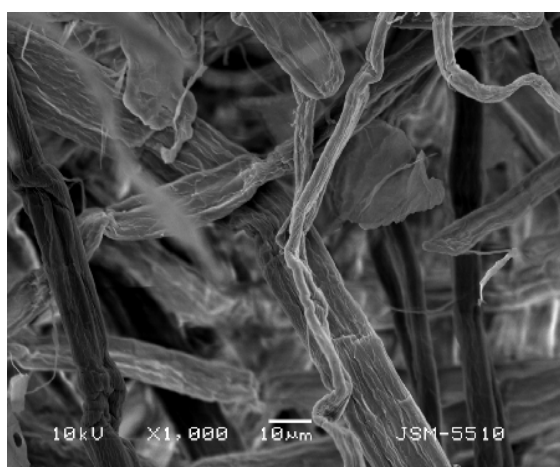
Figure 19. Eucalyptus pulp without enzyme
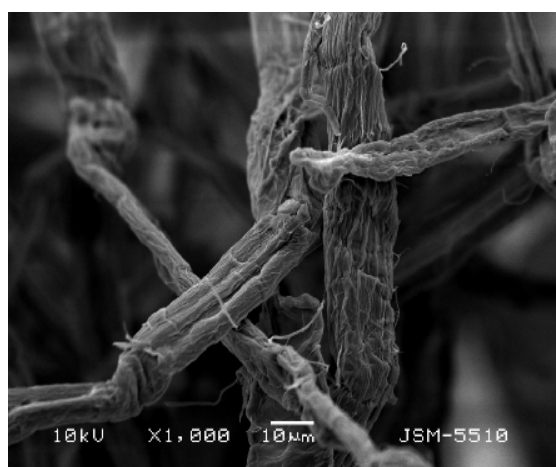
Figure 20. Eucalyptus pulp treated with 0.05% FiberCare® B

Conclusions

The pre-refining cellulase treatment at optimal enzyme dosage significantly improved the beating efficiency and increased the amount of fines. For the Svilocell pulp it was found that the optimal cellulase dosage is 0.0125%, while for the eucalyptus pulp that dosage is 0.05%.

FiberCare® B treatment more significantly reduced Svilocell fiber length and fiber volume and increased the fines fraction, as compared with eucalyptus pulp.

Cellulase did neither affect the fibrillation index, nor the cell wall thickness nor cross section area.

SEM imaging of the pulps showed that the enzyme action modified the fiber surfaces which offer new possibilities in fiber processing.

The established FiberCare® B effects on pulp beating may be considered as a pre-condition for saving of refining energy costs and reduction in paper chemicals. Further investigations will be carried out to find the effects of cellulase treatment on chemical consumption in papermaking and on properties of different paper types.

References

Bajpai P. (1999): Application of Enzymes in the Pulp and Paper Industry. Biotechnol. Prog. 15, 147-157

Blanco A., Díaz P., Martínez J., Vidal T., Torres A. and Pastor F. (1998): Cloning of a new endoglucanase gene from *Bacillus* sp. BP-23 and characterisation of the enzyme. Performance in paper manufacture from cereal straw. Appl. Microbiol. Biotechnol. 50, 48- 54

Jackson L., Heitmann J. and Joyce T. (1993): Enzymatic modifications of secondary fibre. Tappi J. 76(3), 147–154

Jayme G. (1994): Mikro-Quellungsmessungen an Zellstoffen. Wochenbl. Papierfabr. 6, 187–194

King V., Dykstra G. and Glover D. (1998): Chemistry holds key to maintaining speed in today's paper machines. Tappi J. 81(7), 58-61

Mansfield S. and Saddler J. (1997): The use of enzymes to enhance Douglas-fir pulp characteristics. *In*: Biol. Sci. Symp. Tappi Press, San Francisco, California, pp. 279 – 282

Miletzky F. (1996): Biotechnology in the pulp and paper industry. *In:* Biotechnol. Pulp Paper Ind. Recent Advances in Applied and Fundamental Research. *Eds:* Srebotnik, E. and Messner, K. Facultas-Universitätsverlag, Wien, 1996, pp. 9-15

Stock G., Pereira H., Wood T. and Dusterhoft E. (1995): Upgrading recycled pulps using enzymatic treatment. Tappi J. 78(2), 79-88

Weise U. (1998): Hornification. Mechanisms and Terminology. Paperi ja Puu. Paper and Timber 80, 110–115

CHARACTERIZATION OF INITIAL AND MODIFIED SAMPLES OF BLEACHED KRAFT PULP AND COTTON CELLULOSE

Michael Ioelovich

Designer Energy Ltd, Rehovot, Israel

E-mail: bd895892@zahav.net.il

Abstract

Morphology, chemical composition, supermolecular structure and properties of initial and modified samples of bleached Kraft pulp and cotton cellulose have been studied. The initial cellulose samples were characterized by increased content of α-cellulose, absence of lignin and high brightness. The lower ordered pulp had a higher reactivity at acid hydrolysis and alkalization than the more ordered cotton cellulose. Treatment with boiling acid to prepare microcrystalline cellulose lead to increased crystallinity and lateral size of crystallites, while mercerization of the initial cellulose samples caused formation of CII crystalline polymorph, decreasing of crystallinity, lateral size, and length of crystallites. Cellulose properties such as specific volume, accessibility at deuteration, wetting enthalpy and sorption of water vapor, correlated with the content of non-crystalline domains and crystallinity. This permits forecast of some essential properties of the cellulose on the base of its crystallinity degree. And vice versa, testing of sample properties, e.g. sorption of water vapor, permitted estimation of crystallinity and content of non-crystalline domains in cellulose.

Keywords: Cellulose, Structure, Properties, Correlations

Introduction

Various physical, physico-chemical, chemical and biological methods have been used to study structure and properties of cellulose samples. Along with standard, also advanced methods are applied for the characterization of celluloses. One problem is that various companies, institutions and researches have different equipments and investigation methods giving different testing results. Therefore COST Action E54 in 2007-2008 decided to use common pulp samples to be analyzed by the Action members by standard and advanced techniques. A bleached Kraft pulp produced by Södra Cell in Sweden, was a second Common Pulp produced for this purpose. Along with wood pulps, also cotton celluloses take a significant place in papermaking. Cotton can be used for production high-quality and specialty paper types, such as tissue paper, technical papers, albums, drawing, and some printing papers, banknote and document papers, etc. In addition, cellulose is a base material for production of some derivatives such as modified celluloses, e.g. microcrystalline, mercerized and regenerated cellulose, as well as cellulose esters and ethers. In this case reactivity of cellulose plays a vital part.

The purpose of this paper was to characterize original and modified samples of the bleached Kraft pulp and cotton cellulose using standard and advanced methods.

Materials and Methods

Bleached Kraft pulp (Common Pulp II) was received in July 2008. The pulp (Södra Cell, Sweden) contained a mixture spruce (*Picea abies*) and pine (*Pinus sylvestris*) in a weight ratio of about 80:20, and 0.1% Klason lignin, 83.8% cellulose and 14.3% hemicelluloses as analyzed by Stora Enso, Karlstad, Sweden (cf. Table 4c in Heinemann and Ander 2011).

The middle-length fibers "Acala" was used as initial cotton material. Cotton cellulose was prepared by soda cooking of the initial cotton fibers. Cooking solution contained 1% NaOH, 0.5% H_2O_2 and 0.5% non-ionic surfactant Tergitol NP-9. Cooking was carried out at temperature 150 °C for 3 h.

Samples of microcrystalline cellulose (MCC) were obtained by treatment of initial cellulose materials with boiling 2 N HCl for 1h; then the acidic product was washed up to neutral pH, dispersed in water by Waring-blender, and spray-dried. Mercerization of the initial celluloses was carried out by treatment with 20% NaOH at ratio 1:20, room temperature for 24 h with the following washing and drying at 105°C up to constant weight.

X-ray Diffraction

Supermolecular structure (Krässig 1993) of the cellulose samples was tested by improved X-ray diffraction (Ioelovich 1992). Rigaku-Ultima Plus diffractometer (CuK_α – radiation, λ=0.15418 nm) was used for X-ray investigations. Diffractograms were recorded in the φ=2Θ angle range from 5 to 80°. After recording of the diffractograms, the background was separated, corrections for Lorentz factor, polarization, and intensity of primary beam were made, and X-ray patterns were normalized. Then, diffraction intensities from crystalline and non-crystalline regions were separated by computerized method (Vonk 1973). The procedures allowed calculation of degree of crystallinity (X) according to equation

$$\mathbf{X} = \int \mathbf{J_c}\, \mathbf{d\varphi} / \int \mathbf{J_o}\, \mathbf{d\varphi} \qquad\qquad (1)$$

where J_c and J_o are corrected and normalized diffraction intensities for crystalline regions and sample respectively. The part of non-crystalline domains (Y) in cellulose sample was calculated as:

$$\mathbf{Y = 1\text{-}X} \qquad\qquad (2)$$

Improved lateral size of crystallites (**L**) was determined by the modified method. The reflection (200) was isolated, its integral width (**B**) in radians was measured and corrections for instrumental factor (δ_i) and lattice's distortion factor (δ_d) were introduced. The value of **L** was calculated according to equation:

$$\mathbf{L} = \lambda / [(\cos \Theta_o\, (\mathbf{B}^2 - \delta_i^2)^{0.5})^2 - (2\, \delta_d \sin \Theta_o\,)^2]^{0.5} \qquad\qquad (3)$$

where Θ_o – diffraction angle of the reflection (200).

Optical microscopy

Microphotographs of cellulose fibers were made by means of optical microscope "Axioplan" of Zeiss Co.

Deuterium Exchange

Cellulose samples were treated with heavy water (D_2O) at 25 °C and D_2O – cellulose mass ratio 10:1 for 5 h. Excess of heavy water was removed. The samples were dried in P_2O_5 – desiccator at 25 °C for 24 h, and then in a dryer at 105 °C up to constant weight. Amplitude of proton's induction for non-deuterated (I_o) and deuterated (I) cellulose samples was measured on a MNR-relaxometer operating at 42 MHz, with 2.5 µs interval of the $\pi/2$ – pulse (Ioelovich and Gorgeev 1994). Accessibility of cellulose samples at deuteration was calculated by equation:

A = [1 − (I/I$_o$)]/0.3 (4)

Vapor sorption

Sorption of water vapor by cellulose samples was measured at 25 °C and relative vapor pressure p/p$_o$ from 0 to 0.9 using a vacuum Mac-Ben apparatus having helical spring quartz scales.

Wetting enthalpy

Enthalpy of cellulose wetting with water (**ΔH**) was studied by method of isothermal micro-calorimetry at 25 °C using calorimeter TAM III (Wadső and Goldberg 2001).

Specific volume

Specific weight (**V$_{sp.}$**) of the dry sample was tested by pycnometry method in hexane medium (Kalinowski and Urbanczyk 1966)

Chemical composition

Analysis of chemical composition of the pulp was carried out according to standard procedures (Fengel and Wegener 1984; Obolenskaya et al. 1991).

LODP

Level-off DP (Laka et al. 2000) was obtained from testing of characteristic viscosity of diluted solutions of the cellulose samples in Cadoxen after hydrolysis of the samples with 2.5N hydrochloric acid for 1h (Ioelovich and Leykin 2006). Then, an average length of crystallites was calculated:

l = l$_o$ LODP (5)

where l$_o$ =0.517 nm is length of glucopyranose link of cellulose.

Reactivity

The reactivity of cellulose was investigated by treatment with boiling 2.5N hydrochloric acid for 1h and alkalization with solutions of sodium hydroxide at room temperature for 24 h (Ioelovich et al. 1999; 2010).

Results and Discussion

As can be seen from the microphotography, fibers of the bleached Kraft pulp are straight and flat, while fibers of the cotton cellulose have the appearance of twisted bands (Figure 1 and 2).

Analysis of the chemical composition showed that bleached Kraft pulp contains 91.8% α-cellulose and about 14% hemicelluloses. In contrast to the pulp, the cotton cellulose almost did not contain hemicelluloses, while the amount of α-cellulose reached 98.5% (Table 1).
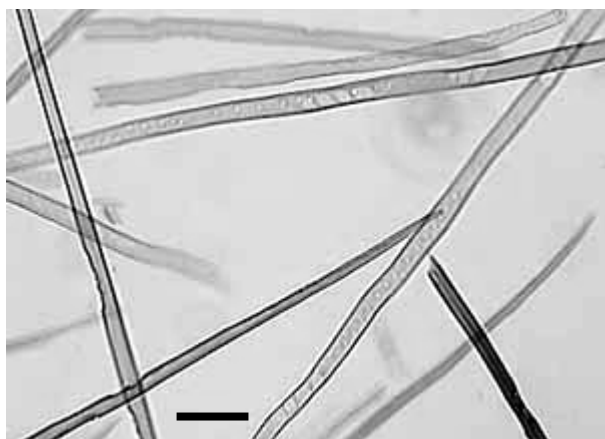
Figure 1. Microphotograph of the Kraft pulp fibers

Scale bars 100 μm
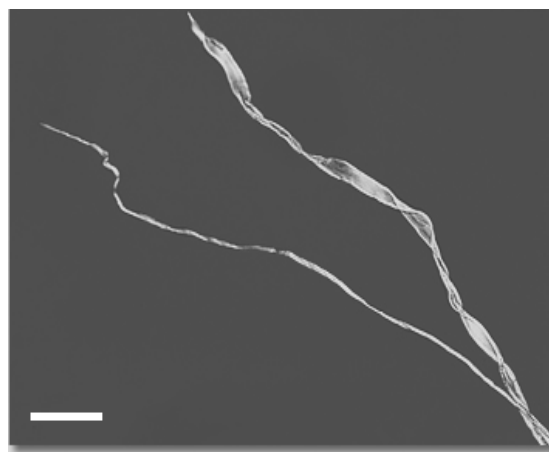
Figure 2. Microphotograph of twisted middle-length cotton cellulose fibers

Table 1. Chemical composition of cellulose fibers

Characteristics	Kraft pulp	Cotton cellulose
α-Cellulose, %	91.8	98.5
Hemicelluloses, %	14.3*	<1
Solubility in 10% NaOH, %	10.3	2.5
Ash, %	0.5	0.2

Note: Analysed by Stora Enso, Karlstad, Sweden

Increased content of α-cellulose, negligible content of lignin and high whiteness mean that these cellulose materials are suitable for both papermaking and production of modified celluloses.

Of great importance for the process of structural modification of cellulose is its reactivity. In this paper the formation process of MCC and mercerized cellulose was studied. The investigation showed that reactivity of the bleached Kraft pulp at acid treatment and alkalization was higher than of the cotton cellulose (Figure 3 and 4).
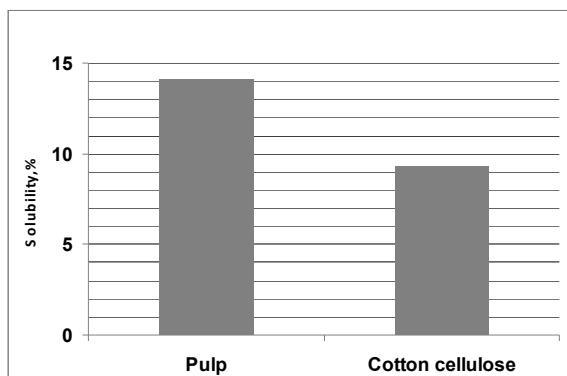
Figure 3. Solubility of cellulose samples at treatment with boiling 2.5 N HCl for 1h
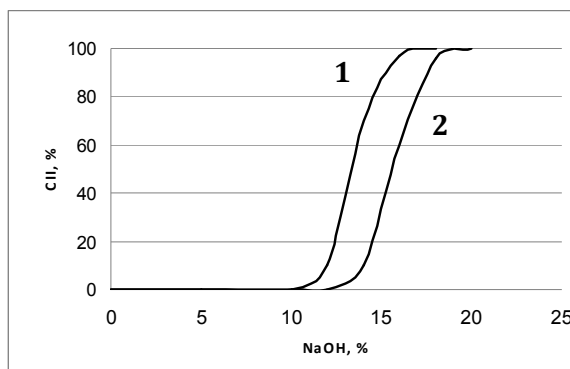
Figure 4. Dependence of CII-content on the concentration of NaOH at alkalization of bleached Kraft pulp (1) and cotton cellulose (2) for 24 h

108

X-ray diffractograms of the initial cellulose samples are typical for $C1_\beta$ – crystalline polymorph (Figure 5 and 6). After acid treatment crystallinity and sizes of crystallites increased and therefore the samples of MCC acquired well resolved peaks related to $C1_\beta$ polymorph (Figure 7, Table 2). X-ray diffractograms of mercerized celluloses are related to CII_β polymorph; they have less resolved peaks due to decreased crystallinity and sizes of crystallites (Figure 8 and Table 2).
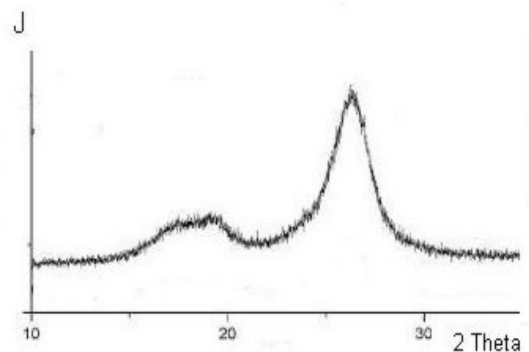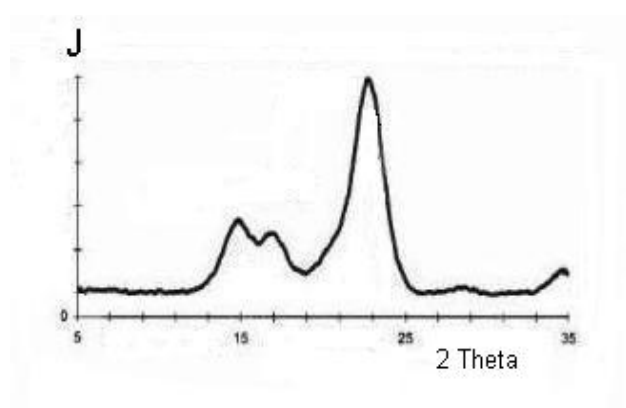
Figure 5. X-ray diffractogram of the bleached Kraft pulp

Figure 6. X-ray diffractogram of the cotton cellulose
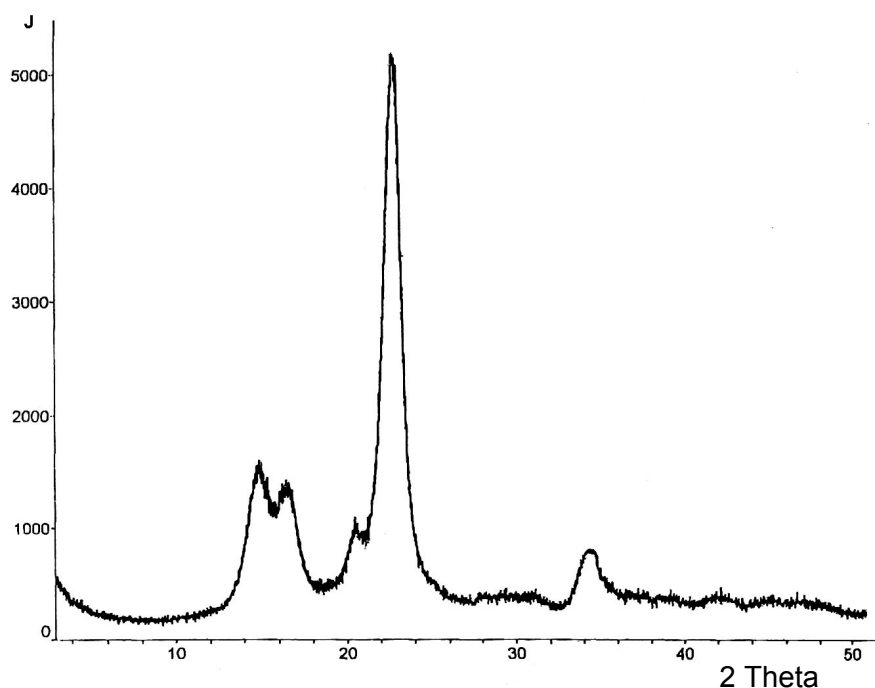
Figure 7. X-ray diffractogram of cotton MCC
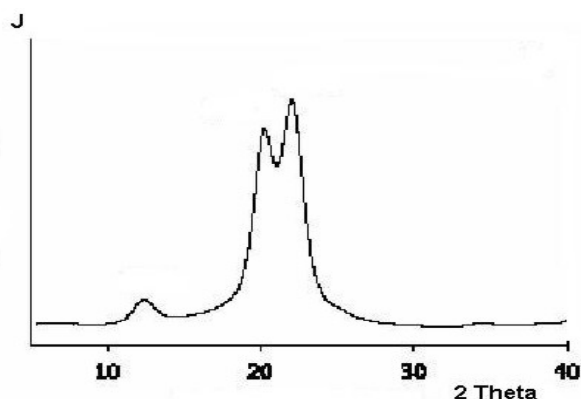
Figure 8. X-ray diffractogram of mercerized cotton cellulose

Values of lateral size (**L**) and length (**l**) of crystallites, crystallinity degree (**X**) and part of non-crystalline domains (**Y**) in cellulose samples are shown in Table 2. Cotton cellulose had a more ordered crystalline structure than the bleached Kraft pulp. Treatment with boiling acid lead to partial hydrolysis of non-crystalline domains, and lateral co-crystallization of crystallites gave an increased crystallinity and lateral size of crystallites. Mercerization of the initial cellulose samples caused transformation of C1 to CII crystalline polymorph – CP (O'Sullivan 1997) that was accompanied by decreased crystallinity, lateral size and length of crystallites.

Table 2. Characteristics of crystalline structure of cellulose samples*

Sample	CP	X	Y	L, nm	l, nm
IP	$C1_\beta$	0.63	0.37	6.7	78
PMCC	$C1_\beta$	0.73	0.27	8.0	78
MP	CII_β	0.53	0.47	5.4	40
IC	$C1_\beta$	0.70	0.30	7.5	110
CMCC	$C1_\beta$	0.78	0.22	11.0	110
MC	CII_β	0.55	0.45	6.0	45

*Note: IP - initial pulp; IC - initial cotton cellulose; PMCC – MCC prepared from pulp;   CMCC – MCC prepared from cotton cellulose; MP – mercerized pulp; MC – mercerized cotton cellulose.

Some physical and physico-chemical properties of the samples were studied (Table 3). As follows from the results, specific volume (**$V_{sp.}$**) was higher for the samples having increased content of non-crystalline domains (**Y**). Hydrophilic properties of the samples, e.g. wetting enthalpy (**ΔH**) and sorption of water vapor (**S**) at **p/p_o** = 0.6, decreased after treatment with boiling acid, but increased after mercerization. Accessibility at deuteration (**A**) was more than content of non-crystalline domains; this indicates that also paracrystalline surface layers of crystallites are accessible to deuterium exchange:

A=Y + α X (6)

where α – accessibility degree of paracrystalline surface layers of crystallites.

Table 3. Properties of cellulose samples

Sample	Y	$V_{sp.}$, cm^3/g	$-\Delta H$, kJ/kg	S, %	A
IP	0.37	0.645	63	7.9	0.46
PMCC	0.27	0.635	46	5.7	0.38
MP	0.47	0.651	80	10.0	0.55
IC	0.30	0.638	51	6.4	0.40
CMCC	0.22	0.630	37	4.7	0.34
MC	0.45	0.649	77	9.7	0.53

Isotherms of water vapor sorption by cellulose samples have a sigma-shaped form that can be described by the following equation:

$$S = S_o Y/[1-k \log (p/p_o)] \tag{7}$$

where $S_o = 50$ % and coefficient k = 6.

As seen from equation 7, increasing content of non-crystalline domains (Y) in the sample leads to rise of the sorption value. This is confirmed with experimental isotherms (Figure 9).
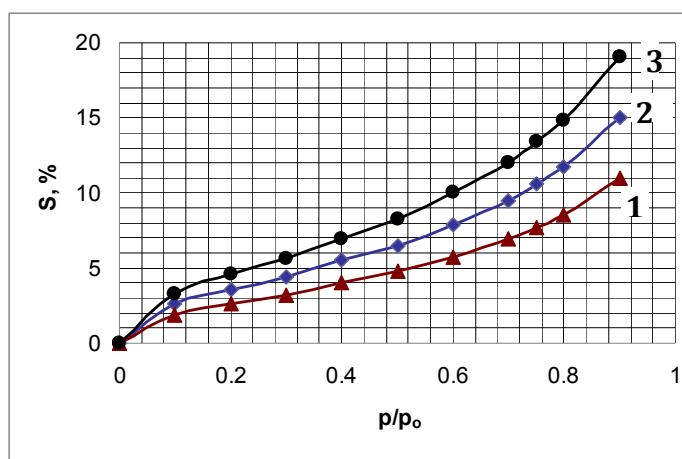
Figure 9. Isotherms of water vapor sorption at 25 °C for samples of PMCC (1), IP (2) and MP (3). Points calculated by Equation 7

Some physical and physico-chemical properties (Z) correlate with part of non-crystalline domains (Y) in cellulose samples. This correlation can be described by means of the linear regression equation:

$$Z = n\,Y + C \tag{8}$$

Coefficients of the regression - n and C, are shown in Table 4.

The Equation 8 makes it possible to predict various properties of the cellulose sample based on its Y-value or crystallinity.

Table 4. Coefficients of the linear regression as in Equation 8

Property: Z	n	C	R*
Sp. volume, $V_{sp,}$ cm^3/g	0.074	0.615	0.98
Wetting enthalpy, $\Delta H,$ kJ/kg	-170	0	0.95
Sorption of water vapor S, % at $p/p_o = 0.6$	21.45	0	0.96
Accessibility at deuteration, A	0.85	0.15	0.93
Solubility at acid hydrolysis, P,%	65	-10	0.90

Note: R – correlation coefficient

Conclusions

The bleached Kraft pulp is characterized by an increased α-cellulose content that is close to 92%. The presence hemicelluloses in the pulp sample can promote fibrillation and forming strong interfiber contacts in the papermaking process. Cotton cellulose has a very high purity degree: the content of α-Cellulose was 98.5% and almost zero hemicelluloses content. Increased content of α-cellulose and high brightness make these cellulose materials useful for papermaking and production of modified celluloses such as microcrystalline cellulose, mercerized cellulose, etc. The lower ordered pulp has higher reactivity at acid treatment and alkalization than the more ordered cotton cellulose. Treatment with boiling acid to obtain MCC leads to increased crystallinity and lateral size of crystallites, while mercerization of the initial cellulose samples caused formation of CII crystalline polymorph, decrease in crystallinity, lateral size and length of crystallites.

The studied physical and physico-chemical properties of the samples, e.g. specific volume, accessibility at deuteration, wetting enthalpy and sorption of water vapor, correlate with part of non-crystalline domains and crystallinity. This permits forecast of some important properties of the cellulose on the base of its crystallinity degree. And vice versa, when testing properties of the samples, such as sorption of water vapor at certain relative pressure or relative humidity, the crystallinity and part of non-crystalline domains in the cellulose can be determined.

References

Fengel D. and Wegener G. (1984): Wood: Chemistry, Ultrastructure, Reactions. Berlin, New York: W. de Gruyter Inc.

Heinemann S. and Ander P. (2011): Standard pulp and paper tests. *In* COST Action E54 "Characterisation of the fine structure and properties of papermaking fibres using new technologies". *Eds*: Ander P., Bauer W., Heinemann S., Kallio P., Passas R. and Treimanis A. Swedish University of Agricultural Sciences. p. 211-232. ISBN 978-91-576-9007-4

Ioelovich M. (1992): Supermolecular structure of native and isolated celluloses. Acta Polymerica. 43: 110-113

Ioelovich M. and Gordeev M. (1994): Crystallinity of cellulose and its accessibility during deuteration. Acta Polymerica 45: 121-123

Ioelovich M. and Larina E. (1999): Parameters of Crystalline Structure and their influence on the Reactivity of Cellulose 1. Cell. Chem. Technol. 33: 3-12

Ioelovich M. and Leykin A. (2006): Microcrystalline Cellulose: Nano-Structure Formation. Cell. Chem. Technol. 40 (5), 313-317

Ioelovich M., Leykin A. and Figovsky O. (2010): Study of cellulose paracrystallinity. BioResources 5(3): 1393-1407

Kalinowski J. and Urbanczyk G. W. (1966): Synthetic Fibers: Analysis and Properties. Moscow: Light Ind.

Krässig H. (1993): Cellulose: Structure, Accessibility and Reactivity, Polymer Monographs, Vol. 11. M. B. Huglin (ed.), Amsterdam: Gordon and Breach Publ.

Laka M., Chernyavslaya S., Treimanis A. and Faitelson L. (2000): Preparation and properties of microcrystalline cellulose gels. Cellul. Chem. Technol. 34: 217-227

Obolenskaya A. V., Elnitzkaya Z.P. and Leonowich A.A. (1991): Practical Works in Wood and Cellulose Chemistry. Moscow: Ecology.

O'Sullivan A.C. (1997): Cellulose: the structure slowly unravels. Cellulose 4: 173-207

Vonk C. G. (1973): Computerization of Ruland s X-ray method for determination of the crystallinity in polymers. J. Appl. Crystallography 6: 148-152

Wadső I. and Goldberg R. (2001): Standards in isothermal microcalorimetry. Pure Appl. Chem. 73(10): 1625-1639

A METHOD CAPABLE TO DETERMINE DAMAGE OF THE OUTER FIBER WALL LAYERS

Rene Eckhart, Ulrich Hirn, Wolfgang Bauer

Institute for Paper, Pulp and Fiber Technology, Graz University of Technology

Kopernikusgasse 24/II, 8010 Graz, Austria

rene.eckhart@tugraz.at

Abstract

Cupri(II)ethylendiamine is normally used to dissolve chemical pulp fibers. If used in a defined concentration and for restricted reaction time it provokes heavy fiber swelling. In areas where the outer layers of the fiber are too weak due to mechanical or chemical damage, they can no longer restrict this swelling process - they break and characteristic swelling reactions can be observed under the microscope.

Images of the swollen fibers were acquired and digital image analysis was used for evaluation of the swelling intensity. For each individual fiber a so called "degree of swelling", representing the swollen proportion of total fiber length, was evaluated. This degree of swelling corresponds to the damage of the outer fiber wall layers. The applicability of the method will be discussed using several results in different fields of interest.

Introduction

This paper presents a novel method capable of delivering information regarding the condition of the outer fiber wall layers of chemical pulp fibers.

The cell wall is composed of two layers, the thin primary wall (P) and the thick secondary wall. The secondary wall is divided into the three sublayers S1, S2 and S3. The orientation of the microfibrils differs between these layers. The fibrils in P are aggregated in a rather stochastic way, the S1 layer has a crossed fibrillar structure and the fibrils within the S2 are highly aligned along the fiber axis. Therefore the S2 layer shows the highest swelling ability. As already mentioned our method is based on chemically induced swelling of chemical pulp fibers. In areas where the more complex structured S1 layer is weakened or damaged during the pulping or stock preparation process, it cannot restrict the chemically induced swelling of the S2 layer and characteristic swelling reactions can be observed (Figure 1). The quantity of such swelling reactions reflects the condition of the outer fiber wall layers. Several methods described in the literature are based on this principle.

Nisser and Brecht (1963) used cupri(II)ethylenediamine to assess fiber wall damage. Hortling et al. (2000) used iron-sodium-tartrate (EWNN) and Unger et al. (1995) quantitatively evaluated swelling and dissolving of pulp fibers in EWNN and LiCl/DiMAc (lithiumchloride/ dimethylacetamide). Ander and Daniel (2004) indicated that polarized light microscopy, electron microscopy and fiber swelling induced by chemicals indeed all indicate cracks in the S1 fiber wall.

Experimental

At our institute we adapted the method of Nisser and Brecht (1963) where cupri(II)ethylendiamine is used as the swelling chemical. Unlike other methods based on chemically induced swelling of pulp fibers that are mentioned in the literature, we did not

observe the swelling reaction itself under the microscope, by means of photographs or video, instead we evaluated the swelling intensity of fibers after controlled treatment with the swelling chemical.

The comparison of pulp samples is restricted to similar samples in terms of raw material (hardwood/softwood) and cooking process (kraft/sulphite). It is impossible to compare for example sulphite and kraft pulp samples on the basis of the same concentration of swelling chemical, as the condition of the outer fiber wall layers is different due to the different characteristics of the cooking liquor (Page 1983). Therefore sulphite fibers already start to dissolve when kraft fibers show the first swelling reactions.

After treatment, the fibers show typical swelling reactions, their quantity depending on the condition of the S1-layer. Images of the treated fiber samples are taken by means of transmitted light microscopy in a prototype. The highly diluted (consistency 0.02 g/l) suspension is pumped through a transparent flow cell made of Plexi glass and CMOS-cameras acquire images in format jpg. For the evaluation of one pulp sample 1500 images are taken. These images contain on average 2500 objects with a minimum length of 250 μm.

As an example, Figure 1 shows seven kraft pulp fibers. Five of the fibers show the typical swelling reactions, two of them were completely unswollen. Swelling type I, called volume swelling, occurs when the S1 layer is already cracked along parts of the fiber and these parts can easily swell during treatment. If the S1, especially of fiber fragments is missing completely and the swelling reaction is not restricted at all, the swelling reaction disintegrates the fiber very fast and swelling type II, so called gel swelling, appears. Swelling type III, called balloon swelling (see also Figure 2), appears when the S1 layer is still intact but weakened or slightly damaged. The S1 layer is cracked in weaker points due to the swelling forces of the S2 and forms constrictions between or aside the occurring balloons.
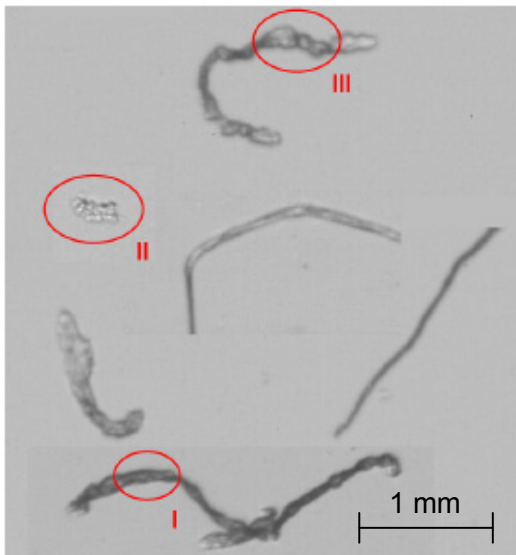
Figure 1(left). Characteristic types of swelling: Volume swelling (I), gel swelling (II), balloon swelling (III)
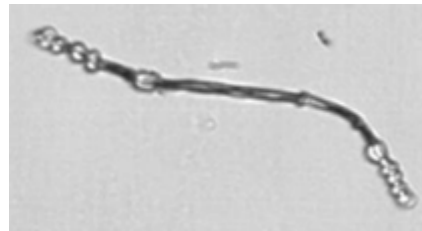
Figure 2 (above). Fiber with a degree of swelling of 36.4 %, which means that 36.4 % of total fiber length are rated as swollen by image analysis

Image analysis algorithms developed at our institute by Hirn (2006) were used to determine the degree of swelling for each individual fiber. Figure 2 shows an example of a partly swollen fiber, with 36.4 % of the total fiber length rated as swollen, therefore 36.4 % of the fiber's S1 wall is considered damaged. In addition, the degree of swelling, fiber length, fiber width, fiber curl and kink index are evaluated for each acquired fiber. A detailed description of the method can be found from the appendix.

The repeatability of the method was tested on the basis of three measurements on a softwood kraft pulp sample. Sampling, treatment with the chemical, image acquisition and analysis were performed three times independently.
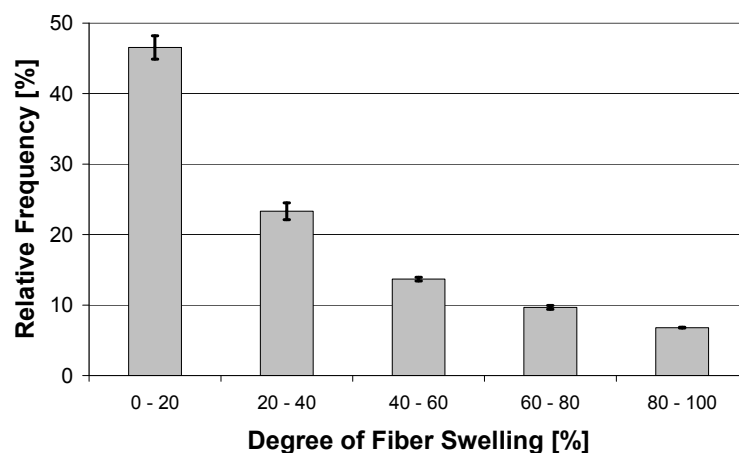
Figure 3. Repeatability on the basis of three fiber swelling measurements. The error bars represent a 95 % confidence interval for the specific class

The average degree of swelling was 30.3 % (swollen fiber length), the standard deviation on the basis of the three measurements was 0.3 %. Figure 3 shows the repeatability of the method in form of 95 % confidence intervals for the frequency distribution of the degree of swelling over five classes. 46 % of the fibers show hardly any damage (0 % - 20 % swollen fiber length) whereas for 7 % of the fibers nearly the whole fiber length was identified as swollen by image analysis (80 % - 100 % swollen fiber length).

Results

In this section we will show the applicability of our newly developed method on the basis of some results in different fields of interest.

1 - Bleaching - Chemical Damage

As fiber damage and degradation of cellulose molecules is always an issue along the fiber production line, we did some investigations on laboratory and industrial bleaching processes, to see if our method can indicate where the damage is done to the fiber in a number of bleaching stages.

Laboratory

As a first experiment and to evaluate if our method has the potential to indicate chemical damage as it occurs in a bleaching stage, a sulphite pulp sample with Kappa number 12 and brightness 55% was bleached in our laboratory in one stage to a brightness of 85.7 %. We used a laboratory cooking vessel. The concentration of the bleaching chemicals and the bleaching parameters were as follows: 3 % NaOH, 5 % H_2O_2, O_2 (at 8 kPa), 95 °C and 90 min.

Figure 4 shows the result of the swelling analysis in form of the frequency distribution of the degree of swelling over five classes for the unbleached and the bleached pulp sample.
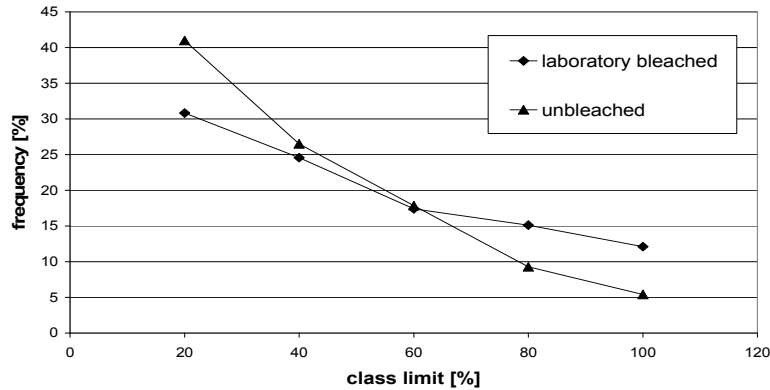
Figure 4. Fiber frequency distribution of the degree of swelling over five classes (0-20, 20-40, 40-60, 60-80 and 80-100% swollen fiber length) for unbleached and laboratory bleached pulp samples

The graph for the bleached pulp sample shows more objects in the classes of high degrees of swelling. The bleaching process leads to a higher proportion of swollen fiber length. Therefore the method is considered capable to indicate chemical damage as it occurred in the laboratory bleaching process under the described parameters.

Industrial scale

In cooperation with our industrial partners, we investigated 5 industrial bleaching sequences, 3 of them sulphite, 2 of them kraft producers to evaluate the method in an industrial application.

Figure 5 shows an exemplary result for one of the sulphite producing fiber lines in form of the frequency distributions of the degree of swelling for samples from the consecutive bleaching stages. As is evident in this diagram, there are only very small differences between the frequency distributions of the samples. It seems that no significant damage is done to the S1 layer in the industrial bleaching process. In fact, if we take a closer look on the classes 0-20% and 80-100% swollen fiber length in Figure 5, it seems that we have a decrease in damage. The unbleached sample shows the highest proportion in the class of high damage and the lowest in the class of the undamaged fibers whereas we see the exact opposite for the sample after the last bleaching stage.
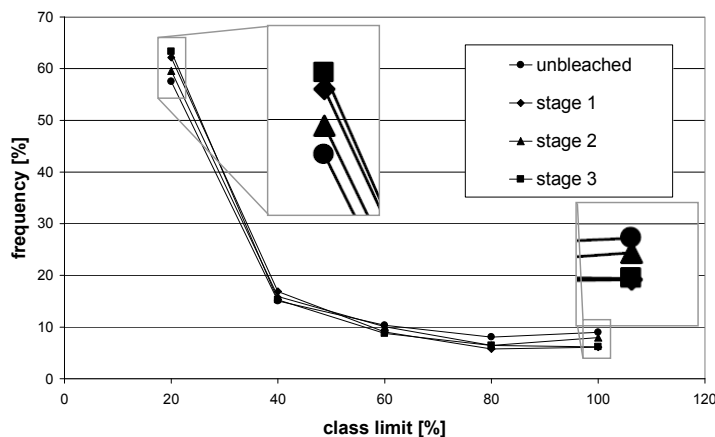
Figure 5. Frequency distribution of the degree of swelling for samples from consecutive bleaching stages

Considering the development of the average degree of swelling over the bleaching sequences, we can see this decrease in swelling reaction for all five investigated fiber lines (Figure 6). This decrease cannot be based on some kind of fiber "healing" during bleaching. We interpret it as a result of the changing amount of negatively charged groups within the fiber during the bleaching process. As the swelling chemical is a positively charged ion, the negatively charged groups within the fiber support the intrusion of its molecules and therefore might accelerate the swelling process. Due to the reduction of the Kappa number the amount of acidic groups within the fiber decreases. The result is a slight decrease of swelling reactions over the bleaching sequence. Maybe this effect superposes eventual detectable damage done to the S1 layer.
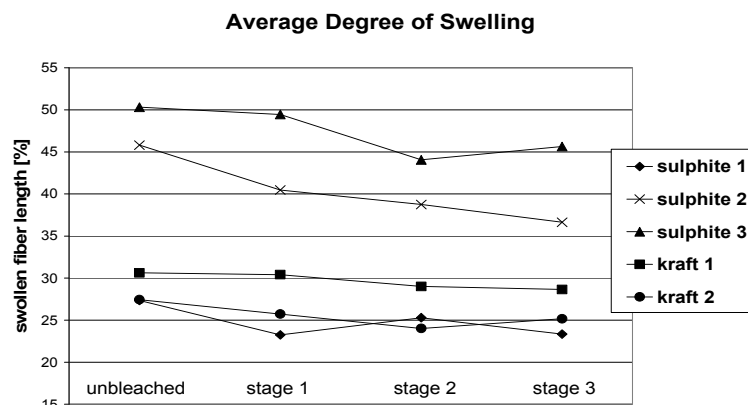
Figure 6. Average degree of swelling of the pulp samples taken after the consecutive bleaching stages

Summary 1

The laboratory experiment shows that the method can detect chemical damage of the S1 layer as it occurs during the bleaching process. Still, the method is unsuited for the evaluation of industrial bleaching sequences, as it cannot describe the fiber damage and the degradation of cellulose molecules in state of the art fiber lines. Furthermore changes in the chemical composition of the fiber wall during bleaching seem to influence the swelling behavior besides the damage of the S1 layer and therefore might lead to misinterpretation of results.

2 - Refining - Mechanical Damage

Investigations were done in laboratory scale (Jokro-mill, PFI-mill, pilot-disc refiner) as well as on industrial aggregates and refining processes.

If we look at the refining process, damage of the S1 layer occurs due to friction on the fiber surface. It may be torn open or even detached due to mechanical stresses. Besides fibrillation, flexibilization and shortening play a major role in the refining process. Flexibilization is not accessible in our method but shortening can be determined on the basis of fiber length development. Therefore the combination of the data on the swelling behavior with data on fiber length of each acquired fiber should allow an extended characterization of refining processes. A softwood kraft pulp sample was refined to an identical breaking length of 7 km with three different laboratory aggregates to determine differences concerning the treatment of the pulp. The investigated aggregates were the Jokro-mill, the PFI-mill and a pilot scale disc refiner. The degree of beating for the two laboratory mill-treated samples was similar at 15.5 SR for the Jokro-mill and 16 SR for the PFI-mill. The disc refined sample had a SR value of 35.

Figure 7 shows the contour plot of the degree of swelling versus fiber length. The two-dimensional frequency distribution of fibers is visualized by gray value. Bright areas represent numerous fibers, dark ones represent only few or no fibers at all. Damage of the fiber wall is indicated by a shift of the high fiber concentrations to the classes of high degrees of swelling, whereas a shift to the left, to shorter length classes corresponds to shortening.

Only little difference can be observed between the plots corresponding to the Jokro and the PFI mill. Comparing the plot corresponding to the disc refiner with those of the two laboratory mills, a high fiber concentration in the region of high degrees of swelling is evident. Another high fiber concentration is still observable at low degrees of swelling. Fewer fibers are situated in between. This shows a rather inhomogeneous treatment in the disc refiner. Those fibers that are reached in the refining zone are mostly heavily damaged, whereas others are not reached and receive no damage at all. Furthermore a shift of the high fiber concentrations to the left – to shorter fiber classes – can be observed due to increased shortening of fibers in the disc refiner.
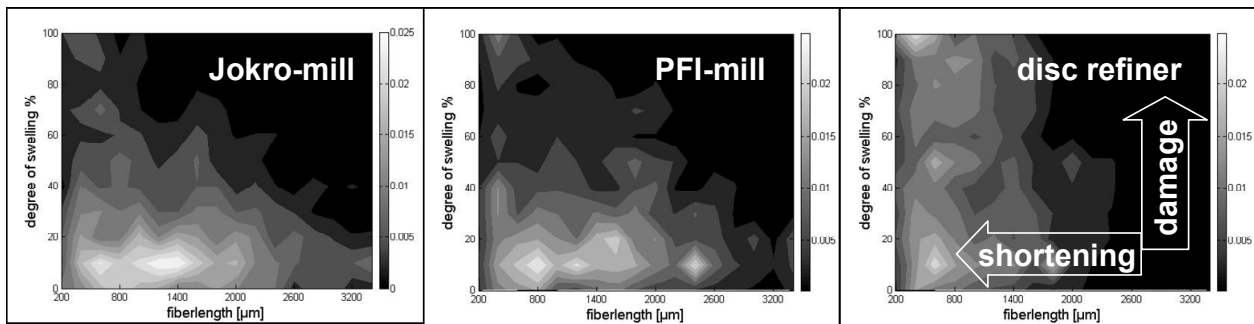
Figure 7. Contour plots of the degree of swelling versus fiber length

If we look at the same results visualized as frequency distributions of the degree of swelling (Figure 8), a difference between the Jokro- and the PFI-mill becomes obvious. Although it can be assumed that all fibers pass the refining zone several times in such laboratory mills, a considerable amount of fibers shows rather no damage of the fiber wall. The laboratory mills develop breaking length more through flexibilization than through fibrillation, shortening or production of fines.
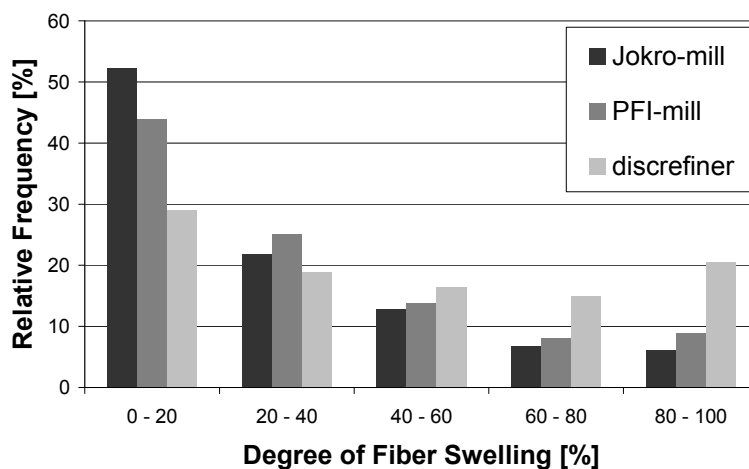
Figure 8. Frequency distributions of the degree of swelling
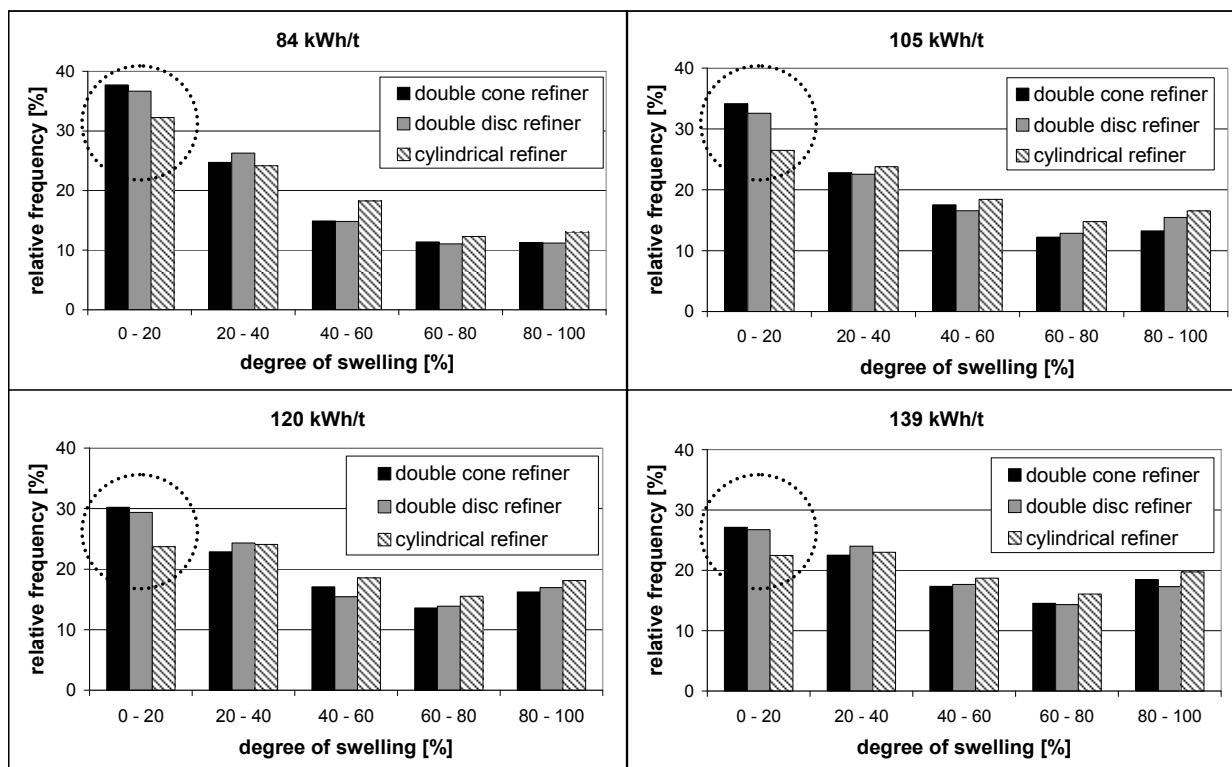
Figure 9. Frequency distributions of the degree of swelling

Still, the PFI-mill treated pulp sample shows less fibers in the class of undamaged fibers (0 - 20 % swollen fiber length) than the Jokro-mill. That is due to higher friction between rotor and housing in the PFI-mill and therefore a more fibrillating effect. In the Jokro-mill, where the rotor rolls more or less in the housing, breaking length descends to an even higher extent from fiber flexibilization. It is developed smoother and more time consuming. Therefore less damage is imposed on the fiber wall.

As damage data is available on every single fiber the method is potentially capable of giving information on the homogeneity of the treatment in a refining process. As an example, Figure 9 shows the fiber damage distributions of a softwood kraft pulp sample, refined with three different industrial aggregates at four points of specific energy consumption. The aggregates were a double cone refiner, a double disc refiner and a cylindrical refiner. The parameters refining consistency and specific edge load were identical for these trials.

The mean calculated damage of the fibers was similar for the double cone and the double disc refiner at all four points of specific refining energy. The pulp sample refined with the cylindrical aggregate showed a slightly higher average degree of fiber swelling. As is shown in Figure 9, the sample refined in the cylindrical aggregate exhibits less objects in the class of rather undamaged fibers of 0 % - 20 % swollen fiber length in all four trials, whereas the distribution over the four remaining classes is quite similar to those of the other aggregates. This result indicates that the higher average fiber damage after treatment with the cylindrical aggregate is not due to higher damage of the fibers that have been treated in the refining zone, which would have resulted in more fibers especially in the classes of 60-80 and 80-100 % swollen fiber length, but due to a higher percentage of damaged fibers. Our conclusion is that in these specific trials, the

cylindrical refiner treated the pulp suspension in a more homogeneous way, as less fibers remain undamaged compared to the other industrial aggregates.

Summary 2

The measurements deliver additional information on the refining process that is not accessible through the degree of beating or breaking length. The method evaluates the refining process directly through single fiber measurement. Each fiber is assessed concerning its wall damage level. Therefore the method is capable to evaluate the homogeneity of fiber treatment. Refining and mechanical damage seems to be the field with the highest applicability of this method.

3 - Comparison of Pulp Samples

Another possible field of application we investigated is the comparison of different pulp samples concerning the fiber damage level and the beatability of these samples. The beatability should be highly correlated to the condition of the fiber wall: weaker fiber wall layers result in a higher degree of swelling; weaker fiber wall layers also cause lower refining resistance; a higher degree of swelling is expected to indicate lower refining resistance. As already mentioned, a comparison with our method is reasonable only in a range of similar pulp samples concerning raw material (hardwood - softwood) and cooking process (sulphite-kraft) as the concentration of the swelling chemical has to be varied based on these properties, to receive meaningful results. Furthermore, as already mentioned earlier, the amount of negatively charged groups within the fiber, which correlates to Kappa number, might contribute to the result.

Therefore six softwood kraft pulp samples with similar brightness (between 85 and 90%) were compared concerning their swelling behavior. The arithmetic mean of the degree of swelling of these pulp samples varied between 23 and 51 %. A difference of 28 % is comparable to the difference we get between an unbeaten sample and the same sample after 250kWh/t in an industrial refiner. This instance demonstrates the major difference due to origin of the pulp, cooking and bleaching parameters and kappa number even among similar pulp samples. As expected, a clear correlation was found between the average degree of swelling and the refining resistance (represented by the number of revolutions in the PFI-mill needed to reach a degree of beating of 23 SR). Figure 10 shows the specific correlation.
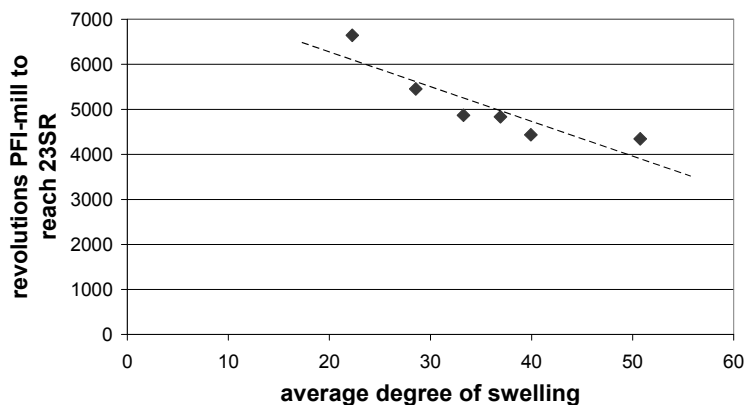
Figure 10. Correlation between degree of swelling and refining resistance

Summary 3

As we expected, the degree of swelling of unrefined pulp samples, is an indicator for the damage-level of the S1 layer, and shows a good correlation to the refining resistance of the specific samples.

Conclusions

The described method is capable to determine the condition of the S1 layer. The highest applicability lies in the field of refining characterization. Combined with data on fiber length development, the method is capable to determine the character of a refining process concerning shortening and fibrillation. Furthermore, as data is available on a single fiber basis, the method can be used to investigate the homogeneity of the refining process. Comparison of different pulp samples is possible within equivalent cooking process type, raw material and similar bleaching level and delivers information concerning the refining resistance.

Acknowledgement

References

Ander P. and Daniel G. (2004): Morphology of spruce fibre dislocations as studied by balloon swelling and acid cleavage - light and electrone microscope observations, *In*: U. Schmitt, P. Ander, J.R. Barnett, A.M.C. Emons, G. Jeronimidis, P. Saranpää, S. Tschegg, *(Eds)*. COST Action E20, "Wood Fibre Cell Walls: Methods to Study Their Formation, Structure and Properties". Swedish University of Agricultural Sciences, Uppsala, Sweden. ISBN 91-576-6803-5, pp. 203-215

Hirn U. (2006): New Methods in Paper Physics Based on Image Analysis, PhD Thesis, Graz University of Technology, Austria

Hortling B., Jousimaa T. and Hyvärinen H.-K. (2000): Investigation of spruce pulp fibres by swelling experiments and light microscopy, in Proc. 10th Int. Conf. CELLUCON 1998, Woodhead Publishing Ltd., pp. 205–208

Nisser H. and Brecht W. (1963): Zwei neue Messkriterien von aufgeschwemmten Fasern zur Beurteilung der Blattfestigkeit. Svensk Papperstidning 66(2), 37–41

Page D.H. (1983): The origin of the differences between sulphite and kraft pulps. J. Pulp Paper Sci. March 1983, TR15-TR20

Unger E., Fink H. and Philipp B. (1995): Morphometrische Untersuchungen des Quell- und Lösevorgangs von Cellulosefasern in EWNN und LiCl/Dimethylacetamid. Das Papier 49(6), 297–307

Appendix

Swelling procedure and analysis

A beaker is filled with 20 g of suspension (consistency 1 g/l) and put on a magnetic stirrer. The swelling reaction is started by adding the swelling chemical to the suspension.

We use commercially available cupri(II)ethylendiamine solution which has to be diluted before use in the swelling reaction as the pure solution would lead to almost immediate dissolution of the fibers. The final concentration of cupri(II)ethylendiamine in the suspension is chosen depending on the pulp sample to be evaluated (sulphite/kraft, hardwood/softwood).

As an example, for a softwood *kraft pulp* sample the concentration of the chemical in the suspension after addition to the solution has to be 16 % whereas 14 % is convenient for a softwood *sulphite pulp* sample. The amount of dilution water added to the chemical is calculated on the basis of the chosen final concentration, the amount of fiber suspension (~20 g) and the amount of pure cupri(II)ethylendiamine solution (~ 7 g). The reaction is stopped 20 sec after addition of the diluted swelling chemical, by dilution with deionized water up to an ineffective concentration of about 1.5 %.

Images of the treated fiber samples are taken. The optical resolution is 6.25 μm/Pixel at an image size of 6.25 x 14.5 mm. Swelling detection is based on following four criteria given below. The image analysis decides for each criterion if the specific fiber section is swollen, not swollen or not determinable (see also Figure 1).

Swelling criteria

1. The absolute width, since the width of swollen fibers is significantly higher than those of unswollen ones.
2. The width-gradient over the length of the fiber.
3. Luminance profile perpendicular to the fiber centerline
4. The gradient of the luminance profile over the length of the fiber.

As a result, every evaluated fiber is assigned a degree of swelling in %.

SOLID STATE NMR CHARACTERISATION OF CELLULOSE ACETATE AND LIME WOOD CELLULOSE

[1]Carmen-Mihaela Popescu, [2] Per Tomas Larsson

[1] Romanian Academy "P.Poni" Institute of Macromolecular Chemistry, 41A Gr. Ghica Voda Alley, Ro.700487, IASI, Romania

[2] Innventia AB, Box 5604, SE-114 86 Stockholm, Sweden

E-mail: mihapop@icmpp.ro

Abstract

This Short Term Scientific Mission (STSM) work performed on the solid state NMR equipment at Innventia AB consisted of determining if and to what extent the fiber fine structure influence the chemical reactivity when cellulose acetate is made from wood fibers. Cellulose acetate is an important commercial product, made from renewable resources at numerous sites around the world, a possible replacement for oil based plastic materials. The changes induced by two important soft-rot fungi *Trichoderma viride* Pers. and *Chaetomium globosum* on lime wood cell wall were also studied by solid state CP/MAS ^{13}C NMR spectroscopy.

Introduction

Solid state CP/MAS ^{13}C NMR spectroscopy is a versatile tool for morphology studies of cellulosic materials. The resolution of CP/MAS ^{13}C NMR spectra is adequate enough to allow chemically equivalent carbons from different magnetic environments to be separated. Cellulose fibers exhibit specific properties that focused the interest toward their use as reinforcing fillers in polymeric composites (Czarnecki et al. 1980, Hermann et al. 1998, Glasser et al. 1999).

The acetylation of cellulose is a typical heterogeneous reaction. On one hand it depends on the accessibility of cellulose elements within the starting cellulosic fibers and on the other hand on the susceptibility of individual cellulose crystallites towards acetylation. The rate and perfection of acetylation is therefore greatly influenced by macro and micro morphology of initial cellulose fibrils (Sassi et al. 1995). Heterogenous acetylation is one suitable way to reduce high polarity, to modify surface properties, to increase the hydrophobic character, and also to control the enzymatic degradation of cellulose fibers.

Wood as a biodegradable natural material (Eriksson et al. 1990) is permanently exposed to degradation processes of environmental, chemical (You et al. 2010) or microbial nature. The extent of deterioration depends on the environmental conditions in which the wood is usually found. Even if wood is considered a durable material there are a number of biological factors that contribute significantly to the degradation of wood. The aim of the STSM project "Cellulose and wood characterisation by CP/MAS ^{13}C NMR spectroscopy" was to obtain information about the supra-molecular structure in order to establish differences which appear after acetylation and after biodegradation by microorganisms. This kind of analysis allowed us to detect small differences appearing after biodegradation of a lime wood species mainly used in art works. The meaning was to find correlations between the degree of structure deterioration and some spectral characteristics, in order to establish new methodology to assess the age of art works.

Materials and methods

Three sets of samples were used: acetylated unbleached and bleached pulp samples, lime wood biodegraded by *Chaetomium globosum* and by *Trichoderma viride*.

Unbleached and bleached kraft pulp fibers (Popescu et al. 2011) were wet-defibrated and air-dried at room temperature several days and then oven-dried at 80 °C for 24h. 1.5 g of each sample were suspended in a mixture of 7.5 mL acetic anhydride and 0.015 mL sulphuric acid as a catalyst and vigorously stirred. Acetylation was performed at 30 °C for different reaction times: 1, 3, 5 and 24 h. After the desired reaction time, each sample was separated by filtration, and washed several times with distilled water and air-dried at room temperature.

The wood samples used were lime wood (*Tilia cordata* Mill). Exposure time for *Chaetomium globosum* was 0, 28 days, 56 days, 91 days and 133 days, and by *Trichoderma viride* 0, 56 days, and 84 days.

The method of investigation was *Cross-Polarization Magic Angle Spinning Carbon-13 Nuclear Magnetic Resonance (CP/MAS ^{13}C-NMR) spectroscopy* as described by Larsson et al. (1997; 1999) and Wickholm et al. (1998).

High-resolution solid state ^{13}C-NMR spectra were recorded at 7.04 T with cross-polarization /magic angle spinning (CP/MAS) in a Bruker Avance AQS 300 WB spectrometer. All powdered samples were packed uniformly in a zirconium oxide rotor. All measurements were performed at 289 ± 1 K. The MAS rate was 5 kHz. A double air-bearing probe was used. Acquisition was performed with a CP pulse sequence, using a 4.5 µs proton 90° pulse, 800 µs ramped (100 – 50%) falling contact pulse and a 2.5 s delay between repetitions. A TPPM15 pulse sequence was used for ^{1}H decoupling. Glycine was used for Hartman-Hahn matching procedure and as external standard for the calibration of chemical shift scale tetramethylsilane (($CH_3)_4Si$) was used. The data point of maximum intensity in glycine carbonyl line was assigned a chemical shift of 176.03 ppm. Deconvolution of the spectra was done by means of Grams/32 program (Galactic Industry Corp.).

Results and Discussion

CP/MAS ^{13}C NMR spectroscopy for cellulose samples

Natural cellulose fibers have a molecular architecture with a high degree of individuality, depending on their biological origin. Typical CP/MAS ^{13}C NMR spectra from cellulose I are made up of six signals from the anhydroglucose unit split into fine structure of the cellulose I fibril. The information in this fine structure is high, but the accessibility of the information is hampered by a severe overlap of the signals (Larsson et al. 1999). The spectra of unbleached and bleached pulp samples, non-acetylated and acetylated showed characteristic signals which are given in Table 1, the assignments being in accord with known literature (Larsson et al. 1997, 1999; Wickholm et al. 1998).

Signals at 171.4 and 20.6 ppm assigned to COO- and CH_3, respectively, in acetyl groups demonstrate that acetylation took place in both unbleached and bleached pulp samples. For a better characterization of the cellulose non-acetylated and acetylated samples, normalization of the C-4 signal from 88.7 ppm was done. This signal is assigned to C-43 carbons situated in crystalline cellulose Iα and Iβ domains together with paracrystalline cellulose and is considered less influenced by the acetylation medium. After normalization the following differences in the spectra of non-acetylated and acetylated <u>unbleached pulp</u> samples were observed.

Table 1. Resonance assignment of CP/MAS ^{13}C NMR spectrum of acetylated pulp samples

Chemical shift (ppm)	Assignments
171.4	COO- in acetyl groups
104.8	C-1 in cellulose Iα, Iβ and less-ordered cellulose
101.4	C-1 in cellulose acetate
88.7	C-4 in crystalline cellulose Iα, Iβ and paracrystalline cellulose
83.7	C4 in amorphous cellulose or less ordered surface cellulose molecules
74.8	C2,3,5 in cellulose and hemicelluloses
72.1	C2,3,5 in cellulose and hemicelluloses
71.4	C2,3,5 in cellulose and hemicelluloses
64.8	C6 in crystalline cellulose Iα, Iβ and paracrystalline cellulose
62.6	C6 in amorphous cellulose or less ordered surface cellulose molecules
20.6	CH$_3$- in acetyl groups

Unbleached pulp

The signal at 104.8 ppm shows a decrease after 1h acetylation and increase with increasing reaction time. The shoulder at 101.4 ppm increased with increasing acetylation time. The C-1 carbon from cellulose acetate remaining in the cellulose samples gave rise to a broad signal, which partly overlaps the C-1 carbon from the cellulose (Sassi et al. 2000). The signal at 83.7 ppm assigned to amorphous cellulose or less ordered surface cellulose molecules increased in intensity. This correlates with a decrease in fibril diameter, maybe acetylation removed layers of fibril surfaces. Also the signals at 74.8, 72.1 and 71.4 ppm, which are assigned to C-2,3,5 carbons from cellulose and hemicelluloses, decreased in intensity after 1h and 3h of acetylation. At longer reaction times these intensities started to increase. This may also be due to acetylation of some xylans, because in these regions signals from both cellulose and hemicelluloses are found. When comparing the region assigned to C-6 a decrease in intensity was observed for the signal at 62.6 ppm with samples acetylated for 1h, 3h and 5h. After 24h an increase in intensity for the acetylated sample was obtained.

Bleached pulp

The same acetylation effect was observed in the case of bleached pulp. However, differences in signal intensities were stronger than for unbleached pulp. This means that the acetylation was more pronounced in the case of bleached pulp sample. After integration of the regions between 30 and 11 ppm, assigned to CH$_3$ from acetyl groups, and 115 and 50 ppm, assigned to C1-6 carbons from cellulose, it was possible to evaluate the acetylation degree (Table 2). Thus, after 5h the acetylation degree was slightly lower for unbleached pulp while it was clearly higher after 24h as compared with the bleached pulp. The unbleached pulp having a less ordered structure than bleached one is more susceptible to acetylation.

Table 2. Acetylation degree against reaction time of unbleached (UB) and bleached (B) pulps

Sample	Acetylation degree	Sample	Acetylation degree
UB – 1h	0.06	B – 1h	0.05
UB – 3h	0.12		
UB – 5h	0.34	B – 5h	0.39
UB – 24h	1.08	B – 24h	0.82

CP/MAS ^{13}C NMR spectroscopy of wood samples

Wood is a complex natural composite material, which contains three major components: cellulose, a poly-β(1-4)-D-glucopyranosyl linear polymer; hemicelluloses in which, the poly-β(1-4)-D-xylopyranosyl polymer substituted by O-acetyl groups, is the major compound; and lignin a polyaromatic three-dimensional amorphous polymer made of phenylpropane units linked through ether bonds. The phenyl rings usually have methoxy substituents. Cellulose represents the crystalline part (fibrils) of wood, which is held together by the hemicelluloses and the lignins. The main function of hemicelluloses and lignins is to support the fibrils. Degradation of any of these wood constituents results in a decrease in the strength of the material.

Microorganisms capable of degrading cellulose produce a battery of enzymes with different specificities, working together. Cellulases hydrolyze the β-1,4-glycosidic linkages of cellulose. Traditionally, they are divided into two classes referred to as endoglucanases and cellobiohydrolases. Endoglucanases (endo-1,4-β-glucanases, EGs) can hydrolyse internal bonds (preferably in cellulose amorphous regions) releasing new terminal ends. Cellobiohydrolases (exo-1,4-β-glucanases, CBHs) acts on the existing endoglucanase-generated chain ends. Both enzymes can degrade amorphous cellulose but, with some exceptions, CBHs are the only enzymes that efficiently degrade crystalline cellulose. CBHs and EGs release cellobiose molecules. An effective hydrolysis of cellulose also requires β-glucosidases, which break down cellobiose releasing two glucose molecules (Eriksson et al. 1990; Leschine 1995, Pérez et al. 2002).

Solid state CP/MAS ^{13}C NMR spectroscopy has been extensively applied to structural studies of natural wood. In native wood the main structural components, cellulose, hemicelluloses, lignin and, to some extent, extractives, give their characteristic shifts to the spectrum. A characteristic of CP/MAS ^{13}C NMR of wood is the broadening of most signals due to the unordered molecular structure of lignin and hemicelluloses and partly cellulose. Relatively sharp signals are assigned to ordered cellulose or hemicelluloses. Conventional CP/MAS ^{13}C NMR measurements followed by signal integration of the reference and decayed wood samples was carried out to obtain information of the chemical changes due to the fungal decay.

In the aliphatic region of spectra, the intensities of the signal at 105 and 89 ppm corresponding to cellulose resonances are altered by the biodegradation.

However, by observing the shoulder at 101.6 ppm assigned to C1 carbons of hemicelluloses, it could be noted that its intensity was reduced. The biodegradation of hemicelluloses reduced the broad background contribution to the aliphatic part of the spectrum, and it may have been responsible for the apparent sharpening of some signals in this region.

After integrating the area of the 112-93 ppm region, it decreased with increased exposure time (Table 1). This is consistent the removal of hemicelluloses and also the transformation of crystalline cellulose in non-crystalline cellulose during exposure to the two soft rot fungi.

Reference and decayed lime wood gave distinct signals at 55.8 ppm from aryl methoxyl carbons of lignin, the percentage contribution of methoxyl C to the total pool of carbons from the NMR spectra increased 5.6% in reference wood to 7.2% upon fungal decay by *C. globosum*, but was constant upon decay by *T. viride*. The resonances between 158-112 ppm are from carbon in aromatic rings from lignin. These are increasing with the increasing time of exposure. One plausible explanation is that there has been an overall increase in lignin content, which could elevate the amount of aromatic rings and methoxyl groups relative to polysaccharides in the altered wood.

Table 3. Composition of lignocellulosic substrates in reference and decayed lime wood as obtained from integration of CP/MAS ^{13}C NMR spectra after exposure to soft-rot fungi

Area Sample	C. globosum		T viride	
	0 days	133 days	0 days	84 days
COO- (177-165 ppm)	3.4	4.8	2.8	4.0
C-3/C-5 of S (158-145 ppm)	3.2	4.1	2.8	4.8
C-1/C-4 of S (145-125 ppm)	3.3	4.2	3.8	5.0
aromatic C	6.5	8.3	6.6	9.8
C-1 (112-93 ppm)	13.7	12.5	15.2	14.0
C-4 (93-80 ppm)	10.9	10.4	11.3	11.2
C-2, 3, 5 (80-67.5 ppm)	41.1	38.8	40.2	40.0
C-6 (67.5-58.5 ppm)	14.1	13.3	-	-
O-alkyl-C	79.8	75.5	66.7	65.2
-OCH$_3$ in lignin (58.5-48 ppm)	5.6	7.2	5.5	5.5
alkyl-C (30.3-29.7 ppm)	1.1	1.1	-	-
CH$_3$ (25-16 ppm)	3.5	3.5	3.6	1.7

In addition, the signals of the methyl and carboxylic carbons of acetyl groups attached to hemicelluloses resonate at 20.6 and 171.4 ppm, respectively as given in Table 1. The signal at 20.6 ppm was well detected in all wood samples, but became broader and had low intensity in wood deacayed by *T. viride*. The integral area of the signal at 171.4 ppm increased up to 4.8% and 4% after 133 and 84 days of exposure (COO- in Table 3), suggesting the generation of new carbonyl moieties by the soft rot fungi.

It appears that the main chemical change in wood during decay by the soft-rot fungus *C. globosum*, was loss of hemicelluloses and cellulose simultaneously with small changes in lignin structure, mainly loss of methoxyl groups, Cα-Cβ bond and β-O-4 bond cleavage. Changes in wood during decay by *T. viride* were due to enzymatic removal of non-crystalline carbohydrates with no distinct increase in lignin signals (Table 3).

Conclusions

All signals assigned to carbons from cellulose were observed by NMR spectroscopy. The signals at 171.4 and 20.6 ppm assigned to COO- and CH$_3$, respectively, in acetyl groups demonstrate that acetylation took place in both unbleached and bleached pulp samples. The degree of acetylation was higher for unbleached pulp than for bleached pulp.

After wood decay a partial removal of carbohydrates was observed for both fungi. *T. viride* degrades the wood by erosion of the fibril surface, while *C. globosum* degrades carbohydrates simultaneously with small changes in lignin structure, mainly small loss of methoxyl groups and Cα-Cβ bond cleavage and loss of β-O-4 linkages.

Acknowledgements

References

Czarnecki L. and White J.L. (1980): Shear flow rheological properties, fiber damage, and mastication characteristics of aramid-, glass-, and cellulose-fiber-reinforced polystyrene melts. J. Appl. Polym. Sci. 25, 1217-1244

Eriksson K.-E. L., Blanchette R.A. and Ander P. (1990): Microbial and Enzymatic Degradation of Wood and Wood Components. Springer-Verlag, Berlin Heidelberg, 407 pp

Glasser W.G., Tai R., Jain R.K. and Kander R. (1999): Fiber-reinforced cellulosic thermoplastic composites. J. Appl. Polym. Sci. 73, 1329-1340

Hermann A.S., Nickel J. and Riedel U. (1998): Construction materials based upon biologically renewable resources—from components to finished parts. Polym. Degrad. Stab. 59, 251-261

Larsson P.T., Wickholm K. and Iversen T. (1997): A CP/MAS13C NMR investigation of molecular ordering in celluloses. Carbohydr. Res. 302, 19-25

Larsson P.T., Hult E.L., Wickholm K., Pettersson E. and Iversen T. (1999): CP/MAS13C NMR spectroscopy applied to structure and interaction studies on cellulose I. Solid State NMR 15, 31-40

Leschine S.B. (1995): Cellulose degradation in anaerobic environments. Annu. Rev. Microbiol 49, 399-426

Pérez J., Muñoz-Dorado J., de la Rubia T. and Martínez J. (2002): Biodegradation and biological treatments of cellulose, hemicellulose and lignin: an overview. Int. Microbiol. 5, 53-63

Popescu C.-M., Totolin M., Tibirna C.M., Popescu M.-C., Ander P. and Vasile C. (2011): Structural and morphological characterization of unmodified and grafted unbleached and bleached softwood kraft pulp fibers. *In* COST Action E54 "Characterisation of the fine structure and properties of papermaking fibres using new technologies". *Eds*: Ander P., Bauer W., Heinemann S., Kallio P., Passas R. and Treimanis, A. Swedish University of Agricultural Sciences. p. 253-266. ISBN 978-91-576-9007-4

Sassi J.F. and Chanzy H. (1995): Ultrastructural aspects of the acetylation of cellulose. Cellulose 2, 111-127

Sassi J.F., Tekely P. and Chanzy H. (2000): Relative susceptibility of the Iα and Iβ phases of cellulose towards acetylation. Cellulose 7, 119-132

You B.R. and Oh S.C. (2010): Nonisothermal kinetics of wood degradation in supercritical methanol. Korean J. Chem. Eng. 27, 1159-1163

Wickholm K., Larsson P.T. and Iversen T. (1998): Assignment of non-crystalline forms in cellulose I by CP/MAS 13C NMR spectroscopy. Carbohydr. Res. 312, 123-129

Chapter 2. New and emerging methods such as microrobotics and microscopic techniques 131-208

MICROROBOTIC PLATFORM FOR MANIPULATION AND MECHANICAL CHARACTERIZATION OF INDIVIDUAL PAPER FIBERS

Pooya Saketi and Pasi Kallio

Micro-and Nanosystems Research Group of Tampere University of Technology, Korkeakoulunkatu 3, 33720 Tampere, Finland

pooya.saketi@tut.fi and pasi.kallio@tut.fi

Abstract

Mechanical characterization of individual paper fibers (IPF)s determines the key parameters which affect the quality of paper sheets. Many of the current laboratory tests are based on bulk paper fiber measurements. This paper introduces a microrobotic platform to manipulate and to characterize paper fibers and fiber bonds at an individual cell level. The platform is able to characterize paper fibers and bonds directly, not in bulk amount or by using indirect estimations. In addition, it provides an infrastructure for fully automated IPF characterization with sufficient amount of data to be used by paper and wood scientists for statistical analysis.

This paper focuses on fiber flexibility, an inverse of bending stiffness. In the IPF flexibility measurement, the platform treats a fiber as a both-ends-fixed beam by using two microgrippers to grasp an IPF from its ends, and to determine the force required to bend the IPF by using a micro force sensor. A machine vision system provides information about the length of the IPFs and the place where the force is applied, which is always in the middle of the IPF. The deflection of the IPF is measured by using a position sensor attached to the force sensor.

Two sets of flexibility tests have been completed with the microrobotic platform. The first set was to determine the effect of tensile stress on bending stiffness, carried out by performing tests while the IPFs were under tension and while they were not under tension. The second set of tests was to compare the flexibility of two different samples, a hardwood and a softwood sample. Finally, the flexibility of a chemically-treated softwood sample was measured as an additional challenge. In addition to the flexibility measurement, this paper discusses manipulating and breaking of individual paper fiber bonds using the platform. Measuring the strength of individual paper fiber bonds requires further development.

Introduction

The development of micro-and nanorobotic technologies and systems and their demonstration in different application sectors has been very active in the recent years (Kim et al. 2008; Krohs et al. 2007; Matsuokaa et al. 2005; Sakaki et al. 2007; Wang et al. 2007). Micro- and nanorobotics have provided significant added value to the research of living cells such as oocytes and embryos manipulated in liquid suspension (Desai et al. 2007; Jager et al. 2000; Park et al. 2004), various adherent eukaryotic cells which need a substrate to grow in, bacterial cells and even sub-cellular components and structures (Arai et al. 2002; Georgiev et al. 2004; Hirvonen et al. 2008; Inoue et al. 2005; Kallio and Kuncova 2006; Kallio et al. 2007; Sun et al. 2004). Other important application areas of micro- and nanorobotic systems are microassembly (Eichhorn et al. 2007; Sardan et al. 2008), manipulation of nanoparticles such as carbon nanotubes (Carlson et al. 2007), and material characterization using nanoindentation methods (Tze et al. 2007), for example. Even though micro- and nanorobotics have been extensively studied in many application areas, the potential of micro- and nanorobotic technologies has been very inadequately utilized in pulp and paper research.

Understanding the properties of papermaking fibers will contribute to the understanding of paper properties as well. For example, researchers and engineers are using mathematical and physical models to estimate the microscale properties of pulp and paper (Hofstetter et al. 2009). The mechanical properties and the chemical composition of papermaking fibers are normally determined by bulk (i.e. average) parameters using sample portions of the papermaking fibers under study. The average bulk parameters, however, do not provide a real possibility for predicting relevant fiber properties and chemical composition. The interest in and the necessity of getting new information and data on papermaking fibers, fiber wall fine structures, and fiber-fiber bonds have increased during the recent years.

In addition to the new measurement data, controlled mechanical treatment and chemical functionalization of *individual paper fibers (IPFs)* could lead to dramatic improvements in the properties of fiber products. The aforementioned controlled functionalization, treatment and characterization of individual fibers request new tools. The methods currently available in industrial and academic fiber research laboratories are typically very laborious to use, require extensive manual preparation and provide a very low yield. Currently available mechanical fiber characterization methods include flexibility and tensile strength measurements. Tensile tests are typically made using micro-tensile testing (Burgert et al. 2003; Eder et al. 2008; Hinterstoisser et al. 2003; Salmén et al. 2004), even though a microrobotic method of nanoindentation has already been reported in the study of the tensile strength properties of single paper fibers (Tze et al. 2007).

Different methods are available to estimate the flexibility of the IPFs. CyberFlex is a commercial product from Papertech, Inc. which measures the flexibility of IPFs by using regular optics and image processing algorithms. The weakness of CyberFlex is its low throughput and a time-consuming procedure for sample preparation. Measurement of wet fiber flexibility by confocal laser scanning microscopy based on the fiber conformability method was reported recently (Yan and Li 2008). In this method, the free span length was measured directly from the transverse view of the fiber span. The collapsibility and the moment of inertia can also be measured from the fiber's cross-section which enables the measurement of the elastic modulus of the IPFs. Measurement of IPF flexibility in a flow cell based device has also been reported (Eckhart et al. 2009). Considering the current fiber flexibility methods to measure the flexibility of individual paper fibers, they all measure the flexibility of the IPFs indirectly.

Micro- and Nanosystems Research Group of the Department of Automation Science and Engineering foresees that micro- and nanorobotic technology facilitates the development of a novel research platform which will allow the required versatile fiber studies at a sufficiently high throughput at an individual cell level in a single instrument.

This paper presents such a versatile microrobotic platform and illustrates fiber manipulation, flexibility measurement and breaking individual paper fiber bonds (IPFB)s as examples of the operations which will be performed with the platform. The most important advantage of the approach used in the platform is the ability to measure the flexibility of the IPFs directly. The platform is also able to manipulate and break individual paper fiber bonds, which is the first step towards individual bond strength measurement. In addition, it provides an infrastructure for a fully automated paper fiber manipulation and mechanical characterization platform.

The rest of this paper is organized as follows. Firstly, it explains the theory and the principles of flexibility measurement, the architecture and conceptual design of the platform, and the technical requirements of the platform. Next, it describes the design and implementation, and the

experiments performed by using the platform. Finally, it elucidates the results and conclusions, and the actions to be taken in continuation of this research.

Theory

The first goal in developing the platform is to measure the flexibility of the IPFs. The principle of the measurement is to utilize the "Beam Theory" (Young and Budynas 2002) in a case, where both ends of the beam are fixed. Figure 1 illustrates a beam with both-ends-fixed boundary condition.
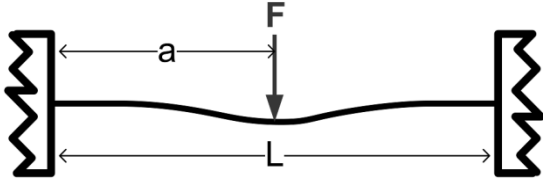
Figure 1. Both-ends-fixed boundary conditions under transverse loading

The maximum deflection, y_{max}, of a both-ends-fixed beam with length L, under a concentrated intermediate load, F, applied on distance, a, from the origin is

$$y_{max} = \frac{-2F(L-a)^2 a^3}{3EI(L+2a)^2} \ at \ x = \frac{2aL}{L+2a} \ if \ a > \frac{L}{2} \tag{1}$$

where E is young's modulus and I is moment of inertia of the beam. Therefore, if the force is applied in the center of the beam, the maximum deflection value is as follows:

$$y_{max} = \frac{-FL^3}{192EI} \ at \ x = a = \frac{L}{2} \tag{2}$$

Flexibility is the compliance of an elastic body to deformation by an applied force; or in the other words, it is the inverse of bending stiffness,

$$Flexibility = \frac{1}{EI} = \frac{192 \ y_{max}}{-FL^3} \tag{3}$$

In the aforementioned analysis, axial loading of the beam was not considered. Figure 2 illustrates a beam with both-ends-fixed boundary conditions under simultaneous axial, P_t, and transverse loading, F.
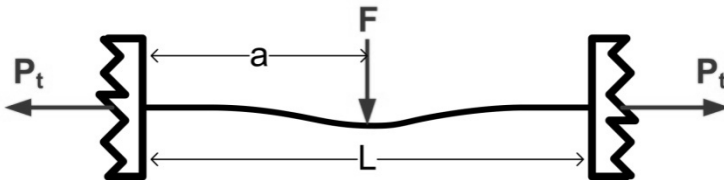
Figure 2. Both-ends-fixed boundary conditions under simultaneous axial tension and transverse loading

Conceptual Design

The architecture of the platform is illustrated in Figure 3. It includes six main functions: sample storage, micromanipulation, force sensing, visualization, dispensing and control.

Figure 3 shows these six functions and their interaction to each other. Each function is divided to sub-functions which are explained in this section in details.
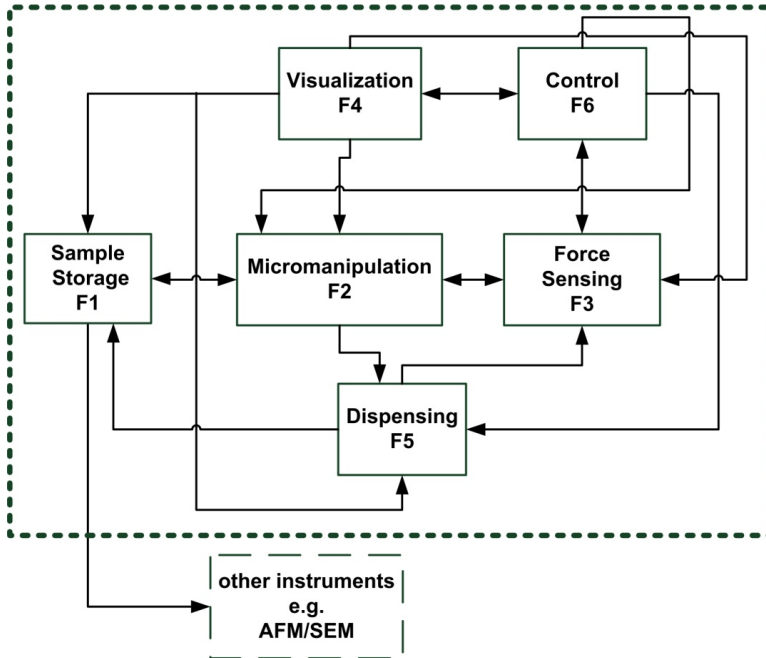
Figure 3. Main functions

Sample storage (F1) consists of three sub-functions: suspension storage, dry storage and frame fixture. To pick up and separate IPFs, it is necessary to disintegrate the dry pulp and make the paper fibers float in the water. Fibers are dried and stored in a paper fiber bank. The individual paper fiber bank (IPF-bank) is a place to store the IPFs sorted based on their type, length and treatment for example. The coordinates of the sorted and stored IPFs and their properties are saved for a later use. The platform also prepares samples for other instruments, such as Atomic Force Microscope (AFM) or Scanning Electron Microscope (SEM).

Micromanipulation function (F2) enables micropositioning, micro-orienting and microgripping of the IPFs. The micropositioning sub-function is used for placing the area of interest – an IPF-bank, a rotary table, a force sensor – in the working space of microgrippers. Micro-orienting facilitates the change of fiber orientation; and microgripping performs the grasping and handling of IPFs. Micromanipulation is also used for moving the dispenser and aligning the dispenser tip on the required targets to shoot droplets for chemical treatment.

Force Sensing function (F3) encompasses two sub-functions, flexibility measurement and bond strength measurement. This function measures the magnitude of force, F, which is applied to the IPFs to bend them and uses information from the other functions such as the length of IPFs, L, from the visualization function (F4) in the control system, to measure the flexibility of IPFs. It also measures the bond strength between two IPFs.

Visualization function (F4) is composed of four sub-functions: imaging, magnification, illumination and signal analysis. Imaging sub-functions acquire visual information to be used as visual feedback in the control function (F6). Considering the IPFs dimensions, a sufficient

magnification and high quality illumination are essential. To accomplish pattern recognition and image analysis as quickly as possible, an independent signal analysis sub-function is required.

Dispensing (F5) encompasses two sub-functions, preparatory-chemical treatment which is required in the sample storage function (F1); and instant chemical treatment which is useful when chemical treatment is needed before the flexibility measurement test.

The most important sub-function of the control function (F6) is the micromanipulation control which controls micropositioning, micro-orienting and microgripping devices. Visualization control sub-function regulates zooming and fine focusing. A user interface sub-function connects all the control sub-functions to the human operator. Force feedback sub-function supplies a sensible force feedback to the human operator. Dispensing control sub-function triggers the dispenser and provides the required droplet size for chemical treatment. The required calculations to measure the flexibility of the IPFs are performed in the measurement algorithm sub-function.

Technical Requirements

This section encompasses technical requirements of the platform to manipulate IPFs, to measure the flexibility of the IPFs and to break individual paper fiber bonds without measuring the bond strength. The major technical requirements for micromanipulation, visualization and force sensing functions stem from the IPF's dimensions and throughput objectives.

Micromanipulation

Whereas characterizing few IPFs is not sufficient to provide valuable statistical information about paper fibers, it is necessary to perform these characterization tests automatically. Based on wood scientists' requirements, five thousand tests per day, 24 hours, provides adequate amount of data for statistical analysis. Six hours calibration and maintenance break for a day is reserved; this leaves 13s for each experiments. Six tasks are identified in a flexibility measurement procedure: IPF recognition and coordinate calculation, IPF orientation and pick up, IPF length measurement, IPF transport to force sensing place, chemical treatment and force sensing and calculation; providing an average of 2.16s for each task.

The micropositioning, micro-orienting and microgripping sub-functions are implemented by using a two degrees-of-freedom (DOF) micropositioner, a rotary table and three microgrippers mounted on XYZ-micropositioners, respectively. The technical requirements of the aforementioned sub-functions are shown in Table 1 which are derived based on the average time of each task, minimum and maximum diameter of IPFs, accessibility of micropositioner to all sections of the platform, the required travel directions, the required resolution and speed, and the accessibility of microgrippers to the rotary table, the IPF-bank and the force sensor.

Table 1. Technical requirements of micromanipulation

	Resolution	Direction	Speed	Travel
Micropositioning	Sub-µm	XY	9 mm/s	4 cm
Micro-orienting[1]	10 µ°	CW-CCW[3]	30°/s	90°
Microgripping[2]	Sub-µm	XYZ-Gripping	9 mm/s	2 cm

1) Diameter: Min.1 cm
2) Gripper Tip Opening: Min. 70µm, Max. 1 mm
3) CW – CCW: Clock Wise – Counter Clock Wise

Visualization

In paper fiber studies, a high optical resolution is necessary to achieve detailed images. Based on the IPF dimensions, the required Field of View (FOV) is around 4.5×2 mm^2. In another hand, a broad image of the test bench and microgrippers is also needed which requires a larger FOV such as 20×8 mm^2. To have a proper image of the paper fibers 3X magnification is required. To have the broad image of the working space 0.25X magnification is required leading to a magnification range of 0.25X - 3.0X. Since a wide range of magnification is needed, a zooming tube microscope is preferred to a constant magnification tube microscope. To know the magnitude of the zoom to estimate the length of paper fiber, a computer controlled motorized zooming system is needed. Considering the size of XYZ-micropositioners, the required working distance of the tube microscope is minimum 5 cm. In flexibility measurement application where only the length of the IPF is measured from the image, the required spatial resolution for the camera is calculated to be 5.0 μm or better.

Force measurement

In order to select a suitable micro force sensor, it is necessary to estimate the amount of force required to measure the flexibility of the IPFs. When two microgrippers are used to grasp the IPFs, the both-ends-fixed boundary conditions of the beam theory are applicable in this case. The formula for calculating bending stiffness and flexibility of IPFs under both-ends-fixed boundary conditions is explained in the Section: Theory. Regarding to the fact that cellulose is the main material in a paper fiber cell wall, it is possible to use the Young's modulus of microcrystalline cellulose, 25±4 GPa (Eichhorn and Young 2001), the geometry of hardwood and softwood and Equation 3 to simulate the required forces to bend an IPF. The simulation shows that the maximum required forces for hardwood and softwood are 206 μN and 29 μN, respectively. Table 2 shows the flexibility values simulated based on the Young's modulus of microcrystalline cellulose and typical average IPF dimensions. In this simulation, it is assumed that the IPF is a symmetrical tube, made of only homogeneous cellulose and the maximum deflection, y_{max}, is 2% of the length of the IPFs. The hardwood/softwood flexibility ratio based on this simulation is 23.

Table 2. Flexibility values based on the Young's modulus of microcrystalline cellulose. Assumption: Maximum deflection is 2% of the length of the IPFs

	Bending Stiffness (Nm^2)×10^{-9}	Flexibility (N^{-1}m^{-2})×10^9
Softwood	29.7	0.34
Hardwood	12.8	7.82

Design and Implementation

This section explains design and implementation of the platform. It includes a survey and selection of the devices used to implement the micromanipulation, visualization and force sensing functions in the platform. Considering the technical requirements of the visualization function, a motorized zoom system providing 0.29X-3.50X magnification and LED coaxial illumination are chosen (Navitar Co.). The camera (XCD-U100 Sony) selected has a 1=1.8" CCD cell chip, a resolution of 1600×1200 pixel and a pixel size of 4.4 μm. After several design iterations, a *Stacked Gantry Crane* configuration, shown in Figure 4, is used in the platform. It provides several benefits, such as having the most compact design without coordinate mapping and with fixed camera.

Table 3 shows the components of platform based on numbering of Figure 4. In this configuration, there are two tailored 4DOF (1, 2), and one 5DOF (3) micromanipulator from SmarAct Co. In addition to the XYZ-positioners and the microgripper, the 5DOF unit includes a positioner for a dispenser (4). The platform includes also a XY-Table (6) of SmarAct on top of which the following equipment are mounted: force sensor (FT-S540 by Femto Tools) (8), a micro-rotary table (SR-1908 by SmarAct) (5), and the IPF-bank (7) to perform the designed tasks. The IPF-bank is made of SU-8, a common epoxy-based negative photoresistant polymer used in lithography, with the height of 200 μm and placed on XY-Table to store the sorted IPFs. Figure 5 shows the top and side view of the current implementation of the platform.
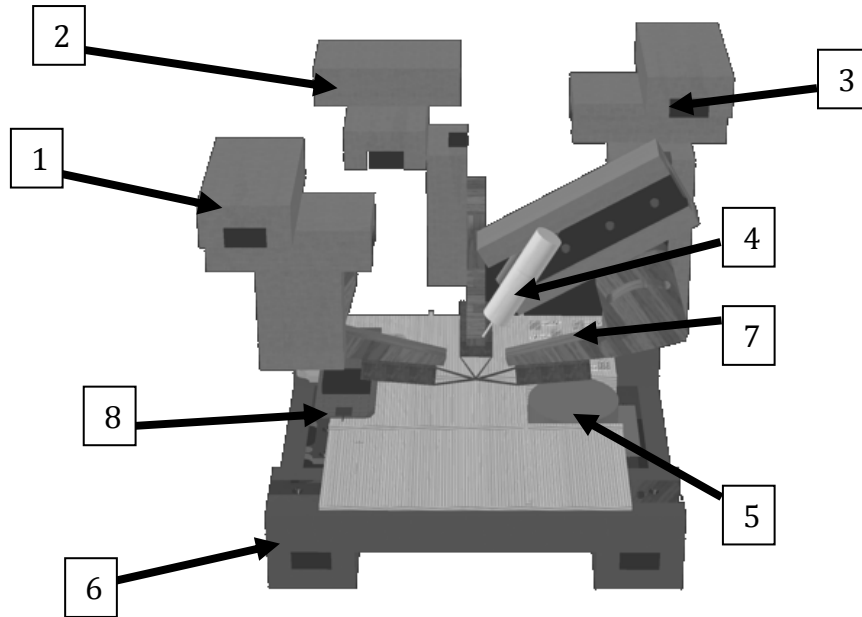
Figure 4. 3D Design of the platform

Table 3. Components of the platform

No.	Component	DOF
1, 2	Microgripper (1, 2)	4 – XYZ+Gripping
3	Microgripper (3)	5 – XYZ+Gripping+Dispenser Positioner
4	Dispenser	--
5	Rotary Table	1 – Rotation in XY-Plane
6	Micropositioner	2 – XY- Plane
7	IPF Bank	--
8	Force Sensor	--
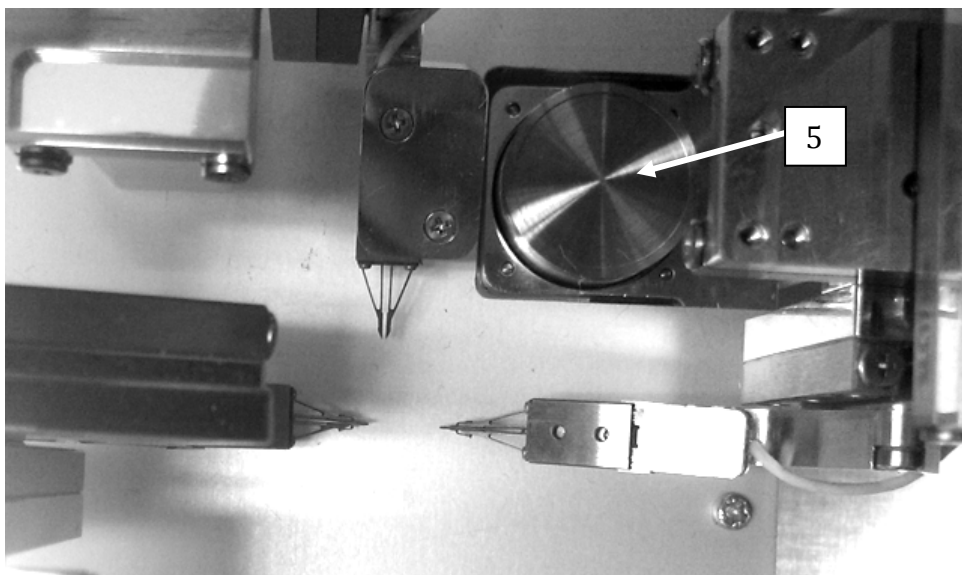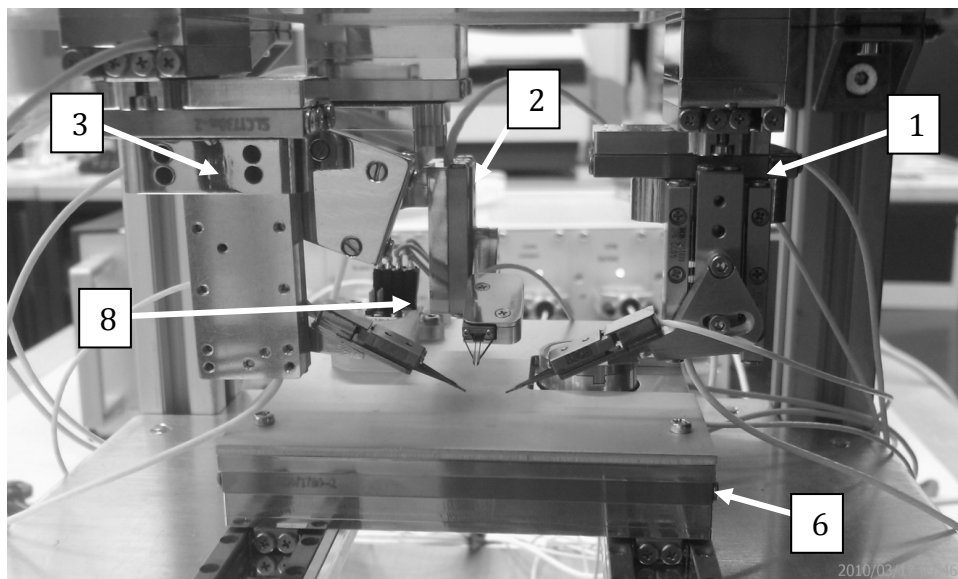
Figure 5. Implementation of the platform. Top: Side-view. Bottom: Top-view

Experiments

This section discusses the experiments on measuring the IPF flexibility and breaking IPFBs using the platform.

Flexibility Measurement

Softwood, hardwood and treated softwood are used as raw materials in the experiments. Sample 1 is bleached Pine kraft pulp which is softwood. Sample 2 is bleached hardwood pulp. As an additional challenge, Sample 1 is treated such that only the S2 and S3 layers and some residues of S1 layer remain in the cell wall.

A small bundle of paper fibers is taken from the pulp sample. The bundle is placed in a Petri dish and it is disintegrated by adding deionized water and shaking. Then the IPFs are soaked for five minutes. Next, the IPFs are placed on the rotary-table by using a pipette. Figure 6 illustrates the process of IPF manipulation and flexibility measurement in 27±2% relative humidity and 25±1°C temperature. The microgrippers pick up the IPF from the rotary-table, (1 and 2), and then straighten the IPF by pulling (3 and 4). The effective length, *L,* of the IPF is measured by using the visualization function. The force sensor is then pushed in the middle of the IPF by using the XY-table and the required amount of force *F* (5 and 6 in Figure 6). The deflection, *y,* of the center point of the IPF is read-out from the position sensor of the XY-table.
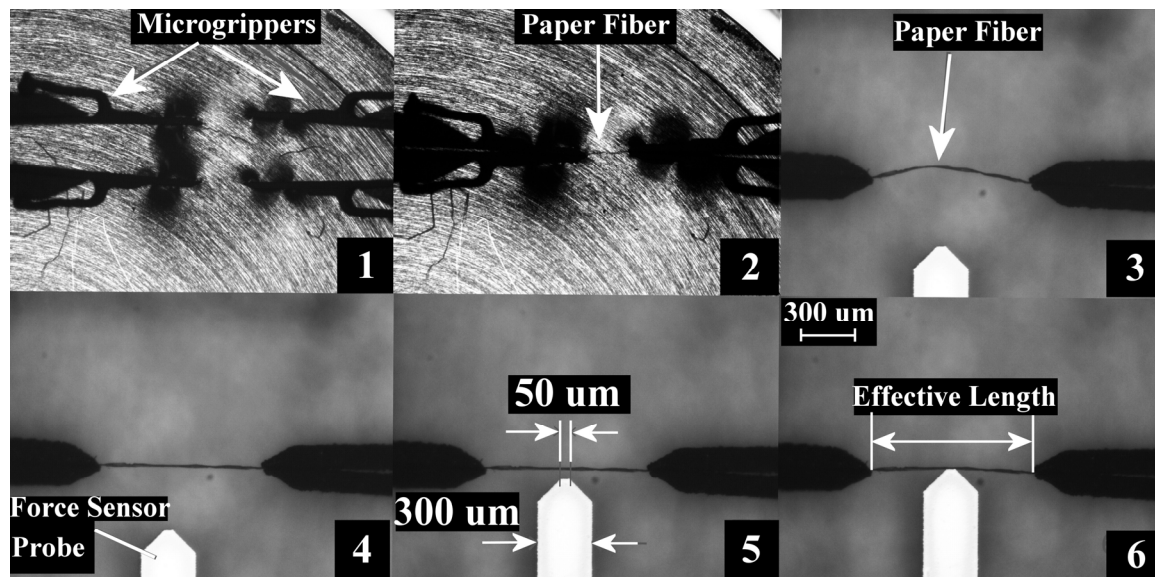
Figure 6. Flexibility measurement using the platform

The vertical alignment of the IPFs is done by using the force sensor probe. Figure 7 illustrates the IPF vertical alignment process. First the force sensor's probe is placed in the middle of the IPF (Figure 7-a). Next, keeping the force sensor's Z-direction coordinate fixed and by moving the force sensor in the XY-plane, the IPF misalignment is recognized (Figure 7-b, c). Then, the IPFs are aligned by adjusting the microgrippers in the Z-direction (Figure 7-e, f). Finally, the IPF alignment is checked before starting the actual tests (Figure 7-d).
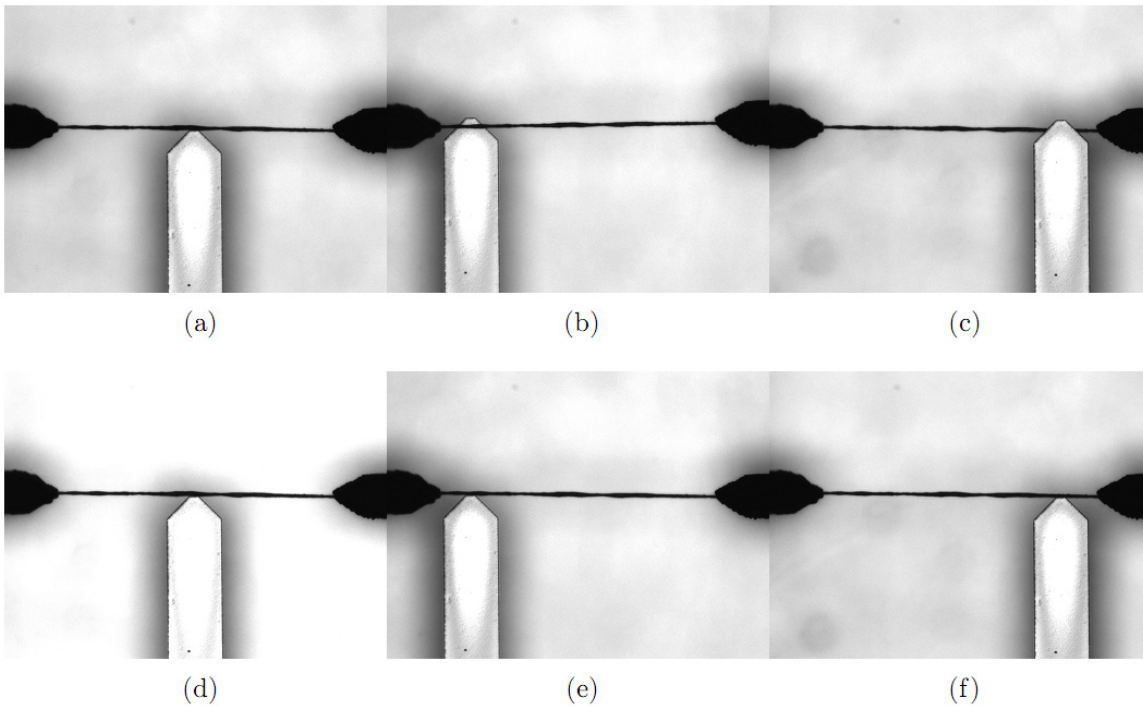
Figure 7. Vertical alignment of IPF. a, b, c: Before alignment. d, e, f: After alignment

Bond Breaking

In order to demonstrate the capability of breaking an individual fiber bond, the bond must first be produced. The following procedure was used in preparing the individual fiber bonds (IPFB). A small bundle of bleached Pine kraft pulp is placed in a Petri dish and it is disintegrated by adding deionized water and shaking. Next, the IPFs are placed randomly between two 4×4 cm^2 Teflon plates by using a pipette. Then, the plates are pressed together and kept in 70 °C for one hour. After the incubation, the IPFBs are identified in a light microscope and moved to rotary table manually by using tweezers. Figure 8 shows an IPFB.
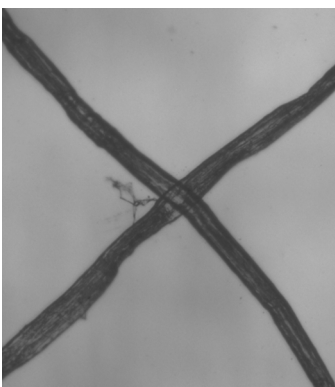
Figure 8. Individual paper fiber bond (IPFB) of bleached Pine kraft pulp

Figure 9 shows the process of breaking an IPFB. The IPFB on the rotary table is identified (Figure 9-a). Next, two parallel axis microgrippers grasp the both ends of IPFB and lift it from the rotary table (Figure 9-b, c). The third microgripper which is perpendicular to the other two microgrippers is used to grasp the crossed IPF (Figure 9-d). After a secure grasp, the third microgripper pulls the crossed IPF until the bond breaks (Figure 9-e, f).
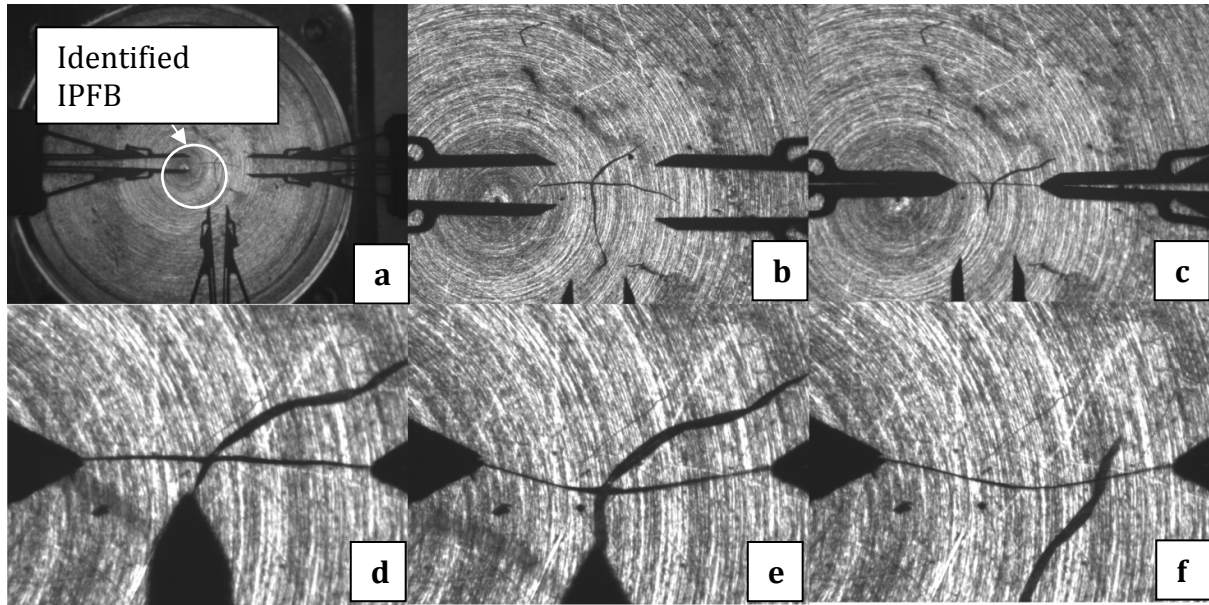
Figure 9. Process of breaking individual fiber bonds (IPFB)

Results and Conclusions

The IPF manipulation, flexibility measurements and breaking an IPFB are demonstrated. The flexibility of three different samples is measured under different boundary conditions. The applied loading is either transverse loading and zero axial tension or simultaneous axial and transverse loading; and the boundary conditions in all tests are both-ends-fixed. Table 4 illustrates all the test results.

Table 4. Results of flexibility measurement

Test	Bending Stiffness $(Nm^2)\times10^{-9}$	Flexibility $(N^{-1}m^{-2})\times10^9$
Softwood – ZAT* (n=10)	0.12±0.042	9.37±4.2
Softwood – UAT** (n=10)	0.30±0.1	3.73±1.37
Hardwood (n=10)	0.0077±0.0044	204.83±170.19
Softwood – S2-S3	0.29 ± 0.24	7.63 ± 6.93

*   *ZAT: Zero Axial Tension*
**   *UAT: Under Axial Tension*

The hardwood IPFs have a higher flexibility compared to softwood IPFs. The hardwood/softwood flexibility ratio based on simulation and experiments are about 23 and 22, respectively; which indicates similar ratio of flexibility values. The IPF model used in the simulation is a symmetrical tube but the measured IPFs are pulp fibers which are asymmetric and they have structural disorders. Furthermore, the simulation assumes that the paper fiber cell wall is made of only homogeneous cellulose; but it also contains hemicelluloses and lignin in addition to cellulose in reality. Therefore, the results based on simulation differ from the average results based on experiments but they have similar hardwood/softwood flexibility ratio.

Although the average flexibility values of the treated softwood fibers seem to differ from the normal softwood, the high coefficient of variation prevents a reliable comparison of the flexibility between the two samples. The IPFs used in the aforementioned tests are pulp fibers and not wood fibers. The pulping process damages the IPF's body seriously. Wood fibers,

however, are screened manually based on their botanical properties, such as latewood or earlywood, fibers or tracheids, etc. This issue is one of the main sources of errors in these measurements. The preliminary flexibility tests with softwood IPFs under axial tension show improvements in the repeatability of the results but the mathematical model which includes the effect of the axial tension needs to be incorporated. Breaking of the IPFBs can be performed successfully by using the platform which is the first step towards individual bond strength measurement.

Future Works

In the continuation of this research the following actions can be taken. The aforementioned tests need to be repeated by using wood fiber samples instead of pulp fiber samples to achieve better standard deviations.

The preliminary flexibility tests with softwood IPFs under axial tension show improvements in the repeatability of the results but the mathematical model which includes the effect of the axial tension needs to be incorporated. It is necessary to integrate an axial force sensor into the platform, to measure the actual flexibility of the IPFs under simultaneous axial and transverse loading. Considering the state of the art on single fiber studies, there is no direct method to measure the IPF-IPF bond strength. This platform provides the infrastructure for such a measurement. A force sensor needs to be integrated in the platform to measure the IPFB strength.

The flexibility tests can be performed in wet conditions either by using a humidity chamber or by performing the test under water. It is possible to place the probe of the force sensor and the tip of the grippers under water. Therefore, by changing the angle of the force sensor, the flexibility tests can be performed under water. A controlled humidity and temperature chamber should be added to the platform, because the standard conditions for testing the IPFs require 50%±2 relative humidity and 20±1°C temperature.

To collect statistically reliable information, it is necessary to make aforementioned teleoperated processes fully automated in the future to perform hundreds of flexibility tests per hour. On the other hand, this platform can be used not only for IPFs but also for other kinds of fibers in microscale.

Acknowledgement

References

Arai F., Sakami T., Maruyama H., Ichikawa A. and Fukuda T. (2002): Minimally Invasive Micromanipulation of Microbe by Laser Trapped Micro Tools. IEEE International Conference on Robotics and Automation (ICRA'02) USA, 1937-1942

Burgert I., Frühmann K., Keckes J., Fratzl P., Stanzl-Tschegg S. E. (2003): Microtensile Testing of Wood Fibers Combined with Video Extensometry for Effcient Strain Detection. Holzforschung 57(6) 661–664

Carlson K., Andersen K. N., Eichhorn V., Petersen D. H., Molhave K., Bu I. Y. Y., Teo K. B. K., Milne W. I., Fatikow S. and Boggild P. (2007): A Carbon Nanofibre Scanning Probe Assembled using an Electrothermal Microgripper. Nanotechnology 18, 34, 7pp

Desai J. P., Pillarisetti A. and Brooks A. D. (2007): Engineering Approaches to Biomanipulation. Annu Rev Biomed Eng, Vol. 9, No. 1, Mar. 2007, pp 35-53

Eckhart R., Donoser M. and Bauer W. (2009): Single Fibre Flexibility Measurement in a Flow Cell Based Device, In Proceedings of Advances in Paper Science and Technology (FRC)

Eder M., Stanzl-Tschegg S. and Burgert I. (2008): The Fracture Behaviour of Single Wood Fibres is Governed by Geometrical Constraints: In Situ ESEM Studies on Three Fibre Types. Wood Sci. Technol. 42, 8 679-689

Eichhorn S.J. and Young R.J. (2001): The Young's Modulus of a Microcrystalline Cellulose. Cellulose 8, 3 197–207

Eichhorn V., Carlson K., Andersen K.N., Fatikow S. and Boggild P. (2007): Nanorobotic Manipulation Setup for Pick-and-Place Handling and Nondestructive Characterization of Carbon Nanotubes. IEEE/RSJ Int. Conf. Intelligent Robots and Systems (IROS'07), USA, 291-296

Georgiev A., Allen P.K. and Edstrom W. (2004): Visually-guided Protein Crystal Manipulation using Micromachined Silicon Tools. IEEE/RSJ Int. Conf. Intelligent Robots and Systems (IROS'04), Japan, 236-241

Hinterstoisser B., Åkerholm M. and Salmén L. (2003): Load Distribution in Native Cellulose. Biomacromolecules 4, 5 1232–1237

Hirvonen J., Ronkanen P., Ylikomi T., Bläuer M., Suuronen R., Skottman H. and Kallio P. (2008): Microcutting of Living Tissue Slices and Stem Cell Colonies by Using Mechanical Tool and Liquid Jet. IEEE RAS & EMBS Int. Conf. Biomedical Robotics and Biomechatronics (BIOROB'08), USA, 612-617

Hofstetter K. and Gamstedt E. K. (2009): Hierarchical Modelling of Microstructural Effects on Mechanical Properties of Wood. Holzforschung 63, 2 130–138

Inoue K., Arai T., Tanikawa T. and Ohba K. (2005): Dexterous Micromanipulation Supporting Cell and Tissue Engineering. IEEE Int. Symp. Micro-NanoMechatronics and Human Science (MHS'05), Japan, 197-202

Jager E. W. H., Inganäs O. and Lundström I. (2000): Microrobots for Micrometer-Size Objects in Aqueous Media: Potential Tools for Single-Cell Manipulation. Science 288, 5475 2335 - 2338

Kallio P. and Kuncova J. (2006): Capillary Pressure Microinjection of Living Adherent Cells: Challenges in Automation. JµM 3, 3-4 189-220

Kallio P., Ritala T., Lukkari M. and Kuikka S. (2007): Injection Guidance System for Cellular Microinjections. Int. J. Robot Res. 26, 11-12 1303 - 1313

Kim K., Liu X., Zhang Y. and Sun Y. (2008): Nanonewton Force-Controlled Manipulation of Biological Cells Using a Monolithic MEMS Microgripper with Two-Axis Force Feedback. J. Micromech. Microeng. 18(2008) 055013 (8pp)

Krohs F., Hagemann S. and Fatikow S. (2007): Automated Cell Characterization by a Nanohandling Robot Station. Mediterranean Conf. Control & Automation (MED'07), Greece, 1-6

Matsuokaa H., Komazakia T., Mukaia Y., Shibusawaa M., Akanea H., Chakic A., Uetakec N. and Saitoa M. (2005): High Throuput Easy Microinjection with a Single-Cell Manipulation Supporting Robot. Biotec. 116, 2 185-194

Park J., Jung S. H., Kim Y. H., Byungkyu K., Lee S. K., Ju B. and Lee K.I. (2004): An Integrated Bio Cell Processor for Single Embryo Cell Manipulation. IEEE/RSJ Int. Conf. Intelligent Robots and Systems (IROS'04), Japan, 242-247

Sakaki K., Dechev N., Park E.J. and Burke R.D. (2007): Development of a Five Degree-Of-Freedom Biomanipulator for Autonomous Single Cell Electroporation. IEEE/RSJ Int. Conf. Intelligent Robots and Systems (IROS'07) USA, 3137-3143

Salmén L. (2004): Micromechanical Understanding of the Cell-Wall Structure. J. Plant Biol. Pathol. 327, 9 873-880

Sardan O., Eichhorn V., Petersen D. H., Fatikow S., Sigmund O. and Boggild P. (2008): Rapid Prototyping of Nanotube-Based Devices using Topology-Optimized Microgrippers. Nanotechnology 19(2008) 495503 (9pp)

Sun Y., Greminger M.A. and Nelson B.J. (2004): Investigating Protein Structure with a Microrobotic System. IEEE Int. Conf. Robotics and Automation (ICRA'04), USA, 2854-2859

Tze W.T.Y., Wang S., Rials T.G., Pharr G.M., Kelley S.S. (2007): Nanoindentation of Wood Cell Walls: Continuous Stiffness and Hardness Measurements. Compos Part A-Appl. Sci. Manufacturing 38, 3 945-953

Yan D. and Li K. (2008): Measurement of Wet Fiber Flexibility by Confocal Laser Scanning Microscopy. J. Mater. Sci. 43, 8 2869–2878

Young W. C. and Budynas R. G. (2002): Roak's Formulas for Stress and Strain - Seventh Edition, McGRAW-Hill

Wang W., Liu X., Gelinas D., Ciruna B. and Sun Y. (2007): A Fully Automated Robotic System for Microinjection of Zebrafish Embryos. Plos One, 2, 9 e862

NANO- AND MICRO- MECHANICS OF SINGLE WOOD PULP FIBRES

[1]Ramesh-Babu Adusumalli, [1]Boopathy Kombaiah, [1]William Mook, [2]Raphaël Passas,

[1]Rejin Raghavan, [1]Johann Michler

[1]Mechanics of Materials and Nanostructures, Swiss Federal Laboratories for Materials Testing and Research, EMPA, CH-3602 Thun, Switzerland

[2]Laboratory of Pulp and Paper Science and Graphic Arts, Grenoble INP-Pagora,

38400 Saint Martin d'Heres Cedex, France

E-mail: adusumalli_2000@yahoo.com; johann.michler@empa.ch

Abstract

Mechanical testing of single pulp fibres is rarely discussed due to the difficulties in handling the specimens. In the present investigation, the nano- and micro-mechanics of single pulp fibres (chemical) are studied by using nanoindentation and a novel in-situ SEM microindentation technique. In order to study the pulp fibres at cell wall scale, single fibres were subjected to indentation tests using a nanoindenter equipped with an AFM scanner. It has been shown that the bleaching process, a routine technique in pulp industry, causes a reduction in cell wall hardness due to the removal of lignin. To understand the fibre deformation and to identify the critical stress level in transverse direction, a novel in-situ scanning electron microscope (SEM) microindentation technique was adopted for the first time to test single industrial pulp fibres. The cell wall deforms by 'elastic' sinking-in and lateral bulging of the microfibrils. In addition, the paper frame set-up used previously (Adusumalli et al. 2006) to test single long fibres has been modified here in order to test both hardwood and softwood pulp fibres in tension. Due to the brittle nature of the pulp fibres, the proposed single fibre tensile tests did not yield promising results, although some successful measurements are reported for softwood pulp fibres.

Introduction

Wood fibre or cell is a complex anisotropic material and is composed of cell wall and lumen. The cell wall consists of a thin primary wall (P), the most external layer, and secondary walls of S1 layer, S2 layer, and S3 layer. The S2 wall, thickest among all cell wall layers, consists of up to 50% partly crystalline cellulose microfibrils wound in a spiral fashion around the stem axis and embedded in a matrix of hemicellulose and lignin (Mark et al. 2002). The spiral angle of the cellulose fibrils is known as micro fibril angle (MFA) and it is considered to be the most influential factor in wood and pulp fibre mechanical properties (Courchene et al. 2006, Lichtenegger et al. 1999, Page and El-Hosseiny 1983). Both, softwood (longer fibres, thinner cell walls in earlywood and thicker cell walls in latewood: 2-10 μm) and hardwood (shorter fibres, cell wall thickness: 2-5 μm) are used as a fibre source for paper and board (Karlsson 2006).

Wood is converted to pulp fibres by a pulping process. Since the middle lamella is readily dissolved away by macerating solutions, chemical pulping or cooking is widely used to separate the cells (fibres) from the middle lamella. Bleaching is performed after cooking in order to increase the brightness of the pulp. Bleaching of chemical pulps is a multi-stage process where the lignin is oxidized, decomposed and finally eliminated from the pulp fibres. As a result of cooking, bleaching and subsequent drying, pulp fibres are more collapsed (reduction in lumen size), thin-walled (P and S1 layers are peeled off) and flattened in shape compared to native

wood fibres (Karlsson 2006). Mohlin et al. (1996) reported the process induced defects such as micro compressions, curls, twists and kinks along the cell length as a result of chemical pulping and refining. Even though it is widely accepted that paper constitutes pulp fibres with process-induced defects as well as natural defects such as pits, not enough studies have been carried out to understand the influence of fibre damage on the paper network. Pulp quality is generally determined by preparing hand sheets and then performing standard paper testing methods such as zero-span tensile tests and short-span compression tests (Mark et al. 2002). Due to the non-uniform geometry and chemical composition of individual pulp fibres, only a few studies have been performed to understand the single pulp fibre deformation and their mechanical properties.

Unlike textile fibres, single pulp fibre tensile tests are not routinely carried out with commercial instrumentation due to their limited length (1-4 mm) and width (15-40 μm). However a few studies can be found in literature about the single fibre testing of pulp fibres, mostly on softwood fibres. Page (1971) and Page and El-Hosseiny (1983) published the results of 1.2 mm long single spruce pulp fibres and also reported a correlation between MFA and elastic modulus. Mott et al. (1995) studied the virgin and recycled pulp fibres (1.2 mm long) and found that natural defects such as bordered pits are crack initiators in single fibre tensile testing. In most of the single fibre tests, the ball and socket method was used to fix the fibres between two droplets; load is measured through the load cell while the tensile test is carried out either under light microscopy (Gilani 2006) or environmental scanning electron microscopy (ESEM) (Burgert et al. 2005; Mott et al. 1995). Elongation in tensile test is measured either with cross-head movement or image analysis. Recently Eder et al. (2008) studied the earlywood and latewood single fibres by subjecting them to tensile testing under ESEM. Similarly single fibre testing of bast fibres and man-made fibres were also quoted elsewhere (Adusumalli et al. 2006). Dunford and Wild (2002) studied the mechanical behaviour of single pulp fibres using cyclic transverse compression. Xing et al. 2008 studied the influence of thermomecahnical refining pressure on pulp fibre properties using the nanoindentation technique.

Mohlin et al. (1996) reported that fully bleached commercial pulps are more deformed than unbleached pulps. Deformation such as kinks, angular folds and twists which are prone to change the direction of the fibre axis are found to have a negative effect on the tensile index, compressive strength, etc. So in the present study, the influence of bleaching on single pulp fibre properties is conducted. Here, the paper frame set-up was modified for the tension test in order to fix the fibres of small length commonly seen in hardwood fibres. Since the aim of the present study is to understand the pulp fibre properties at cell wall dimensions, nanoindentation is performed for the first time on fibre cross-sections to measure the hardness and elastic modulus of the S2 cell wall. Since the indentation displacement range is generally between 0.1 to 2 μm, it is possible to probe localised areas of collapsed pulp fibre cell walls having thicknesses of 2 to 5 μm. Nanoindentation of wood fibre cell walls was studied by several authors (Gindl et al. 2004, Wu et al. 2009, Zickler et al. 2006). Since the tensile and nanoindentation tests are performed in the longitudinal direction, a third test is introduced in this chapter to understand the "localised" deformation and fracture behaviour of a single pulp fibre in the transverse direction. This novel technique allows real time correlation between the cell wall deformation and the response from the load cell in addition to advantages of the scanning electron microscope (SEM) over an optical microscope used in other studies. In the present paper the in-situ SEM microindentation of transverse pulp fibres is explained and preliminary results are reported.

Materials and methods

Softwood pulp (Scots pine, *Pinus sylvestris*) as a dry sheet and hardwood pulp (Eucalyptus, *Eucalyptus globulus*) as pellets produced in the laboratory were used as raw materials for the

present study. Kappa numbers of unbleached hardwood (HWUB), bleached hardwood (HWB), unbleached softwood (SWUB) and bleached softwood (SWB) were 13, 1.5, 29 and <1 respectively. Unbeaten kraft fibres are selected for the present study. In order to prepare the samples, few grams of pulp were suspended in water, stirred magnetically for five minutes, until fine fractions of pulp were obtained, and a drop of pulp solution was placed on a glass slide and allowed to dry at room temperature. For nanoindentation, the pulp suspension was allowed to flow in one direction by keeping the glass slide tilted in position for 24 hours at room temperature. For tensile and microindentation tests, dried single fibres were carefully extracted using micro tweezers.
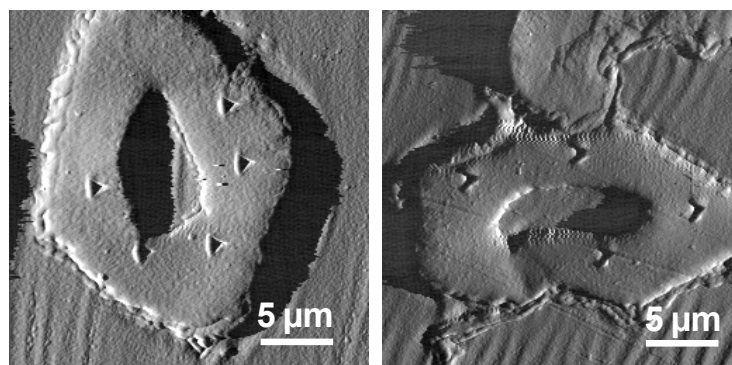
Figure 1. Hysitron scanning probe microscope image of bleached (left) and unbleached (right) hardwood pulp fibre cross sections after indentation testing. Note the pyramidal impressions on cross sections from nanoindentation tests. Prior to nanoindentation, both fibres were embedded in epoxy and micro-tomed until smooth surface was achieved. The depths of the indents are approximately 200 nm.

Nanoindentation

Fibre-bundles (partially aligned) were removed from the glass slide and placed in a silicone mould using micro tweezers. Using alternating vacuum-pressure treatment, pulp fibres were embedded in epoxy resin and cured at 60 °C for 8 hours (Spurr 1969). Cured epoxy blocks were removed from the silicone mould and a razor blade was used to cut the epoxy blocks until fibre cross sections were exposed along the surface which was further polished until a smooth surface was achieved. A microtome with a diamond rotating knife was used to further cut the surface down to the 1 μm level. Specimens prepared with this method revealed smooth surfaces as shown in Figure 1. A detailed description of the sample preparation for nanoindentation can be found in the literature (Adusumalli et al. 2010a). After sectioning, the epoxy blocks were fixed to aluminium disks using cyanoacrylate adhesive and mounted on the magnetic sample holder of a Hysitron TriboIndenter (Hysitron, Inc. Minneapolis, 55344 USA) as shown in Figure 2. Indentation was performed at ambient temperature and relative humidity. Pulp containing latewood fibre cell wall cross sections was identified using the nanoindenter's optical microscope. In the case of hardwood pulps, only libriform fibres were considered. The indenter tip then scanned the chosen surface regions (with scan sizes up to 50 X 50 μm^2) using normal forces of approximately 200 nN such that the pulp cell wall could be found and centred underneath the tip. Indentation could be conducted with a lateral accuracy of ±100 nm at the middle of the latewood fibre cell wall having thicknesses greater than 2.5 μm. For all tests, post indentation images were taken using scanning probe microscopy. Indents performed close to the cell wall borders were not considered.
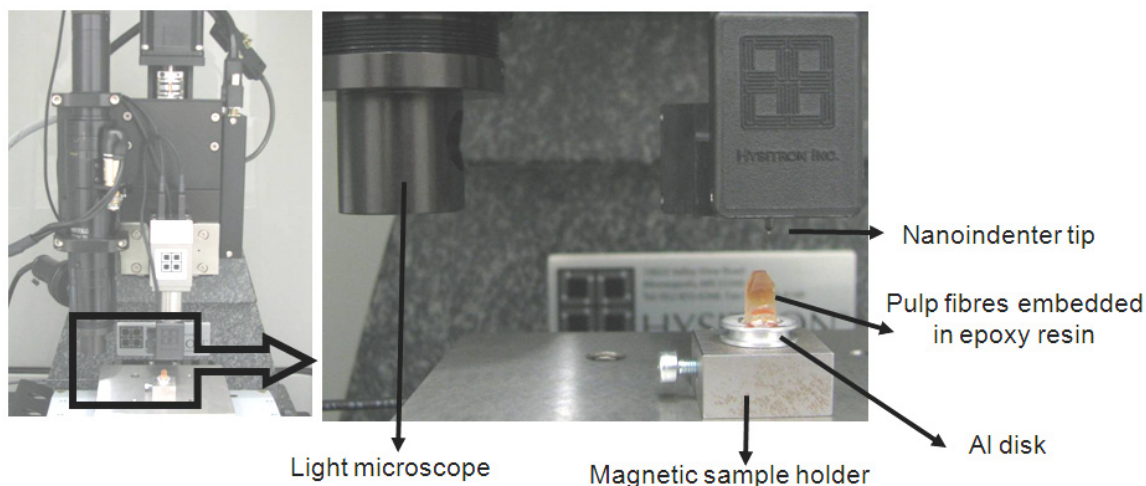
Figure 2. Set-up for nanoindentation of single pulp fibre cell walls using Hysitron TriboIndenter

On average 3-5 indents were placed on each fibre cross section. Each indent was composed of four loading cycles with increasing peak load from 20 µN in steps of 40 µN, resembling cyclic indentation (Figure 3). A maximum load of 160 µN was selected to avoid the edge effects caused by low cell wall thickness, collapse behaviour of pulp fibres and to stay within the displacement range where the area function had been calibrated for the specific indenter tip. For all steps the loading and unloading speed was 20 µN / s and the holding time at peak load was 12 s to monitor the visco-plastic creep. An ultra sharp cube corner tip made of diamond was used to perform the indents on the fibre cross sections. The load–displacement curves obtained from all experiments were evaluated according to the Oliver-Pharr method (Oliver and Pharr 1992) where peak load (P_{max}), depth at peak load (h) and initial slope of the unloading curve (S) are used to measure the hardness (P_{max} / A). Contact area A at P_{max} was determined from the known shape of the indenter which is calibrated by indenting a material with known properties (in this case fused quartz). Reduced elastic modulus (E_r) as shown in Equation (1) is almost identical to E in the case of soft materials and is termed indentation modulus throughout this paper.

$$Er = \frac{1}{2}\sqrt{\pi}\frac{S}{\sqrt{A}} \qquad (1)$$

Microindentation

For microindentation, ten long single pulp fibres (~ one mm length) are fixed at both ends with epoxy droplets on ten different conductive glass slides which contained indium tin oxide as a top layer to minimize charging during SEM imaging. Then, each conductive glass slide was fixed to the SEM stub using double sided carbon tape and sputter coated with a 6 nm thick gold-palladium layer to avoid further charging. Microindentation was carried out at 0 % moisture content of the pulp fibres in an environment of 10^{-6} mbar and 296 K inside a Zeiss DSM962 SEM. A detailed description of the in-situ SEM microindentation set-up is available elsewhere (Rabe et al. 2004). As shown in Figure 4, a conical diamond indenter (cone angle of 43º) ending in a flat-top (diameter of ~ 2 µm) was used in the present study. For all the tests, deformation was carried out at a constant displacement rate of 100 nm/s and corresponding load (P) vs. displacement (h) curves were obtained.
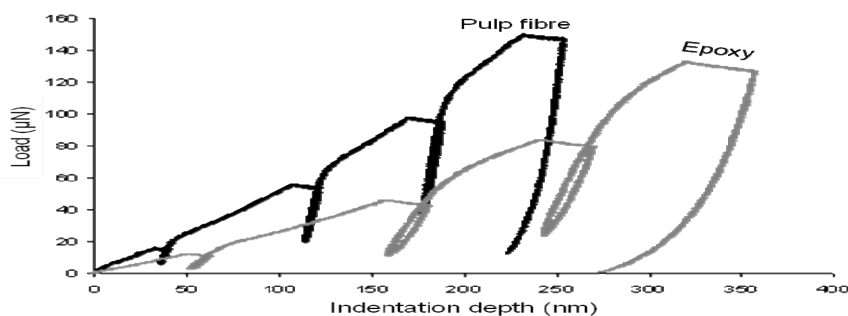
Figure 3. Typical load-displacement graph of a nanoindentation experiment
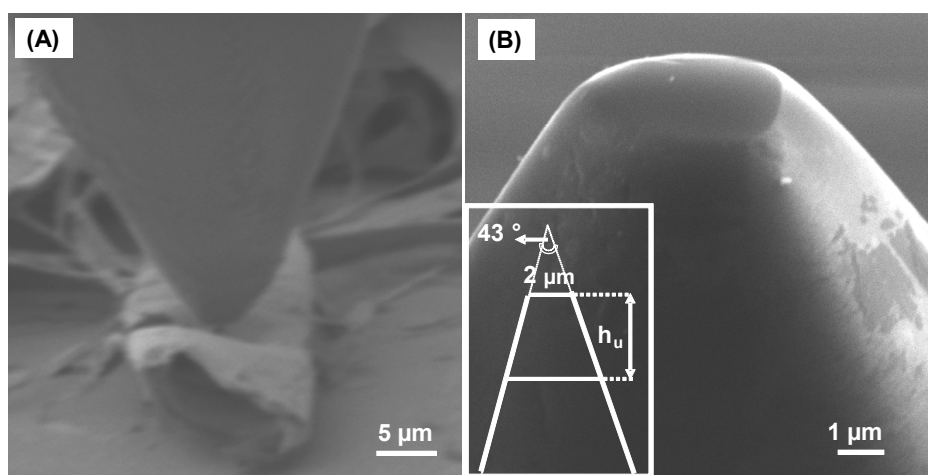
Figure 4. (A) In-situ SEM microindentation of the pulp fibre in transverse direction. Flattened cross section of the pulp fibre and the shape of the lumen can be observed. (B) SEM image of the indenter tip having the flat-top surface. Inset picture corresponds to the schematic diagram of the flat-top conical micro-indenter showing conical angle and depth of penetration h_u.

Single fibre tensile test

Under a stereomicroscope, dried single fibres were extracted using small tweezers and fixed to the paper frame with cyano acrylate glue as shown in Figure 5. The paper frame set-up, generally used for single fibre testing of brittle fibres such as carbon fibres (ASTM D3379-75), has been modified for pulp fibres. Initially, one paper frame (yellow) was cut with gauge lengths ranging from 0.5 mm to 3 mm in order to test both softwood and hardwood fibres. After fixing of the fibre ends to the yellow frame, it was fixed to another paper frame (black) and two side edges of the yellow paper frame were cut free using a fine razor blade under a stereo microscope. The whole set-up was then clamped to the tensile jaws as shown in Figure 5a, and the two side edges of the black frame were cut free very carefully, thus, only the fibre was subjected to tensile forces as shown in Figure 5b (image was taken after tensile test). Before clamping, fibre diameter (average of three measurements) and gauge length were measured using a stereomicroscope. The tensile test was carried out in an UTS machine equipped with a 10N load cell and elongation was measured through cross-head movement. All tests were carried out with a displacement rate of 500 μm / min and at environmental conditions of 25 °C and 55 % relative humidity.
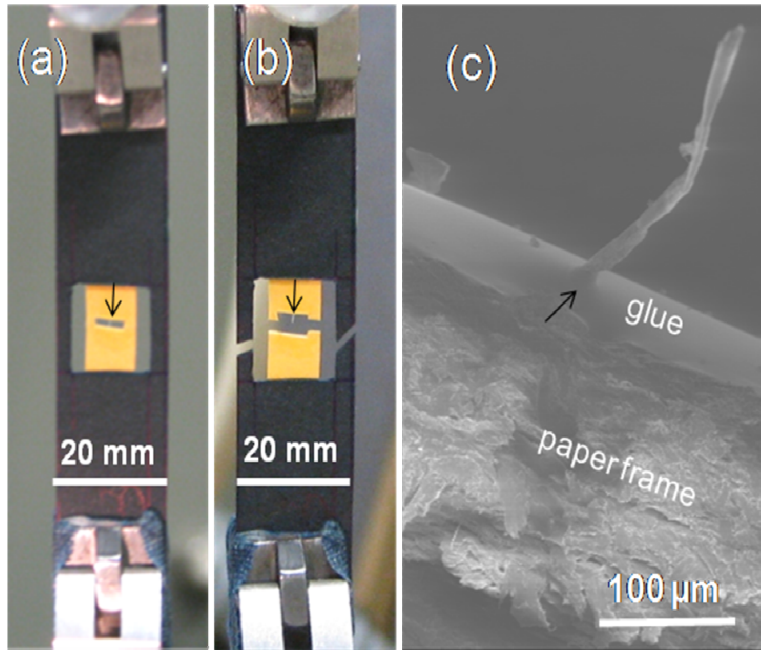
Figure 5. Double paper frame (yellow and black) set-up developed for tensile testing of single pulp fibres (see the black arrow) which are glued to the yellow paper frame. a) Set-up before tensile testing. b) Set-up after tensile testing revealing the fibre break at the middle. c) SEM image of the fibre shown in b. Fibre twist, which causes the fibre to break in tension, can be seen in the SEM image.

Results and Discussion

Nanoindentation

Figure 6 shows an optical micrograph of pulp fibres embedded in epoxy resin and sectioned until a smooth surface is achieved as explained in the previous section. This micrograph was taken prior to nanoindentation using normal reflected light microscopy in order to map the latewood cell cross-sections. Undoubtedly, this micrograph reveals not only fibre cross sections but also some tilted (misaligned fibre cross sections) and longitudinal sections due to the fibre misalignment. Since pulp fibres are 1-3 mm length, highly deformed and irregular in their aspect ratio, it is difficult to achieve a specimen with all fibres aligned in one direction. Additionally, since the indentation modulus is influenced by this fibre misalignment (Konnerth et al. 2009), care is taken to select only longitudinally-aligned fibre cross sections which are free from other artefacts such as microtome knife markings. One way of checking the fibre alignment is to compare the shapes of the fibre cross section before indentation (Figure 6a) and after indentation followed by 10-20 μm sectioning of surface material (Figure 6b). This technique is followed in our experiments by progressive sectioning of 17 μm thick material as explained in Figure 6.

The scanning probe microscopy image of residual indents on pulp fibre cell wall after nanoindentation is shown in Figure 1. Both fibres are collapsed (decrease in lumen) and compressed such that the lumen exhibits variability in its cell wall thickness. However no variability in indentation modulus E_r and hardness H was observed across the cell wall. This is most likely because indents were performed on very localised areas of the cell wall where minimal cell wall defects were found. It is therefore assumed that E_r and H values obtained from nanoindentation tests are higher than average values. When typical load – depth curves are observed (Figure 3), both pulp and epoxy (embedding medium) revealed elasto-plastic behaviour during loading and unloading in addition to creep while holding at the peak load. Indentation

modulus and hardness values of different pulp grades are displayed in Figure 7 and 8 respectively. On average, more than 30 measurements were used for each fibre type. In many tests, a slight decrease in Er and H was observed with increasing indentation depth.
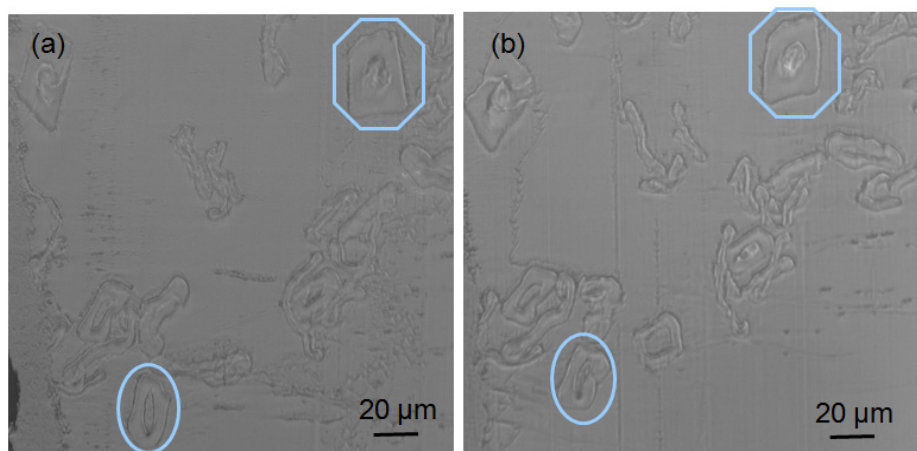
Figure 6. Optical micrograph of the smoothly polished pulp fibre-epoxy nanoindentation specimen. Image (a) is taken prior to the <u>first</u> nanoindentation test and image (b) is taken prior to the <u>second</u> nanoindentation test, both tests are performed on the same cell wall cross sections. After first nanoindentation test, specimen was brought to the polishing lab and 17 µm thick material was sectioned progressively from the top surface and the same cell wall cross sections were identified under light microscope (See the oval and hexagonal areas). Subsequently specimen was brought again to the nanoindenter to perform the second test. This technique was followed to understand the influence of fibre misalignment in nanoindentation measurements.

Similarly nanoindentation of viscose and lyocell fibres also revealed a decrease in hardness and elastic modulus with increasing indentation depth (Gindl et al. 2006). This is most likely not due to the surrounding epoxy but due to the difficulties in detecting the surface contact at low loads (Jakes et al. 2007). Quantitative analysis of nanoindentation data revealed an average Er and H of 12.2 ± 1.6 GPa and 0.42 ± 0.05 GPa respectively for S2 cell walls of unbleached Scots pine pulp. For S2 wall of spruce latewood, Zickler et al. (2006) reported average Er and H of 14.2 GPa and 0.40 GPa respectively. Gindl et al. (2004) reported Er of 16.2 GPa and H of 0.43 GPa for the latewood Norway spruce (MFA 20°). So the values of the unbleached softwood pulp are in good agreement with the values presented by Zickler and Gindl. Er of 9.1±1.6 GPa and H of 0.43±0.05 GPa were obtained for unbleached eucalyptus pulp. Wu et al. (2009) reported a Er of 20.2 GPa and H of 0.49 GPa as an average values of 10 hardwood species. In Figure 7 and 8, Er and H of the epoxy resin were determined to be 4.6 GPa and 0.24 GPa respectively which were measured under the same conditions as the cross section measurements. Gindl and Gupta (2002) presented the Er and H of same epoxy resin as 3.1 GPa and 0.10 GPa respectively, where a berkovich tip was loaded to a peak force of 500 µN.
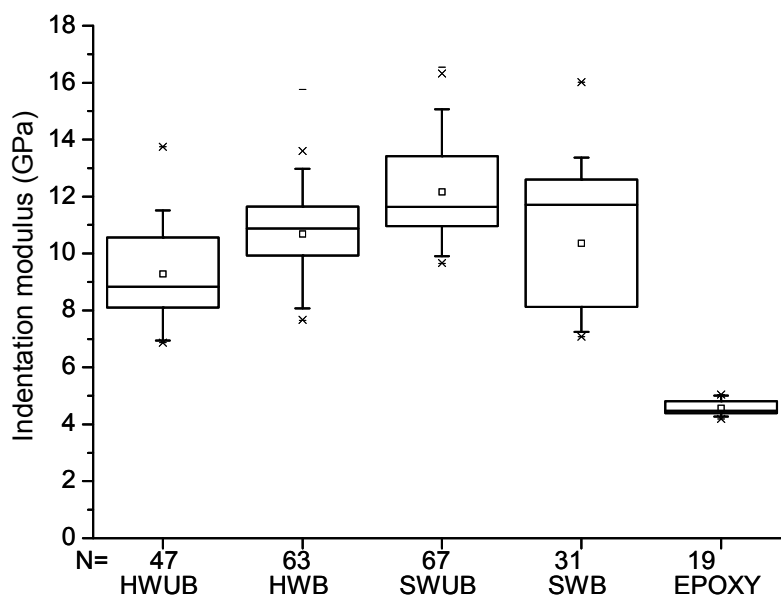
Figure 7. Nanoindentation results showing indentation modulus or reduced elastic modulus of pulp fibre cell walls and epoxy resin (HWUB= Hardwood unbleached; HWB= Hardwood bleached; SWUB= Softwood unbleached; SWB= Softwood bleached; N= number of samples). The box and whisker plot shows the mean value (small square in the box), median (horizontal line inside the box), the 50% interquartile range (box), maximum and minimum values (whiskers) and outliers.

Regarding the Er shown in Figure 7, unbleached hardwood showed significantly lower values than unbleached softwood. After the bleaching treatment, both hardwood and softwood revealed a similar Er value of ~11 GPa for a similar Kappa number of ~1 (lignin content 0.2%). For a similar indentation depth, Gindl et al. (2006) reported an Er of ~ 11 GPa for lyocell fibre composed of 100 % cellulose. Since Er is directly proportional to MFA as revealed by several nanoindentation studies (Gindl et al. 2004, Wu et al. 2009), it is difficult to interpret the Er values of different pulp grades shown in Figure 7 without the MFA measurements. But unfortunately it is also difficult to evaluate the accurate MFA of pulp fibres especially where indentation is performed, although some studies have been reported in literature (Donaldson 1991, Pleasants et al. 1998).

Hardness values measured from nanoindentation are shown in Figure 8. Since H is a plastic property of the material unlike Er, MFA does not influence the hardness value which could be the reason that no difference in H was observed between softwood and hardwood in the present study. This supports the recent study that nanoindentation hardness is related to the cell wall matrix (Konnerth et al. 2009). Similary Wu et al. (2009) also found no significant trend between nanoindentation hardness and MFA of ten hardwood species. In general, bleaching treatment increases the ductility of the cell wall assembly by degrading the lignin, which eventually leads to lower hardness values compared to the unbleached fibres of both hardwood and softwood as shown in Figure 8. This can be understood as follows: the lignin content of the wood is around 23 % and cell wall hardness is around 0.42 GPa (unpublished data). Based on the Kappa numbers measured in this study, the lignin content of the unbleached softwood and hardwood pulp is around 4.4 % and 2 % respectively. Even though lignin content decreased significantly from wood to unbleached pulps, the hardness value remained constant i.e. ~0.42 GPa. The lignin content of the bleached fibres was measured to be 0.2 % and their hardness values were in the range of 0.36 GPa. That means removal of the lignin-hemicellulose matrix during bleaching

plays a significant role in stress transfer between cellulose microfibrils. When the lignin content was further reduced to zero percentage in lyocell fibres, the hardness value drops drastically to 0.24 GPa, in which only hydrogen bonding and van der Waals bonding takes place between cellulose-cellulose molecules.
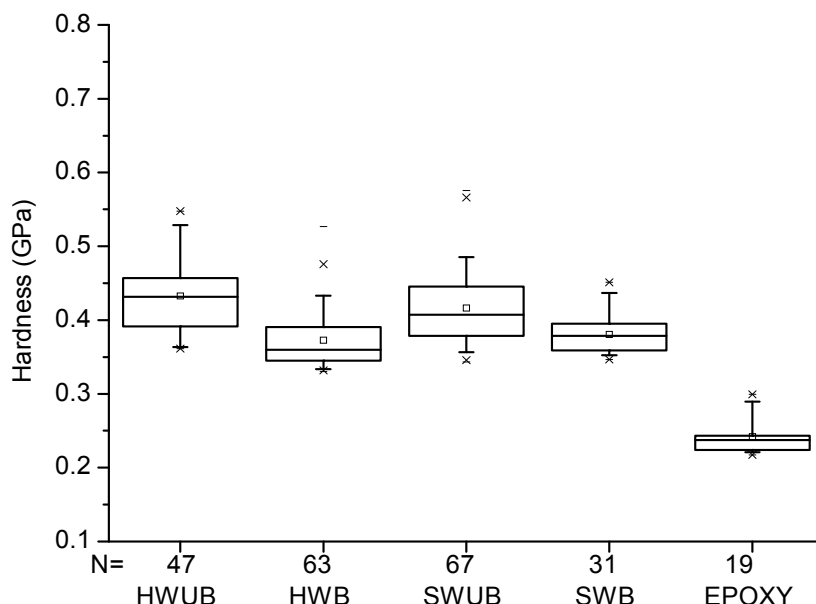
Figure 8. Nanoindentation results showing the hardness of pulp fibre cell walls and epoxy (HWUB= Hardwood unbleached; HWB= Hardwood bleached; SWUB= Softwood unbleached; SWB= Softwood bleached; N= number of samples.

Microindentation

Figure 9 shows the typical P-h curve obtained from in-situ SEM microindentation of single pulp fibre in transverse direction. Insets are SEM micrographs revealing the real-time deformation and fracture sequence of the fibre. At the beginning of the indentation test, non-linear behaviour of the P-h curve arises due to the non-uniform geometry of the fibre and results in proper contact with the glass substrate (not shown in Figure 9). The deformation and failure sequence of the fibre shown in Figure 9 is described as follows. Initial deformation was accommodated by sinking-in of the upper cell wall, followed by cracking, which corresponds to the kink or load drop in the P-h curve. Crack propagation occurs along the longitudinal axis of the fibre, while the initiation seems to be dominated by stress concentrations at the surface. As the load increases, a second crack was initiated at ~ 10 mN. The two cracks propagated along the axis to a length of around 10 μm, most likely parallel to the micro fibril angle (MFA). Crack formation led to local collapse of the cell wall and the indenter punched through the upper cell wall. Continued indentation into the lumen and the lower cell wall yielded an increase in the steepness of the P-h curve due to substrate effects (Figure 9). The cracks formed on upper cell wall, close to unloading, and a residual imprint of the conical punch can be seen in the pulp fibre.
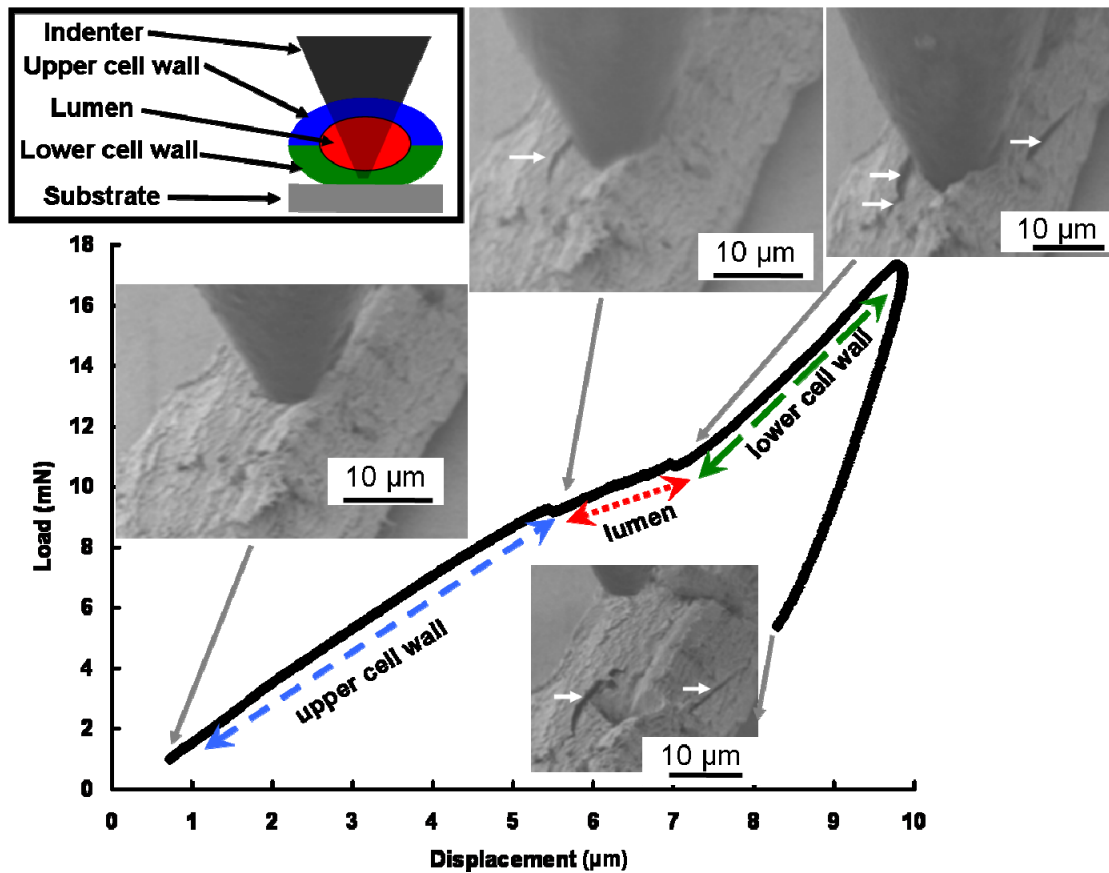
Figure 9. Load (P) - displacement (h) curve and corresponding SEM video sequence of microindentation test. Arrows labelled in SEM micrographs represent crack initiation and crack propagation probably along the microfibril angle. Schematic mechanism of the microindentation test is shown in inset (top left).

Tougher responses were observed during the deformation of other fibres. It is understood that the fibre geometry will play a significant role when a fibre is subjected to lateral compression, because fibre collapse precedes the cell wall compression (Mark et al. 2002, Nyrén 1971). But, it is important to note that, in the present study, the load was applied locally, which leads to large stresses and correspondingly large strains. Hence, the P-h curve shown in Figure 9 is mostly based on the indentation response of the cell walls and specific to the given geometry of the fibre and indenter. Based on these assumptions, the critical stress required to initiate a crack or deformation in the cell wall was calculated for three successful measurements (Adusumalli et al. 2010b). Failure sequence of single fibres subjected to longitudinal compression differs from the failure sequence found in this study. Loosening of the fibrils, piling-up of the fibrillar walls and eventual fibril fracture as reported by Sachs (1986) during longitudinal compression were also observed in the present study. But, as shown in Figure 9, SEM micrographs did not reveal any slip bands similar to those observed during longitudinal compression of single pulp fibres.
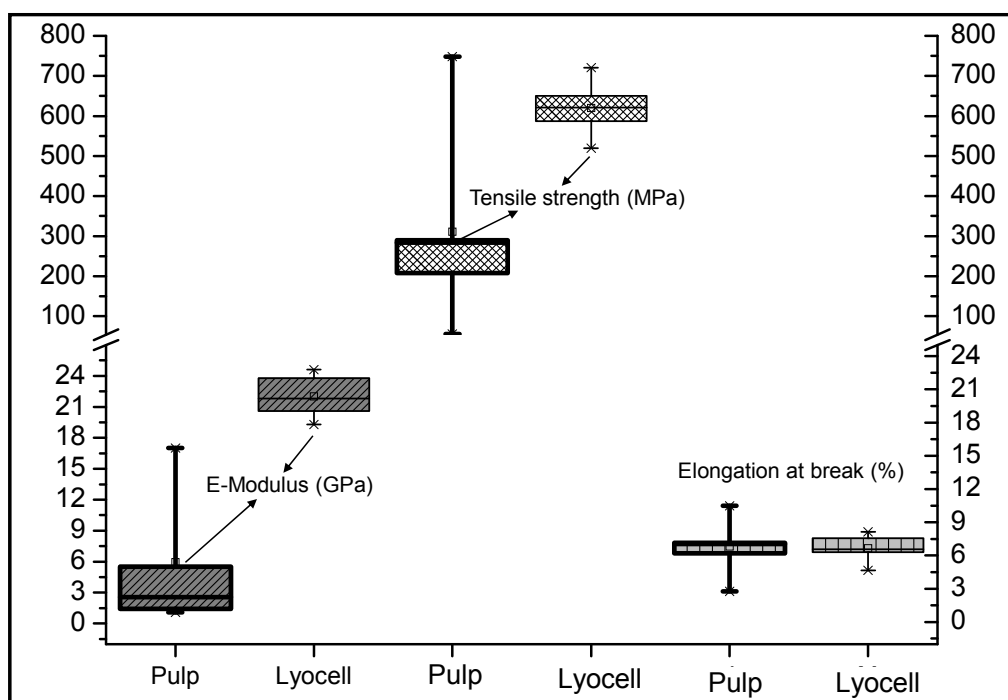
Figure 10. Tensile properties of bleached soft wood pulp and lyocell fibres obtained from single fibre testing. Box-and whisker diagram showing the tensile modulus (left), strength (centre) and elongation at break (right) (average of 9 measurements).

Single fibre tensile test

Double paper frame set-up developed to test single fibres did not yield enough results in case of hardwood fibres (lengths are between 500-800 μm). Fibre lengths exceeding 1 mm such as softwood fibres and bleached fibres (ductile and flexible compared to unbleached fibres) can be tested easily by the set-up developed in this test series. On average 10 fibres were tested and results of the successfully measured bleached softwood pulp and lyocell fibres are displayed in Figure 10. Here, lyocell is taken as reference fibre. Elastic modulus (E-modulus) was obtained from the initial slope of the stress-strain curve (Figure 11). Good agreement was found between lyocell tensile values shown in Figure 10 and values presented in literature (Adusumalli et al. 2009). Tensile strength of approx. 300 MPa and E-modulus of approx. 3 GPa was measured for bleached soft wood pulp. Standard deviations are very high for single pulp fibres due to their natural variability.

For the successful tensile measurements, SEM fractographs were taken by sputtering the fibre with a 20 nm gold-platinum coating. In case of wood and pulp fibres, it is well known that increasing micro fibril angle will decrease the tensile modulus and strength. Similar results are shown in Figures 11-13, where SEM fractographs are compared to the tensile stress-strain curves. The curve shown in Figure 11a corresponds to high strength and modulus due to low twist (presumably low MFA), in which cleavage occurred across the fibre (Figure 13). The curve shown in Figure 11b corresponds to low strength and low modulus due to extreme fibre twists (presumably high MFA) in which angular cleavage is typically found (Figure 12). Both fibres revealed no significant difference in their elongation at break, since the amorphous matrix (low in quantity for bleached fibres) controls the strain of the fibre, whereas strength and modulus depend on cellulose nanofibrils which are oriented around the fibre axis. Considering the unsuccessful measurements, in most cases, fibre breakage occurred while cutting the black paper

frame using the razor blade. Page et al. (1983) tested only softwood fibres with span lengths of 1.2 mm and they used a hot wire to burn the paper frame. Tensile testing of hardwood single fibres will remain a challenge until some in-situ techniques are adopted.
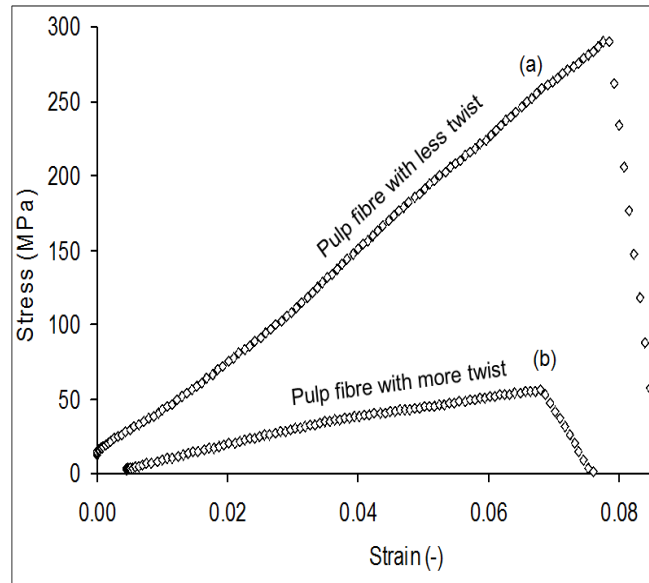
Figure 11. Stress-strain diagram of untwisted (a) and twisted (b) single bleached softwood pulp fibres obtained from tensile test. The corresponding SEM fractographs of fibre a and b are shown in Figure 13 and Figure 12, respectively.
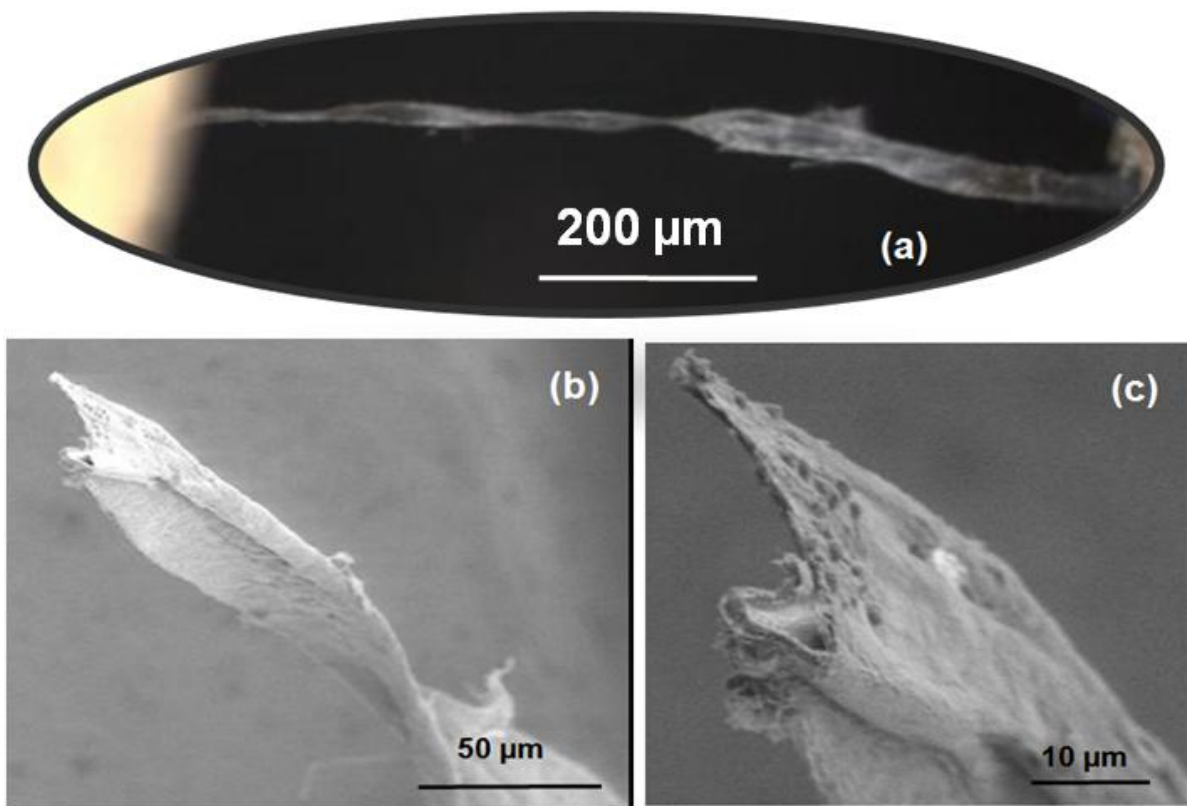
Figure 12. Stereomicroscopic image of the single pulp fibre prior to tensile test (a). Severe twists can be observed in the fibre (a and b). SEM fractographs of the same fibre after tensile test (b,c). Angular cleavage is found as a typical tensile failure mode for all twisted fibres.
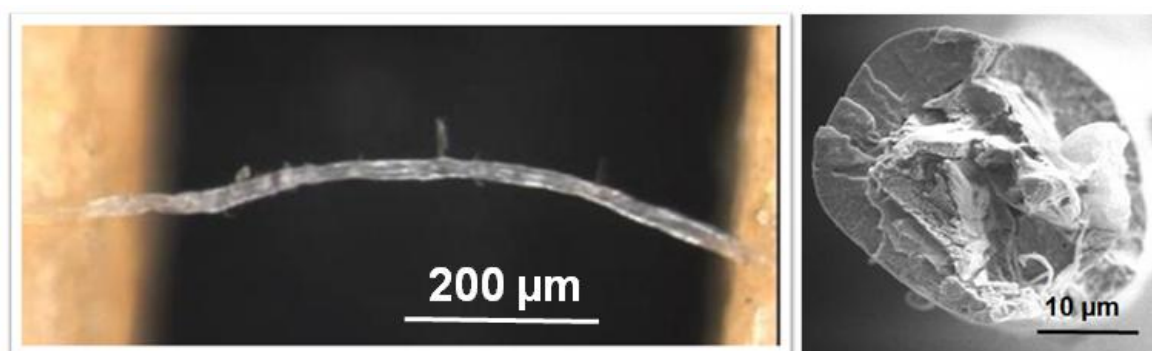
Figure 13. Stereomicroscopic image of the single pulp fibre prior to tensile test (left). Almost no twists can be observed in the fibre shown here. SEM fractograph of the same fibre after tensile test (right). Cleavage across the fibre diameter was found as a typical tensile failure mode for all untwisted fibres.

Conclusions

We have shown that nanoindentation can be used as a tool to estimate changes in the mechanical properties of cell walls caused by bleaching and also to study the differences in cell wall mechanical properties between hardwood and softwood. After kraft cooking, prior to bleaching, indentation modulus of 12 GPa was observed for softwood pulp which is 25 % higher than for hardwood pulp. But, bleaching treatment decreased the hardness value of both softwood and hardwood pulps indicating the importance of critical kappa number (lignin content) during residual delignification. After cooking, bleaching and drying stages, both hardwood and softwood fibres have similar E_r (~10.5 ± 2.1 GPa) and H (~ 0.377 ± 0.033 GPa)

The deformation response of single pulp fibres was studied in-situ SEM microindentation, which revealed correspondence between the cell wall failure mechanisms and the P-h curve response. The failure sequence of single fibre cell walls begins with sinking-in and lateral bulging of the microfibrils followed by cell wall fracture. It was found that a critical stress of ~ 50 MPa is required to initiate cracks in the cell wall, which propagate parallel to the microfibril angle.

Chemical pulp fibres of bleached softwood were successfully tested in tension by using a newly developed double paper frame set-up. A correlation was also observed between scanning electron microscopy (SEM) fractographs and tensile stress-strain curves. But, by this method it is difficult to test fibres of small length (hardwood) and low flexibility (unbleached).

Acknowledgement

References

Adusumalli R-B., Reifferscheid M., Roeder T., Weber H., Sixta H. and Gindl W. (2006): Mechanical Properties of Regenerated Cellulose Fibres for Composites. Macromol. Symp. 244, 119-125

Adusumalli R-B., Keckes J., Martinschitz K., Boesecke P., Roeder T., Weber H., Sixta H. and Gindl W. (2009): Comparison of molecular orientation and mechanical properties of lyocell fibre tow and staple fibres. Cellulose 16(5), 765-772

Adusumalli R-B., Mook W., Passas R., Schwaller P. and Michler J. (2010a): Nanoindentation of single pulp fibre cell walls. J. Mat. Sci. 45(10), 2558 – 2563

Adusumalli R-B., Raghavan R., Schwaller P., Zimmermann T. and Michler J. (2010b): In situ SEM microindentation of single wood pulp fibres in transverse direction. J. Electron Microscopy 1-5, DOI: 10.1093/jmicro/dfg025

ASTM D 3379-75 (1982): Standard test method for tensile strength and youngs modulus for high-modulus single filament materials, Philadelphia, U.S.A.

Burgert I., Eder M., Frühmann K., Keckes J., Fratzl P. and Stanzl-Tschegg S. (2005): Properties of chemically and mechanically isolated fibres of spruce (Picea abies [L. Karst].). Part-3: Mechanical characterisation. Holzforschung 59, 354-357

Courchene C.E., Peter G.F. and Litvay J. (2006): Cellulose microfibril angle as a determinant of paper strength and hygroexpansivity in *Pinus taeda* L. Wood Fibre Sci. 38(1), 112-120

Donaldson L.A. (1991): The use of pit apertures as windows to measure microfibril angle in chemical pulp fibres. Wood Fibre Sci. 23(2), 290-295

Dunford J.A. and Wild P.M. (2002): Cyclic transverse compression of single wood pulp fibres. J. Pulp Paper Sci. 28(4), 136-141

Eder M., Stanzl-Tschegg S. and Burgert I. (2008): The fracture behaviour of single wood fibres is governed by geometrical constraints: in situ ESEM studied on three fibre types. Wood Sci. Technol. 42, 679-689

Gilani M. S (2006): A micromechanical approach to the behaviour of single wood fibres and wood fracture at cellular level. PhD Thesis, EPFL Lausanne, Switzerland

Gindl W. and Gupta H.S (2002): Cell wall hardness and Young's modulus of melamine-modified spruce wood by nanoindentation. Composites Part A. 33, 1141-1145

Gindl W., Gupta H.S., Schöberl T., Lichtenegger H.C. and Fratzl P. (2004): Mechanical properties of spruce wood cell walls by nanoindentation. Appl. Phys. A 79, 2069-2073

Gindl W., Konnerth J. and Schöberl T. (2006): Nanoindentation of regenerated cellulose fibres. Cellulose 13, 1-7

Jakes J.E., Stone D.S. and Frihart C.R. (2007): Nanoindentation size effects in wood. Proc. 30th Annual Meeting Adhesion Society, Inc, Tampa Bay, Florida, USA. pp: 15-17

Karlsson H. (2006): Fibre Guide – Fibre analysis and process applications in the pulp and paper industry. ISBN: 91-631-7899-0. AB Lorentzen & Wettre

Konnerth J., Gierlinger N., Keckes J. and Gindl W. (2009): Actual versus apparent within cell wall variability of nanoindentation results from wood cell walls related to cellulose microfibril angle. J. Mat. Sci. 44, 4399-4406

Lichtenegger H., Reiterer A., Stanzl-Tschegg S.E. and Fratzl P. (1999): Variation of cellulose microfibril angles in Softwoods and Hardwoods – A Possible strategy of mechanical optimization. J. Structural Biology 128, 257-269

Mark R.E., Habeger Jr C.C., Borch J and Lyne M.B. (2002): Handbook of Physical Testing of Paper. ISBN: 0-8247-0498-3. Marcel Dekker, Inc. Vol. 1, Chapter 13 edited by Paavilainen L, Fibre Structure pp. 699-720

Mohlin U.B., Dahlbom J. and Hornatowska J. (1996): Fibre deformation and sheet strength. TAPPI 79(6), 105-111

Mott L., Shaler S.M., Groom L.H. and Liang B.H. (1995): The tensile testing of individual wood fibres using ESEM and video image analysis. TAPPI 78(5), 143-148

Nyrén J. (1971): The transverse compressibility of pulp fibres. Tech. Sect., CPPA 72(10), T321-T323

Oliver W.C. and Pharr G.M. (1992): An improved technique for determining hardness and elastic modulus using load and displacement sensing indentation experiments. J. Mat. Res. 7, 1564-83

Page D.H. and El- Hosseiny F. (1983): The mechanical properties of single wood pulp fibres. Part 6. Fibril angle and the shape of the stress-strain curve. J. Pulp Paper Sci., 9, 1-2

Page D.H., El-Hosseiny F. and Winkler K. (1971): Behaviour of single wood fibres under axial tensile strain. Nature 229, 252-253

Pleasants S., Batchelor W. J. and Parker I.H. (1998): Measuring the fibril angle of bleached fibres using micro-Raman Spectroscopy. APPITA 51(5), 373-376

Rabe R., Breguet J-M., Schwaller P., Stauss S., Haug F-J., Patscheider J. and Michler J. (2004): Observation of fracture and plastic deformation during indentation and scratching inside the scanning electron microscope. Thin Solid Films 469-470, 206-213

Sachs I.B. (1986): Microscopic observations during longitudinal compression loading of single pulp fibres. TAPPI July, 98-102

Spurr A.R. (1969): A low viscosity epoxy resin embedding medium for electron microscope. J. Ultra Structural Research 26, 31-43

Wu Y., Wang S., Zhou D., Xing C. and Zhang Y. (2009): Use of Nanoindentation and Silviscan to determine the mechanical properties of 10 hardwood species. Wood Fibre Sci. 41(1), 64-73

Xing C., Wang S., Pharr G.M. and Groom L.H. (2008): Effect of thermo-mechanical refining pressure on the properties of wood fibres as measured by nanoindentation and atomic force microscopy. Holzforschung 62, 230-236

Zickler G.A., Schöberl T. and Paris O. (2006): Mechanical properties of pyrolysed wood: a nanoindentation study. Phil. Mag. 86(10), 1373-1386

TOWARDS AUTOMATED MANIPULATION AND CHARACTERISATION OF PAPER-MAKING FIBRES AND ITS COMPONENTS

[1]Manuel Mikczinski, [1]Malte Bartenwerfer, [2]Pooya Saketi, [3]Sabine Heinemann, [4]Raphaël Passas, [2]Pasi Kallio and [1]Sergej Fatikow

[1]Division Microrobtics and Control Engineering, University of Oldenburg, D-26111 Oldenburg, Germany

[2]Micro and Nanosystems Research Group, Tampere University of Technology, FI-33101 Tampere, Finland

[3]VTT Fibre Processes, Fibre Converting (Espoo), FI-02044 VTT, Finland

[4]Grenoble-INP/PAGORA, F-38402 Saint Martin d'Hères, France

Corresponding author: manuel.mikczinski@informatik.uni-oldenburg.de

Abstract

Papermaking has a long history and is dominated by experience. The understanding of structure and ultrastructure and their formation mechanisms is fundamental but far from complete. Experiments and tests are performed to unveil the ultrastructure and find out more about fibre properties and the fibre-fibre and fibril-fibre connection establishment during paper-making.

The following pages are dealing with the development and evaluation of novel systems and methodologies addressing this topic. The work was performed in a joint workshop organised between the University of Oldenburg, VTT, Grenoble-INP/PAGORA and Tampere University of Technology. Adopting nanomanipulation techniques used to handle and assemble individual carbon nano tubes (CNT) is a promising approach. Although organic material behaves differently than the more organised inorganic structures like CNTs, the existing systems and techniques are good starting points. Three different systems were used during the workshop at the University of Oldenburg. One of these systems was developed from scratch for this workshop. It is a modular micro/nanomanipulation system offering a high flexibility in manipulations. After introducing these systems, different manipulation techniques are performed and presented. The gained experiences were used to perform a number of preparing steps and characterisation experiments which are not yet available in larger scale applications in the presented resolution, e.g. the compression testing of single fibres with force feedback. Also other techniques as for example focused ion beam cutting and deposition on single fibres were performed. All presented material was used to evaluate existing systems and to create recommendations for future systems.

Introduction

Producing different paper is a versatile challenge. Especially printing paper is available in a huge number of different weight classes and qualities. Producing these papers with certain properties requires a detailed knowledge about the materials and processes. Insight into the paper structure is of major interest to check the obtained results. Several properties need to be controlled to validate the processing and material. Changes take place not only on sheet level but also on fibre and fibril level. Data that is gathered in the post-processing state must be compared to data collected in raw state. Going from the sheet level down to the fibre or even fibril level several conditions change. Visualisation system, working environment, and manipulation systems will change due to technical reasons. Visualisation in a scanning electron microscope (SEM) is

already performed to obtain insights into the surface structure of fibres or to make fibrils visible, as seen with Chinga-Carrasco (2010) and Turner and Reynolds (2009). With the SEM the working environment changes from atmospheric conditions into a chamber with reduced pressure to enable the use of the electron beam. This makes remotely controlled manipulation systems necessary. The use of these micro- or nanomanipulation systems requires in turn new methodologies but enables also new experiments.

The COST Action E54 was initiated to contribute to the following questions aiming at the "Characterisation of the fine structure of papermaking fibres using new technologies". The main objective of the Action is to generate new knowledge on the micro- and nanostructure of papermaking fibres and properties required for the efficient and sustainable use of fibres. Specific attention is paid to the influence of the chemical and mechanical pulping processes and fibre treatment on the fine structure and composition of different papermaking fibres.

Single fibre investigations are subject of Working Group 2 in this Action, entitled "Treatment and characterisation of individual fibres by microsystem technologies." The group focuses on the development of new instruments by which individual fibres can be treated and fibre structures can be investigated at lab scale. Interaction between microsystem technology developers and paper scientists in Europe providing a good transfer of knowledge between those groups is highly desired and has started within this COST Action. This paper represents one of the first results of this networking.

Working with Single Fibres

There are two general processes to get a fibre deliberated from the wood matrix in a tree – mechanical treatment by grinding or refining (e.g. the TMP process), and chemical treatment (e.g. cooking). Depending on these processes, the separated fibres have a characteristic appearance e.g. in the light microscope (Figure 1). In the first case, the wood matrix is broken down to single particles with minor material loss. Usually yields are 90-95%. The fibres appear rarely intact, they are mainly broken or their outer layers are partly peeled off (Figure 1a). In the second case, approx. 50% of the wood (lignin and some carbohydrates) is dissolved by chemicals and removed. The remaining fibres are intact with smooth and close surfaces (Figure 1b).

The properties of such fibres vary considerably with the wood species and growth site. The wood fibre properties vary also by the growth rate, and the age of the wood influence fibre properties to a large extend. Both the fibre length and the fibre wall thickness increase with wood age. The juvenile wood fibres are shorter, narrower, and have thinner walls than mature wood. Typically, the juvenile wood pulps have lower strength properties and higher light-scattering coefficient as reported by Tyrväinen (1995).

In general a tree of a faster growth rate contains more earlywood and more lignin than a slow grown tree. The growth rate influences the cross-sectional dimensions of fibres. Sirviö (2000) and Sarén et al. (1999) showed that faster growing trees develop thinner walled fibres than slowly growing trees in average. Microfibril angle decreases rapidly with the age of the tree, being larger for earlywood than latewood and larger for fast-grown than for slowly grown trees as reported by Sarén et al. (1999) and Lichtenegger et al. (1999). Vehniäinen (2008) reports that a fast grown tree of the same diameter contains less heartwood compared to a slowly grown tree.
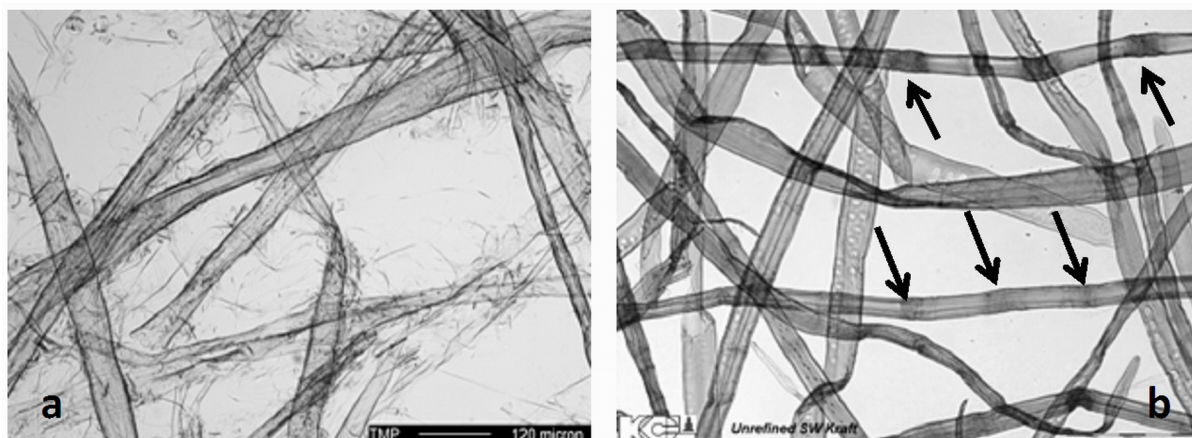
Figure 1. Softwood fibres in the light microscope – mechanical pulp (TMP) showing broken fibres and peeled fibre surfaces with high degree of fibrillation (a), and chemical pulp with intact fibres and untouched surfaces (b). Some weak points (compression areas, dislocations marked with arrows) are visible (Photos: KCL (today VTT))

Typical fibre characterisation tests provide average values of dimensions such as length, width, and wall thickness computed from 5,000 to 100,000 single fibres using automated fibre analysers. Of course the parameter distributions are delivered as well, but only little of this information can be traced back to the single fibre. But knowledge about single fibre properties and behaviour in manufacturing processes is essential for their use in traditional, advanced and future products, which might not only be paper.

In recent years, it became of greater interest to study the basic reactions of wood fibres on process impacts throughout the mechanical pulping process with the aim to understand the interaction of single fibre development and specific energy consumption as seen in Vehniäinen (2008). Understanding the occurrence and development of such morphological features as shown in Figure 2 would enable e.g. to revise the energy-intensive mechanical pulping process towards more efficient energy use and higher raw material exploitation.

Chemical pulp fibres are characterised by strong (crystalline), and weak (amorphous) structures of the fibre wall. Those weak structures are called dislocations, which is a structure containing slip lines and slip planes that are easily seen in polarised light microscopy. Small dislocations affect fibre flexibility and are not considered detrimental for papermaking. Large dislocations also give fibre flexibility, but due to the less ordered or more open amorphous cellulose structure in the dislocations, they can be the target for chemical, mechanical or enzymatic attacks as reported by Ander et al. (2008). Effects of such attacks on single fibres are shown in Figure 3. To understand, where in a fibre the highest effect occurs and how it develops with certain treatments is another reason to study single fibres instead of collecting average values.
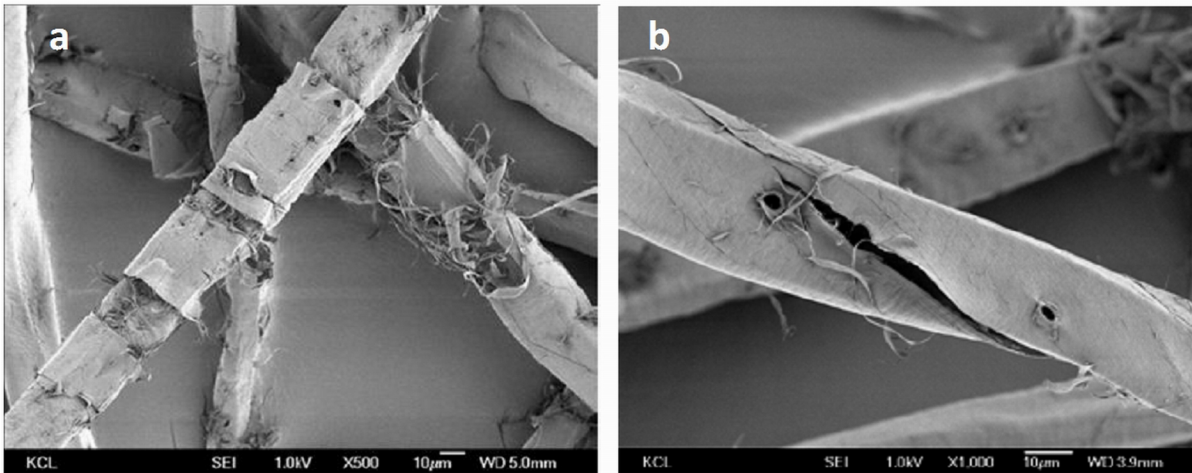
Figure 2. SEM-images of softwood mechanical pulp fibres (TMP) – Bands of combined middle lamella and P and S1 layer around long fibres in 3rd stage pulp (a), split thin-walled earlywood fibre with slit propagation in the direction of fibril angle (b) (Photos KCL (today VTT), scale bar always 10 µm)
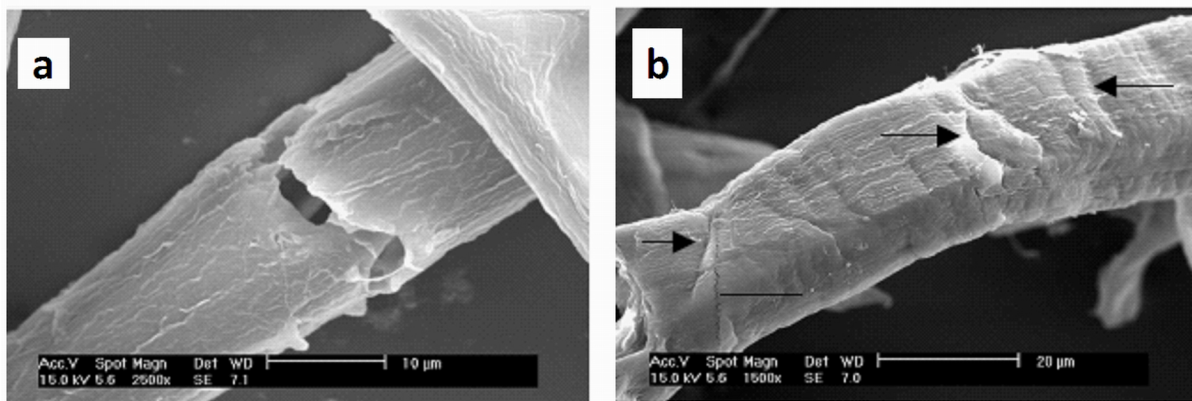
Figure 3. SEM-images of softwood chemical pulp fibres – Further degradation after HCl attack cleaving both the S1 and S2 fibre walls (a); and (b) early phase of cellulase (0.3 mL Celluclast) action producing numerous clefts/grooves in the outer fibre wall (black arrows). An artefact crack is shown at the line to the left (see Ander et al. 2008)

Micro- and Nanorobotics

A variety of experimental setups are already developed for manipulation and characterization task on different materials, with main focus on inorganic materials, though. Depending on the size of the particles and objects, the most common approaches for mechanical characterisation measurements are the determination of elastic forces and of thermal vibration frequencies for micro- and nanoscale-objects, as reported by Poncharal (1999) and Lukic (2005).

The division Microrobtics and Control Engineering developed a setup for characterisation measurements on CNTs over the past years. The setup consists of a coarse and a fine positioning system allowing realization of multistep-based experiments. The setup was used to determine the Young's modulus of vertical aligned multi walled carbon nanotubes (CNTs) as well as the conductivity of single walled carbon nanotube bundles, as described by Eichhorn (2010, 2010a). The performed mechanical characterisation measurements were based on the determination of the bending stiffness and bending behaviour of CNTs.

Due to this basic experience, the system can be adapted for different kinds of characterisation tasks and objects. On the one hand, the requirements on an experimental setup for organic

materials are even higher; on the other hand at least a possible redesign effort is minimized by the versatility of the existing system. Therefore, this is the first system to be adopted and is described in more detail in the Mechanical Setup section.

Working Environment

The working environment includes the main chamber in which experiments are conducted, the visualisation system, and the inserted manipulation facilities. Using the scanning electron microscope (SEM) is a necessity for visualisation at the scale of interest.

System Environment

The principle of the SEM is to obtain images from the detection of secondary or backscattered electrons. Those are produced during interaction between a focused electron beam and the material. The electron beam is generated in the column part of the SEM and its energy is controlled by the accelerating voltage parameter. In the column, the pressure should be as low as possible in order to facilitate extraction of the electrons (10^{-4} to 10^{-10} Pa, respectively for a tungsten cathode and for a field emission gun). The electron/matter interactions occur in the microscope chamber and the chamber-pressure is very important on one hand to reduce the electron beam diffusion and on the other hand to amplify the signal given by the secondary electrons.

In order to reduce the electrical charging effect of the sample, one can choose between three possibilities. The first one is to prepare the sample by deposition of a thin layer of conductive material (carbon, gold, palladium…). The second one is to decrease the electron beam energy (low accelerating voltage e.g. 1kV) and the last one is to introduce gas (e.g. water vapour) in the chamber (low vacuum and environmental mode). Fibres are living cells and are to be considered as biological samples. That means that they are sensitive to the energy of the electron beam and they could be hydrated. The advantage of the Environmental SEM (ESEM) is to allow the observation of such a sample. In this mode, the pressure in the chamber varies from ca. 130 Pa to about 2700 Pa. The water phase diagram (Figure 4) shows that if the sample temperature is controlled, it is possible to keep it hydrated. From a papermaker point of view, this is of great interest because it is conceivable to study the fibre deformation (hornification phenomena) during drying and rewetting cycles.

Two different SEMs were available for the experiments. Low-pressure experiments were performed in a Quanta 600 of FEI, Netherlands, with a tungsten cathode as electron source. Other experiments were conducted in a LYRA 3 FEG / XMH of Tescan, Czech Republic, which works with a field emission gun and is also equipped with a focused ion beam (FIB) column. With this microscope, fibres can be visualized at a low accelerating voltage (typically 1.5 kV) without any sample preparation until a magnification of X5,000 times. To achieve high magnification, specimens are coated with a thin gold layer. This was performed in a Polaron SC7620 sputter coater. The specimens were coated with the minimal energy and duration of approximately 30 seconds.

Both SEMs are used with their original stage and only added manipulator units or systems, which are described in more detail in the following subsection.
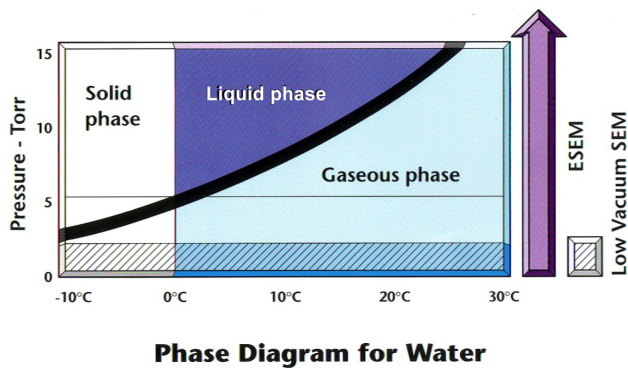
Figure 4. Phase diagram of water (1 Torr = 133 Pa, from FEI company)

Mechanical Setup

There are lots of restrictions for mechanical positioning and manipulation systems that are used inside the SEM for micro- and nanomanipulations. For example, they need to be very small, offer a high repeatable accuracy, and show virtually no drift.

Three systems were developed to work in the SEMs for different purposes. First, there is a mechanical testing station (I) for direct measurements between two aligned objects. The second system rebuilds an atomic force microscope (AFM) to be used inside the SEM (II). The restriction of strict tool-specimen alignment is overcome by the third system (III), which is designed in a more modular fashion. It offers flexible positioning of the manipulators relative to the specimen.

Mechanical testing, like tensile strength, indentation, or compression requires a good alignment between the tool and the object to be tested. The first setup (I) offers this on a bar-like base (Figure 5-I). On this base two types of positioners are installed for coarse and fine positioning. Coarse positioning is performed by linear axes by SmarAct GmbH, Germany. These axes are working with the slip-stick principle and offer a high relative resolution of ca. 50 nm along the complete axis movement. Due to the principle they are fast and offer not only the stepping movement but also a scanning movement. For fine positioning Physik Instrumente axes with a stroke of ± 100 μm are used from the Hera product line. These are built with flexure hinges and ensure a frictionless and drift-free movement. A capacitive sensor is used to measure the movement. The resolution of these axes is less than 2 nm, which makes them ideal for high resolution mechanical testing. The measurement tool is fixed on the coarse positioning side, whereas the specimen is mounted on the fine positioning side. The specimen can either be mounted on a flat or an angled stub, as required by the chosen property to be tested. In turn, the tool or any other end effector needs to be aligned accordingly.

The second setup (II) is already more specialised. To combine the advantages of both techniques this systems represents an atomic force microscope (AFM) inserted in a SEM, see Figure 5-II. As a commercial AFM is generally designed to move the probe, this setup uses a movable scanning tip. It consists, as well as the first system, of a coarse and a fine positioning unit. SmarAct axes with a high stiffness are used for positioning the scanning tip on the patch to be scanned. The scanning motion is performed by means of the fine positioning axes by Physik Instrumente. In this way the region of interest stays in sight of the SEM view. Additionally, this setup is capable of delivering a force feedback to the operator via a Phantom Desktop haptic device by SensAble Technologies. But every mode requires some settings that does not allow for using the modes (AFM and force feedback manipulations) simultaneously.
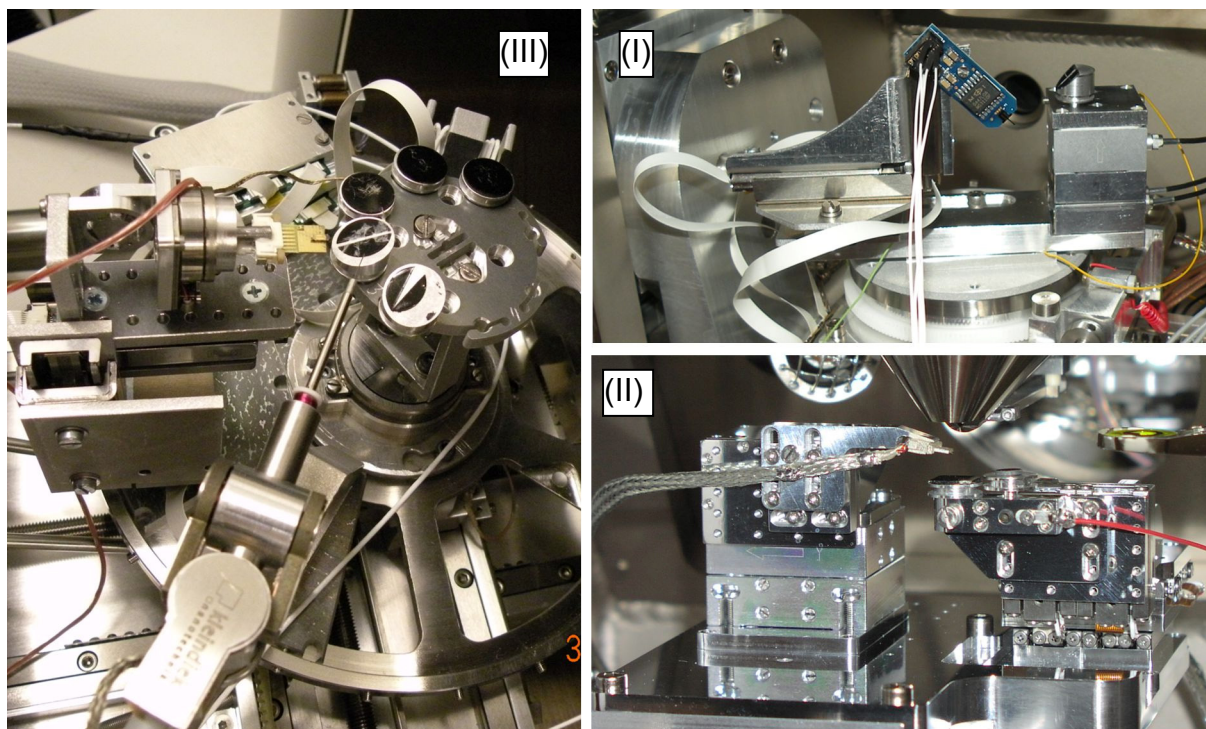
Figure 5. The mechanical setups used for the experiments. In (I) the coarse positioning axes with the measurement tool (left) and the fine positioning axes with the sample (right) can be seen. (II) shows the AFM setup mounted inside the SEM chamber. This time the coarse positioning carries the sample (right) and the fine positioning moves the tool (left). The third setup can be seen in (III). All tools come from an outer position and centre around the samples, which can be revolved. In this way any tool can reach any sample. On the left side a microgripper on its carrier-pcb is facing the second sample in the sample carousel. From the bottom comes the sharp metal tip in the field of view. The angle between the tools can be adjusted beforehand to ensure a close collaboration on the sample

The third system used is a fully modular positioning and manipulation system (III). Many tasks in micro- and nanorobotics benefit from two or more endeffectors manipulating the specimens. This is especially true for organic materials as paper-making fibres. On a round disc-like base different positioning / manipulation units are mounted. Every module is set into a groove on the base disc and fixed with setscrews. Due to the angled border of the pie piece-like module bases and the groove in the base-disc every module is clamped and perfectly fixed. By combining the different modules a large variety of manipulations becomes possible. Even different angles between the tools can be easily achieved due to the round shape. Every module is designed to take a specific combination of positioners, e.g. linear or rotary axes. These multi-degree-of-freedom positioners can be equipped with any kind of end effector to form a manipulator unit. Typical end effectors are for example sharp metal tips from tungsten wire (STM-tips), force sensors, or micro- and nanogrippers.

Automation Approaches

Not just in industry but also in research are many processes automated. Many steps in experiments require a large number of specimens to be handled or tested. In some cases this work causes fatigue and concentration losses with the experimenter. Especially the work with organic specimen like biological cells is laborious work as reported earlier (Desai et al. 2007).

Automating an experimental setup does not just mean to replace a manual handle with a motor and program a controller to send a signal to the motor which performs the required movement. It starts earlier with determining the necessary steps to be performed. Experimental protocols are the first thing to be examined. From these, the necessary tools can be derived. The next step is planning the automation system mechanically. After programming the automation sequence in accordance to the protocols, the automations system needs to be validated. From the information technology point of view, it is beneficial to divide the automation software in a low-level and a high-level control. The low-level control deals with converting control signals into driving signals of e.g. the motors. In the high-level control structure the testing protocol is implemented. In this way, it is possible to program the protocol without direct knowledge about the specific driving signals.

However, here the focus is on the mechanical side. What facilities are necessary is determined by the tests, which should be performed. An automation system could start for example with separating fibres from pulp samples. Before outlining a mechanical system testing procedures need to be formulated.

Testing Procedures

Microscopic analysis of fibres is very important, as already mentioned above. The visualisation of special features of the fibre wall in micro and nano scale has already been well developed, but the bottleneck of all such procedures is the high time demand and the required accuracy for sample preparation. A large number of tests have to be performed to achieve statistical results due to natural variability (see also section "Working with Single Fibres" above). Furthermore, it is necessary to avoid human artefacts on the analysis in order to have a repeatable method which could be applicable as a standard. It is also interesting to keep in mind that a paper machine produces about 1,000 tons of paper per day. If some analyses are needed to check the product quality, a quick measurement is mandatory.

The idea therefore was to study the suitability of certain procedures for a fully automated testing principle on single fibres. Such a method would be interesting both from scientific and from commercial point of view.

As a start-up, three different tasks were performed during the workshop on the single fibre level:

1) Basic fibre manipulations (e.g. gripping or slicing with a metal tip),
2) Fibre compression testing with force measurement, and
3) Charged particle beam manipulations: cross-sectional cutting and depositing metals on the fibre surface.

Automation System

The first step in individual paper fibre (IPF) characterisation is sample preparation. Wood fibres are natural fibres and they have high level of asymmetry compared to synthetic nanowires, like CNTs. This asymmetry problem is even worse in case of pulp fibres due to damages caused in pulping process. Combination of asymmetry problem and the paper fibre dimensions, tens of micrometres in diameter and few millimetres in length, make paper fibres a challenging material to manipulate on individual cell level.
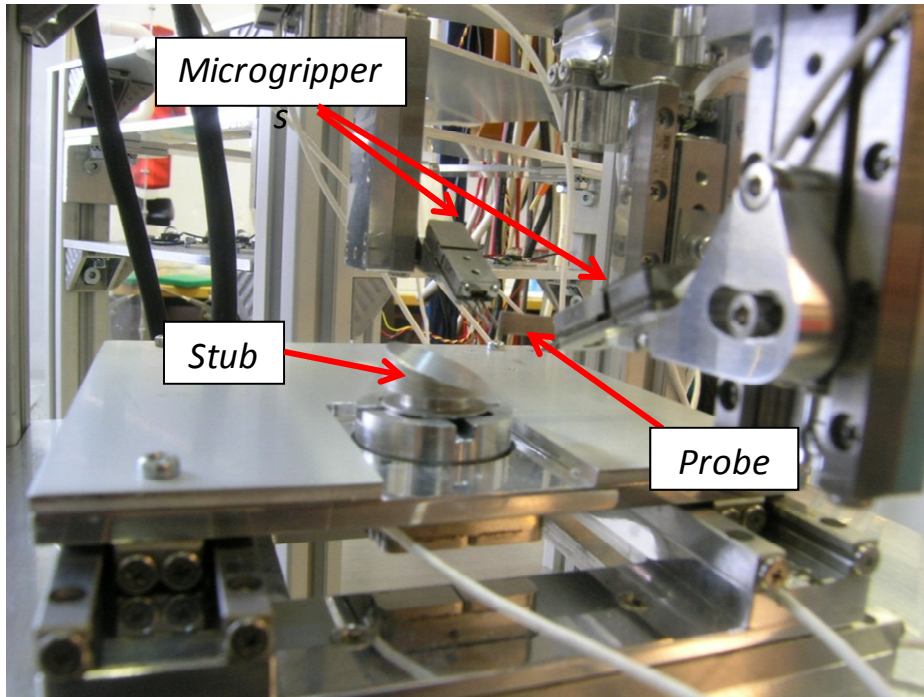
Figure 6. Individual paper fibre manipulation platform (IPFMP)

An individual paper fibre manipulation platform (IPFMP) is developed in MST-Group of Tampere University of Technology. IPFMP is used to manipulate and sort the IPFs to prepare the samples. IPFMP operates two microgrippers (SmarAct™) to grasp the individual paper fibres (IPFs) and a self-tailored probe to place the IPFs on stubs (SEM sample holder). Figure 6 shows the IPFMP and its components.

The pulp fibre samples are disintegrated in a Petri dish by adding DI-water. Then the IPFs are placed on rotary table by using a pipette. Carbon pads are placed on the SEM stubs in a V-shape. This facilitates to match the length of the IPF with the gap between the pads. The two microgrippers are used for picking-up an IPF from the suspension, straighten it and let it dry. One of the microgrippers releases the IPF and the second microgripper is used for carrying the IPF on the V groove of the carbon pads to the place where the gap matches the length of the IPF. Afterwards, the fibres are placed on the carbon pads on each stub either with one-end-fixed and/or both-ends-fixed configurations. Figure 7 illustrates the schematic fibre placement configuration on the stubs. A probe is used to place the ends of the IPF on the carbon pads.
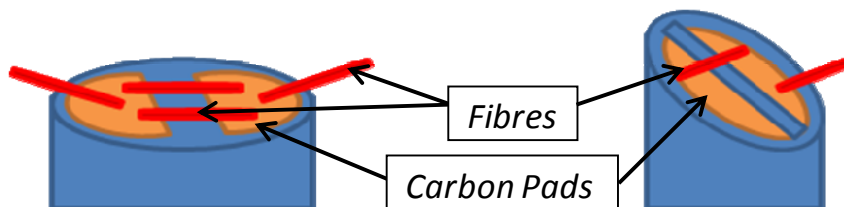
Figure 7. Schematic of fibre placement configuration

Two IPFs from each sample are placed with the both-ends-fixed configuration and the other two are placed with the one-end-fixed configuration on the stubs. Figure 8 shows the IPF placement configuration; or in other words, boundary conditions of the IPFs.
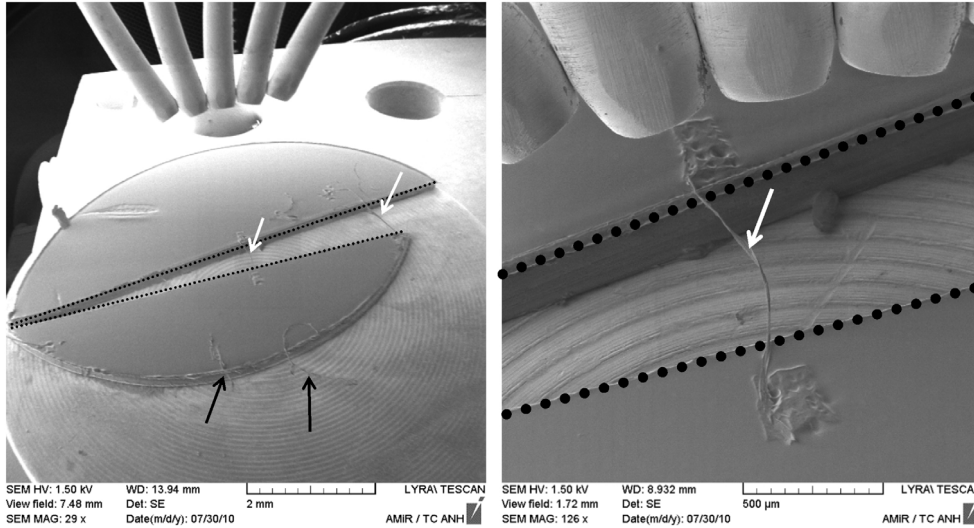
Figure 8. Boundary conditions of the IPFs. White arrow: Both-ends-fixed. Black arrow: One-end-fixed. From top the gas injection system (GIS) can be seen which is used for deposition experiments

The above mentioned process is performed in a tele-operated mode. The sample preparation time is around 15 min/IPF. But most of the time is used to let the fibre dry. Although, preparing less than 40 samples and characterizing these IPFs does not provide statistically reliable data, the need for an automated IPF sample preparation platform is obvious. As a sub-system of an automated manipulation and characterisation paper fibre platform, IPFMP provides an infrastructure for a fully automated IPF sample preparation platform which could prepare stacks of samples for characterisation in adequate time.

The next step in automating fibre testing is the delivery of the prepared sample stub in the SEM. During the workshop this was done manually. But opening and closing the SEM and wait for the vacuum system to reduce the pressure for one or two samples is far from optimal. This means either a sample stock must be available inside the SEM or an automated vacuum lock for samples must be installed.

Subsequently, the testing takes place. Depending on the preferred tests, different testing modules must be installed. These can either be chosen beforehand or in the best case the automation system can rearrange the setup according to the operator's wishes. In the latter case, also the testing and measurement tools must be palletised.

SEM Experiments and Results

1) Basic Fibre Manipulations

Some basic manipulation techniques like pushing, pulling, gripping, relocating, and fixing a fibre or its components in a certain place have to be learned. Only with this knowledge an automation system will work reliable and correctly. During the workshop, manipulations with a sharp tungsten wire tip, which are normally used for scanning tunnelling microscopy (STM), were performed. The tip was used to hold a fibre in place by fixing it on the carbon glue pad or

to push fibres over the pad's surface. By pushing the nanoscale tip through the fibre and moving it sideways the fibre was sliced. The piece of cell wall which was ripped apart stuck to the tip and could be transferred to other places without losing it. From this point a gripper was used to grip the free-standing part of the cell wall. The biggest problem during these manipulations was the lack of knowledge about the third dimension. It was not clearly visible if the tool was already in contact with the fibre or not. Due to the material, the fibres were bending downwards without changing position in the visual plane.
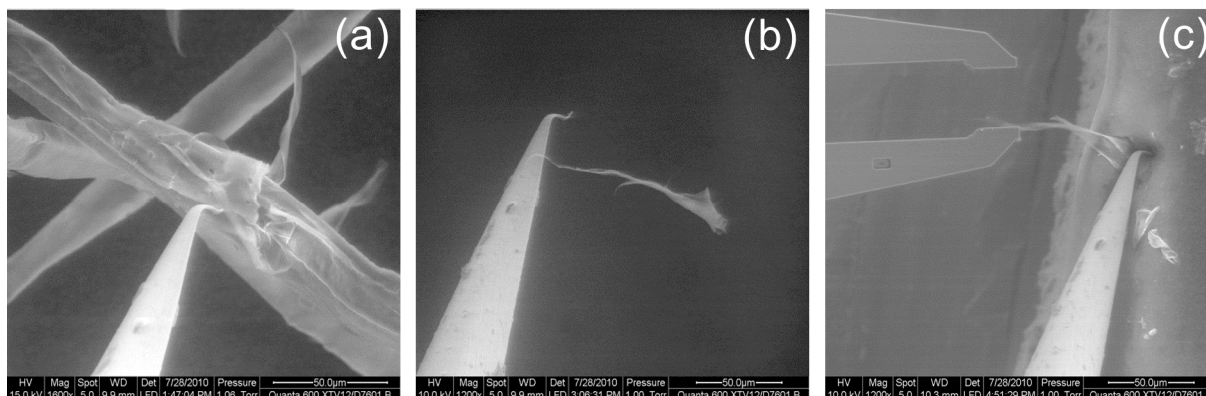
Figure 9. From (a) to (c) a number of manipulations can be recognised. (a) shows the penetration of the STM-tip into the fibre wall. The piece of fibre cell wall that was ripped off is sticking to the STM-tip (b). The last picture shows the collaboration of two different tools on the same object: a gripper coming from the left and the STM-tip, which is fixing the fibre wall layer at the carbon pad of the SEM stub

2) Fibre Compression Testing

First compression tests support the experimental setup for the mechanical characterisation (setup I). Figure 10 shows an unrefined paper fibre fixed between two pieces of carbon glue pads, as prepared by the IPFMP. The fibre does not touch the metal surface, is still flexible, and can be pressed against the surface easily to achieve an actual compression. The metal surface itself is used to provide a quasi-rigid sample for the sensors calibration, which is needed to determine the intrinsic stiffness.
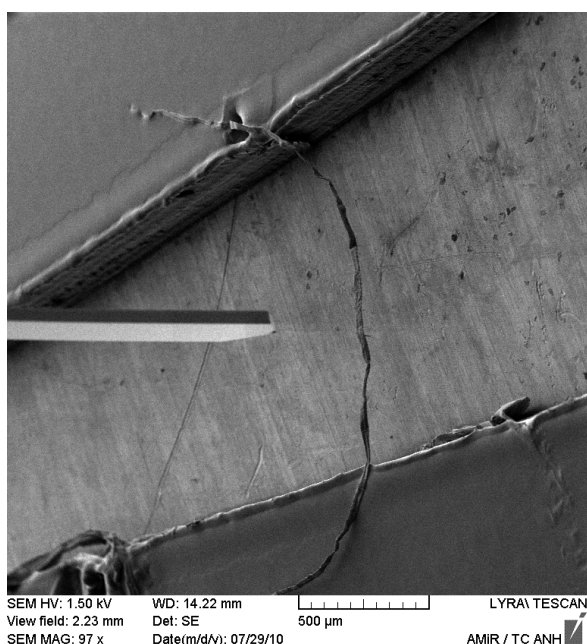
Figure 10. A COST unrefined paper fibre fixed between two pieces of carbon glue pads. The force sensor (left side) pushes the fibre to the underlying metal plane and causes a compression of the fibre subsequently. The fibre has a diameter of ca. 23.2 µm, but a non-round cross-section

Several compressions on different paper fibres were performed, while monitoring displacement and force. A typical measurement curve is shown in Figure 11. Two distinguishable parts are observable: a) the low-force region, where the force sensor pushes the fibre towards the surface and b) the high-force region, where the actual compression is performed.

Loading and unloading curve show hysteresis and a slight different shape; typical for elasticity measurements. Only the unloading part of the curve is taken into account, since this part contains primarily information of the material's elasticity without being affected by parasitic forces.

The results of the force displacement measurements reveal a non-fatigue-behaviour of the fibres and a stiffness of about 2000 N/m. The determination of a corresponding material property −e.g. Young's modulus- would be interesting, but is possible only with an extensive knowledge of the fibre's cross-section.
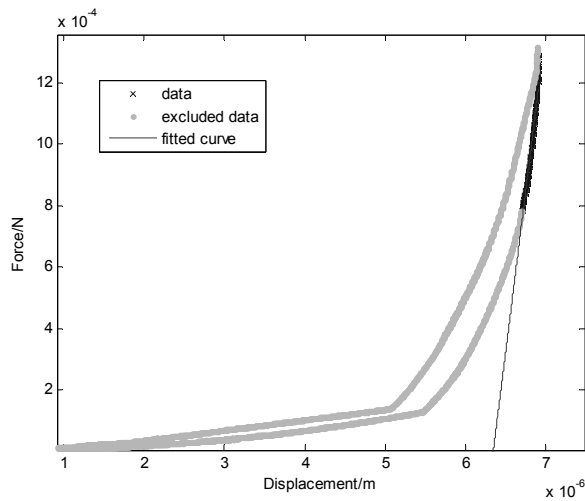
Figure 11. Typical force-displacement measurement curve on a paper fibre. Only the first 40% of the unloading curve (black x-markers) were used for the elasticity calculation (black line)

3) Charged Particle Beam Manipulations

Cutting across single free standing fibres with a focused ion beam (FIB) and subsequent manipulation of the cut areas as well as depositing metals, platinum (Pt) and tungsten (W), from the gaseous phase by ion beam induced deposition (IBiD) are discussed in the following sub-section.

Figure 12 shows a series of SEM images taken during a cutting sequence. The tests were performed on single fibres which were not separated before testing as explained above. Air-dried unrefined softwood chemical pulp from the 2nd common COST sample, described elsewhere in this book by Heinemann and Ander (2011) was fixed on the stub and a free-standing fibre loop was chosen for the test. FIB cutting was applied to all cuts with 630 pA and aperture 6. For the manipulation of cut fibre parts, a piezoresistive AFM cantilever was used with the AFM-in-SEM system, which is capable of manipulations with force feedback. Two neighboured cuts were performed subsequently (Figure 12a). For cut 1, the total cutting time was calculated with 150 sec. This long time was applied because obviously nothing had happened to the fibre although the beam was hitting the substrate (white line beneath cut 1 in Figure 12a) The same beam conditions were applied to cut 2, but already after a few seconds, the fibre moved in cut 1 which was evidently broken (no continuation in longitudinal fibre orientation, i.e. the left side of the fibre turning a bit upwards). Since the cut piece was still hold onto the fibre, manipulation by the

AFM cantilever should move it apart (Figure 12b). The mechanical action did not succeed, and another ionic beam, having the same conditions as before, was set to cut 2. Immediately after the first energy input, the cut fibre part was released at cut 1 and bend down towards the substrate. The cross-sectional shape of the cut fibre became visible for cut 1 (Figure 12c and d). The magnification of the cross-section in Figure 12d explains why so different energy amounts by time had to be applied to create the cut – the fibre was partly folded (U-shaped), which could not be seen from above when choosing the cutting position, and the ion beam had to go through the fibre in principle twice in the folded regions.

Bending down and fibre repelling were observed also for other cut fibre parts and explained by charging effects.
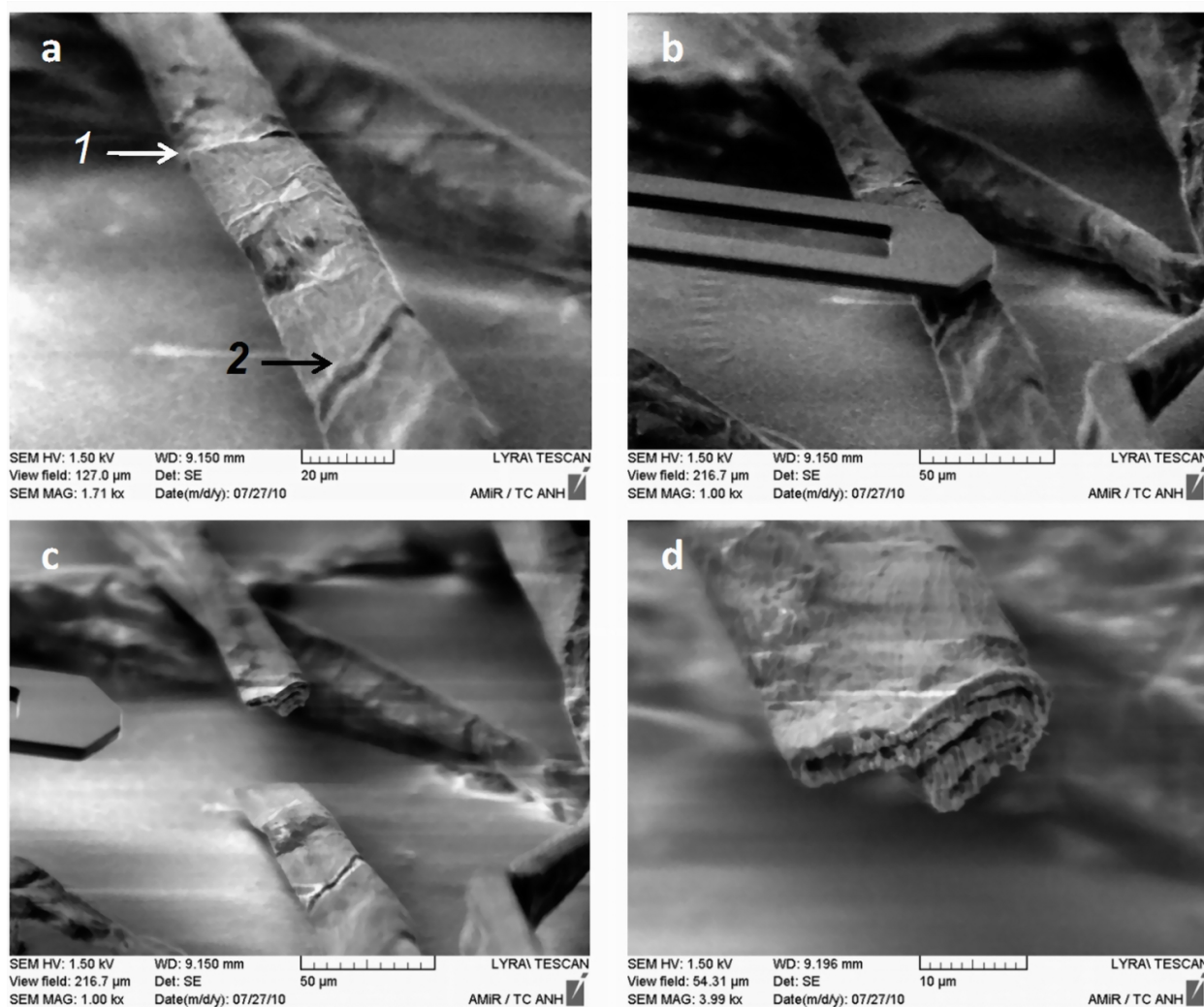
Figure 12. Cross-cutting of a single fibre (softwood chemical pulp unrefined) and manipulation with AFM cantilever using FIB mode (630 pA, aperture 6). Fibre after two neighboured cuts 1 and 2 (a), manipulation of the cut piece by AFM cantilever (b), breaking of cut 1 (c), and magnified cross-section of the cut fibre at cut 1 (d)
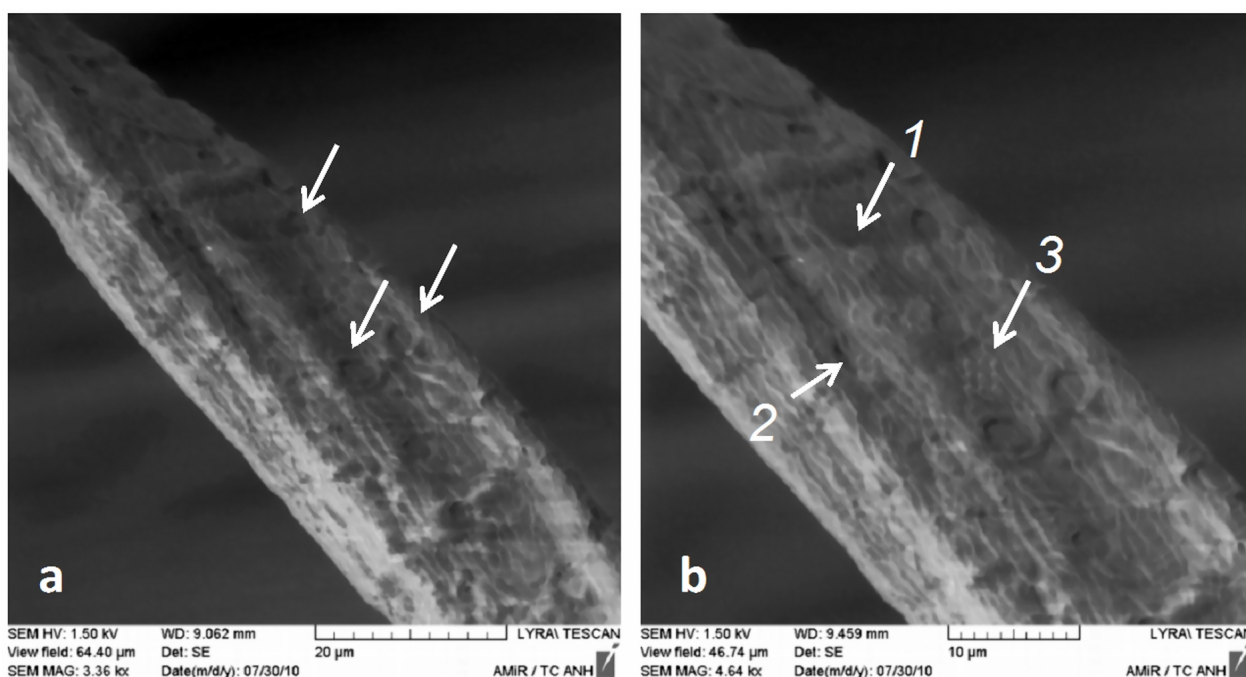
Figure 13. Deposition experiments using electron and ion beam induced deposition (EBiD/IBiD) with platinum (Pt) and tungsten (W) on a free standing softwood fibre of refined chemical pulp. Fibre surface before deposition, natural circular features such as closed bordered pits marked with white arrows (a), results of three deposition trials (b): Trial 1: 4-spot grid, radius 1 µm, gap 4 µm, parallel mode (Pt), trial 2: 4-spot grid, radius 0.25 µm, gap 1 µm, serial mode (Pt), trial 3: 9-spot grid, radius 0.25 µm, gap 1 µm, serial mode (W)

Electron or ion beam induced depositions (EBiD resp. IBiD) use the charged particle beam to decompose precursor molecules which are injected into the vacuum chamber of the SEM. Many precursors are delivered in gaseous state close to the deposition spot by a gas injection system (GIS). The charged beam cracks the adsorbed precursor molecules and the non-volatile fragments become a solid deposition. The volatile fragments are pumped away by the vacuum system. More about the use of EBiD and IBiD can be found in Fatikow (2008). The deposition experiments were performed at refined samples of the softwood chemical pulp from the 2nd common COST sample, described elsewhere in this book by Heinemann and Ander (2011). A free-standing single fibre was used, which was prepared as described above (see Figure 8). The depositions were done with Platinum (Pt) and Tungsten (W) with three different patterns (Figure 13). To separate native circular structures on a dry fibre surface, features such as closed bordered pits were registered from the fibre before deposition treatment (white arrows in Figure 13a). The resulting three grid patterns are visible in Figure 13b. Pattern 1 was a 4-spot grid (2x2 matrix) with a spot radius of 1 µm and a gap width of 4 µm performed as parallel process with Platinum. Also pattern 2 was performed with Platinum as a 4-spot grid with a spot radius of 0.25 µm and a gap width of 1 µm, but as serial process (spot-by-spot). The serial process was also applied to pattern 3, which was a 3x3 matrix with the same spot radius and gap width as for pattern 2, but using a tungsten precursor.

Outlook

The results of the first manipulation applications on single fibres in SEM and AFM-in-SEM techniques were promising and a good start-up for developing a fully automated testing principle on single fibres.

The combination of micro/nano manipulators and the SEM/AFM technology have a high potential to improve investigations on the morphology of fibres and fibrils, e.g. by following deformations during drying and wetting and thus contributing to hornification tests.

The application of the FIB technology will contribute to investigations on structural properties and on the fine fibre structure e.g. by tests of the fibre compressibility or peeling resistance. Instead of simple cross-sectional cutting the surface and fibre-wall ablation by this charged particle beam needs to be tested, as it could reveal more of the inner structure of the fibre and make specific structuring of the fibre possible.

Concerning the compression testing the folding of the fibres must be known. On the one hand the presented setup can measure the folding stiffness and on the other hand the compression stiffness of the fibre alone. This folding-problem needs to be taken into account in future setups: Either another fibre must be chosen or the setup is able to unfold the fibre. With these modifications the cross-section will be known and a corresponding material property can be determined.

Future research also has to address the difficulties in manipulating and processing these paper fibres in three dimensions. A contact detection tool which is sensitive in three dimensions would ensure safer working with the often delicate tools made from silicon.

Questions for future research can possibly be answered with micro- and nanorobotic systems. Some of those questions could be for example:

- Single fibre properties such as transversal and cross-sectional dimensions, bendability and tensile strength including fibre wall structure at the breaking point
- Characterisation of bonds between fibres, between fibres and fibrils, and between fibres and vessels regarding the bonding strength
- Fibre wall delamination, cross-sectional shape and effect on fibre deformation (compression force)
- Peeling characteristics of fibre layers: Removing of single fibre wall layers considering the peeling off force
- Special focus on the nano scale: Bundles of fibrils, microfibrils, nanofibrils.

However, an automated system as outlined in the Automation System-section is not yet realised. Some of the biggest efforts have to be spent on the handling of such irregular, naturally grown structures like paper fibres. But using robotics, that work at the micro and nanoscale, will certainly offer future-proof solutions.

Acknowledgement

References

Ander P., Hildén L. and Daniel G. (2008): Cleavage of softwood kraft pulp fibers by HCl and cellulases. BioResources 3(2): 477-490

Chinga-Carrasco G. (2010): Micro- and nanostructures of wood pulp fibres. COST Action E54 Workshop, May 10-12, Coimbra, Portugal 2010

Desai J.P., Pillarisetti A. and Brooks A.D. (2007): Engineering Approaches to Biomanipulation. Anu. Rev. Biomed. Eng. 9:35-53

Eichhorn V., Bartenwerfer M. and Fatikow S. (2010): Nanorobotic Strategy for Nondestructive Mechanical Characterization of Carbon Nanotubes. Bentham J. Micro and Nanosystems 2(1): 32-37

Eichhorn V., Fatikow S., Sukas O. S., Hansen T., Bøggild P. and Occhipinti L. (2010a): Novel Four-Point-Probe Design and Nanorobotic Dual Endeffector Strategy for Electrical Characterization of As-grown SWCNT-Bundles. In: IEEE International Conference on Robotics and Automation, Anchorage, Alaska, USA, May 3-8, 2010

Fatikow S. (2008): Automated Nanohandling by Microrobots. Springer-Verlag, London 2008

Heinemann S. and Ander P. (2011): Standard Pulp and Paper Tests, *In* COST Action E54 "Characterisation of the fine structure and properties of papermaking fibres using new technologies". *Eds*: Ander P., Bauer W., Heinemann S., Kallio P., Passas R. and Treimanis A. Swedish University of Agricultural Sciences. p. 211-232. ISBN 978-91-576-9007-4

Lichtenegger H., Reiterer A., Tschegg S. and Franzl P. (1999): Variation of cellulose microfibril angles in softwoods and hardwoods – A possible strategy of mechanical optimization. J. Struct. Biol. 128(3): 257-269

Sarén M.-P., Serimaa R., Andersson S., Paakkari T., Saranpää P. and Pesonen, E. (1999): Structural variations of tracheids in Norway spruce (*Picea abies* [L.] Karst.). J. Struct. Biol. 128(2): 101-109

Sirviö J. (2000): Variation in tracheid properties of Norway spruce. Dissertation. University of Helsinki, Department of Forest Resource Management. Helsinki, Finland: Yliopistopaino, Publications 25, 35 p.

Turner P. and Reynolds A. (2009): New insights into the cellulose micro-fibril structure of the wood cell wall. COST Action E54 Workshop, May 4-6, Tampere, Finland, 2009

Tyrväinen J. (1995): The influence of wood properties on the quality of TMP made from Norway spruce (*Picea abies*) wood from old growth forests, first thinnings and sawmill chips. In: 1995 Int. Mech. Pulping Conf, Ottawa, Canada, 12-15 June 1995. Montreal, Canada: CPPA, Proceedings, p. 23

Vehniäinen A. (2008): Single fiber properties – a key to the characteristic defibration patterns from wood to paper fibers. Dissertation. Helsinki University of Technology, Department of Forest Products Technology. Espoo, Finland: KCL Communications 12, 95 p.

FIBER CROSS SECTION PROPERTIES ESTIMATED WITH AN AUTOMATED SERIAL SECTIONING TECHNIQUE

[1]Johannes Kritzinger, [2]Michael Donoser, [1]Ulrich Hirn and [1]Wolfgang Bauer

[1]Institute for Paper, Pulp and Fiber Technology, Graz University of Technology

Research Studio Austria µSTRUCSCOP

Kopernikusgasse 24/II, 8010 Graz, Austria

[2]Institute for Computer Graphics and Vision, Graz University of Technology

{johannes.kritzinger, michael.donoser, ulrich.hirn, wolfgang.bauer}@tugraz.at

Abstract

An accurate analysis of pulp fiber cross section properties in the dry state is commonly performed based on images obtained with scanning electron microscopy (SEM) or confocal laser scanning microscopy (CLSM). Sample preparation and digitization is a time consuming process for both techniques, especially if a reasonable number of fiber cross sections has to be analyzed. This paper introduces an automated serial sectioning technique and newly developed image analysis algorithms for the analysis of fiber cross section properties in a sheet of paper. A 3D data set, consisting of consecutive cross sections, allows the analysis of several thousand fiber cross sections within reasonable time. This technique was used to study the effect of beating in a PFI mill on fiber cross section properties. An increase in fiber collapse as well as a decrease in the fiber wall thickness was observed.

Introduction

The paper network is composed of individual fibers which highly vary in their shapes and dimensions. These variations can attributed to two major sources. The first source is the variation of fiber dimensions within the same kind of wood species, due to e.g. growing conditions, location in the stem or location in annual ring (earlywood vs. latewood). The second source of variations originates from the wood species used. Softwoods are almost fully composed of tubular tracheids with an average length of 2 to 3 mm and a width of 20 to 35 µm. Hardwoods are made up from very thin walled vessel cells and tracheids which are significantly smaller than those in softwoods.

Measurement of longitudinal properties like the fiber length, kink and curl is well established and usually performed in flow cells, i.e. in the wet state (e.g. Turunen et al. 2005; Hirn and Bauer 2006). Some of these flow cell based devices also characterize average wet state fiber cross section properties as e.g. fiber wall thickness, however at a rather low level of resolution. Exact analysis of fiber cross section properties requires significantly higher resolution and thus more sophisticated measuring techniques. In fact, there is currently no measurement equipment available which is able to determine fiber cross section properties at high resolution in a statistically reasonable manner and within a reasonable time. Several approaches have been suggested since fiber cross section properties have crucial effects on paper quality. Mechanical properties of single fibers like fiber strength are affected by changes in the cross section dimensions (Hartler and Nyrén 1970). Cracks in the fiber wall can cause changes in the scattering coefficient or surface smoothness in the final sheet (Nesbakk et al. 2001). Thin walled fibers collapse easier than thick walled ones and these collapsed fibers are more flexible and form denser fiber networks (Jang and Seth 1998; Gregersen and Niskanen 1999). This again has

an impact on the final paper in terms of higher paper strength, a lower paper thickness and increased paper smoothness (e.g. Dinwoodie 1965; Oluwafemi and Sotannde 2007).

CLSM
(Batchelor et al. 2006)

SEM
(Chinga et al. 2007)

X-ray tomography
(Antoine et al. 2002)
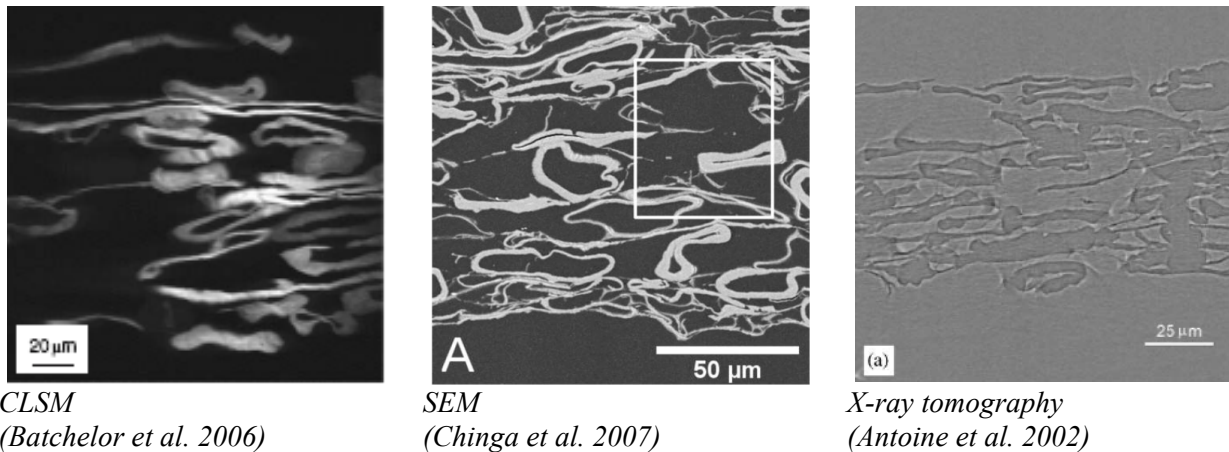
Figure 1. Paper cross section used for the analysis of fiber cross section properties obtained with different digitization techniques

A typical analysis routine of fiber cross section properties consists of three steps: digitization of fiber cross sections – detection and segmentation of fiber cross sections – measurement of fiber cross section properties. The first step is very important since image quality and image contrast are the determining factors for the later steps. Different techniques are used for the digitization of fiber cross sections; scanning electron microscopy (SEM) and confocal laser scanning microscopy (CLSM) are the most common techniques, X-ray tomography (μCT) is an emerging technique within the last decade. Exemplary images obtained by the various methods are shown in Figure 1.

The optical sectioning capability of CLSM is used to produce 3D datasets of the sample to be analyzed. Fiber cross section analysis is performed in two different ways, optical sectioning through the fiber thickness of individual fibers mounted on a microscope slide (Ho et al. 1991; Jang et al. 1992) and digitization of prepared paper cross sections (Dickson 2000a; He et al. 2003a). The latter technique again can be divided into digitization of paper cross sections at a small depth range (Dickson 2000a; b) and at significantly different depth from 0 to 10 μm (He et al. 2003a; b). In general, the use of CLSM is limited because of two reasons; a rapid diminishing of the signal intensity with increasing depth of the vocal plane and the need of a fluorescent dye because of the weak auto fluorescence of fibers used in paper making. Another problem for both techniques is that touching fibers cannot be separated because there are just weak boundaries visible in the grey scale images.

Scanning electron microscopy (SEM) in backscatter mode is used because of the very high resolution achievable and the high contrast between embedding medium and fibrous materials, see Figure 1 (b). The common way in the analysis of fiber cross section properties with SEM is the use of individual cross sections (e.g. Reme and Helle 2001; Reme et al. 2002; Nesbakk and Helle 2002; Chinga-Carrasco et al. 2009). The fibers have to be orientated perpendicular to the image plane. Therefore different preparation steps are necessary. Image analysis is difficult as with CLSM, because touching fibers again do not show a visible borderline. There are also some attempts to analyze fiber cross section properties from 3D data sets obtained with SEM. Different approaches like serial grinding (Chinga et al. 2004) or also serial sectioning (Aronsson et al. 2002) are used but the time involved is very high in both cases.

X-ray tomography is a non destructive technique capable for the analysis of fiber cross section properties. Synchrotron radiation based digitization yields in acceptable image quality (e.g. Antoine et al. 2002; Rolland du Roscoat et al. 2005), see Figure 1 (c), without the need of contrast material or embedding of the sample. Again, only grey scale images are obtained and thus there is also a lack in image analysis in the case of touching fibers.

Serial sectioning in principle fulfills the basic requirements for a digitization system in fiber cross section analysis; a high resolution combined with sufficient image quality, digitization of a large sample within a reasonable time and the capability to digitize fibers in a sheet of paper.

This paper describes the use of an automated serial sectioning combined with light microscopy and newly developed image analysis routines for the analysis of fiber cross section properties. The technique is used to show the effect of beating in a PFI mill on fiber cross section properties.

Materials and methods

As with other techniques, our method to analyze fiber cross section dimensions consists of three subsequent steps. First, the 3D structure of a paper sample is digitized at high resolution using the automated serial sectioning technique. Second, newly developed image analysis algorithms are used to detect individual fibers. And third, several properties of the fiber cross sections are evaluated.

Automated serial sectioning

(a) Schematic diagram of the prototype built   (b) Photograph of the prototype built
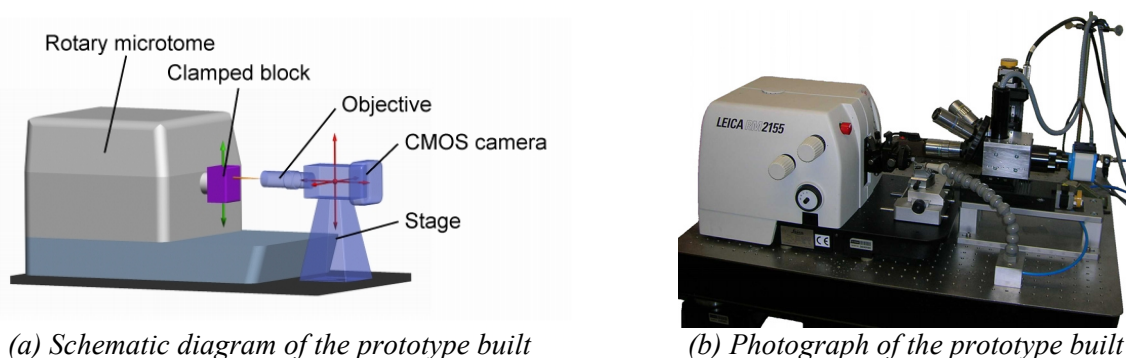
Figure 2. Layout of the prototype built; (a) shows a schematic diagram indicating the major components and directions of motion and (b) depicts a photograph of the prototype built

The digitization concept has already been introduced by Wiltsche et al. (2005). This concept combines automated microtomy and light optical microscopy, see Figure 2 (a) and (b). The microtome cuts off thin slices from a resin embedded paper sample. After each cut the surface of the block is scanned with a microscope mounted on a moveable stage in front of the microtome. Slicing and imaging are fully automated and a 3D digital representation of the analyzed paper sample is obtained. Fiber cross section analysis is performed at a resolution of 0.6 μm and at a cut thickness between 1 and 3 μm. The time needed for a slicing and imaging of a typical cross section is about 1 minute. A small cut out of a digitized paper sample is shown in Figure 3, representing a low weight coated (LWC) paper. The spatial distribution of the coating layer as well as changes in the cross sectional appearance of some fibers is already visible in this small cut out.
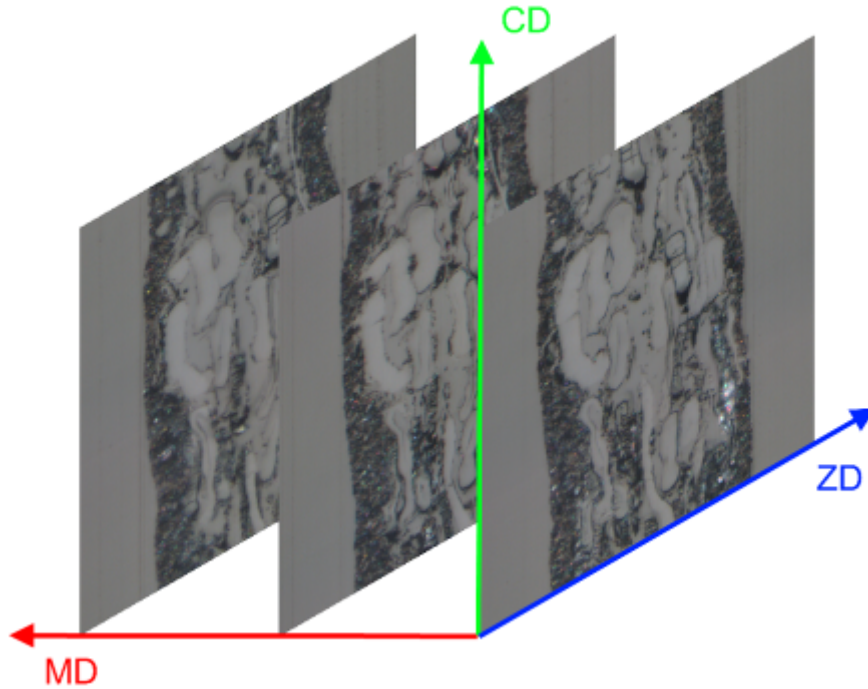
Figure 3. Cutout of a 3D dataset obtained with the automated serial sectioning technique. Several structural features, like the coating layers or fiber cross sections are visible in this image

The digitized 3D paper structure data sets can then be analyzed with a novel semi-automatic image analysis routine which allows the tracking of individual fibers through the entire image sequence.

Image analysis

A tracking algorithm was developed which segments individual fiber cross sections only based on the boundary image contrast which is clearly visible in Figure 5 (a). Tracking of fiber cross sections is formulated in a probabilistic framework to improve robustness. Maximally Stable Extremal Regions (MSERs) are used to obtain accurate fiber segmentations in every frame. The concept is explained in detail in Donoser et al. (2008). The detection of individual fiber cross sections is still a major research topic.

The tracking of fibers is initiated with manually segmented fiber cross sections in a first frame. This manual segmentation may cause a selection of some specific classes of fiber cross sections which has to be considered in the interpretation of the results.

The result of tracking is a sequence of so-called label images, where the segmentations of the cross sections of each fiber are identified by a unique ID. Figure 5 (b) shows obtained results where each ID is shown in a distinct color. Please note, that this allows direct access to each individual fiber which makes an independent analysis of all segmented fibers possible.

Evaluation of fiber cross section properties

This brief outline is based on Kritzinger et al. (2008; 2009). A very important step in the analysis of fiber cross section properties from 3D image data sets of actual paper samples is the calculation of a true fiber cross section. Since fibers are usually not oriented perpendicular to the cut plane, the dimensions of the measured cross sections in the images are overrated compared to

their real sizes. By allowing access to a sequence of cross sections our method enables us to correct this overrating. The change of the cross section location of a fiber in the fiber network is estimated based on the fiber centroid coordinates. The trend of this centroid coordinates is calculated using a polynomial fit. The local slope of this fit is used as a measure to transform the measured cross section to the true sized one.
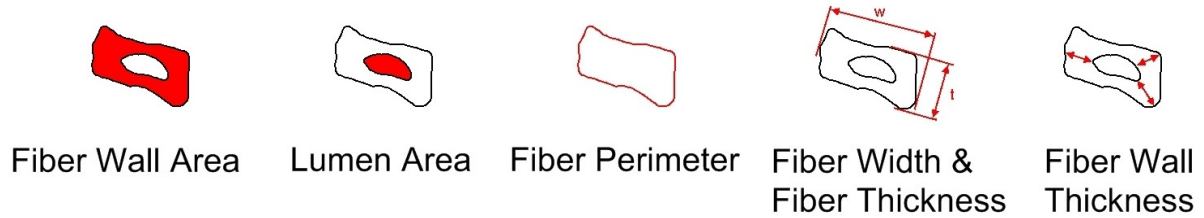
Figure 4. Fiber cross section properties extracted from resized cross sections

The transformed cross sections are then analyzed concerning fiber wall area, lumen area, fiber perimeter, fiber width and fiber thickness as well as fiber wall thickness, as illustrated in Figure 4. Furthermore the fiber cross sections are classified into three groups, collapsed fibers, fibers with visible lumen and fibers with a broken fiber wall. The calculation of distributions of single properties as well as correlations between the properties of the fiber cross sections like the fill factor (ratio between fiber wall area and the total area of the cross section – wall area and lumen area) completes the analysis routines. New approaches are developed to analyze changes of cross sectional properties along the fiber main axis.

Results and Discussion

The capability to analyze fiber cross section properties with an automated serial sectioning technique is shown in the following. The first example shows the effect of beating in a PFI-mill on fiber cross section properties. The second example shows some limitations of the automated serial sectioning technique. The last example is an outlook on future work in the field of fiber morphology.

(a) Paper cross sections with one fiber highlighted   *(b) Label image (different sample) with extracted fiber cross sections along image sequence*
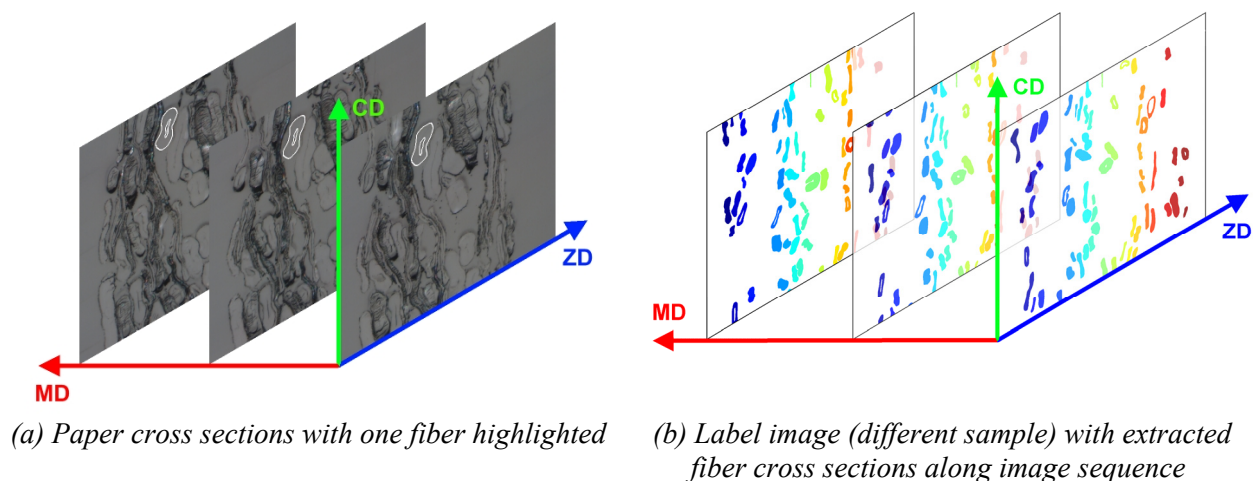
Figure 5. Detection of fiber cross sections in paper cross sections

Mean (vis.): 4.41 [µm] Std.dev. (vis.): 1.08 [µm]
Mean (col.): 3.08 [µm] Std.dev. (col.): 1.16 [µm]
Mean (bro.): 4.27 [µm] Std.dev. (bro.): 1.56 [µm]

Mean (vis.): 3.25 [µm] Std.dev. (vis.): 0.951 [µm]
Mean (col.): 2.64 [µm] Std.dev. (col.): 1.09 [µm]
Mean (bro.): 3.1 [µm] Std.dev. (bro.): 1.13 [µm]

(a) Unbeaten pulp   *(b) 6 000 rev. in PFI-mill*
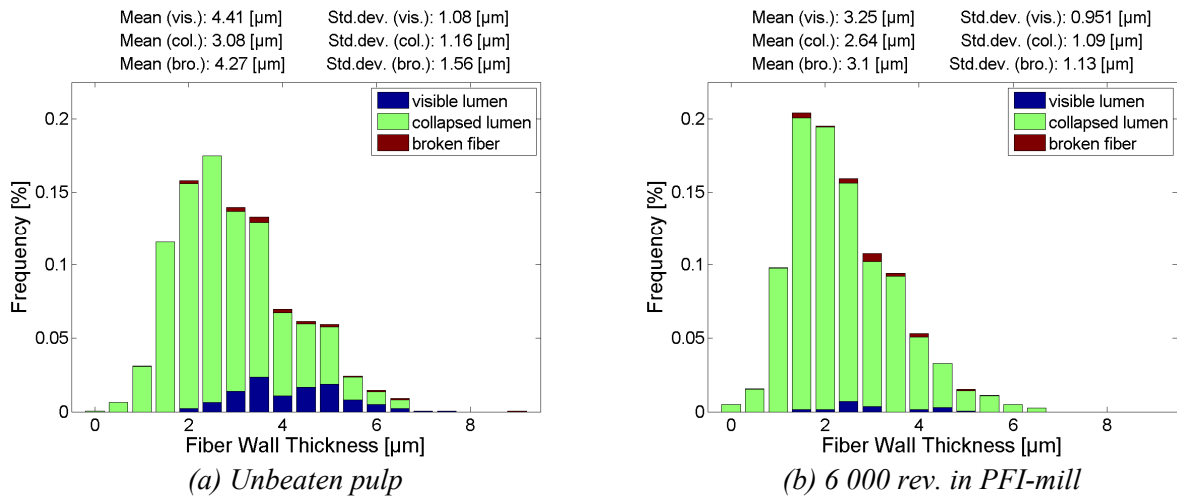
Figure 6. Effect of beating on fiber wall thickness distribution and fraction of collapsed fibers. The mean wall thicknesses and standard deviations of the corresponding distributions are given for the three different classes of fiber cross sections

(a) Unbeaten pulp   *(b) 6000 rev. in PFI-mill*
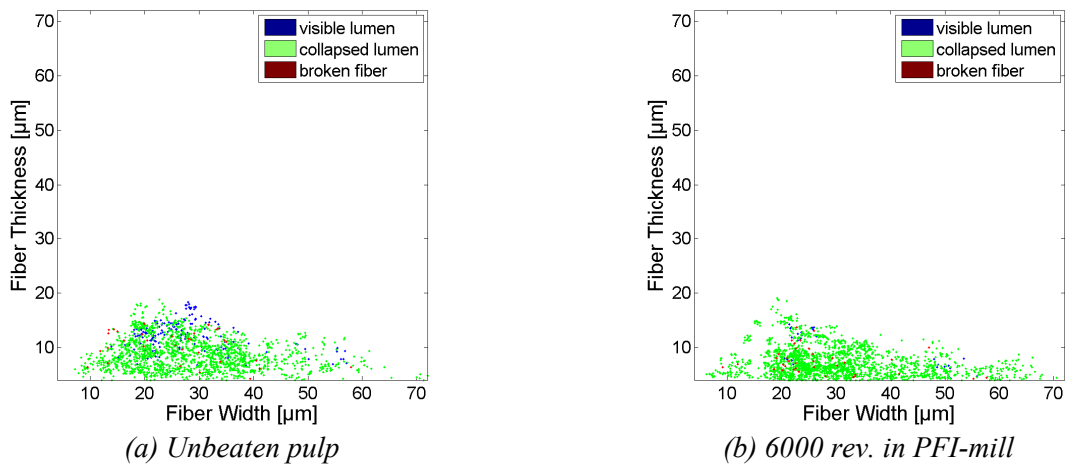
Figure 7. Effect of beating on the correlation of fiber thickness and fiber width

Effect of beating on fiber wall thickness

A flash dried bleached softwood (spruce) kraft pulp was used to analyze the effect of laboratory beating in a PFI-mill on fiber cross section properties. Three beating levels have been analyzed; unbeaten, 2 000 and 6 000 revolutions in the PFI mill. Small cutouts of typical cross sections of standard hand sheets (Rapid Koethen method) made from the pulps are presented in Figure 8, (a) for the unbeaten pulp and (b) for the pulp after 6 000 revolutions in the PFI-mill.

(a) Unbeaten pulp   *(b) 6000 rev. in PFI-mill*
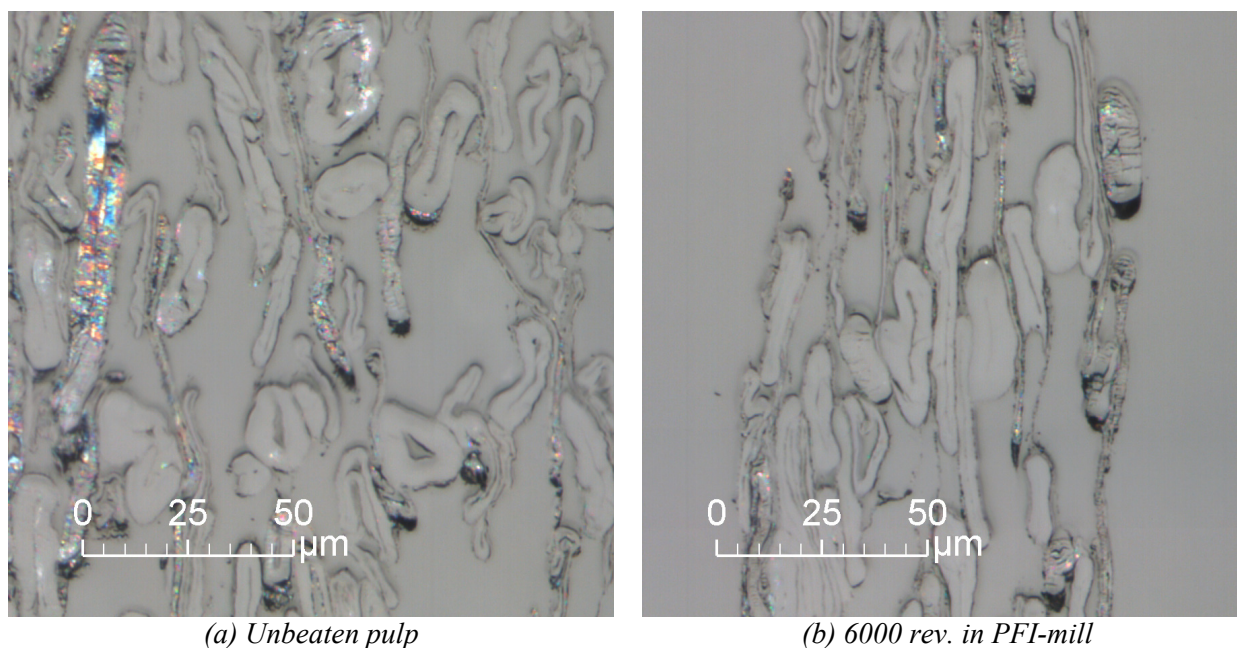
Figure 8. Effect of beating on fiber cross sections prepared in hand sheets

Several effects of beating on fiber and paper structures can already be seen in these images. The unbeaten pulp contains a fraction of fibers with visible lumen and the fibers are strongly deformed in many cases. The paper structure appears very porous. Beating leads to several changes in the structures. The fibers after beating are almost fully collapsed. The increased flexibility of the fibers is obvious because of the denser network respectively the lower void volume between the individual fibers. The higher network strength achieved in beating can be imagined because of the apparently larger contact areas between the fibers.

Several subsequent cross sections with a length of more than 2 mm have been digitized. The distance between the cross sections was set to 1 μm. An average of 2 000 fiber cross sections has been analyzed in each case. The most important results obtained in fiber cross section analysis are summarized in Table 1. Fiber wall area and fiber wall thickness are significantly reduced in the beating process. The actual reasons for this effect have not been found so far, however there might be some peeling of outer layers at the fiber wall or a compression of the fiber wall. The fiber width, the major length of a fiber cross section, is slightly increased, whereas the fiber thickness is decreased significantly. This is an indication for strong fiber collapse during beating. The fiber perimeter is not affected by different beating levels. The fill factor confirms the observations made in Figure 8. This value is always close to one which indicates strongly collapsed cross sections at all beating levels. The fraction of fibers with a visible lumen is decreased during beating from about 11% in the unbeaten pulp to approximately 2% after 6 000 revolutions in the PFI mill. To the same extent, the fraction of collapsed fibers increases. The fraction of fibers with a broken fiber wall is hardly affected during beating in a PFI-mill.

A more detailed analysis of fiber wall thickness data is presented in Figure 6, showing the wall thickness distribution for (a) the unbeaten pulp and (b) the pulp after 6 000 revolutions in the PFI-mill. The bars are split into fractions of fibers with visible lumen (blue part), fibers with collapsed lumen (green part) and fibers with a broken fiber wall (red part). As has been already discussed, the fraction of fibers with visible lumen is strongly decreased after beating in the PFI-mill. The fiber wall thickness seems to be an influencing parameter on the resistance of fiber collapse. As can be seen in the mean values collapsed fibers tend to have a thinner fiber wall

than the fibers with a visible lumen. The mean values also indicate that the decrease of the fiber wall thickness during beating is more pronounced for fibers with visible lumen and fibers with a broken wall than for already collapsed fibers.

Table 1. Effect of beating with a PFI-mill on fiber cross section properties obtained with automated serial sectioning and image analysis)

Cross section property	Unbeaten pulp	2 000 rev. in PFI-mill	6 000 rev. in PFI-mill
# Fiber cross sections	~1 900	~2 100	~2 100
Fiber wall area [µm²]	170.2 ± 3.2	150.1 ± 3.0	142.8 ± 2.7
Fiber wall thickness [µm]	3.25 ± 0.06	2.75 ± 0.05	2.66 ± 0.05
Fiber width [µm]	28.58 ± 0.49	31.26 ± 0.54	30.84 ± 0.52
Fiber thickness [µm]	9.01 ± 0.14	7.28 ± 0.12	6.97 ± 0.12
Fiber perimeter [mm]	69.17 ± 0.99	69.42 ± 0.98	67.95 ± 0.93
Fill factor [ ]	0.990	0.997	0.997
Visible lumen [%]	10.90	4.14	1.83
Collapsed lumen [%]	87.32	93.93	96.20
Broken fiber wall [%]	1.78	1.96	1.97
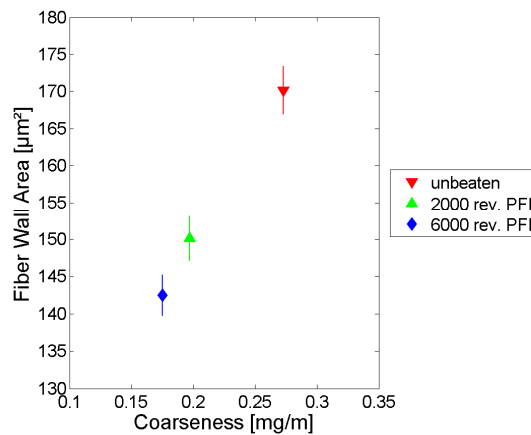
Figure 9. Correlation of fiber wall thickness (serial sectioning) and coarseness (kajaani FS-200). A strong correlation between the two different measuring techniques can be found

Figure 7 shows the correlation between fiber thickness and fiber width, (a) for the unbeaten pulp sample and (b) for the pulp after 6 000 revolutions in the PFI-mill. Values for the fiber width are considerably larger than for the fiber thickness. This indicates a strong deformation from a roundish like to a flattened cross section. Beating again shows some effects. The fiber thickness values are more concentrated below 10 µm, whereas the fiber width is hardly affected as was already summarized in Table 1.

A validation of the results obtained with the novel technique is presented in Figure 9, where a correlation of the fiber wall area obtained in the dry state with the serial sectioning technique and the coarseness measured with a kajaani FS200 in the wet state is shown. The fiber wall area as a measure for the fiber volume is thought to influence the coarseness of a pulp which can be interpreted as another method to measure the fiber volume. The data show a strong correlation, a decrease in the fiber wall area corresponds to a decrease in the coarseness. This can be seen as proof, since two completely different measuring systems show a similar trend of the properties investigated.

Fiber cross section analysis in mechanical pulp

As with other techniques, the automated serial sectioning technique has also its limitations in the analysis of fiber cross section properties. As can be seen in Figure 10, there are some pulp grades, where almost no fiber cross sections can be detected. These samples are cross sections of hand sheets from different mechanical pulps, (a) stone ground wood – SGW, (b) pressure ground wood – PGW and (c) thermo mechanical pulp – TMP. The main structures in these images result from fines and parts of the fiber wall.

| *(a) SGW* | *(b) PGW* | *(c) TMP* |
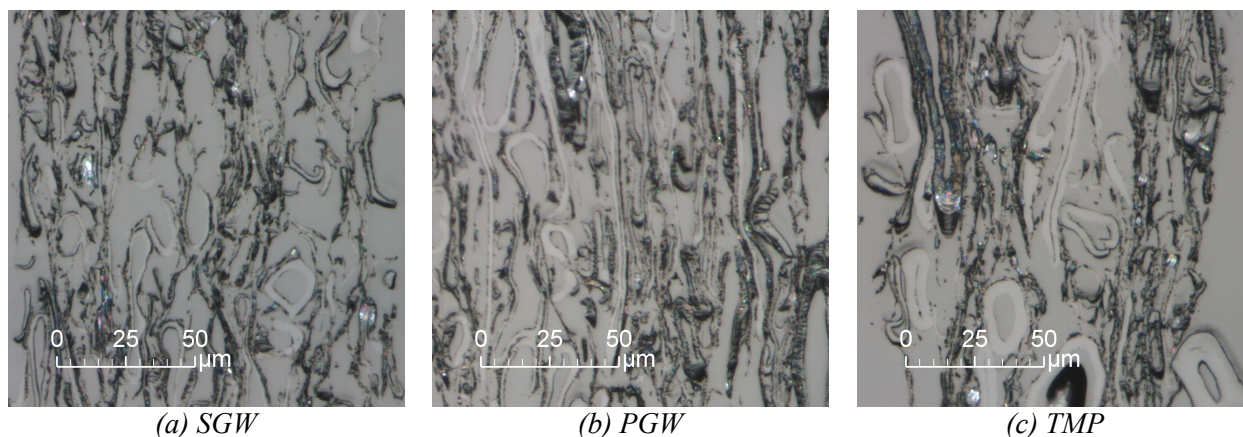
Figure 10. Cross sections of different mechanical pulp grades obtained with the automated serial sectioning technique

Other research groups concentrate on the analysis of fiber cross section properties in mechanical pulps (e.g. Reme et al. 2002). The fraction of fibers with a broken fiber wall and the degree of collapse are important characteristic measures for these pulps. The analysis in this case is usually limited to fractions of the different fiber classes which are typically obtained with Bauer-McNett fractionation. This seems to be the preparation method of choice in this case. A total, representative analysis of fiber cross section properties however is not possible anymore.

Change of cross section properties along fiber main axis

Also the variance of cross section properties along the fiber main axis is a question of interest. As an example Figure 11 shows 10 subsequent cross sections of a hand sheet made from spruce kraft pulp. The distance between each frame is 6 μm. Two fibers are outlined, one black and the other one white. The white fiber collapses and decollapses within the image sequence over a distance of just 60 μm. Apart from the rapid changes in fiber collapse the values measured for fiber wall properties are varying strongly within this small distance. Fiber wall thickness varies 20-30%, fiber wall area varies 10-25% and fiber perimeter varies around 15%.

Similar results have been reported by Bardage et al. (2002) and due to the new method developed, are now easy to access giving the basis for further discussion.
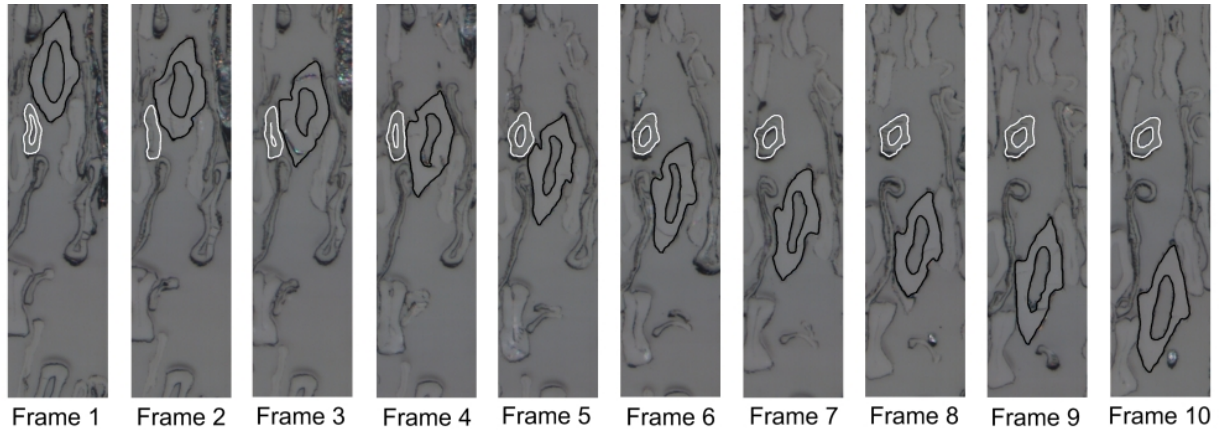
Figure 11. Changes of cross sectional shape along the image sequence. Collapse and decollapse of a cross section during passing another fiber.

Table 2. Changes of chosen cross sectional properties along the image sequence presented in Figure 11. Frame #1 and Frame #10 cannot be evaluated because of a lack of information for the currently used cross section resizing routine

Frame #	2	3	4	5	6	7	8	9
Fiber wall thickness [µm]								
Black fiber	4.88	4.96	4.83	4.61	4.37	4.42	4.10	4.38
White Fiber	2.82	2.99	3.30	3.36	3.41	3.60	3.70	3.71
Fiber wall area [µm²]								
Black fiber	343	337	332	336	321	339	305	346
White fiber	103	103	106	105	108	119	122	123
Fiber perimeter [µm]								
Black fiber	96	99	100	104	102	106	100	112
White fiber	52	50	48	47	45	49	49	47

Conclusions and Outlook

The combination of a microtome, light optical microscopy and proper image analysis is capable to analyze fiber cross section properties in a sheet of paper. Compared to other techniques, serial sectioning is able to access a reasonable number of fiber cross sections within a short period of time and a sufficient image quality. The image analysis routines are in principle able to handle thousands of cross sections that have to be evaluated to obtain statistically significant results. Further improvements of image analysis routines are however still necessary to minimize the necessary user interactions and the time needed for analysis.

The effect of beating on fiber cross section properties was shown in the first experiments. A noticeable decrease of fiber wall area and fiber wall thickness was found at increased beating levels. The fraction of fibers with a visible lumen was found to be decreased from about 11% for the unbeaten pulp to about 2% for the pulp after 6 000 revolutions in the PFI-mill. The fiber width was almost unaffected, whereas the fiber thickness decreased during beating.

A promising approach is the possibility to extract data about changes in cross section morphology within individual pulp fibers. Measurement of dimensional variations within fibers is important since these have a large impact on fiber flexibility, strength and conformability. A novel field in fiber morphology research can be opened with this technique.

Acknowledgement

References

Antoine C., Nygard P., Gregersen Ö.W., Holmstad R., Weitkamp T. and Rau C. (2002): 3D images of paper obtained by phase-contrast X-ray microtomography: image quality and binarisation. Nucl. Instrum. Methods Phys. Res. Sect. B-Beam Interact. Mater. Atoms 490, 392-402

Aronsson M., Henningsson, O. and Sävborg Ö. (2002): Slice-based Digital Volume Assembly of a Small Paper Sample. Nord. Pulp Paper Res. J. 17(1), 29-33

Bardage S.L., Daniel G. and Singh A. (2002): Three-Dimensional Analysis of the Collapse Behavior of Kraft-Cooked Norway Spruce Fibers. Wood Fiber Sci. 34(3), 382-390

Batchelor W.J., He J. and Sampson W.W. (2006): Inter-fibre contacts in random fibrous materials: experimental verification of theoretical dependence on porosity and fibre width. J. Mater. Sci. 41, 8377-8381

Chinga G., Johnsen P.O. and Diserud O. (2004): Controlled serial grinding for high-resolution three-dimensional reconstruction. J. Microsc.-Oxf. 214(1), 13-21

Chinga G. Solheim O. and Mörseburg K. (2007): Cross-sectional dimensions of fiber and pore networks based on Euclidean distance maps. Nord. Pulp Paper Res. J. 22(4), 500-507

Chinga-Carrasco G., Lenes M., Johnsen P.O. and Hult E.-L. (2009): Computer-assisted scanning electron microscopy of wood pulp fibres: Dimensions and spatial distribution in a polypropylene composite. Micron 40(7), 761-768

Dickson A.R. (2000a): Quantitative analysis of paper cross-sections. Appita J. 53(5), 292-295

Dickson A.R. (2000b): The quantitative microscopic analysis of paper cross-sections: sample preparation effects. Appita J. 53(5), 362-366

Dinwoodie J.M. (1965): The relationship between fiber morphology and paper properties: A review of literature. Tappi J. 48(8), 440-447

Donoser M., Kritzinger J., Mauthner T. and Bischof H. (2008): A probabilistic approach for tracking fibers. Proc. 19th International Conference on Pattern Recognition (ICPR), Tampa, Florida, December 2008. ISBN 978-1-4244-2175-6

Gregersen Ø.W. and Niskanen K. (1999): Measurement and simulation of paper 3D-structure. Proc. COST E11 meeting, 1999

Hartler N. and Nyrén J. (1970): Transverse Compressibility of Pulp Fibers II. Influence of Cooking Method, Yield, Beating, and Drying. Tappi J. 53(5), 820-823

He J., Batchelor W.J., Markowski R. and Johnston R.E. (2003a): A new approach for quantitative analysis of paper structure at the fibre level. Appita J. 56(5), 366-370

He J., Batchelor W.J. and Johnston R.E. (2003b): The behavior of fibers in wet pressing. Tappi J. 2(12), 27-31

Hirn U. and Bauer W. (2006): A review of image analysis based methods to evaluated fiber properties. Lenzinger Berichte 86, 96-105

Ho F.J., Robertson A.G. and Seth R.S. (1991): Optical sectioning of pulp fibers using confocal scanning laser microscopy. Tappi J. 74(10), 217-219

Jang H.F., Robertson A.G. and Seth R.S. (1992): Transverse dimensions of wood pulp fibres by confocal laser scanning microscopy and image analysis. J. Mater. Sci. 27, 6391-6400

Jang H.F. and Seth R.S. (1998): Using confocal microscopy to characterize the collapse behavior of fibers. Tappi J. 81(5): 167-174

Kritzinger J., Donoser M., Wiltsche M. and Bauer W. (2008): Examination of fiber transverse properties based on a serial sectioning technique. Proc. Progress in Paper Physics Seminar 2008, Helsinki, Finland, June 2008. ISBN 978-951-22-9391-9, pp. 157-160

Kritzinger J., Donoser M. and Bauer, W. (2009): Estimation of fiber cross section properties from image data obtained by a serial sectioning technique. Proc. COST E54 meeting Tampere, Finland, May 2008. pp. 63-65

Nesbakk T., Mörseburg K. and Helle T. (2001): Relationship between fibre properties and cross sectional paper characteristics of mechanical pulp handsheets. Proc. 3rd Biennial Gullichsen Coll. 2001

Nesbakk T. and Helle T. (2002): The influence on the pulp fibre properties on supercalendered mechanical pulp handsheets. J. Pulp Pap. Sci. 28(12), 406-409

Oluwafemi O.A. and Sotannde O.A. (2007): The Relationship between Fibre Characteristics and Pulp-sheet Properties of *Leucaena leucocphala* (Lam.) De Wit. Middle-East Journal of Scientific Research 2(2), 63-68

Reme P.A. and Helle T. (2001): Quantitative Assessment of Mechanical Fibre Dimensions During Defibration and Fibre Development. J. Pulp Pap. Sci. 27(1), 1-7

Reme P.A., Johnsen P.O. and Helle T. (2002): Assessment of Fibre Transverse Dimensions using SEM and Image Analysis. J. Pulp Pap. Sci. 28(4), 122-128

Rolland du Roscoat S., Bloch J.F. and Thibault X. (2005): Synchrotron radiation microtomography applied to investigation on paper. J. Phys. D-Appl. Phys. 38, A78-A84

Turunen M., LeNy C., Tienvieri T. and Niinimäki J. (2005): Comparison of fibre morphology analysers. Appita J. 58(1), 28-32

Wiltsche M., Donoser M., Bauer W. and Bischof H. (2005): A new slice based concept for 3D paper structure analysis applied to spatial coating layer formation. Proc. 13th Fund. Res. Symposium, Cambridge, UK, September 2005. ISBN 0-9545273-3-2, pp. 853-899

IMPROVED CHARACTERIZATION OF CHANGES IN FIBRE CROSS SECTION DURING SHEET FORMING AND DRYING USING OPTICAL FIBRE ANALYZER DATA AND A SERIAL SECTIONING TECHNIQUE

[1]Warren Batchelor, [2]Johannes Kritzinger, [2]Wolfgang Bauer, [3]Timo Kuntzsch and [3]Gert Meinl

[1]Monash University Victoria, Australia

[2]Graz University of Technology, RSA µSTRUCSCOP, Austria

[3]PTS Heidenau, Germany

E-mail: timo.kuntzsch@ptspaper.de

Abstract

The contribution describes the combination of analysis methods to characterize fibre cross sections in wet and dry state aiming at a better understanding of shrinkage and pressing effects and related fibre collapse and deformation. The experimental results measured for a range of different pulp samples by an optical fibre analyzer and a serial sectioning technique are presented and discussed. Furthermore a new numerical approach for describing the transformation of fibre cross sections from wet to dried state is introduced and evaluated.

Introduction

The development of physical models for paper property prediction and their practical use require detailed knowledge regarding individual fibre characteristics such as their morphological parameters and their arrangement in a fibre network of the formed sheet. Regarding fibre bonding, fibre cross sections are one of the most important issues controlling bonded surfaces as shown in Figure 1, for instance in terms of Relative Bonded Area (RBA). Batchelor and He (2005) and Batchelor et al. (2007) presented approaches to estimate RBA of fibres in a given sheet by using the apparent density of the sheet and (mean) fibre cross section dimensions. The method itself needs the knowledge of fibre diameter in the dried sheet.
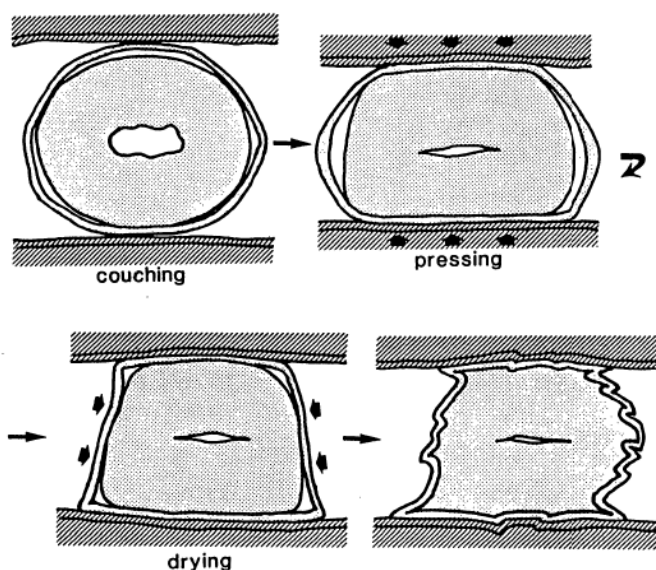
Figure 1. Fibre bond formation process (from Nanko and Ohsawa 1989)

Cross section information of thousands of fibres is typically provided by some fibre analyzers which measure morphological fibre properties in a dilute suspension. The fibre cross section dimensions determined in the wet state differ considerably from those in a well dried paper sheet because of fibre shrinkage and pressing effects, which lead to fibre collapse and deformation (Figure 1).

During the last few years, as a result of innovative image acquisition and processing techniques, morphological data of fibre cross sections within dried sheets have become available. The combination of analysis methods to characterize fibre cross sections in wet and dry state allows a better understanding of pressing and drying mechanisms and can be used to derive and to improve corresponding simulation models.

This contribution will compare characteristics of fibre cross-sectional dimensions (i.e. Fibre Width, Fibre Wall Thickness and Fibre Wall Area) measured in suspension and in the dried sheet. The fibre cross-section dimensions in suspension were measured by a kajaani FiberLab^{TM} instrument (Metso Automation), while a serial sectioning technique applied to handsheets was used to measure cross-sectional dimensions within the dried sheet. For allocation of representative results fibre populations of about 20000 fibres in suspension and 2000 fibre cross sections in the corresponding handsheets have been analysed. The results were evaluated with regard to pressing and drying processes. Moreover a new numerical approach for describing the transformation of fibre cross sections from wet to dried state will be introduced and discussed.

Experimental

Pulp samples

The following unrefined pulp samples were selected in order to compare fibre cross section in suspension and in dried handsheets:

- BCTMP (Bleached Chemi-Thermomechanical Pulp, aspen)
- BEKP (Bleached Eucalyptus Kraft Pulp)
- NBSK (Northern-Bleached Softwood Kraft, spruce)
- Sulfite (Softwood sulfite pulp, spruce)

Further on to study the effect of refining on fibre cross section a Northern Unbleached Softwood Kraft Pulp (UBSK, pine/spruce) was used and refined on a laboratory disc refiner with a Specific Edge Load of 2.0 J/m and with Specific Net Refining Energy input of 0, 50 and 100 kWh/t.

Measurement methods

FiberLab^{TM} V3.0 was used to measure the fibre cross sections in suspension. For this purpose all pulp samples were reslushed and diluted.

Working principals of optical fibre analyzers and some quality comparisons were described in more detail by Turunen et al. (2005) and Guay et al. (2005). Comparing FiberLab^{TM} fibre wall thickness data with results from an alternative image processing systems, Richardson et al. (2003) recommended the use of FiberLab^{TM} fibre wall thickness data carefully. Nevertheless FiberLab^{TM} is an established fibre analyzer for fibre wall thickness measurement of large fibre populations featuring a proven ability to detect changes relevant to raw material or process effects (see e.g. Reyier 2008).

Rapid-Köthen former was used to form standard handsheets for each pulp sample. A serial sectioning technique and image processing tools were applied for fibre cross sectional analysis in handsheets (see Kritzinger et al. 2008).

Results and Discussion

Starting with Fibre Wall Area the measured data confirm that the ratio of the Fibre Wall Area *A'* in handsheet and those in suspension *A* varies between 1:2.5 (chemical pulp) and 1:4 (mechanical pulp). Concerning the correlation of Fibre Wall Thickness data seen in Figure 2 of handsheet and suspension indicates the same corresponding behaviour of chemical (dashed line) and mechanical (continuous line) pulps. In addition to the measured data, Figure 2 contains data from Reyier (2008), where fibre wall thickness of TMP fibres before (TMP Feed) and after various fractionation steps (TMP Stream 1, TMP Stream 5) in a hydrocyclone were compared. "Handsheet" data were measured by Reyier on freeze dried fibres, a method which is described in more detail by Reme et al. (2002). The data for TMP are well on the line of BCTMP.
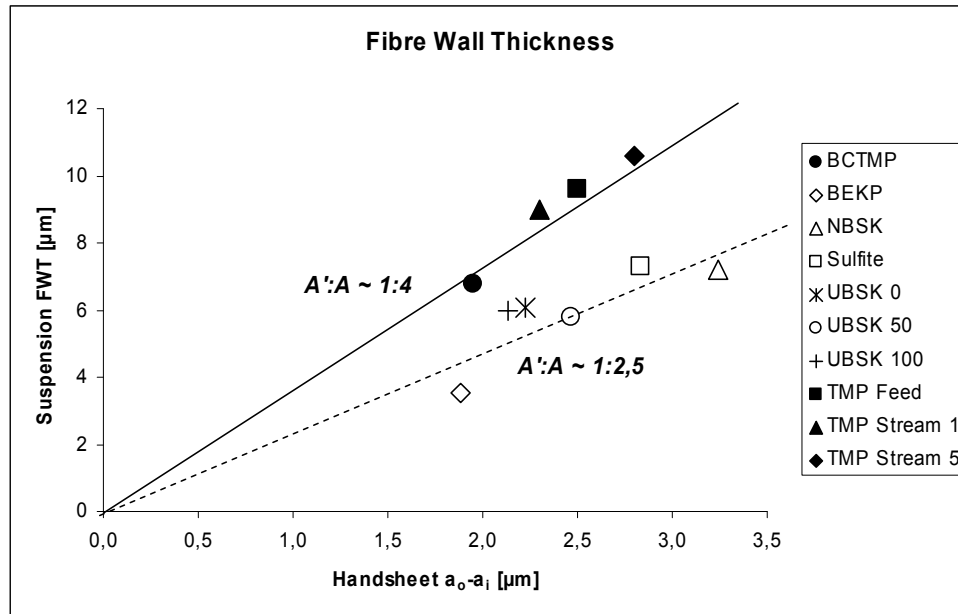
Figure 2. Mean Fibre Wall Thickness in suspension (FWT) and in handsheet (a_o-a_i ; explained in Figure 4)

The results also show that there are no major differences in the average Fibre Wall Area visible before and after refining. The same observation was made for other mean values of cross sectional dimensions. Only the amount of totally collapsed fibres indicates the refining impact. The latter number increased steadily from 85 % (unrefined) to 95% as refined (100 kWh/t).
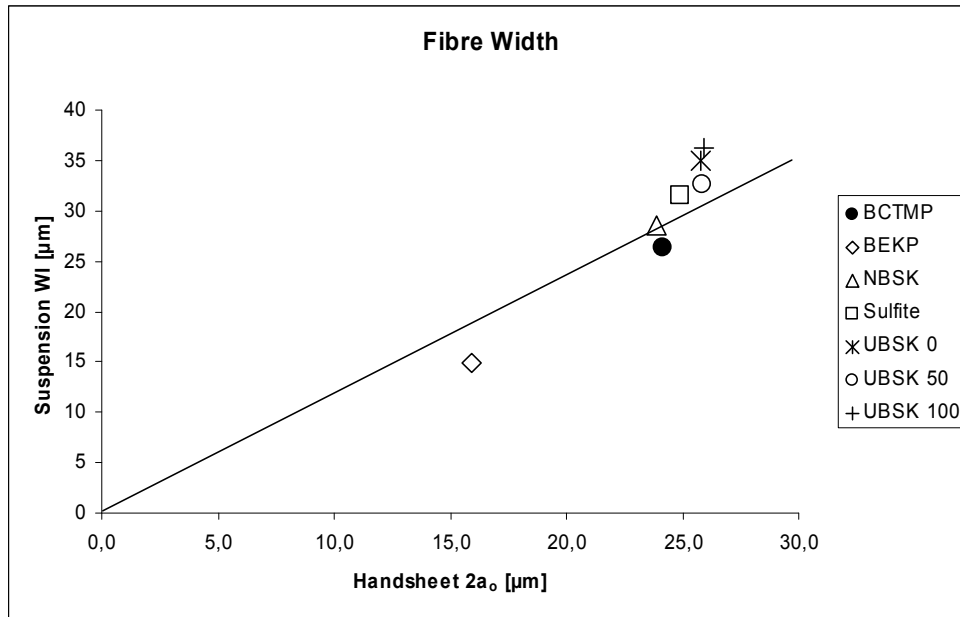
Figure Width

Figure 3. Fibre width in suspension (WI) and in handsheet ($2a_o$; explained in Figure 4)

Based on the measured data for fibre width (Figure 3) and fibre wall thickness, the transition of the fibre cross section from swollen state to dried and compressed state can be divided into two processes (Figure 4), which occur simultaneously during paper making – the drying process (shrinkage of the fibre cross section) and the compressions process (due to the forces which act on the fibres during wet pressing).
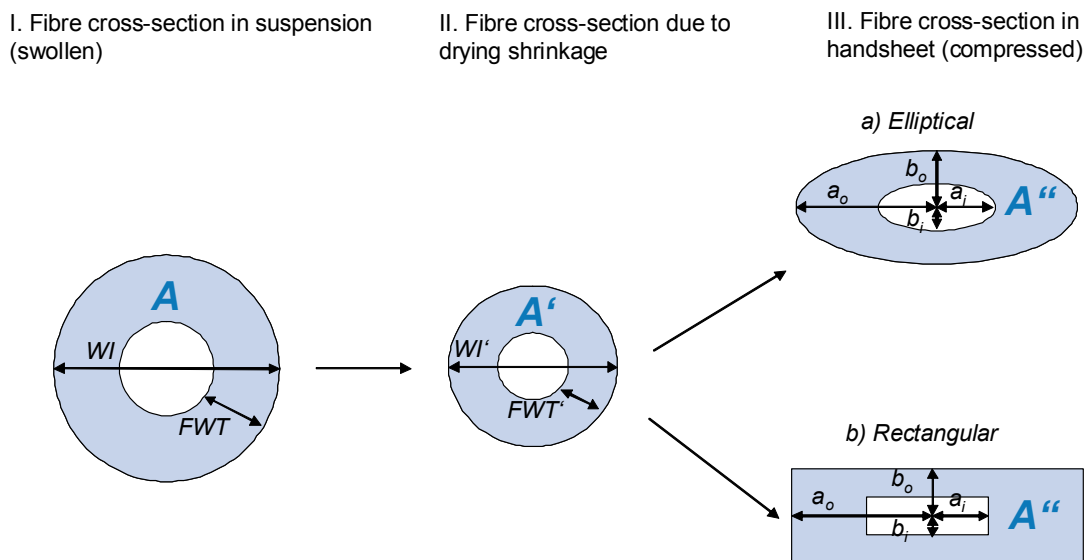
Figure 4. Two processes (drying shrinkage and compression), which occur during sheet forming and corresponding fibre cross section characteristics. The fibre cross section in handsheet can be drawn as elliptical or rectangular

The drying process I→II (A→A' in Figure 4) can be characterized mathematically by a similarity transformation. Comparing Fibre Wall Area A before and A'' after shrinkage (the latter equals A' if we assume fibre wall material incompressibility) leads to a similarity ratio [$\sqrt{A''/A}$] of about 0.66 for chemical pulp and 0.5 for mechanical pulp. Applying this ratio to WI and FWT yields the corresponding values WI' and FWT' of the dried but uncompressed fibre.

For the second step, the compression process II→III in Figure 4, it is important to account for invariants. According to observations by He et al. (2003) the fibre cross section area does not change significantly due to various wet press levels, i.e. *A'=A''*. A second assumption that was made is *FWT'=b$_o$-b$_i$*. i.e., the difference of outer and inner minor axis remains constant. As a third assumption let us assume that fibre perimeter also remains constant.

Now the procedure followed for the transformation to elliptical shape was to prescribe the values of the outside semi-minor ellipse axis, b_o, as a fraction of *WI'*. The inside semi-minor ellipse axis, b_i, was then calculated by subtracting the wall thickness *FWT'* of the fibre *A'* from b_o. The outside and inside semi-major axes, a_o and a_i were calculated from the area invariance *A'=A''* and by assuming that the perimeter of the ellipse was constant and independent of the fractional, very slight reduction in thickness given by 2b_o/WI'.

The procedure described above can be applied with minor modifications to both cases, elliptical or rectangular fibre cross section in handsheet. A calculation example is shown in Figure 5 for the BEKP sample (elliptical case) for various b_o values. In this case the measured value for a_o can be described properly supporting the proposed procedure. However further refinement is ongoing to explain all observed effects, e.g. with regard to fibre collapse.
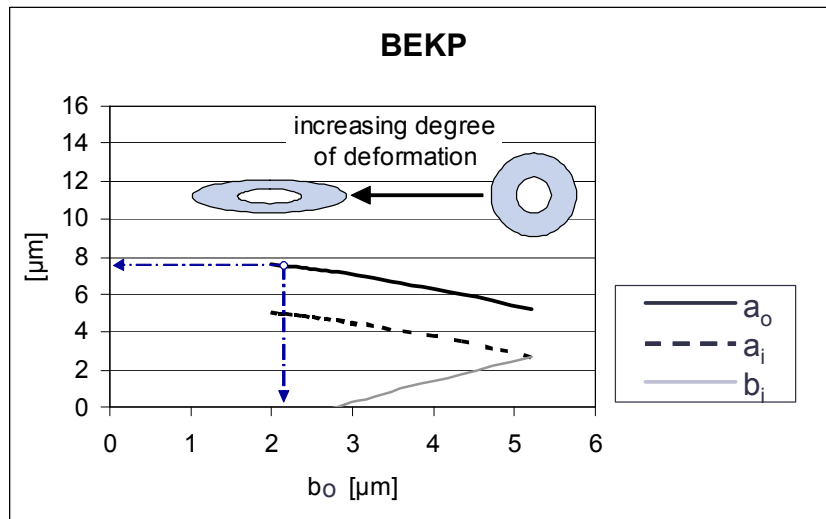
Figure 5. Calculation of a$_o$, a$_i$, b$_i$ as a function of b$_o$ for BEKP. The following input data were used: A''= 59.7 µm^2, Perimeter: 32.5 µm, b$_o$ - b$_i$ = 4.9 µm. The arrows refer to the measured values of b$_o$ and a$_o$

Conclusions

Different measurement methods were combined to characterize fibre cross sections in wet state (suspension) and in handsheets after shrinking and drying. All handsheets showed highly deformed fibres, for all investigated chemical pulp samples little or no lumen was found. Fibre shrinkage and deformation/compression were described using similarity transformations. A circular cross section for fibres in suspension and an elliptical shaped cross section for fibres in handsheets were assumed. The relation between cross section data measured by FiberLab[TM] in suspension and those of the dried and compressed fibres in handsheets can be described by two affine transformations, which differ for chemical and mechanical pulps. Fibre deformation seems to occur in a similar way for all investigated pulp samples.

From analysis of fibre cross sections after moderate refining (up to 100 kWh/t net refining energy) no significant changes were observed neither in suspension nor in dried handsheets. The only significant change was that the number of collapsed fibres increased, with increasing refining energy, which was probably caused by fibre stiffness reduction.

References

Batchelor W.J. and He J. (2005): A new method for determining the relative bonded area. Tappi J. 47(6), 23-28

Batchelor W., Kibblewhite R.P. and He J. (2007): A new method for measuring RBA applied to the Page equation for the tensile strength of paper. TAPPI Paper Physics Conference 2007

Guay D., Sutherland N., Rantanen W., Malandri N., Stephens A., Mattingly K. and Schneider M. (2005): Comparison of Fiber Length Analyzers. Proc. TAPPI Practical Papermaking Conf., May 22-26, 2005, Milwaukee, Wisconsin

He J., Batchelor W.J., Markowski R. and Johnston R. (2003): A new approach for quantitative analysis of paper structure at the fibre level. Appita J. 56(9) 366

Kritzinger J., Donoser M., Wiltsche M. and Bauer W. (2008): Examination of fibre transverse properties based on a serial sectioning technique. Proc. Progress Paper Physics Seminar: June 2-5, 2008, Espoo, Finland

Nanko H. and Ohsawa J. (1989): Mechanisms of fibre bond formation. In: Fundamentals of Papermaking. Ed: C.F. Baker, Mechanical Engineering Publications Ltd., London, 1989, p. 783

Reme P.A., Johnsen P.O. and Helle T. (2002): Assessment of Fibre Transverse Dimensions using SEM and Image Analysis. J. Pulp Paper Sci. 28(4), 122

Reyier S. (2008): Bonding Ability Distributions of Fibers in Mechanical Pulp Furnishes. Licentiate Thesis, Mid-Sweden University, Sundsvall 2008

Richardson J.D., Riddell M.J.C. and Burrel P. (2003): Experience with the FiberLab V3.0 analyser for measuring fibre cross-section dimensions. Proc. 57th Appita Annual Conference and Exhibition: May 5-7, 2003, Melbourne, Australia

Turunen M., LeNy C., Tienvieri T. and Niinimäki J. (2005): Comparison of fibre morphology analysers. Appita J. 58(1) 28

CHARACTERIZATION OF TMP FIBER WALL STRUCTURES BY MICROSCOPIC TECHNIQUES

[1]Sabine Heinemann, [2]Shaoxia Wang, [2]Jouko Peltonen, [1]Marjatta Kleen

[1]P.O. Box 1000, 02044 VTT (Espoo), Finland

[2] Center of Excellence for Functional Materials (FUNMAT), Laboratory of Paper Coating and Converting, Åbo Akademi University, Porthansgatan 3, 20500 Turku, Finland

Corresponding author: sabine.heinemann@vtt.fi

Abstract

Effect of pH on micro and nano scale surface structure of 1st stage TMP latewood fibers from Norway spruce was investigated. The fibers were analyzed by light microscopy, Atomic Force Microscopy (AFM) and Field-Emission Scanning Electron Microscopy (FE-SEM). Fibers at rather neutral pH level were found to be partly covered by reminants of outer fiber wall layers and partly by areas of exposed inner fiber wall. The outer fiber wall areas appeared as intact bands surrounding the fiber and were clearly rougher than areas of exposed inner fiber wall. In addition, the pH level affected the roughness of the outer fiber wall areas.

Introduction

Process development, including improved understanding of the fiber surface development, plays a key role in modern mechanical pulping. Both the physical and the chemical surface properties of pulps are very important, since they influence fiber charge, fiber bonding, wettability, adsorption, adhesion and consumption of papermaking chemicals.

The refining process includes two stages – fiber separation and fiber development – which can occur simultaneously (Karnis 1994). In the fiber separation stage, wood chips are broken up into smaller particles, whereas fiber development proceeds via delamination and peeling of the fiber surface. Basically, the outer fiber wall layers, i.e. primary wall (P) and outer secondary wall (S1), are peeled off leaving the inner secondary wall (S2) exposed. The way how the refining process affects the fiber surfaces depends on several factors, e.g. the refining energy input and the possible pretreatment of the wood chips with steam or chemicals prior to refining.

The conventional chemical used in softwood CTMP process is sodium sulfate (Na_2SO_3). In comparison to the TMP process, this chemical improves the purity of the softwood pulp as well as its absorption ability and strength, though the refining energy demand to a certain freeness level is increased by addition of the chemical. Some other chemicals, e.g. buffered sodium oxalate, have been tested mainly in search of suitable processes for TMP production at lower specific energy consumption (Meyer et al. 2004; 2005). Such process applies acidic pH of about 2. On the other hand, very little is known about how the acidic treatment changes the fiber surface morphology.

The morphology of mechanical pulp fiber surfaces can be studied by different microscopy techniques, e.g. with Atomic Force Microscope (AFM) (Börås et al. 1999; Gustafsson 2004; Hanley et al. 1994; Kangas et al. 2004; Koljonen et al. 2003; Shaune et al. 1994; Snell 2001; Stenius et al. 2008; Österberg 2006), with light microscopy or with Scanning Electron Microscopy (SEM) (Braaten 1997; Daniel et al. 2009; Fernando and Daniel 2008; Johnsen et al. 1995; Lidbrandt and Mohlin 1980; Reme et al. 1998). A SEM equipped with a field emission gun (FE-SEM) produces images of fiber surfaces at high magnifications and can be used to study fine surface details (Kangas et al. 2004).

The aim of this work was to collect versatile information about the surface structures of spruce TMP fiber walls and how they were changed by acidic environment. Different microscopy techniques were used to study the fiber surface structures focusing on the differences between the inner and outer fiber wall areas of spruce TMP fibers treated with water and hydrochloric acid.

Materials and sample preparation

Samples

The investigations were carried out on samples from latewood-enriched, i.e. thick-walled, long fibers separated from 1st stage spruce TMP (*Picea abies*). This type of material has the highest sensitivity in responding to the initial defibration process in mechanical pulping. The long fibers were separated from the pulp by Bauer-McNett cascade fractionation. The remaining material over 14 mesh and 28 mesh was mixed. The latewood content of this material was 42 % as measured by microscopy, which is high compared to the normal 15-20 %. Selected properties of these long fibers are given in Table 1.

Table 1. Average properties of the fibers in the long fiber fraction before chemical treatment

	Long fibers
Freeness, mL	760
Length-weighted fiber length, mm	2.12
DDJ-fines content, % [1]	1.7
Fiber wall thickness, μm	5.21
Fiber width, μm	35.48
Cell-wall index CWI [2]	0.294

1) *Fines proportion of a pulp sample, separated by Dynamic Drainage Jar (DDJ) using a 81 μm mesh screen*
2) *Cell wall index is calculated as the ratio of double fiber wall thickness and fiber width (see also Heinemann and Ander 2011)*

Adjusting of pH levels

The long fibers were treated with hydrochloric acid (AC) to get a pH of approx. 2.5. Reference treatment (REF) was performed with deionized water at pH 6. The conditions for all treatments are given in Table 2. In all cases, fiber consistency was 2 % and the treatment temperature 130°C. All mechanical treatments, such as mixing and stirring, were the same for all trials.

Table 2. Fiber treatment conditions

Sample name	**Treatment**	**Amount of chemical on oven-dry fiber (mmol/g)**	**Initial pH**	**Treatment time (min)**	**Total contact time (min)**
REF	Water		6.0	15	53
AC	HCl	1.14	2.5	15	51

Preparation of single fibers for analysis

A special single fiber analysis procedure for inspection with different microscopy techniques was developed. This enabled the imaging of one and the same fiber with all microscopy methods. Moist fibers with visible bands of intact outer fiber wall were selected under the light microscope. The fibers were placed as parallel as possible onto a round glass plate of 15 mm diameter. The ends of the fibers were fixed with water-proof tape, and the glass plate was then

brought to an object slide fixed with a drop of water-glycerin. Finally, a drop of water was set onto the fibers, and they were covered with cover slide and brought to cool and dark storage room.

For AFM measurements, dry fibers are preferred. The fibers fixed on the glass plates and covered with standard cover glass were permitted to dry gently in the storage room. Before AFM imaging, the cover glass was carefully removed. By this procedure, minor changes in the surface structure cannot be avoided, and some shrinking was observed. These minor changes are assumed not to affect the comparison of the samples, since the same preparation procedure was applied on all the samples.

After AFM measurement, the same glass plates with fibers fixed on them were studied by FE-SEM. The glass plates were mounted to the samples holders, and the fibers were sputtered directly on the glass support.

Methods

Light microscopy

Each single unstained fiber was first inspected at light microscope applying bright field, polarization, surface scatter and combinations of these optical techniques. These illumination modes provide possibilities to visualize distinctive parts of the fiber wall – bands of intact outer fiber wall, and exposed areas of inner fiber wall. Additionally, selected fibers were stained with Rhodamine Red and Toluidine Blue to further improve the visibility of morphologically different fiber wall areas.

Images were taken from all inspected single fibers. The positions of the different fiber wall parts were marked to localize them again when analyzing the fibers by AFM and FE-SEM.

Atomic Force Microscope (AFM)

The AFM measurements were carried out at ambient conditions with a Nanoscope IIIa (Digital Instruments Veeco Meterology Group, Santa Barbara, CA) instrument. The microscope was placed on an active vibration isolation table (MOD-1, JAS Scientific Instruments), which was itself placed on a massive stone table to eliminate external vibration noise. All images were obtained with a J-scanner in tapping mode and using silicon cantilevers (NSC15/NoAl, μmasch TM) with a radius of curvature of the tips less than 10 nm. The free vibration amplitude of the cantilever was 80 ± 5 nm, and a damping ratio (tapping amplitude/free amplitude) within 0.60-0.75 was used for imaging. Topographical and phase images were recorded simultaneously using a scan speed of 0.8-1 Hz with a pixel resolution of 512 x 512. Mean values and deviations of roughness parameters were calculated from about 8 sample spots sized 3 x 3 μm each.

RMS (Root Mean Square) roughness, kurtosis and skewness were found to be the most suitable roughness parameters for characterization of surface differences between the outer and the inner fiber wall areas.

RMS roughness S_q is defined as the standard deviation of height within the sampling area:

$$S_q = \sqrt{\frac{1}{MN} \sum_{k=0}^{M-1} \sum_{l=0}^{N-1} \left[z(x_k, y_l) - \mu \right]^2} \qquad (1)$$

Where μ is the mean height:

$$\mu = \frac{1}{MN} \sum_{k=0}^{M-1} \sum_{l=0}^{N-1} z(x_k, y_l) \tag{2}$$

These equations are valid for an M x N rectangular sampling area with lateral directions x and y and vertical direction z (Image Metrology 2007).

Kurtosis S_{ku} is a measure of the peakedness or sharpness of the surface topography, and it is defined as:

$$S_{ku} = \frac{1}{MNS_q^4} \sum_{k=0}^{M-1} \sum_{l=0}^{N-1} [z(x_k, y_l) - \mu]^4 \tag{3}$$

S_{ku} equals 3.0 for a Gaussian-like surface. Values smaller than 3.0 indicate a broad (heterogeneous) height distribution, whereas values larger than 3.0 refer to a surface with height distribution narrower than that of a Gaussian surface (Stout 2000, Image Metrology 2007).

Skewness S_{sk} describes the asymmetry of the height distribution histogram, and is defined as:

$$S_{sk} = \sum_{k=0}^{M-1} \sum_{l=0}^{N-1} [z(x_k, y_l) - \mu]^3 \tag{4}$$

If S_{sk} is 0, a symmetric Gaussian like height distribution is indicated. $S_{sk} > 0$ indicates a flat surface with peaks and $S_{sk} < 0$ refers to a surface dominated with valleys. Values numerically greater than 1.0 may indicate extreme valleys or peaks on the surface (Image Metrology 2007).

Field Emission Scanning Electron Microscope (FE-SEM)

The morphology of pulp fibers was imaged using a Field Emission Scanning Electron Microscope (FE-SEM, Jeol JSM 6335F). A low acceleration voltage (1 kV) was used. Fibers were sputter-coated with a thin layer of Au-Pd. The same areas as already studied with the light microscope and measured by AFM were localized in FE-SEM.

Results and Discussion

TMP fiber wall surface structures studied by light microscopy

The appearance of the studied TMP fibers is illustrated in Figure 1. Different parts of the fiber walls can be easily recognized, i.e. areas of intact outer fiber wall, which appear as bands around the fiber without longitudinal slits, and exposed inner fiber wall areas, which are seen as swollen areas by light microscopy. The dimensions of the outer wall bands and their distribution along the fiber axis depend on TMP process conditions and are connected to fiber flexibility and eventually to paper properties (Vehniäinen 2008; Heinemann 2008).
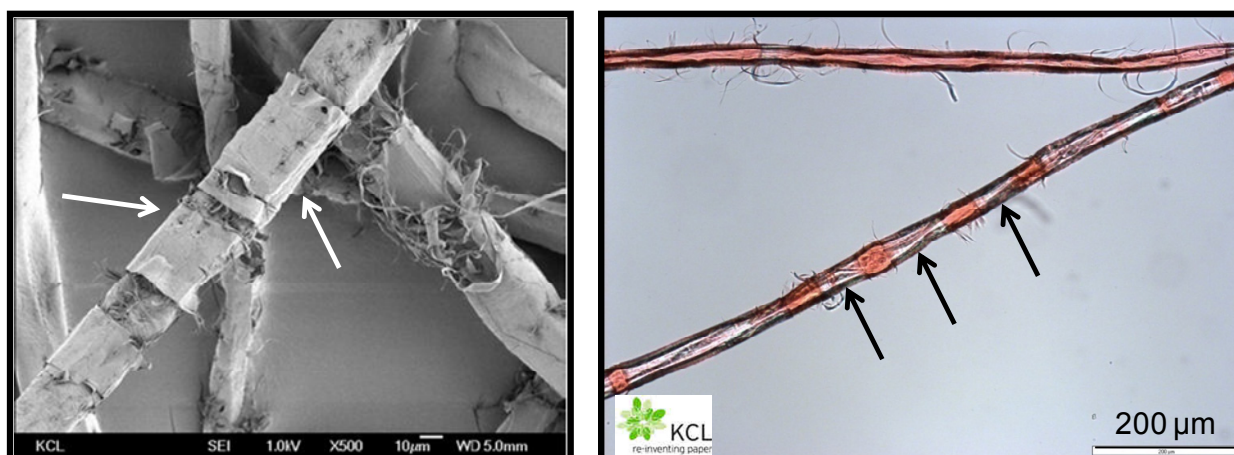
Figure 1. Surface structures of TMP fiber walls – intact outer (marked with arrows) and developed inner fiber wall areas as imaged by SEM and light microscopy (photo: KCL (today VTT))

Figure 2 shows how the different surface structures become visible at light microscopy when various illumination modes and optical staining methods are used. It is possible to recognize morphological differences between intact outer fiber wall and exposed inner fiber wall using only bright field illumination with transmitted light (1). The optical contrast can be improved by polarized light (2), by circular modified polarized light (3) and by more unconventional illumination mode with surface-scattered light (4). Staining of the fiber with suitable stains and observation in transmitted light (5 and 6) was a further step to improve the optical contrast between the outer and the inner fiber wall areas. As seen from Figure 2, there was a clear distinction between the intact outer fiber wall (P/S_1 wall) areas and the exposed inner fiber wall (S_2) area in all applied light microscopy procedures. The most suitable stains were Rhodamine Red (5) and Direct Red. In this work, Rhodamine Red (5) was mainly used.

1 – normal transmitted light
2 – polarized light
3 – modified polarized light
4 - surface light
5 – normal transmitted light (Rhodamine)
6 – normal transmitted light (Rhodamine/Toluidine Blue)
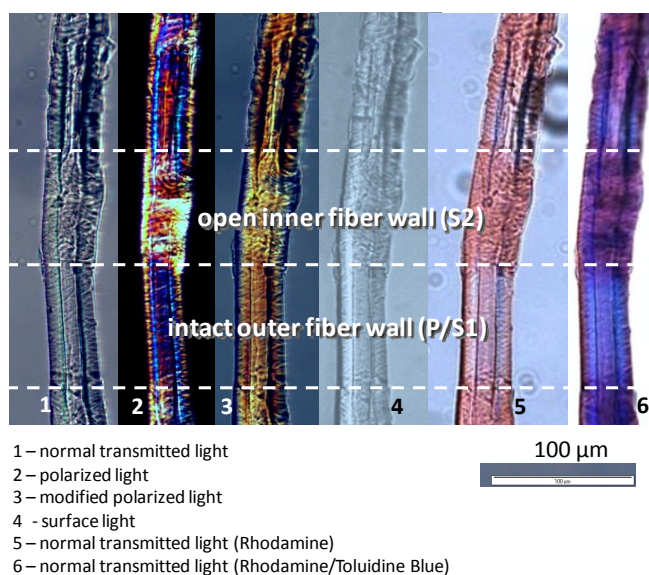
Figure 2. Intact outer fiber wall areas and exposed inner fiber wall area along fiber length axis revealed by different light microscopy techniques

TMP fiber wall surface structures studied by AFM

The same single fibers that were studied with the light microscope were further investigated by AFM and FE-SEM. AFM topographical and phase images were measured from different areas (i.e. inner and outer layers) of the fiber surfaces.

Figure 3 shows a representative topographic image and the corresponding phase contrast image from the inner wall of a fiber treated with hydrochloric acid. The topographical image resolves not only main bundles, but also individual microfibrils and the roughness of the surface structure. The diameter of the microfibrils is 10-30 nm which is in very good agreement with literature values (Kollmann et al. 1968).

The phase image, in addition, reveals more details of the fiber fine structure because the contrast is proportional to the viscoelastic interactions between the surface and the oscillating tip. The marked area in Figure 3 represents a relatively even and smooth area and therefore, by topography, a visually homogeneous part of the regarded surface. The phase image of the same marked area, however, reveals that the surface in fact is heterogeneous. This is indicated by the locally varying phase contrast arising from such locally different viscoelastic properties, i.e. different material components appear on the surface. The softer the material the darker the color in the images. In comparison with the reference fiber (not shown here), besides microfibrils, additional granular components (the darker area in the image) are visible in the phase image of the hydrochloric acid treated fiber. In other words, the hydrochloric acid treatment resulted in a morphological change of the TMP fiber surface caused by some granular, softer material.
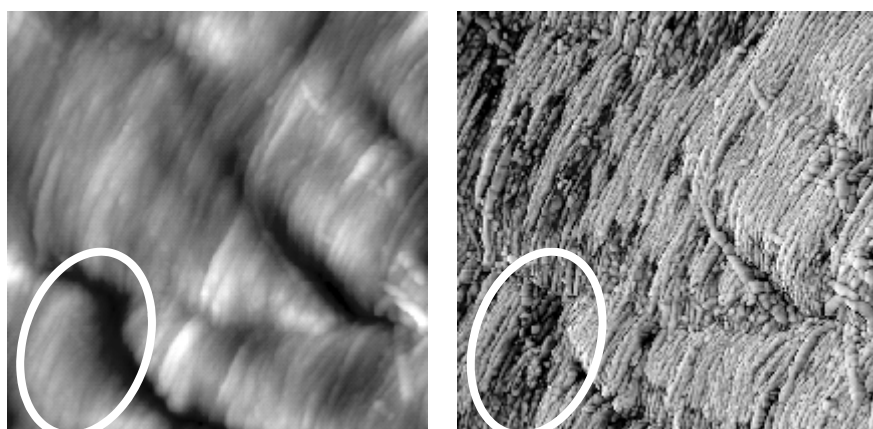
Figure 3. AFM topography (left) and phase (right) images of a spruce TMP long fiber treated with hydrochloric acid. The images are 3 μm x 3 μm

In order to evaluate structural features and differences in the differently treated fibers, phase contrast images of fiber surfaces were used. A collection of them is shown in Figure 4. The topographical images (not shown here) were used for roughness analysis. The fibril angles were estimated from the AFM phase images of fibers that were always positioned vertically before starting the AFM measurement. The estimated fibril angles assured that distinctive outer and inner fiber wall areas from the studied fibers were evaluated. The fibril angle, RMS roughness (S_q), kurtosis (S_{ku}) and skewness (S_{sk}) values are given in Figure 4 for the shown images.

Although the fibril angles were only estimated from the AFM phase images, a clear difference in fibril angle values was found between the inner and the outer fiber walls (Figure 4). This result probably explains the formation of the band-like outer fiber wall parts (Figure 1) in the refining process.

a) REF samples
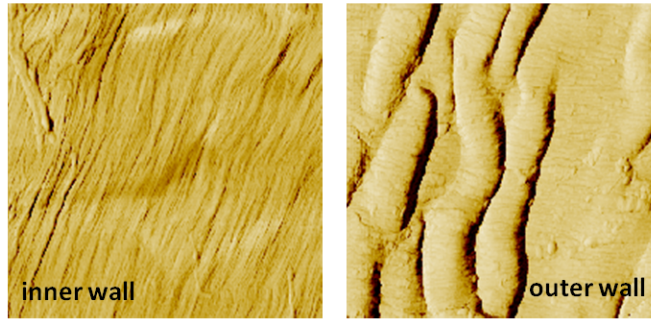
Fibril angle, °	20	78
S_q, nm	14.2	45.7
S_{ku}	4.49	2.80
S_{sk}	0.26	-0.18

b) AC samples
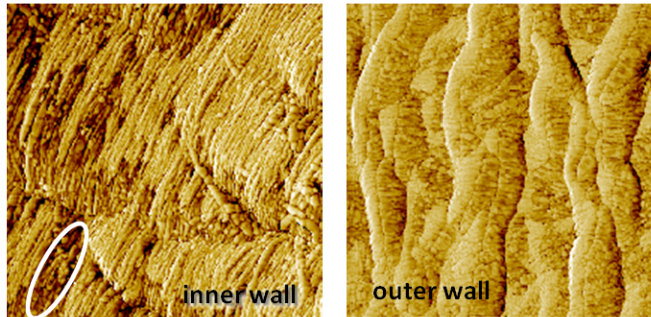
Fibril angle, °	25	89
S_q, nm	23.6	47.0
S_{ku}	4.38	2.06
S_{sk}	-0.78	0.07

⭕ area of "phase contrast"

Figure 4. AFM phase images, fibril angle and surface roughness parameters of reference fiber (REF), and fiber treated with hydrochloric acid (AC). The images are 3 μm x 3 μm

The inner and outer fiber walls of the reference pulp (REF) can clearly be distinguished due to their different visual appearance and characteristic roughness parameter values (Figure 4a). For fibers treated with hydrochloric acid (AC), granular structures were observed in the phase image (Figure 4b) of the inner walls in addition to the fibrilar structure. Furthermore, the dark-light local contrast differences in the phase contrast image refer to inhomogeneities in the viscoelastic properties of the inner wall. This kind of heterogeneity is concluded to be caused by the AC-treatment, because corresponding heterogeneity is not visible in the reference sample REF (Figure 4a). In addition, the hydrochloric acid treatment seemed to have resulted in formation of patch-like structures on the surface of the outer wall.

The mean RMS roughness values (S_q), calculated as an average from all measurements of each type of wall area, and their corresponding standard deviations are given in Figure 5a. No significant difference in roughness of the inner walls was found between the different pH levels. Independent of the chemical treatment, the outer fiber wall surfaces were clearly rougher than the inner fiber wall surfaces. Practically no difference could be observed between the samples treated with hydrochloric acid (AC) and water (REF).
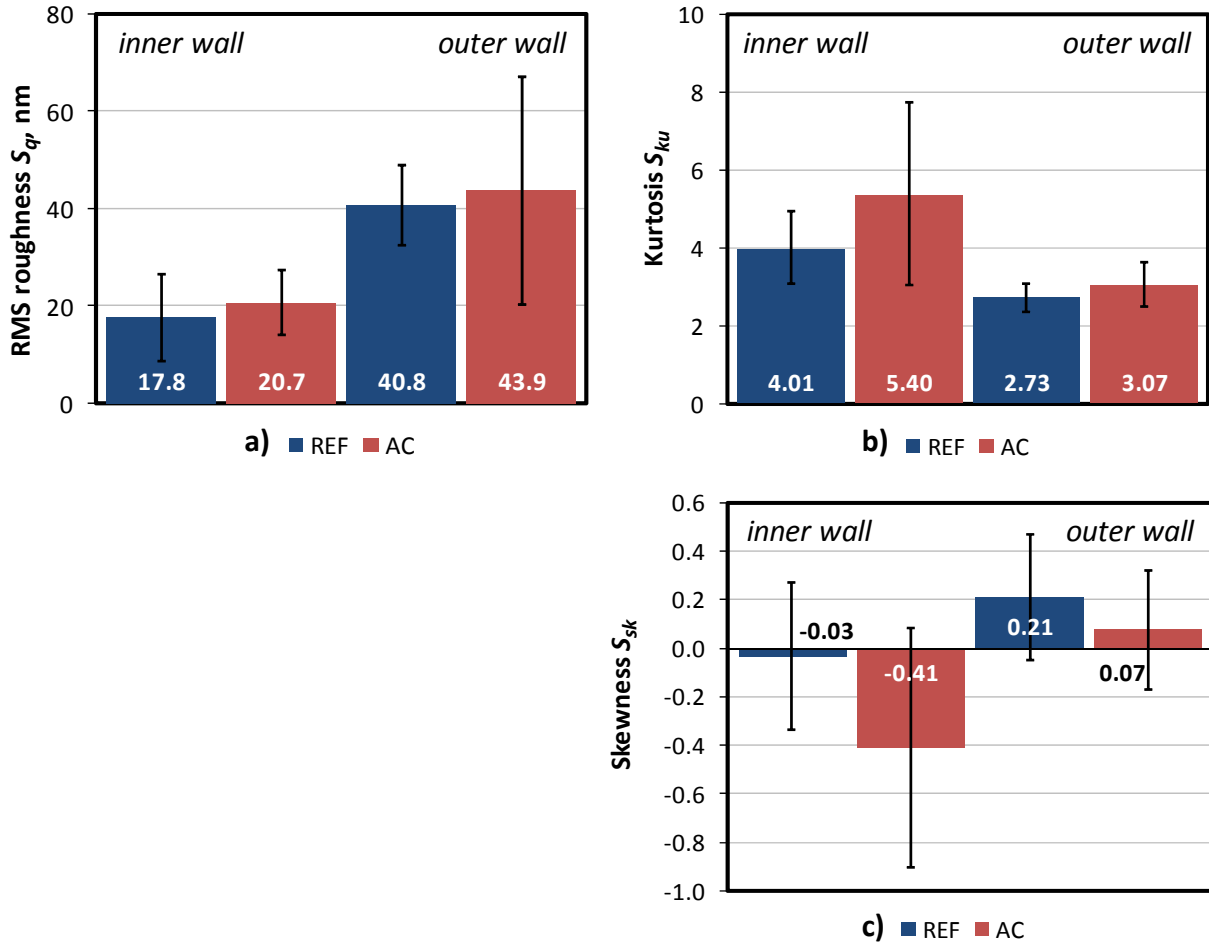
Figure 5. RMS roughness (a), Kurtosis S_{ku} (b), and Skewness S_{sk} (c) of inner and outer fiber wall areas (for averages, 9 images, varying from 4 to 12 were evaluated)

The results of the height distribution analysis (roughness parameter kurtosis, S_{ku}) are shown in Figure 5b. In each sample type, the value of this parameter was larger for the inner fiber wall areas than for the outer fiber wall areas. The inner walls of the acid-treated sample (AC) showed clearly higher kurtosis indicating that this treatment caused a larger change in the surface peak distribution of the inner wall areas. The AC-treated samples also showed a substantial difference in kurtosis between the inner and the outer fiber wall areas. The kurtosis values of the outer fiber wall parts were quite close to 3, i.e. for these parts of the fiber surfaces Gaussian distribution was the most representative. The results suggest that no visible changes were introduced to the surface height distribution of the outer fiber wall areas by changing the pH in the treatment.

Skewness (S_{sk}) was slightly negative for all measured inner fiber wall areas (Figure 5c). This stands for a surface dominated by valleys (surface pores). This is distinctive especially for the acid-treated fibers (AC) indicating that this treatment created most surface pores in the inner wall areas. The outer fiber walls had skewness values close to zero or slightly positive which

means that the surfaces were less porous than the surfaces of inner fiber wall areas, especially in the reference sample (REF).

RMS roughness of each analyzed area was plotted in relation to the corresponding fibril angle (Figure 6). The roughness values of the inner fiber wall parts scatter clearly less than those of the outer fiber wall parts as already seen in the average values in Figure 5a. Although the fibril angles were only estimated from the AFM phase images with the fibers carefully positioned before analysis, a clear classification between the inner and the outer fiber walls was found. This result probably explains the formation of the band-like outer fiber wall parts in the refining process – fiber wall layers with high fibril angles have a lower resistance against peeling perpendicular to the fiber length axis.
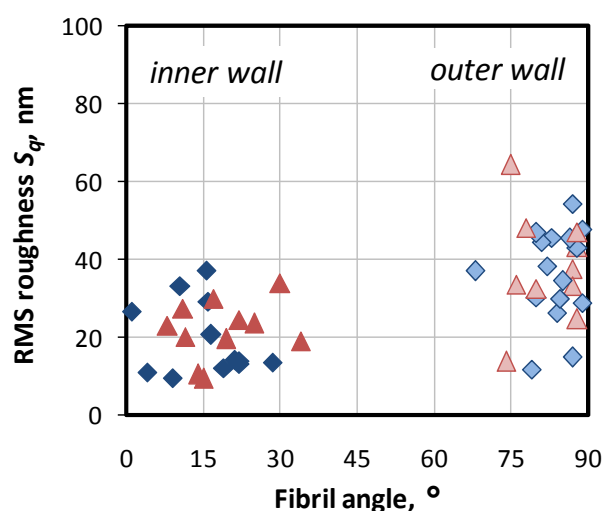
Figure 6. Distinction of inner and outer fiber wall roughness by fibril angle

TMP fiber wall surface structures studied by FE-SEM

The same single fibers, which were measured by AFM, were also studied by FE-SEM to compare the information obtained with these two analysis techniques.

FE-SEM confirmed the relatively smooth surface of the inner fiber wall of the reference fibers (REF, Figure 7) as already was seen by AFM (Figures 4 and 5). Also the fibers treated with hydrochloric acid (AC) were found by FE-SEM to have similar structures (Figure 8) as found by AFM.

Obviously, the high resolution of FE-SEM gives high-quality information comparable to AFM in visual characterization of fiber surface structures. The strength of AFM lies in additional possibilities to measure surface roughness and other surface structural characteristics.
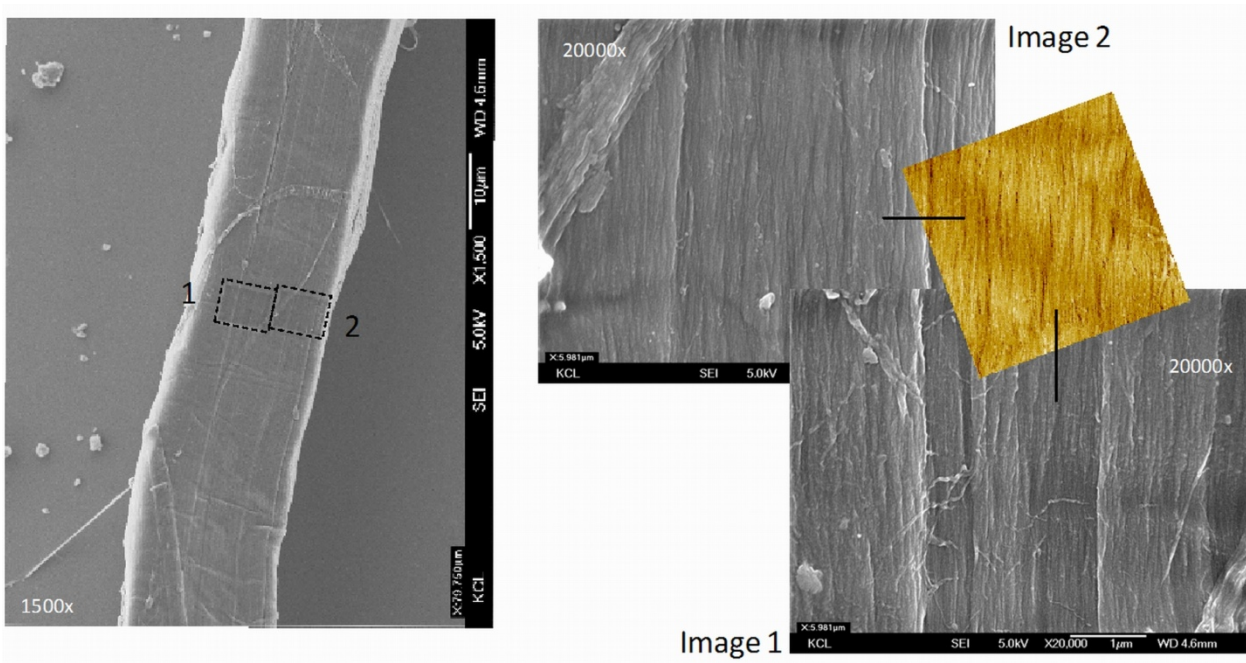
Figure 7. FE-SEM images of inner fiber wall surface – reference sample (REF) – Insert: AFM image of comparable fiber wall structure with corresponding size (not from exactly the same position of the fiber wall)
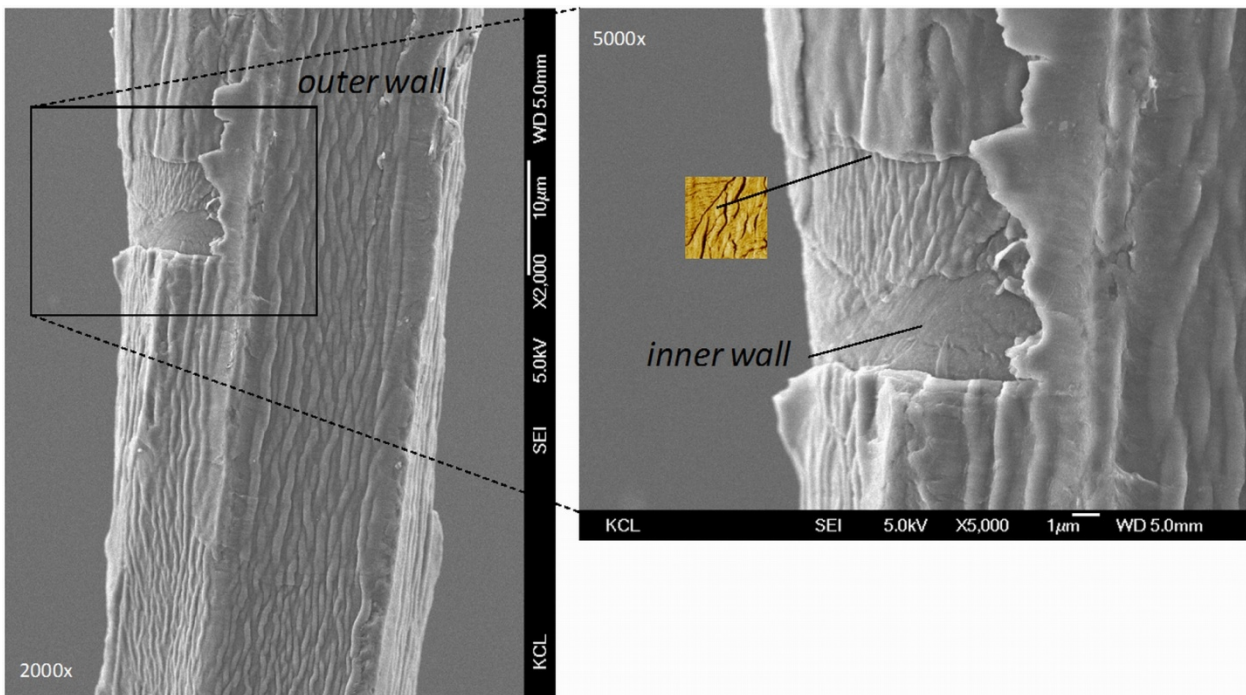
Figure 8. FE-SEM images of outer and inner fiber wall areas of samples treated with hydrochloric acid (AC) – Insert: AFM image of comparable fiber wall structure with corresponding size (not from exactly the same position of the fiber wall)

Conclusions

Light microscopy, AFM and FE-SEM are very suitable tools to characterize fiber wall surface structures. Single fiber examination with a combination of these techniques provided deeper insight into fiber wall surface structure. Distinction between the outer and the exposed inner fiber wall areas in TMP refined fibers can easily be done by light microscopy in transmitted light on fibers stained with Direct Red or Rhodamine Red. AFM measurements deliver roughness data of the outer and inner fiber wall areas and FE-SEM can be used to illustrate the locations in macro scale of the structures which can be measured in micro and nano scale by AFM.

Using AFM, the surface structures of the inner and outer fiber wall areas were clearly distinguishable based on their fibril angle and RMS roughness measures. The reminants of the outer fiber wall areas in all studied samples were found rougher than the exposed inner fiber wall areas. The hydrochloric acid treatment modified the fine structure of the inner wall surfaces and revealed the appearance of a granular and viscoelastic heterogeneous structure.

References

Braaten K.R. (1997): The impact of fiber geometry, fiber splitting and fibrillation on light scattering. 1997 Int. Mech. Pulp. Conf. (IMPC), Stockholm, June 9-13, 349-353

Börås L. and Gatenholm P. (1999): Surface composition and morphology of CTMP fibers. Holzforschung, (53): 188-194

Daniel G., Bardage S., Fernando D., Hafrén J. and Ander P. (2009): Energy consumption in refining of Scots pine and Norway spruce TMP is governed by fibre morphology and ultrastructure. Int. Mech. Pulp. Conf., Sundsvall, Sweden. May 31-June 4, 2009. SPCI and Mid Sweden University, p. 82-86

Fernando D. and Daniel G. (2008): Exploring pine fibre development mechanisms during TMP processing; Impact of cell wall ultrastructure (morphological and topochemical) on negative behaviour. Holzforschung 62(5): 597-607

Gustafsson J. (2004): Surface characterization of chemical and mechanical pulp fibres by AFM and XPS. Doctoral thesis, Åbo Akademi University, Turku, Finland

Hanley S.J. and Gray, D.G. (1994): Atomic force microscope images of black spruce wood sections and pulp fibres. Holzforschung (48): 29-34

Heinemann S. (2008): Quantitative description of the TMP fiber wall. Wochenbl. Papierfab. 136(11-12): 658-665

Image Metrology, The Scanning Probe Image Processor, SPIPTM, User's and Reference Guide Version 4.4, 2007, Copenhagen

James P.J., Antognozzi M., Tamayo J., McMaster T.J., Newton J.M. and Miles, M.J. (2001): Interpretation of contrast in tapping mode AFM and shear force microscopy. A study of Nafion. Langmuir. (17): 349-360

Johnsen P.O., Skinnarland I., Helle T. and Houen P.J. (1995): Distribution of lignin and other materials on particle surfaces in mechanical pulps. 1995 Int. Mech. Pulp. Conf. (IMPC), Ottawa, Canada, 93-107

Kangas H., Pöhler T., Heikkurinen A. and Kleen M. (2004): Development of the mechanical fibre surface as a function of refining energy. J. Pulp Paper Sci. 30(11): 298-306

Kangas H. and Kleen M. (2004): Surface chemical and morphological properties of mechanical pulp fines. Nordic Pulp Paper Res. J. 19(2): 191-199

Karnis A. (1994): The mechanism of fibre development in mechanical pulping. J. Pulp Paper Sci. 20(10): J280-J288

Koljonen K., Österberg M., Johansson L.-S. and Stenius P. (2003): Surface chemistry and morphology of different mechanical pulps determined by ESCA and AFM. Colloids and Surfaces A: Physicochem. Eng. Aspects (228): 143-158

Kollmann F.F.P. and Côté W.A. (1968): Principles of wood science and technology: I. Solid Wood. Springer-Verlag, Berlin

Lidbrandt O. and Mohlin U.-B. (1980): Changes in fiber structure due to refining as revealed by SEM. IPC Int. Symp. Fundamental Concepts of Refining, Appleton, USA, 61-74

Meyer V., Ruel K., Petit-Conil M., Valtat G. and Kurek B. (2004): Modification of the cell wall structure by oxalate associated with energy savings during mechanical pulping. 9th Int. Conf. Biotechnol. Pulp Paper Ind., Durban, South Africa, 10 – 14 October 2004, pp. 95–96

Meyer V., Ruel K., Kurek B. and Petit-Conil M. (2005): Oxalate pretreatment of poplar and spruce chips before mechanical pulping: Energy savings related to biochemical and ultrastructural modifications. 2005 Int. Mech. Pulping Conf., Oslo, Norway, 7 – 9 June 2005, pp. 102–106

Reme P.A., Helle, T. and Johnsen P.O. (1998): Fibre characteristics of some mechanical pulp grades. Nordic Pulp Paper Res. J. 13(4): 263-268

Snell R., Groom L.H. and Rials T.G. (2001): Characterizing the surface roughness of thermomechanical pulp fibers with atomic force microscopy. Holzforschung 55: 511-520

Stenius P. and Koljonen K. (2008): Surface characterization of mechanical pulp fibers by contact angle measurement, polyelectrolyte adsorption, XPS and AFM. Characterization of Lignocellulosic Materials. *In:* Hu, T. Q. (*Ed.*), Characterization of Lignocellulosic Materials, Blackwell, Oxford, pp. 36-59

Stout K.J. (2000): Development of Methods for the Characterisation of Roughness in Three Dimensions, Penton Press, London

Vehniäinen A. (2008): Single Fiber Properties ─ A Key to the Characteristic Defibration Patterns from Wood to Paper Fibers. Doctoral thesis, Helsinki University of Technology, Espoo, Finland

Österberg M., Schmidt U. and Jääskeläinen A.S. (2006): Combining confocal Raman spectroscopy and atomic force microscopy to study wood extractives on cellulose surfaces. Colloids and Surfaces A: Physicochem. Eng. Aspects. (291): 197-201

STANDARD PULP AND PAPER TESTS

[1]Sabine Heinemann, [2]Paul Ander

[1]P.O. Box 1000, 02044 VTT (Espoo), Finland

[2]CRUW, Dept. Forest Products/Wood Science, Swedish Univ. of Agricultural Sciences (SLU)
P.O. Box 7008, SE-75007 Uppsala, Sweden

sabine.heinemann@vtt.fi and paul.ander@slu.se

Abstract

Within the COST Action E54 "Characterization of the fine structure and properties of papermaking fibers using new technologies", common pulp samples from a Södra Cell pulp mill were tested applying a variety of standard testing methods but also of new and unique measuring technologies. The data were collected and summarized, providing extended knowledge about the quality of that pulp grade like never before.

Introduction

As announced by the title of the COST Action, new technologies and unique methods should be applied to characterize the fine structure and properties of papermaking fibers. Two common pulp samples were selected and distributed to all participating partners who could provide methods and technologies for fine fiber characterization. To perform all the tests and analyses with one and the same pulp sample from a common chemical pulp production line opened the unique opportunity to collect characteristics and information about this pulp exceeding all experiences so far. The other advantage of these efforts was an improved comparability of the applied methods and technologies.

New and unique technologies are presented within this book in separate articles. This article is to summarize the results from standard measurements. Standard methods in that sense can be typical laboratory testing methods described e.g. in ISO standards, but also some special methods which are introduced and proved but common for certain laboratories only.

Common pulp samples

The common pulp was softwood chemical pulp from spruce (*Picea abies*) and pine (*Pinus sylvestris*), delivered in two sample sets, both from a Södra Cell pulp mill in Sweden.

In the first sample set, the percentage relation spruce:pine was 79:21. The trees for that sample came probably from Southwest Sweden. Pulping was done by batch kraft cooking, the bleaching sequence was Q(complexing agent) OP Q+PAA(peracetic acid) PO. Also unbleached pulp was included into the first sample set. The factory sampling was carried out at the end of May 2007.

The second sample set was similar to the first one. Only bleached pulp of Södra Green 85Z quality was used. The percentage relation spruce:pine was 81:19, and the factory sampling was done at the beginning of June 2008.

Applied methods

All pulp tests start usually with microscopic inspection for morphological characterization. Light microscopy with different illumination modes (e.g. polarization, phase contrast, staining in transmitted light) are the simplest methods and easy to apply. More advanced methods are

Atomic Force Microscopy (AFM) and Electron Microscopy (SEM, ESEM) to get more information about the small-scale structures of the fibers. AFM is also used for fiber surface characterization.

Fiber dimensions are usually determined by automated fiber analyzers. Several commercial devices were applied, such as kajaani FiberLab, kajaani FS300, L&W FiberMaster, L&W FiberTester, MorfiLab and Cyberflex. Within this paper, data from kajaani FiberLab were used.

From the pulp slurries, several drainability parameters were measured (Schopper-Riegler value, Canadian Standard Freeness, Water Retention Value, Fiber Saturation Point, Specific Filtration Resistance, Specific Surface area, and Drainage time Rapid Köthen).

The refining resistance was tested with a laboratory beater (JOKRO mill). Additionally, a pilot scale refiner was used. Handsheets were made for physical testing of strength and optical properties.

Assessment of spruce-pine ratio (SLU, Sweden)

The spruce-pine ratio in the common pulp sample was studied by means of polarized light microscopy. This illumination mode is very useful to visualize the typical window pores in pine earlywood fibers (Figure 1). Additionally, SEM can be applied to characterize fiber cleavage more detailed (Figure 2).
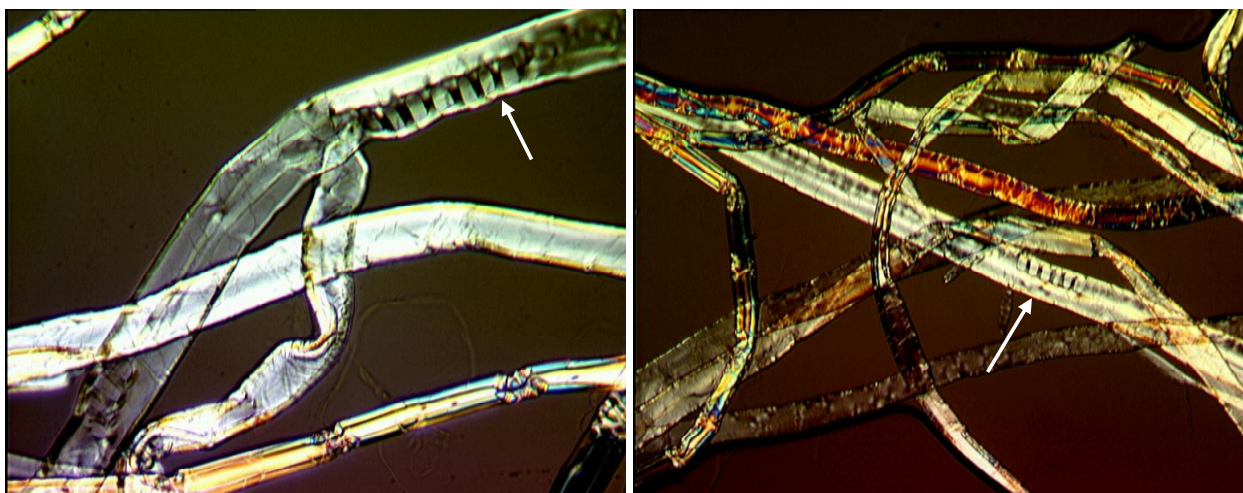
Figure 1. Earlywood fiber from unbleached pulp (left, magnification 20x), and from bleached pulp (right, magnification 10x). Typical window pores in pine fibers marked with white arrow, Polarized light

In the Polarized Light method (PLM), fiber images were inspected, and typical pine earlywood fibers were counted. For example, from 28 counted unbleached earlywood fibers, 8 were recognised as pine fibers, thus giving 29% pine fibers and subsequently 71% spruce fibers in the earlywood. From 48 counted bleached earlywood fibers, 13 were found to be from pine, and the proportion becomes 27% pine fibers and 73% spruce fibers. In another image, when both earlywood and latewood fibers were present (like Figure 1 right), 91 fibers in total were counted, from which 19% were pine earlywood fibers, and subsequently 81% spruce earlywood fibers. The average of all these counted proportions gave 25% pine fibers and 75% spruce fibers in the earlywood. Assuming that the same ratio can also be found from the latewood, one gets 79% spruce fibers and 21% pine fibers in total.
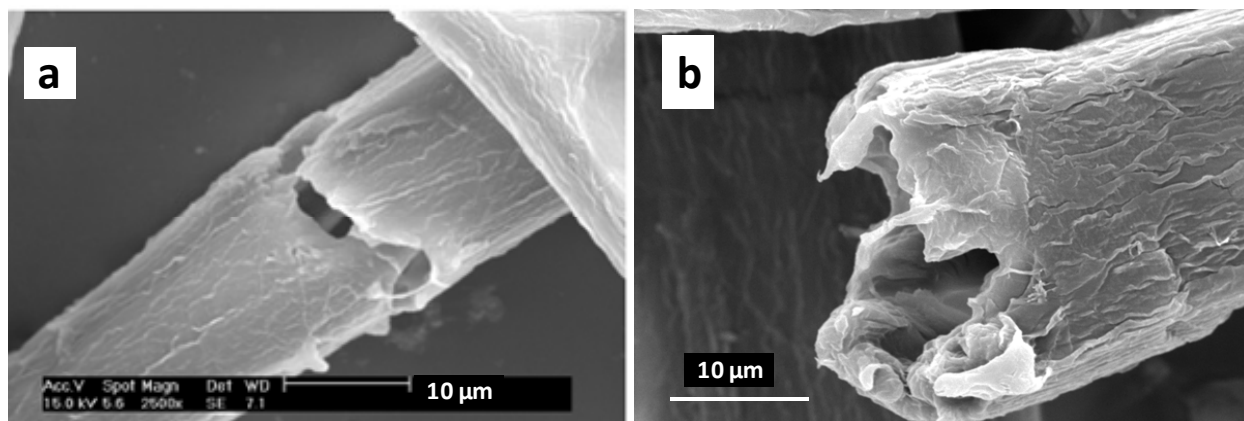
Figure 2. SEM-images of the cleavage of softwood chemical pulp fibres – Further degradation after HCl attack cleaving both the S1 and S2 fiber walls (a), complete cleavage of the fiber, also revealing the cell lumen (see Ander et al. 2008)

This is the spruce-pine ratio calculated for the first common pulp sample (79:21). The ratio in the second sample was 81:19. From an earlier Södra Cell pulp, a ratio spruce:pine of 84:16 was found.

HCl-method for cleavage determination (SLU, Sweden)

A standard method to obtain cleavage per fiber was developed (Ander et al 2005; 2008, Ander and Daniel 2006). The parameter "cleavage per fiber" evaluates dislocations and weak points in the fiber. It is defined as

$$Cleavage\ per\ fiber = \frac{L_0}{L} - 1$$

with L_0 being the length-weighted fiber length in mm for the control in water, and L the length-weighted fiber length in mm for the HCl-treated sample.

Cleavage by HCl shown in the SEM is given in Figure 2 for a softwood kraft pulp (Ander et al. 2008). Cellulases also cleave fibres in dislocations. In addition, cleavage of latewood dislocations by HCl is shown using PLM (Ander et al. 2011).

Procedure

- Never-dried pulp fibers (dry weight 100-250 mg) were swelled for 10-15 minutes in 20 mL water in a 100 mL Erlenmeyer flask and stirred with a 25 mm stirring bar.
- Treatment with 40 mL 1 M HCl pH 0 at 80-82°C for 4h in a reciprocal water bath without using the stirring bar.
- Completion of cleavage with 25 mm stirring bar at 150 rpm for 30 minutes during cooling to near room temperature.
- Fibre washing with 0.2 M phosphate buffer pH 7 on Munktell filters 1002, 1003 or glass filters G2 or G3. Polarized light microscopy can be done directly on the cleaved fibres. For electron microscopy, the fibres must be washed with water to remove the buffer.
- Fiber length analysis with commercial automated fiber analyzer (e.g. FiberMaster or kajaani FiberLab)
- Calculation of the cleavage per fiber from length-weighted fiber lengths

The procedure is illustrated in Figure 3.

Figure 3. Procedure steps of the HCl-method for fiber cleavage: Swelling of fibers in 20 mL water with stirring (above left), shaking fiber in 1M HCl for 4 h at 80-81°C in the water bath - plastic lid closed during treatment (above right), close up of water bath (below left), and cooling down with stirring for 30 min (below right)

Drainability by RAPID-KÖTHEN method - RK number (drainage time)

Drainage time according to RAPID-KÖTHEN – shortly called RK number – is a rather old testing method, which is performed during handsheet forming in Rapid Köthen sheet molds. There is no standard anymore, but it has once been described as a testing method in the collection of Zellcheming Technical Leaflets (1961). The RK number stands for the time, which takes a volume of 6 L of aqueous fiber slurry to drain in the RAPID-KÖTHEN handsheet former from 8 L to 2 L under atmospheric pressure. The initial pulp consistency is 0.03% which corresponds to the concentration for a 75 g/m²-handsheet. The testing device and an idealistic drainage curve are given in Figure 4.
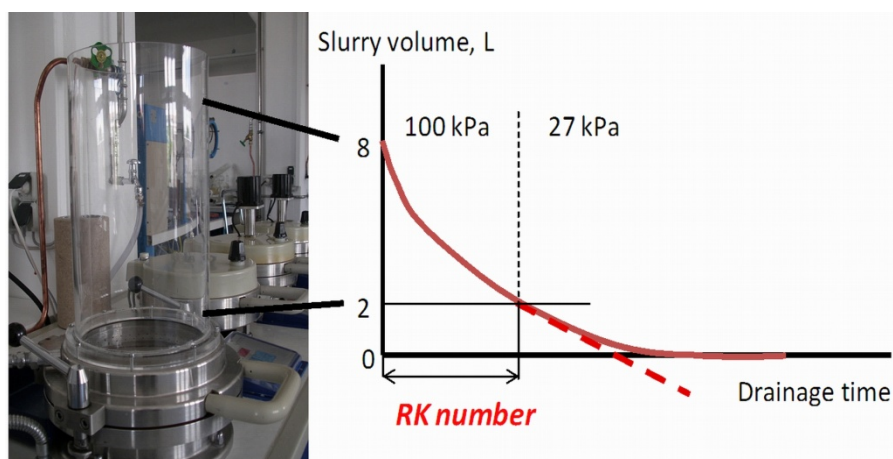
Figure 4. RAPID-KÖTHEN sheet mold – dewatering column (left), and idealistic drainage curve with RK number

Drainage time can also be measured with conventional sheet formers during handsheet forming, but the resulting parameter is different to the RK number due to several procedure deviations (Table 1).

Table 1. Comparison of methods for drainage time assessment

	RK number	**Drainage time**
Method description	Zellcheming Technical Leaflet V/7/61	T221 cm-99 (SCAN-M9:76)
Sheet forming procedure	RAPID KÖTHEN sheet former (ISO 5269-2)	Conventional sheet former (ISO 5269-1)
Procedure point of measurement	Drainage time stopped 2 L above the screen	Drainage stopped when all water has passed through the screen
Applied drainage pressure, kPa	100 (atmosphere)	27 (vacuum)
Applied handsheet grammage, g/m²	75	60

Specific surface area and specific filtration resistance

These parameters also characterize the dewatering behavior of pulps, but they have been used more to describe the bonding ability of the fibers, e.g. to predict static strength properties (tensile index, breaking length). The methods to determine both parameters have been developed rather parallel.

Specific surface area is the result of the permeability method, which was in this sense first published about 60 years ago (Robertson and Mason 1949, Mason 1950), and mainly applied on mechanical pulps (Brecht and Schanz 1957, Forgacs 1963). More details about this parameter "hydrodynamic specific surface area" can be found from elsewhere in this book (Heinemann and Neclaw 2011). The tests in this investigation of the common pulp sample were performed with the Dresden Permeability Tester (Heinemann 1985).

Specific filtration resistance is the result of the filtration method (Ingmanson 1952, Ingmanson and Whitney 1954, Ingmanson and Andrews 1959). A special apparatus for the characterization of mechanical pulp was developed by Mannström (1967, 1972) and was also used for the pulp tests.

There are essential differences between the two methods.

Specific surface area is understood as the surface area of fibers in a compressed water-swollen fiber pad that is accessible for flowing water molecules, and thus, the so called hydrodynamic specific surface area is a function of the flow rate through a fiber pad. Because the flow rate is measured AFTER building-up the fiber pad for different compressions steps, there is no effect of fiber conformability during the measurement. The resulting parameter is given as specific surface area in m²/g.

The filtration method estimates specific surface area from the filtration behavior of fiber slurries based on the principle of cake filtration, which means a complete deposition of the solid material onto the filter medium and building of a filter cake proportionally to the corresponding filtrate volume with the cake structure remaining constant. The resulting specific filtration resistance is thus a function of the flow rate during fiber pad (cake) creation. Because the flow rate is measured DURING building up the fiber pad by defined drainage of a fiber suspension over a wire screen, the effect of fiber conformability cannot be neglected. No constant height of the fiber pad (or filter cake) can be adjusted, therefore the specific filtration resistance is given in m/g.

Dimension-based parameters

All dimension-based parameters reported in this paper were measured with kajaani FiberLab™. Additionally to the basis parameters fiber length, fiber width and fiber wall thickness, further parameters were calculated and discussed.

• *Aspect ratio*

The parameter "Aspect ratio" AR is normally used for non-fibrous particles. Applied to fibers, it is an expression for the "slenderness" of the material. The smaller the value the more thread-like are the particles.

$$AR = \frac{Fiber\ width}{Fiber\ length} = \frac{W}{L_{C,i}}$$

• *Mork's value*

The parameter "Mork's value MV" is not widely known as such. The original idea was to separate earlywood and latewood fibers within a pulp sample and giving proportions of the fiber types (Mork 1928). A fiber with a lumen at least as wide as the double fiber wall thickness CWT was declared to be earlywood. In practical cases, fibers with only marginal differences in lumen size and double fiber wall thickness, which were classified to be earlywood, often behaved like latewood. That is why it is better to use the mean value of all calculated Mork's values of the respective fibers instead of a summarized proportion. Additionally, a deviation of this value can be provided (Heinemann and Vehniäinen 2009).

$$MV = \frac{Fiber\ wall\ thickness}{Lumen} = \frac{2 \times CWT}{(W - 2 \times CWT)}$$

- *Cell wall index CWI*

The cell wall index is something similar like the Mork's value, but it is related to the fiber width instead of fiber lumen.

$$CWI = \frac{Fiber\ wall\ thickness}{Fiber\ width} = \frac{2 \times CWT}{W}$$

- *Cross-sectional area CSA, volume index VI*

The cross-sectional area CSA and the volume index VI are standard parameters delivered from kajaani FiberLab™ in the cross-sectional parameter package. These values consider a fiber to have a circular shaped cross-section.

The cross-sectional area CSA is therefore calculated as annulus from fiber width W and fiber wall thickness CWT. The volume index VI describes then a tube with the cross-section CSA and the central-line length of the respective fiber.

$$CSA = \pi \cdot CWT(W - CWT)$$

$$VI = CSA \cdot L_c$$

External fibrillation

External fibrillation occurs to fibers undergoing mechanical treatments such as refining. Parts of the outer fiber wall are opened or released; the fibrils of the inner fiber wall become accessible and can be separated from their original position in the fiber wall. Figure 5 shows such fibrillated fibers how they appear in the light microscope.
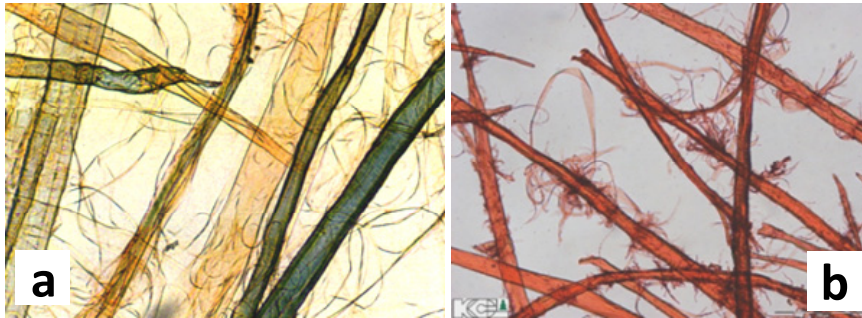
Fibrils released from fiber surface   Fibrils still connected to the fiber surface

Figure 5. External fibrillation of softwood fibers from long fiber fractions. Fibrils released from or slightly attached to the fibers (a), fibrils still strongly attached to the fibers (b) (micrographs: VTT/KCL)

Fibrillation index is a parameter provided by automated fiber analyzer kajaani FiberLab™. It is defined as the ratio between the area of fibrils and the total fiber area in the evaluated image:

$$Fibrillation\ index = \frac{A_{fibril}}{A_{total}} \times 100\%$$

Only fibers with attached fibrils are considered (such as shown in image b of Figure 5). Released fibrils are recorded either as short fibers or as fines depending on their length and visibility (optical contrast).

Assessment of the refining resistance

For the assessment of the refining resistance, the bleached pulp from the second sample set was treated in the JOKRO mill at Dresden University of Technology for 15, 45, and 60 minutes. The resulting pulps were tested in Dresden and at VTT (KCL) in Finland according to the trial plan shown in Figure 6. Some part of the pulp was also refined in the laboratory refiner at PTS Heidenau/Germany.
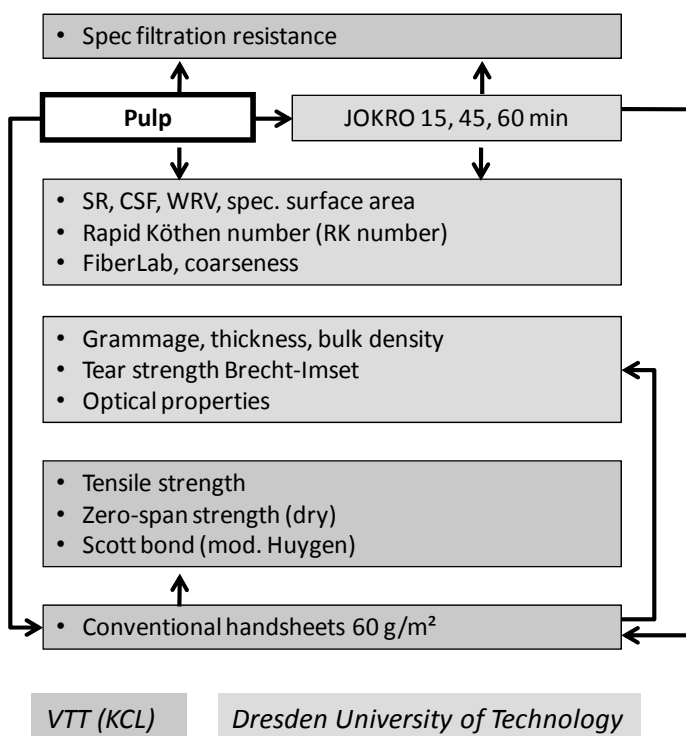
Figure 6. Testing program of refining resistance with laboratory equipment. Blue: Trials performed at VTT(KCL), red: trials performed at Dresden University of Technology

• *JOKRO mill*
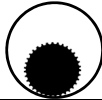
The JOKRO mill is a laboratory device for classifying pulp characterization and quality control. It was developed approx. 80 years ago by Jonas and Kross (Jonas 1933). Several investigations were done with that laboratory apparatus in comparison with former laboratory beaters (Ekstam 1957, Jayme and Buettel 1965, Hechler 1968), but in principle, this laboratory mill has not been changed neither in design nor in working procedure since more than 30 years (Kleinert 1977). It is a standardized machine (DIN 54360) and preferably used in German speaking regions of Europe. Figure 7 shows the JOKRO mill design; Table 2 compares the applied standard beating conditions with those of the PFI mill. The only measurable variable of the JOKRO mill procedure is the treatment time.

The beating is performed at the upper limit of LC refining (6%). The beating pressure is determined by the centrifugal forces given by the rotational speed of the beating roll (2.85 rps), and the beating gap is determined by centrifugal forces <u>and</u> oven-dry sample mass.

Figure 7. JOKRO mill – design

Table 2. Standard design and procedure parameters of the JOKRO mill in comparison with the PFI mill

	JOKRO mill	**PFI mill**
Beating tool in scaled size		
External diameter of the beating roll	89.15 mm	201 mm
Number of bars	35	33
Bar width	2 mm	5 mm
Groove width / groove depth	6 mm / 3 mm	14 mm / 30 mm
Bar length	60 mm	50 mm
Surface oft he container	Knurled 55°	Smooth
Material oft he beating container	Bronze	Stainless steel
Net beating pressure	n.m.	3.33 N/mm
Rotational speed of the beating roll	2.85 rps	24.3 rps
Oven-dry pulp sample per run	6 x 16 g = 96 g	30 g
Water quality[1)	Distilled water, 20°C	Standard water (ISO 14487), 20°C
Initial pulp consistency	6 % (60 g/L)	10 % (100 g/L)

- *PTS Laboratory refiner*

The PTS laboratory refiner belongs to the small-scale pilot machines for simulation purposes. It is shown in Figure 8. Selected parameters applied for the performed pulp treatment are summarized in Table 3. Only one refining point was carried out.
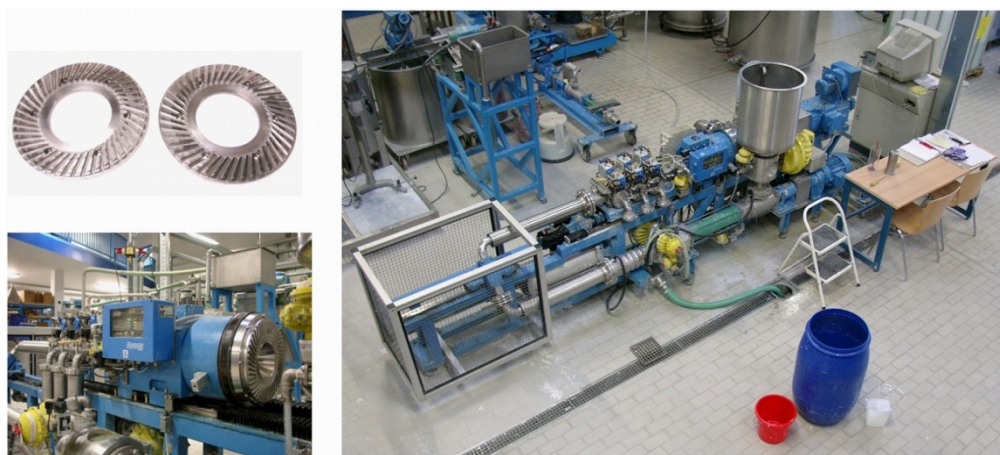
Figure 8. PTS laboratory refiner (courtesy of PTS)

Table 3. Selected parameters applied for the performed pulp treatment in the PTS Refiner

Type	Disc
Consistency	4 %
Specific edge load	2 Ws/m
Cutting length per second	2.85 km/s
Cutting angle	60°
Specific refining energy	150 kWh/t

Results and Discussion

Unrefined samples

- *Microscopic appearance*

Unrefined unbleached fibers were inspected with FIB-SEM technology (Orlandi 2007). Clear differences were seen between moist (above) and dried (below) fibers in Figure 9.

Straight fibers with smooth surfaces are found for the moist pulp. Dislocation regions can be specified (red arrows in Figure 9a).

Free drying forms typically extremely twisted fibers (Figure 9c) with surface shrinkage and closed bordered pits (white arrows in Figure 9d).

- *Results from chemical and physical testing*

The results of pulp testing are summarized for the unbleached and the two bleached samples in Table 4. Table 4a contains the chemical characteristics, drainability data and parameters from automated fiber analysis with kajaani FiberLab. Table 4b collects the results of handsheet testing – parameters of strength and optical properties. The results from carbohydrate analysis are found in Table 4c.
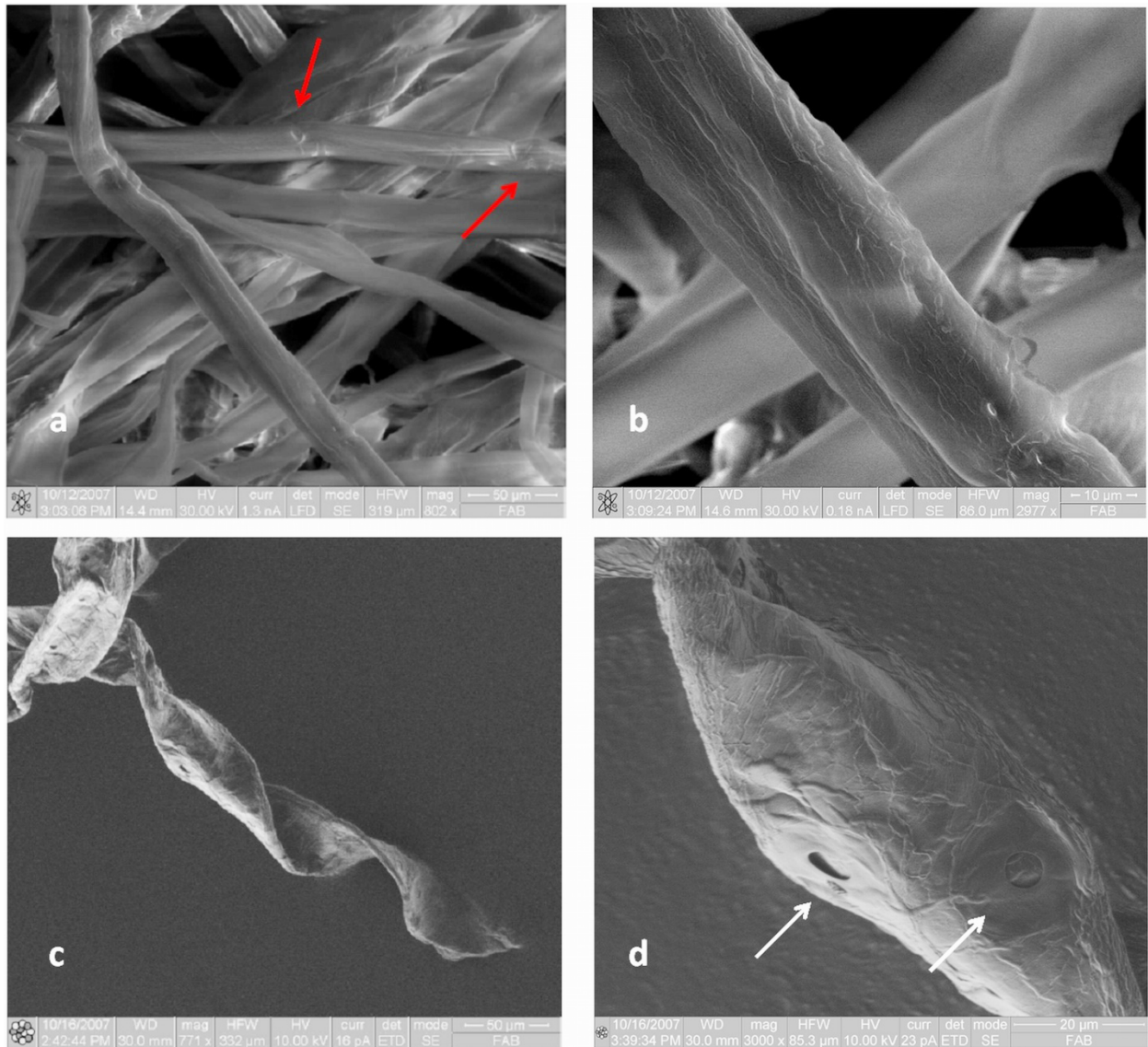
Figure 9. FIB-SEM appearance of the unbleached pulp sample: initial wet (above), and dried (below). Dislocation regions (red arrows), surface shrinkage and closed bordered pits (white arrows) can be specified (see Orlandi 2007)

Table 4a. Characteristics of the unrefined common pulp – chemical and physicochemical parameters, drainability data, and parameters from dimensional measurements with automated fiber analyzer kajaani FiberLab

Sample (set number) Sampling time		Unbleached (1) May 2007	Bleached (1) May 2007	Bleached (2) June 2008
Total charge/Carboxyl groups	meq/kg	81	58	
Surface charge PolyDADMAC	meq/kg	20	24	
Intrinsic viscosity	mL/g	1109	728	
Kappa number		26.8	3.2	
Lignin	%	4.0	---	---
Cleavage/fiber		3.62	6.11	---
SR	units	---	---	12
CSF	mL	730	720	742
Specific filtration resistance	10^8 m/g	---	---	16
Specific surface area	m²/g	1.02	1.16	1.09
Water retention value TUD	g/g	1.35	1.25	0.99
Water retention value VTT	g/g	1.59	1.43	1.16
Fiber saturation point FSP	g/g	1.25	1.18	---
Drainage time RK	s	---	---	2.0
Arithmetic central-line fiber length (FiberLab)	μm	1200	1150	1100
Length-w. central-line fiber length L_C (FiberLab)	μm	2460	2370	2370
Fiber width W (FiberLab)	μm	29.3	27.8	26.64
Fiber wall thickness CWT (FiberLab)	μm	8.2	7.9	8.18
Aspect ratio (FiberLab)		40.96	41.37	41.291
Mork's value (FiberLab)		---	---	1.593
CSA (FiberLab)	μm²	---	---	91.52
Fiber wall index CWI (FiberLab)		---	---	0.614
BMcNett R16	%	48.3	43.8	---
BMcNett R30	%	36.1	38.6	---
BMcNett R50	%	9.9	10.6	---
BMcNett R100	%	3.7	4.1	---
BMcNett D100	%	2	2.9	---
Fines (FiberLab)	%	---	---	33.37
Length-w. fines (FiberLab)	%	2.6	2.7	3.12
Volume index VI (FiberLab)	10^3 μm³	---	---	96.2
Coarseness	μg/m	---	---	237
Curl index (FiberLab)	%	15.1	20.2	21.6
Fibrillation index (FiberLab)	%	---	---	3.253

Table 4b. Characteristics of the unrefined common pulp – parameters of strength and optical properties, measured from laboratory handsheets

Sample (set number) Sampling time		Unbleached (1) May 2007	Bleached (1) May 2007	Bleached (2) June 2008
Apparent bulk density	kg/m³	528	559	455
Bulk (stack)	cm³/g	1.9	1.79	2.20
Tensile index	Nm/g	29.8	27.5	15.9
Stretch	%	2.1	3.4	2.4
Tensile energy absorption index (TEA index)	J/g	0.479	0.748	0.296
Tensile stiffness index	kNm/g	4.59	3.81	2.48
Modulus of elasticity	N/mm²	2420	2129	1128
Breaking length	km	3.04	2.81	1.62
Tear-Index (Elmendorf)	mNm²/g	20.2	20.3	---
Tear-Index (Brecht-Imset)	mNm²/g	---	---	17.08
Internal bond mod. Huygen	J/m²	100	132	77
Zero-span tensile index wet	Nm/g	135	101	123
Brightness R_{457}	%	---	---	85.86
Opacity	%	---	---	74.42
Transparency	%	---	---	30.60
Light-scattering coeff.	m²/kg	---	---	33.41
Light-absorption coeff.	m²/kg	---	---	0.11
CIELab L*		---	---	96.95
CIELab a* (green)		---	---	-0.62
CIELab b* (yellow)		---	---	4.86

Table 4c. Characteristics of the unrefined common pulps – Results from carbohydrate analysis, done by Stora Enso, Karlstad, Sweden

Sample (set number) Sampling time		Unbleached (1) May 2007	Bleached (1) May 2007	Bleached (2) June 2008
Arabinose	%	0.7	0.6	0.6
Galactose	%	0.4	0.2	0.2
Glucose	%	84.0	85.1	85.2
Xylose	%	7.9	7.5	7.3
Mannose	%	7.0	6.6	6.7
Arabinose anhydro	mass-%	0.6	0.6	0.6
Galactose anhydro	mass-%	0.4	0.2	0.2
Glucose anhydro	mass-%	78.8	83.7	83.8
Xylose anhydro	mass-%	7.3	7.2	7.0
Mannose anhydro	mass-%	6.6	6.5	6.5
Total carbohydrates anhydro	mass-%	93.6	98.1	98.2
Klason lignin	%	3.9	0.2	0.1
Acid soluble lignin (205 nm)	mass-%	0.5	0.5	0.6

Refined samples

Microscopic characterization
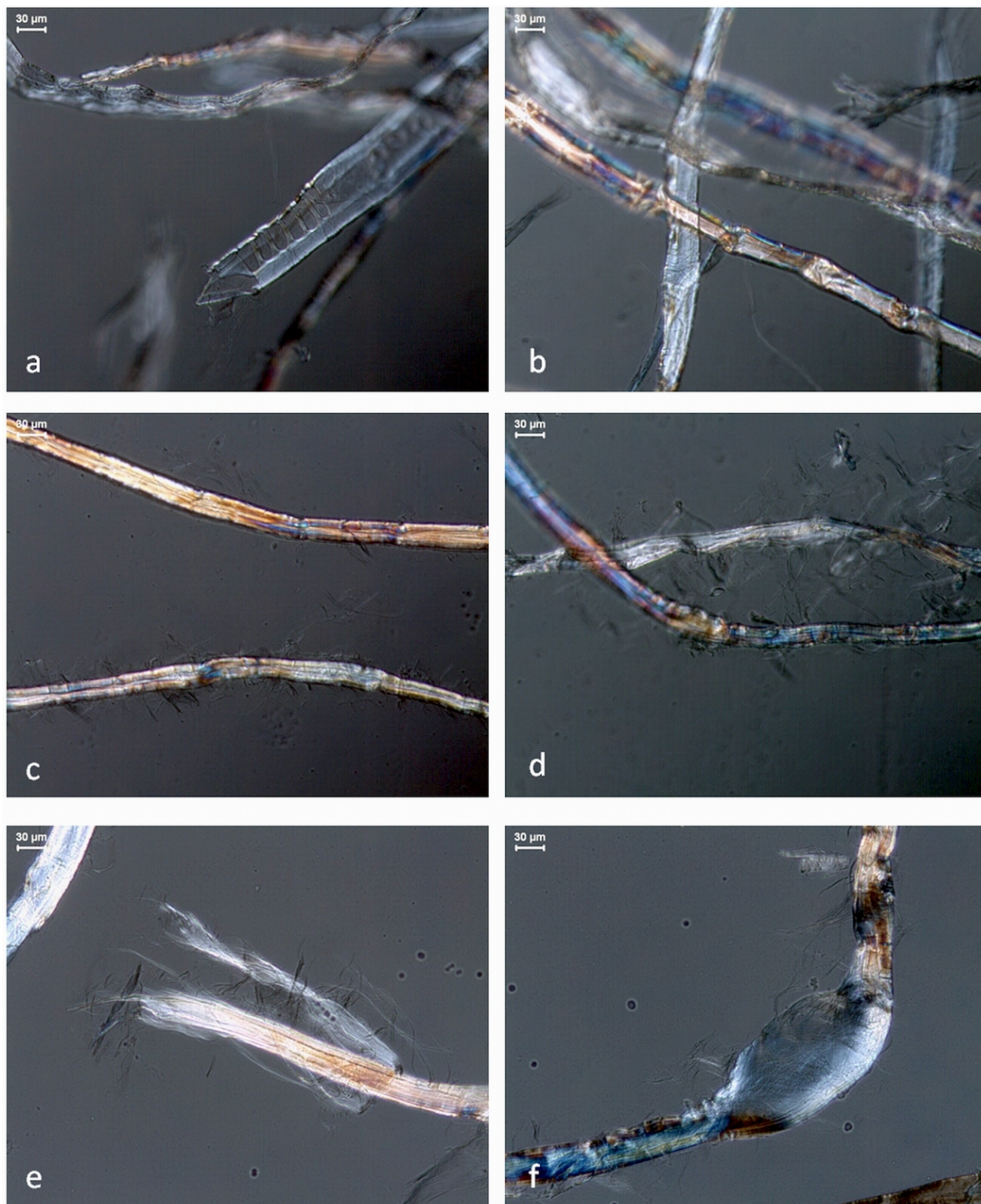
Figure 10. Microscopic appearance of pulp fibers in modified polarized light. a) cut earlywood pine fiber in the unrefined sample, b) smooth and untouched fiber surface in the unrefined sample, c) outer fibrillation starts slightly after 15 min JOKRO mill beating, d) more external fibrillation after 45 min JOKRO mill beating, e) strong peeling effects after 60 min JOKRO mill beating, f) strong internal fibrillation after 60 min JOKRO mill, fiber structure disappears partly

Figure 10 shows special features seen in the light microscope developed with the refining treatment. Modified polarized light was used to improve the visibility of details (position of polarization filters less than 90° and λ¼-filter).

Already in the unbeaten pulp, non-intact fibers were found to a certain extend. This could be caused by mechanical impact from disintegration which might affect the fibers in their weakest points (Figure 10a). But the greater part of the fibers was untouched with a smooth surface as seen in Figure 10b. Dislocation areas could easily be distinguished. After 15 minutes beating time, outer fibrillation started slightly (Figure 10c) and increased clearly when the treatment continued (Figure 10d, 45 minutes). After 60 minutes, external fibrillation can appear like partly peeled parts of the outer fiber wall (Figure 10e). That also internal fibrillation takes place, shows the fiber in Figure 10f, where the fiber wall structure partly disappeared. Even in this low magnification, the fibrilar structure of the total fiber wall can be recognized.

Drainability behavior

The development of pulp quality with any refining treatment is traditionally followed by the development of drainability using either Schopper-Riegler value or CSF. Although these parameters are so complex that they cannot react as sensitive to process effects as they should, also in this report, Schopper-Riegler is used as the basis parameter to follow the property development in the JOKRO beating.

All results concerning drainability are summarized in Figure 11.

As expected, JOKRO beating increased dewatering resistance. Linearity was found between RK number and Schopper-Riegler, non-linearity between CSF and Schopper-Riegler (Figure 11a). Specific filtration resistance and specific surface area increase with Schopper-Riegler, specific filtration resistance linearly like RK number (Figure 11b). Swelling occurred immediately after the treatment start as seen with water retention value (Figure 11c). This can be explained by immediate start of peeling reaction – removal or opening of the resistant outer fiber wall gives access for the water to the swellable inner fiber wall (see also Figure 12c, where peeling is explained as decrease of fiber wall thickness).

PTS refining produced pulp with comparable parameters for Schopper-Riegler, CSF, RK number, specific filtration resistance and specific surface area (bright dots in Figure 11). But swelling was different, with the same explanation (see Figure 12c).

Fiber dimensions and related parameters

Fiber dimensions and calculated dimension-based parameters are summarized in Figure 12.

Fiber length decreased gently with refining (Figure 12a). Fiber width decreased with refining as a result of the peeling (Figure 12b). Also Aspect Ratio decreased, which means that peeling exceeded fiber shortening – the fibers became slender with refining (Figure 12b). Fiber wall thickness decreased as result of peeling (Figure 12c). Mork's value MV (Figure 12c) and Fiber wall index CWI (Figure 12d) show similar curve shapes – strong decrease in the beginning of the treatment and then constancy throughout the rest of the refining process. Mork's value MV and fiber wall index CWI are two-dimensional parameters. Cross-sectional area CSA is based on a three-dimensional model (annulus), and thus with somewhat different response on refining (Figure 12d).
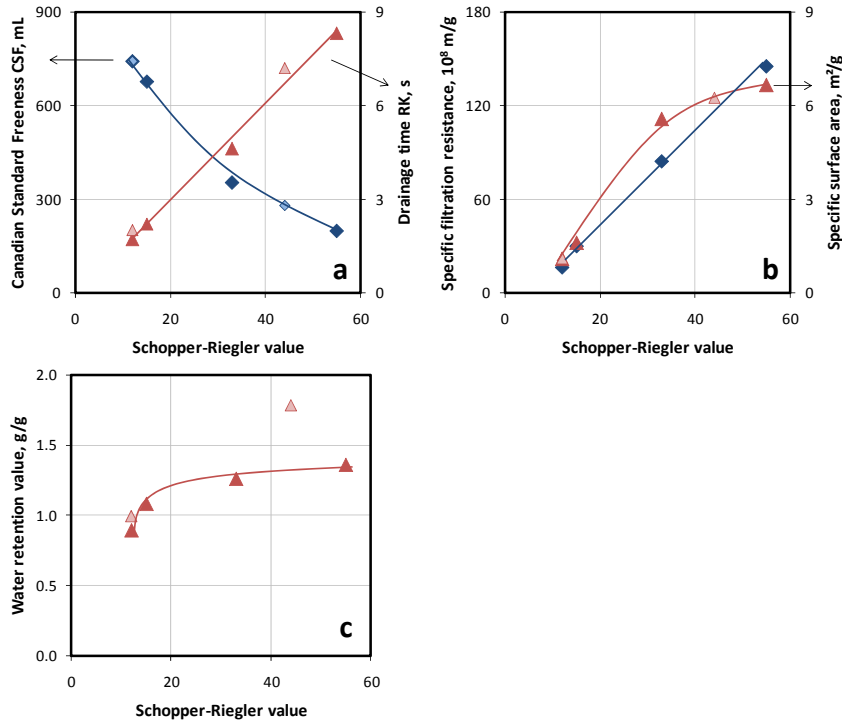
Figure 11. Development of drainability behavior versus Schopper-Riegler – Canadian Standard Freeness CSF and RK number (a), specific filtration resistance and specific surface area (b), and water retention value (c). Dark dots: JOKRO beating, bright dots: PTS refining
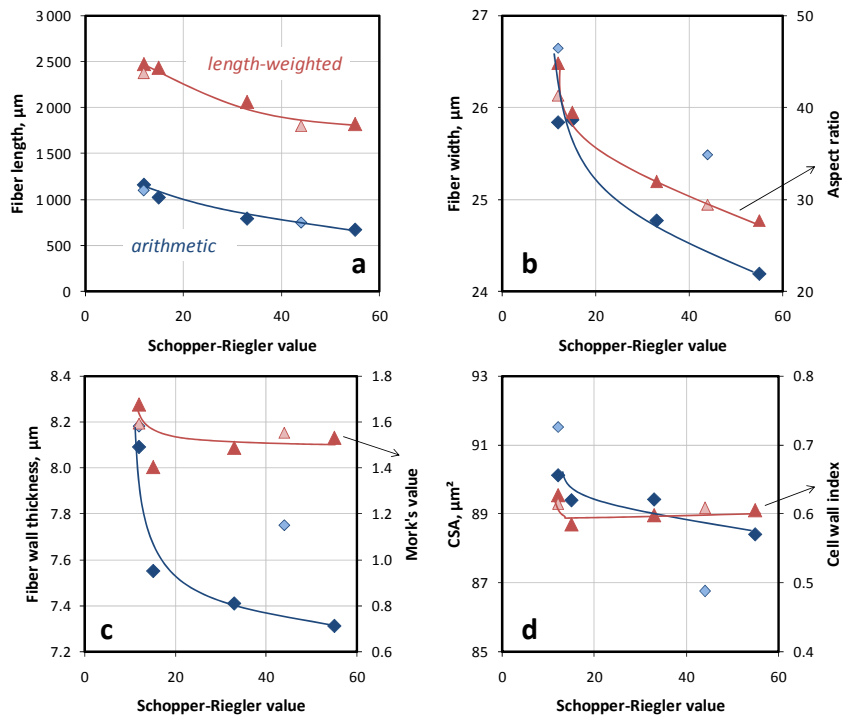
Figure 12. Fiber dimensions, measured with and calculated from kajaani FiberLab™ - Fiber length (a), fiber width and aspect ratio (b), fiber wall thickness and Mork's value (c), and cross-sectional area CSA and cell wall index (d). Dark dots: JOKRO beating, bright dots: PTS refining

PTS refining produced pulp with different swelling behavior (see Figure 11c). But this high swelling was not connected to lower fiber width or fiber wall thickness (Figure 12b and Figure 12c). The fibers have obviously a hydroskin, which causes apparent higher values for cross-sectional dimensions. This affects also the values of calculated data such as cross-sectional area CSA (Figure 12d). A slightly lower length-weighted fiber length and this apparent high fiber width lead to similar Aspect ratio (Figure 12b).

Distribution curves of the length-weighted fiber length (Figure 13) show that there is no immediate response on refining considering fiber length. The distribution curves of the unrefined sample (SR 12) and that after 15 min JOKRO beating (SR 15) are rather similar.
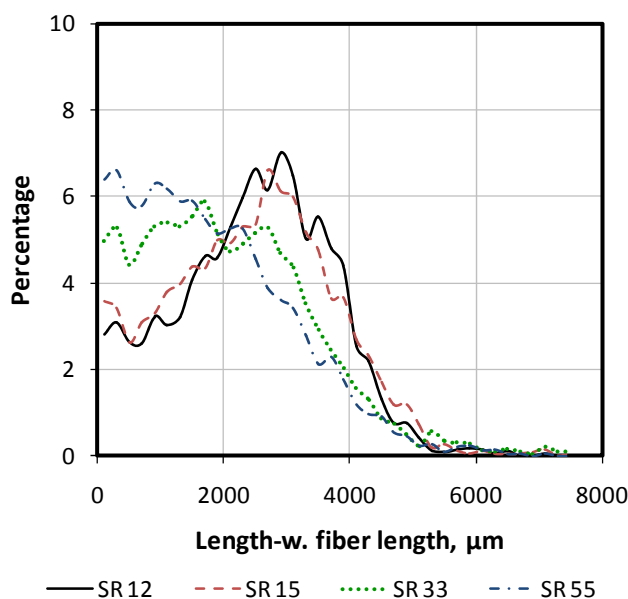
Figure 13. Distribution of length-weighted fiber length, measured with kajaani FiberLab™

The peeling of the fiber wall as described in Figure 12 is one source for the fines production, which is a usual effect of chemical pulp refining. The development of fines is shown in Figure 14a. Like the peeling occurred more in the beginning of refining, also the production of fines is higher in the beginning of the refining treatment (blue curve in Figure 14a). The strong increase in length-weighted fines (red curve in Figure 14a) corresponds to an increasing creation of thread-like fibrilar fines. PTS refining produced lower fines amount.

The refining type – fibrillating or cutting – can be characterized by fiber length (length-weighted fiber length) and bonding ability (specific surface area). Figure 14b gives a theoretical idea about the refining types. For the application of that theory to the sample pulp, relative values were calculated for length-weighted central-line fiber length and specific surface area, always based on the values of the unrefined pulp. The result is shown in Figure 14c. A slight decrease of fiber length and a strong increase of specific surface area stand for preferably fibrillation during the refining procedure.

This fibrillation is confirmed by the increasing fibrillation index (Figure 15b).
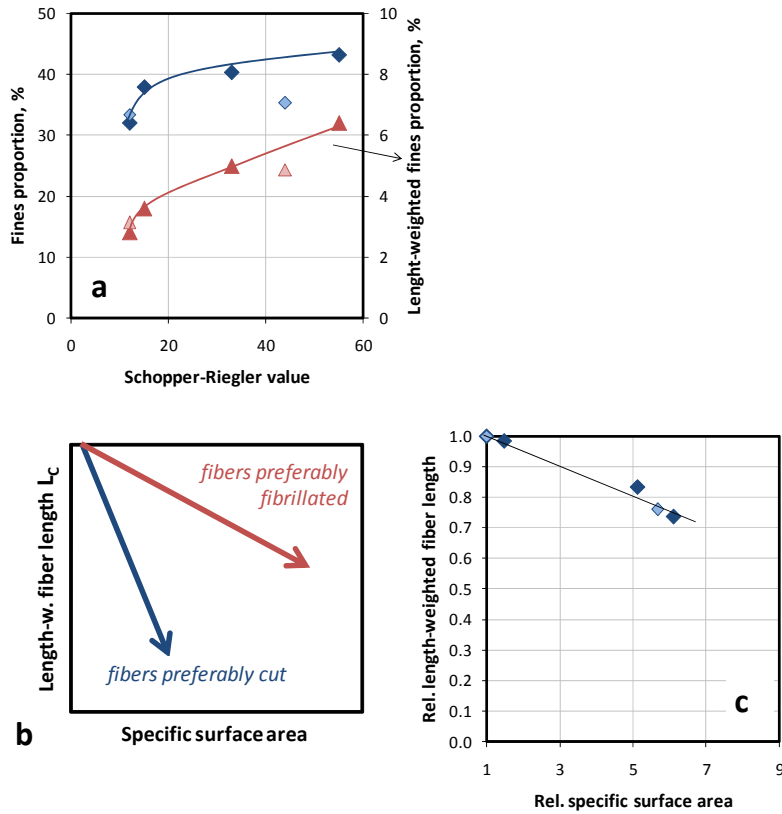
Figure 14. Development of the fines proportion (a). Characterization of the refining type by fiber dimensions (length-weighted fiber length) and bonding ability (specific surface area) – theoretically (b), and for the performed JOKRO beating (c). Dark dots: JOKRO beating, bright dots: PTS refining
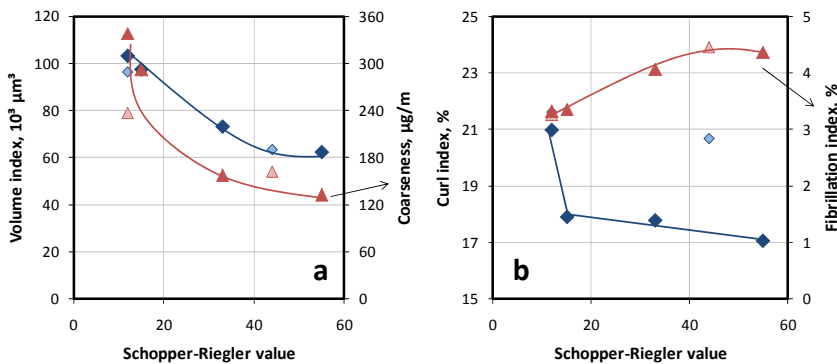
Figure 15. Further parameters from automated fiber analysis with kajaani Fiberlab™ - Volume index VI and coarseness (a), curl index and fibrillation index (b). Dark dots: JOKRO beating, bright dots: PTS refining

Coarseness is a parameter that also tells something about the fiber response in refining. Considering the fiber wall density as constant, this value also can describe whether a refining is more of the cutting or of the fibrillation type. The smaller the change of coarseness the higher the proportion of cut fibers. The clear decrease of coarseness confirmed the preferably fibrillation treatment in the JOKRO mill (Figure 15a).

For a reliable coarseness measurement, the initial sample concentration (oven-dry sample mass) has to be provided as exact as possible before the test, and the test itself has to be performed without blockage of the capillary system. Because this is not always possible, the parameter volume index VI can be used as well. The volume index VI developed in the same tendency

(Figure 15a). There is also a close connection between volume index and aspect ratio when calculated from the same basis data (see Figure 12b).

The curl index describes the deviation of the fiber direction along the fiber length axis from a straight line. It is calculated from the relation between projected fiber length and central-line fiber length. Refining energy causes fiber straightening in the most cases, which can also be seen for the common pulp sample at the beginning of the treatment (Figure 15b). PTS refining did not cause fiber straightening.

Strength properties

Conventional handsheets were produced according to standard ISO 5269-1. From the sheets, strength parameters and optical properties were tested.

Strength properties are summarized in Figure 16.

Tensile index, zero-span wet tensile index (Figure 16a), tensile stiffness index and modulus of elasticity (Figure 16b), stretch (Figure 16c), and internal bond (Figure 16d) increased with refining, especially at the beginning of the treatment. The development of bonding ability in z-direction is strongly correlating with the fibrilar character of the fines (see Figure 16a). Bulk decreases at the beginning of refining with decreasing fiber wall thickness and increasing fines proportion (Figure 16c). Unfortunately, the available dimension-based parameters cannot describe real fiber flexibility.

Tear index was measured with the standardized Brecht-Imset apparatus (DIN 53115). This tearing test is more related to the practical tearing behavior of a paper than the Elmendorf-test (Brecht and Imset 1933, Seth and Blinco 1990). The common pulp sample shows the typical shape of a Brecht-Imset tearing curve (Figure 16d). The maximum occurs when long AND fibrillated fibers are in the sample, which happened in the beginning of the refining treatment.
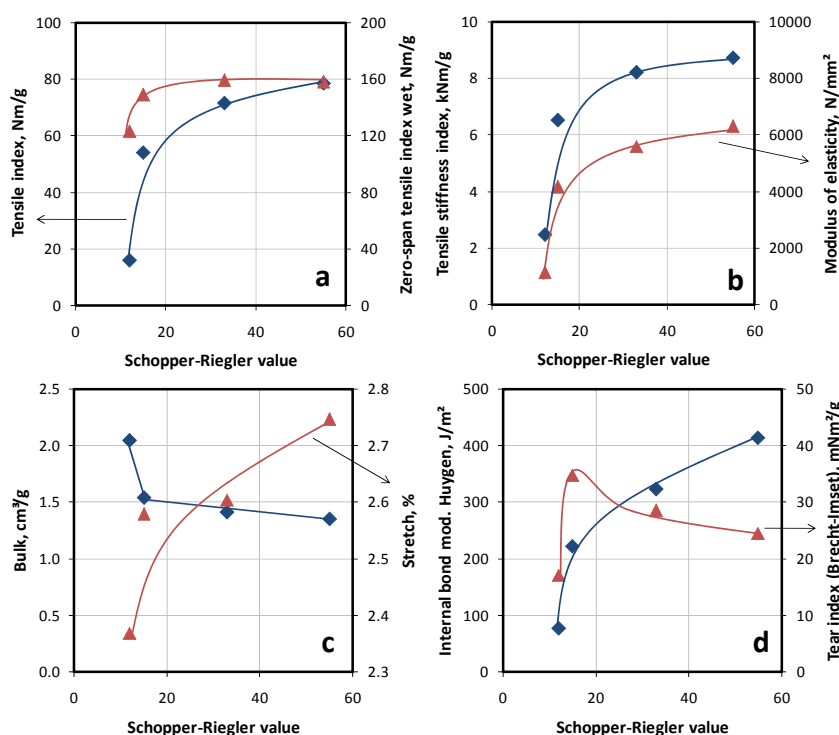
Figure 16. Strength properties of handsheets – Tensile index and zero-span wet tensile index (a), tensile stiffness index and modulus of elasticity (b), bulk and stretch (c), and internal bond and tear index (d)
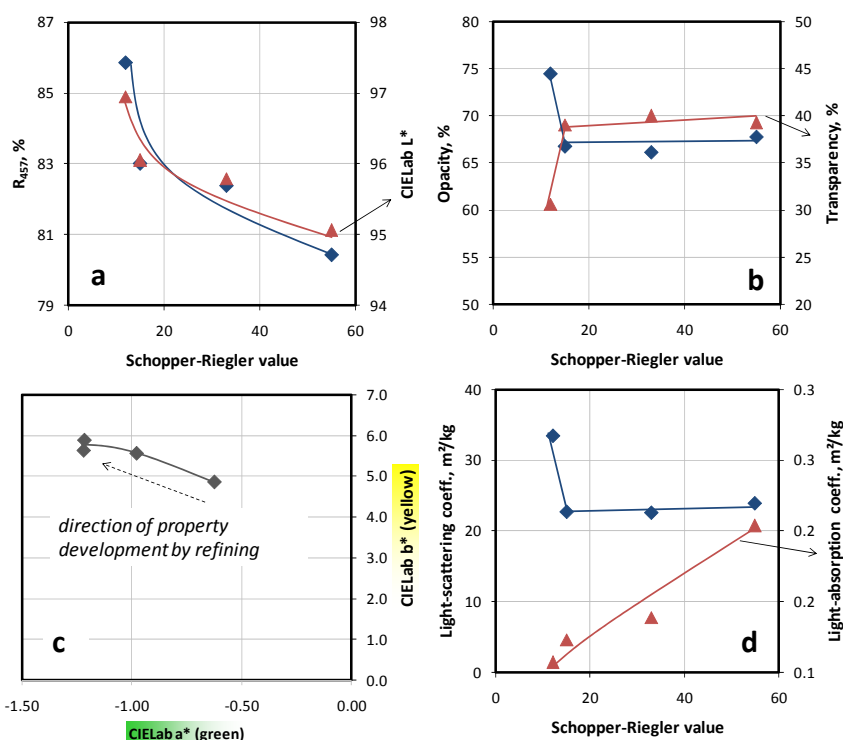
Figure 17. Optical properties of handsheets – Brightness R_{457} and lightness L (a), opacity and transparency (b), color position in the CIELab system (c), and light-scattering and light-absorption coefficients (d)*

Optical properties

Optical properties of the handsheets are summarized in Figure 17. Refining decreases brightness, seen for the two corresponding parameters R_{457} and L* (Figure 17a). A drop in brightness is usually connected with an increase of the light-absorption coefficient (Figure 17d). Opacity, transparency and light-scattering coefficient are affected by the sheet structure. After the first value drop, these parameters remained constant throughout the subsequent refining process (Figure 17b and Figure 17d). The same tendency could be seen for the development of the handsheet density (bulk, Figure 16c): The denser the sheet the lower light scattering and porosity. The color position of the sample in the CIELab system was determined for the unrefined sample (Figure 17c). The name of the pulp brand "Södra green" was confirmed, because the color position was found for the green-yellow quadrant. The brightness drop and the increase of light absorption are also seen in the color development – with refining, the color position moves towards higher color saturation, i.e. the sample becomes darker.

Conclusions

A lot of data were collected from the common pulp samples. The focus in this paper was on refining behavior in laboratory scale (JOKRO mill).

At the beginning of the refining treatment, fibers became more straight (strong decrease of curl index), and only cross-sectional dimensions were changed (strong decrease of fiber width and fiber wall thickness).

Changes towards shorter fiber length occurred later in the refining procedure. But also the peeling effect continued, and fibrilar fines were produced. It cannot be proved whether the lower mean value for fiber length comes from fiber shortening (cutting) or whether it comes from a higher proportion of released coarse fibrils long enough to be classified as short fibers. The decrease in cross-sectional dimensions speaks for this possibility.

The pulp response on mechanical treatment as performed in a JOKRO mill (and also in the PTS Refiner) is preferably fibrillation due to slight decrease in fiber length and significant increase in bonding ability (specific surface area).

Acknowledgements

References

Ander P., Daniel G., Garcia-Lindgren C. and Marklund A. (2005): Characterization of industrial and laboratory pulp fibres using HCl, Cellulase and FiberMaster analyses. Nordic Pulp Paper Res. J. 20(1), 115-120

Ander P. and Daniel G. (2006): Dislocation counting and comparison of pulp fibre properties after HCl-treatment and fibre length determination. Proc. 5th Plant Biomechanics Conference, Stockholm, Vol. I. August 28 – September 1, 2006. *Ed.*: L. Salmén. STFI-Packforsk, Stockholm, Sweden, ISBN 91-86018-12-4, pp. 169-174

Ander P., Hildén L. and Daniel G. (2008): Cleavage of softwood kraft pulp fibers by HCl and cellulases. BioResources 3(2), 477-490

Ander P., Henniges, U. and Potthast A. (2011): SEC studies on HCl treated softwood and birch kraft pulps. *In* COST Action E54 "Characterisation of the fine structure and properties of papermaking fibres using new technologies". *Eds*: Ander P., Bauer W., Heinemann S., Kallio P., Passas R. and Treimanis A. Printed by: Swedish University of Agricultural Sciences, pp. 65-72. ISBN 978-91-576-9007-4.

Brecht W. and Imset O. (1933): Ein neues Gerät zur Messung des Durchreisswiderstandes von Papieren (A new apparatus for assessment of tear strength of papers). Wochenbl. Papierfab. 64 (48), 848-853

Brecht W. and Schanz D. (1957): Attempt to characterize mechanical pulp fines by assessing its specific surface area. Wochenbl. Papierfab. 85(23), 891-898

Ekstam T. (1957): Investigations on beating with the "JOKRO-Mühle". Paperi ja Puu 39(6), 309-316

Forgacs O.L. (1963): The characterization of mechanical pulps. Pulp Paper Mag. Can. 64(C), T89-T118

Hechler E. (1968): Beating trials with the JOKRO mill. Das Papier 22(7), 396-406

Heinemann S. (1985): Contribution to determine the mass-specific surface area and its effect on strength behavior of pulps. Doctoral Thesis, Dresden University of Technology, Faculty of Engineering

Heinemann S. and Neclaw A. (2011): Hydrodynamic specific surface area – The Dresden method and its results for pulps affected by different additives. *In* COST Action E54 "Characterisation of the fine structure and properties of papermaking fibres using new technologies". *Eds*: Ander P., Bauer W., Heinemann S., Kallio P., Passas R. and Treimanis A. Swedish University of Agricultural Sciences, pp. 233-246. ISBN 978-91-576-9007-4

Heinemann S. and Vehniäinen A. (2009): The character and properties of mechanical pulps. *In* Mechanical Pulping, Bd. 5 of the series Papermaking Science and Technology, 2nd edition, chapter 15, p. 456 – 514, Lönnberg, B. *(Ed.)*, Helsinki: Paperi ja Puu Oy, 2009 (ISBN 978-952-5216-35-6)

Ingmanson W.L. (1952): An investigation of the mechanism of water removal from pulp slurries, Tappi Journal 35(10), 439-448

Ingmanson W.L. and Andrews B.D. (1959): The effect of beating on filtration resistance and its components of specific surface and specific volume. Tappi J. 42 (1), 29-35

Ingmanson W.L. and Whitney R.P. (1954): The filtration resistance of pulp slurries. Tappi J. 37(11), 523-534

Jayme L.G. and Büttel H. (1965): Acquisition of fine deviations in pulp behavior during beating in the JOKRO mill. Atti del Congresso Europeo di Tecnica Cartaria Venedig 1965, Proceedings, p.131-146

Jonas K.G. (1933): The beating actions in the hollaender and in the JOKRO mill. Der Papierfabrikant 31(36), 473-483

Kleinert R. (1977): Upgrading the JOKRO mill for standard laboratory beating. Zellstoff und Papier 26(9), 261-266

Mannström B. (1967): On the characterization and quality control of mechanical pulp. Paperi ja Puu 49(4a), 137-146

Mannström B. (1972): Characterization of refiner mechanical pulp. Das Papier 26(10A), 657-664

Mason, S.G. (1950): Specific surface of fibers – Its measurement and application. Tappi J. 33(8), 403-409

Mork E. (1928): Die Qualität des Fichtenholzes unter besonderer Rücksichtnahme auf Schleif- und Papierholz (The quality of spruce wood considering especially its use for ground wood and pulp wood). Der Papierfabrikant 26(48), 741-747

Orlandi M. (2007): FIB Analysis of unbleached kraft pulp. COST E54 Workshop, 24-25 October 2007, Brussels/Belgium

Robertson A. and Mason S.G. (1949): Specific surface of cellulose fibres by the liquid permeability method. Pulp Paper Mag. Can. 50(13), 103-110

SCAN-M9 (1976): Mechanical pulp – Drainage time (withdrawn Scandinavian standard, informative only)

Seth R.S. and Blinco K.M. (1990): Comparison of Brecht-Imset and Elmendorf tear strengths. Tappi J. 73(1), 139-142

TAPPI standard T221 cm-99 (1999): Drainage of pulp

Zellcheming Technical Leaflet (1961): Common method for strength assessment of pulps, Part G: Testing of dewatering behaviour, Zellcheming Technical Leaflet V/7/61 (withdrawn as standard, informative only)

HYDRODYNAMIC SPECIFIC SURFACE AREA – THE DRESDEN METHOD AND ITS RESULTS FOR PULPS AFFECTED BY DIFFERENT ADDITIVES

[1]Sabine Heinemann and [2]Aleksandra Neclaw

[1]P.O. Box 1000, 02044 VTT (Espoo), Finland

[2]Eska Graphic Board, P.B. 90, 9610 AB Sappemeer, The Netherlands

sabine.heinemann@vtt.fi

a.neclaw@eskagraphicboard.com

Abstract

Hydrodynamic specific surface area and compressibility are suitable parameters to characterize the behavior of fibrous material in draining processes such as sheet forming and pressing as well as the strength of the resulting sheets. Obvious data differences caused by effects of raw material or pulping processes made the hydrodynamic specific surface area becoming a parameter of interest in investigations of alternative additives based on commercial products from bio-based industries. The experiments and discussion presented in this paper were part of a Master Thesis with the objective to assess the impact of different, alternative papermaking additives on paper web dewatering intensity in the wet-end part of paper machine with a clear focus on the influence and the role of additives and fibers. Alternative bio-based additives which can be used as a valuable papermaking additive without negative effect on paper quality were targeted. The effect of those additives on the dewatering behavior of pulp suspensions with different papermaking alternative additives using process effects, and correlations between different dewatering methods were studied.

The hydrodynamic specific surface area and compressibility parameters made clear distinctions between the applied alternative bio-based pulps, which could improve the dewatering of the mixed pulp slurry to a certain extend. The interactions between the pure reference made from recovered fibers and the character of the alternative pulps, described by properties such as e.g. dimensions, dimensional distribution, moisture content, and chemical composition, have a high variability. The results show that not always the optimal trial parameters could be applied, but at least some of the alternative materials such as the sugar-based Betacal, the wooden sawdust, but also deinking sludge have a potential to adjust suitable dewatering properties for certain base pulps. Additionally, citrus pulp and probably also potato peelings have a chance for application in this sense.

Introduction

Hydrodynamic specific surface area and compressibility are suitable parameters to characterize the behavior of fibrous material in draining processes such as sheet forming and pressing as well as the strength of the resulting sheets. The method as such was developed about 60 years ago (Robertson and Mason 1949; Mason 1950), and mainly applied on mechanical pulps (Brecht and Schanz 1957; Forgacs 1963). A lot of research has been focused on this measuring method during the following years about the permeability theory, optimization of the testing principle and suitable applications for pulp characterization and prediction of paper properties (Emerton 1955; Robertson 1957; Ingmanson and Andrews 1959; Thode 1959; Ingmanson and Andrews 1963; Campbell 1965; Grén and Hedström 1967; Labreque 1968; Han 1969; Cowan 1970; Grén 1972; Schweizer 1975; Yan and El-Hosseiny 1978). A commercial device – the Pulmac

Permeability Tester – was launched at the end of that research period (Cowan 1970), but is not commercially available anymore.

A next boom for the method has been in the middle eighties of the last century including new apparatus developments and applications (Ljungkvist 1983; Unger et al. 1983; Unger and Heinemann 1983a,b and 1985).

Recent developments and applications have started in the late nineties (Kumar and Ramarao 1995; Ramarao 1999; Das et al. 2001; Wang et al. 2002). Nevertheless, the method has its limitations for on-line application and is therefore not widely known or in use, although the testing results are more reliable and distinct testing pulps better than corresponding dewatering parameters such as Canadian Standard Freeness or Schopper-Riegler (Heinemann 1985).

In the following discussion, hydrodynamic specific surface and specific volume by permeability method was measured with the Dresden Permeability apparatus (Unger et al. 1983; Heinemann 1985 and 2010). Obvious data differences gained with this testing device and caused by effects of raw material or pulping processes made these parameters becoming of interest in investigations of alternative additives based on commercial products from bio-based industries.

The experiments and discussion presented in this paper were part of a Master Thesis with the objective to assess the impact of different, alternative papermaking additives on paper web dewatering intensity in the wet-end part of paper machine with a clear focus on the influence and the role of additives and fibers (Judasz 2009). Alternative bio-based additives which can be used as a valuable papermaking additive without negative effect on paper quality were targeted. The effect of those additives on the dewatering behavior of pulp suspensions with different papermaking alternative additives using process effects, and correlations between different dewatering methods were studied.

Theory and background of the permeability principle

The hydrodynamic surface area of fibers is defined as fiber surface area in a compressed water-swollen fiber pad that is accessible for streaming water molecules, and its dimension is m²/g. The method is based on liquid permeability method first published by Robertson and Mason (1949), which is an application of the permeability principle by Kozeny (1927).

For the porous fiber wall, an internal and an external surface can be defined. In water-swollen fibers, internal surface area is not accessible for water molecules which flow along the external fiber surface. Only the external surface is in contact with the streaming/flowing water. Therefore, the hydrodynamic specific surface area describes an external surface and is a function of flow rate through a compressed fiber pad under defined hydrostatic pressure, reflecting the flow resistance caused by fiber surface character (Emerton 1955; Heinemann 1985).

According to Robertson and Mason (1949), the permeability behavior of a compressed pad of water-swollen fibers is linear for a certain range of concentration at the given sample mass g. Linearity can be expressed by a straight-line equation (equation 1).

$$(Kc_F^2)^{1/3} = \left(\frac{1}{2 S_m^2}\right)^{1/3} - V_m c_F \left(\frac{1}{2 S_m^2}\right)^{1/3} \tag{1}$$

K   permeability parameter
c_F fiber pad concentration
S_m specific surface area
V_m specific volume

This straight line is part of the so-called Kozeny-Carman plot, which is created by data pairs of the value $(Kc_F{}^2)^{1/3}$ versus c_F. (Figure 1). The data pairs are gained from flow rate measurements through a stepwise further compressed fiber pad. Practically, a defined amount of oven-dry, air-free sample material is compressed in a vessel between 2 wire screens from which one is moving with a piston, and the other is fixed. For each compression step, hydrostatic pressure, flow rate, wire screen distance and liquid temperature is measured. After the full number of compression steps, the fiber pad is removed, and the oven-dry mass is determined. The fiber pad concentration c_F and the permeability factor K are calculated using equations according to Darcy (flow rate through a porous material with unknown porosity) and according to Hagen-Poiseuille (flow rate through a material with known number of circle-cylindrical pores). From these calculated values, the parameters for the Kozeny-Carman plot – $(Kc_F{}^2)^{1/3}$ and c_F – are taken.
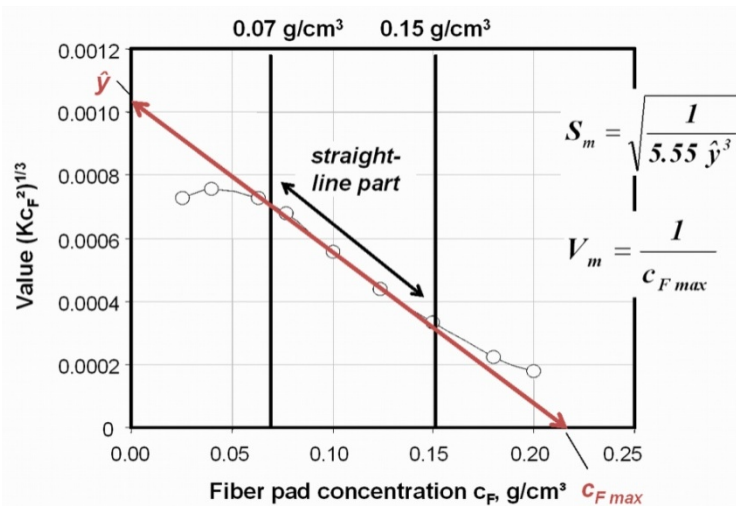
Figure 1. The Kozeny-Carman plot, based on laboratory refining of softwood kraft pulp, with extrapolation of the straight-line part to the y-axis (ŷ) for calculation of the specific surface area S_m, and extrapolation to the x-axis ($c_{F\ max}$) for calculation of the specific volume V_m.. (See Heinemann 2010)

The shape of the Kozeny-Carman plot (Figure 1) is reflecting different states of the particle-flow interaction depending on the concentration of the compressed fiber pad. At concentrations smaller than 0.07 g/cm³, fibers can freely move under hydrostatic pressure, and the flow rate increases with increasing pad consistency. At about c_F=0.07 g/cm³, fibers cannot flow anymore with hydrostatic pressure, they start to find their "best place" under compression pressure. This concentration is the starting point of the straight-line part in the Kozeny-Carman plot. The upper concentration limit for the linearity, c_F = 0.15 g/cm³, was defined due to construction limits of the first testing apparatus ever built (Robertson and Mason 1949; Brecht and Schanz 1957). It was found that the straight-line equation can be applied also for higher fiber pad concentrations, especially for pulps with less compressible fibers. In other cases, fibers cannot move anymore under compression pressure and start to collapse – the flow rate increases again, and the Kozeny-Carman plot flattens (Heinemann 1985).

In a compressed fiber pad, all particles are in contact with their neighbours, and only part of the fiber surface is free to be in contact with flowing water. For the total specific surface area, particles are assumed NOT to be in contact with any neighbour. Computation of specific surface area is carried out by extrapolation of the straight-line part to the y-axis (C_F=0, i.e. no contact to any neighbour). From the y-intercept (ŷ), specific surface area S_m is calculated according to equation 2.

$$S_m = \sqrt{\frac{1}{5.55\ \hat{y}^3}}$$

(2)

Extrapolation of the same straight-line part to the x-axis $((Kc_F{}^2)^{1/3}=0$, i.e. no flow through the fiber pad) describes the theoretical situation, that all fibers are in full contact to each other and no free fiber surface is left in the fiber pad. At this intercept, the specific volume of all fibers V_m can be calculated just by reversing the intercept value c_{Fmax} (equation 3).

$$V_m = \frac{1}{c_{F\,max}}$$

(3)

Specific surface area is a good tool to characterize refining behavior of chemical pulps when expressed together with length-weighted fiber length (Figure 2).

A gradual increase in specific surface area with moderate decrease of fiber length stands for preferably fibrillation treatment during laboratory beating (valid for all tested kraft pulps – pine, Douglas fir, eucalyptus, and birch). A strong decrease of fiber length immediately after the beginning of treatment without any noticeable increase of specific surface area stands for all pulps with low refining resistances, which are preferably shortened in laboratory beating (spruce sulfite pulp, straw kraft pulp). Figure 2 shows also, that a development of specific surface area occurs also for such pulps, but only later in the refining process, and at much lower fiber length.
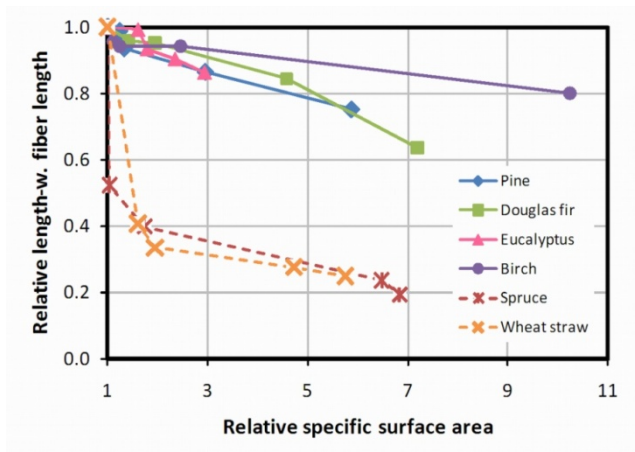
Figure 2. Relative length-weighted central-line fiber length versus relative hydrodynamic specific surface area for laboratory beating of chemical pulps in the JOKRO mill. Basis for relativization was always the unbeaten reference pulp (See Heinemann 2010)

Although it has often been postulated, there is neither a clear correlation between specific surface area and Schopper-Riegler value nor with Canadian Standard Freeness (Unger and Heinemann 1983a).
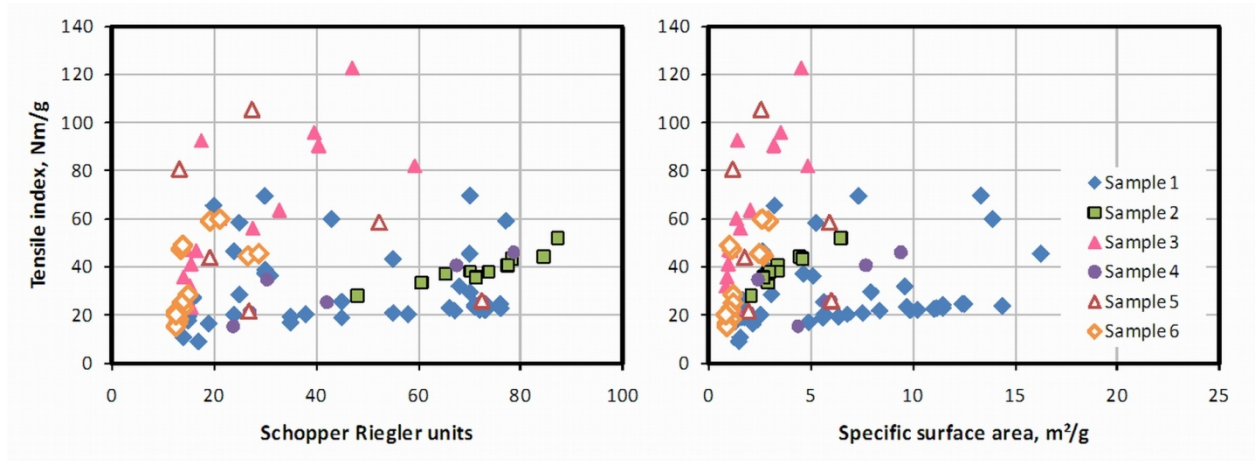
Figure 3. Development of tensile index for 6 samples differing in raw material, pulping and refining processes, versus Schopper-Riegler units (left), and versus specific surface area (right) (See Heinemann 2010)

For parameters, which describe the bonding behavior (like tensile index), a better correlation can be found with specific surface area than with the Schopper-Riegler value (Figure 3). For some samples, drainability expressed in Schopper-Riegler units might already be enough to describe the development of tensile index (sample 2 in Figure 3), but for other samples, a better sample distinction can be made with specific surface area than with Schopper-Riegler (or Canadian Standard Freeness).

The compressibility is a complex property depending on dimensions, stiffness and swelling degree of the fibers. An empirical equation (equation 4) based on fiber pad concentration and compression pressure was found suitable for papermaking fibers (Ingmanson 1953; Wilder 1960; Grén 1972). Especially the parameter n was found to describe the compressibility behavior of the tested pulp sample.

$$c_F = c_{F0} + m \times p_K{}^n \tag{4}$$

c_F	Concentration of the fiber pad in g/cm³
c_{F0}	Initial concentration of the fiber pad in g/cm³
p_K	Compression pressure in kPa
m, n	Conformability parameters

An application of this compressibility assumption was made with the Dresden Permeability Tester (Figure 4, Heinemann 1985). The values for the parameter n (0.31 for groundwood and 0.35 for softwood kraft pulp respectively) were close to values found earlier elsewhere (Grén 1972), and demonstrate that the unbeaten kraft pulp fibers with their higher flexibility are better compressible than the groundwood material containing not only rather stiff fibers but also other material broken down from the wood matrix in a wide dimensional distribution.
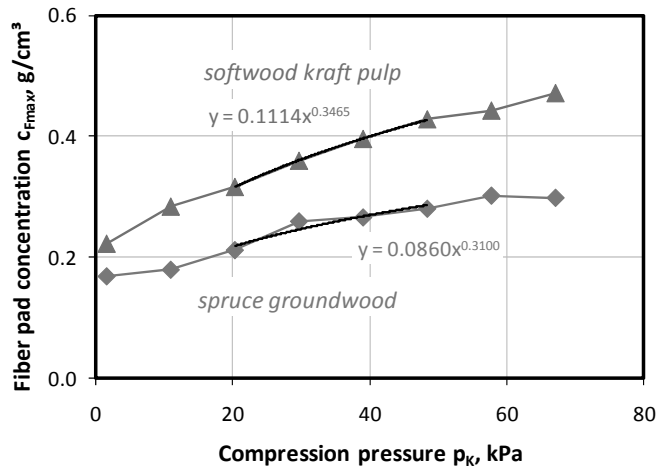
Figure 4. Maximum fiber pad concentration c_{Fmax} depending on compression pressure p_K for unbeaten softwood kraft pulp and spruce groundwood, measured with the Dresden Permeability Tester (see Heinemann 1985). Trend lines with equations describe the compressibility behavior in the medium compression range between 20 and 50 kPa

Experimental

Tested materials

Experiments were performed to investigate the effect of alternative additives on drainability and flow behavior respectively.

The reference pulp was made from pure recovered fibers, using fluting from Smurfit Kappa Roermond Paper, consisting in 60% OCC and 40% MOW (mixed office waste).

Commonly available substances from the papermaking industry and collaborating bio-based industries were used as alternative additives (in alphabetical order): apple pulp, Betacal (a side-product from sugar industry), beer fines fresh and dried, citrus pulp, deinking sludge, onion skins, potato pulp (potato peelings), and sawdust with diameters of 100µm and 320 µm. The main components of some of these materials are given in Table 1.

Table 1. Main components of selected alternative additives

Alternative additives	Cellulose [g/kg]	Hemicellulose [g/kg]	Lignin [g/kg]	Ash [g/kg]
Apple pulp	285			25
Betacal	-	-	-	43
Beer fines	220	480	60	
Sawdust C100	450-550	100-200	250-300	5
Sawdust C320	474	214	246	2
Citrus pulp	130			40
Deinking sludge	356	94	205	250
Onion skins	245			90

The samples for the permeability tests were prepared by adding 5%, 10%, and 15% of oven-dry alternative additives to oven-dry reference pulp, resulting in two sample groups. One group included the samples which were measured almost immediately after preparation. The other group contained samples with at least 2 hours of swelling time between sample preparation and sample testing. In opposite to the normally applied permeability method, the pulp samples were not air-free.

Testing equipment

No commercial device for testing hydrodynamic specific surface area is available. The trials were performed with the unique Dresden Permeability Tester, first published by Heinemann (1985). Figure 5 shows the simplified testing principle for permeability measurements (= measurement of the flow rate through a more or less compressed fiber pad). Additionally, compression tests can be performed to a certain extent with the same device as part of the permeability measurements (Figure 6). Constant device parameters are summarized in Table 2.
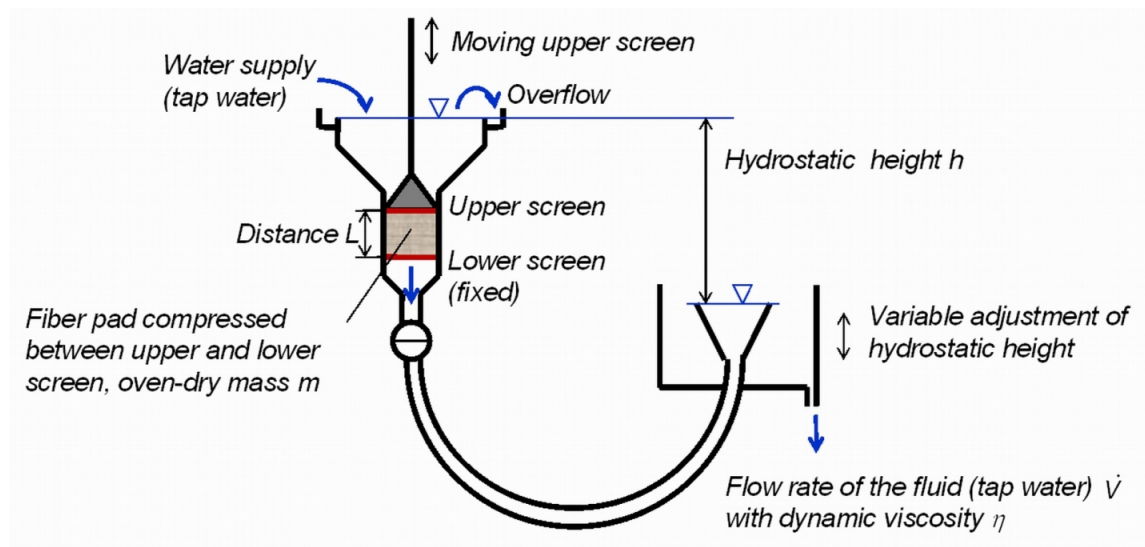
Figure 5. Simplified testing principle of the Dresden Permeability Tester (see Heinemann 2008)

Table 2. Constant and adjustable device parameters

Cross-sectional area of the compression vessel	12.57 cm²
Hydrostatic pressure	0 – 8.8 kPa (0 – 88 mbar)
Sample mass oven-dry	1.8 – 2.5g
Minimum compression pressure (applied for flow-rate measurements during step-wise fiber pad compression	1.56 kPa (15.6 mbar)
Maximum compression pressure applied for compressibility tests	67.1 kPa (0.67 bar)
Step size for compression pressure in compressibility tests	9.37 kPa (93.7 mbar)
Number of compression steps	At least 3
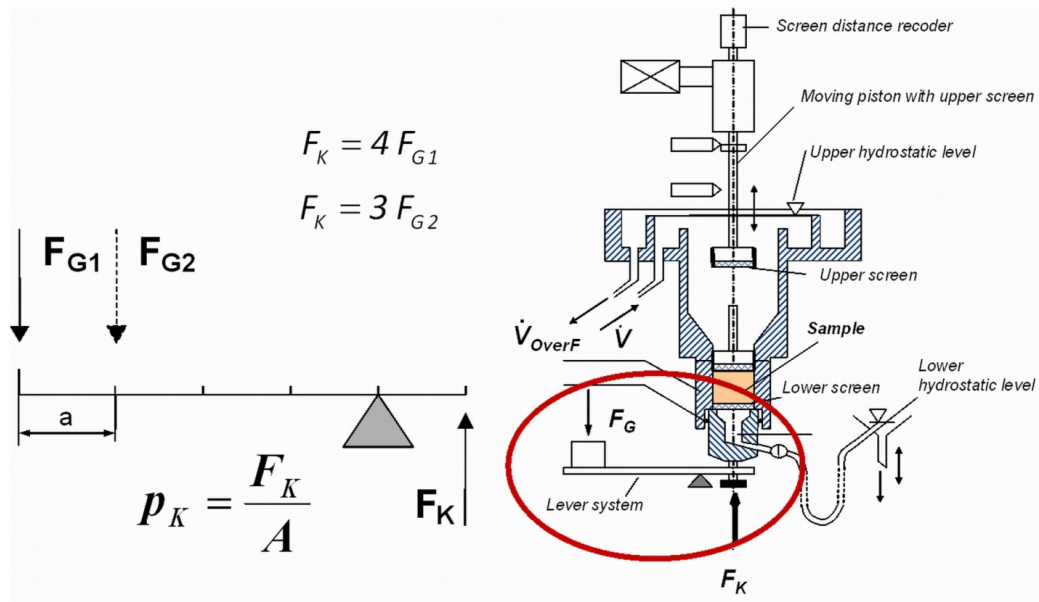
Figure 6. Lever system for compression tests. The conformability of the fibers in the compressed fiber pad is defined as the maximum fiber pad concentration which can be reached with maximum compression pressure of 67.1 kPa after a number of defined compression steps for flow rate measurements at compression pressure of 1.56 kPa (see Heinemann 1985)

Trial performance including sample preparation

The following steps were performed for repeatable assessment of specific surface area and compressibility:

- Grinding the alternative additive materials in a kitchen coffee grinder if necessary
- Placing the recovered paper into the disintegrator
- Adding the alternative pulps in proper proportion to the disintegrator
- Disintegrating of the material mix with 15000 revolutions at 2% consistency
- Filling those samples which needed to swell into special containers (consistency 2%)
- Placing the pulp either directly after disintegration or after swelling into a dilution tank, filling the tank up to a volume of 10 liters, and determining the slurry consistency
- Taking the proper sample amount corresponding to 2 g oven-dry material from the dilution tank
- Performing the permeability test with six compression steps
- Performing the conformability test with compression pressure of 67.1 kPa

The applied procedure parameters are summarized in Table 3.

Table 3. Applied procedure variables

Hydrostatic pressure (lowest pressure applied to avoid undesired effects on the internal fiber pad structure)	1.0 – 1.5 kPa (10 – 15 mbar)
Sample mass oven-dry	2 g
Minimum compression pressure (applied for flow-rate measurements during step-wise fiber pad compression	1.56 kPa (15.6 mbar)
Maximum compression pressure applied for compressibility tests	67.1 kPa (0.67 bar)
Swelling time for selected samples	At least 2 h
Number of compression steps	6
Range of fiber pad concentration during the 6 compression steps	0.069-0.143 g/cm³
Range of achieved maximum fiber pad concentration	0.45 to 0.60 g/cm³

Testing results

The tests were performed to precise the effect of adding alternative materials to the reference pulp from recovered fibers on the dewatering behavior of the resulting pulp suspensions. Hydrodynamic specific surface area and compressibility was measured for three different proportions of oven-dry additives, partly also a 2-hours-swelling was performed.
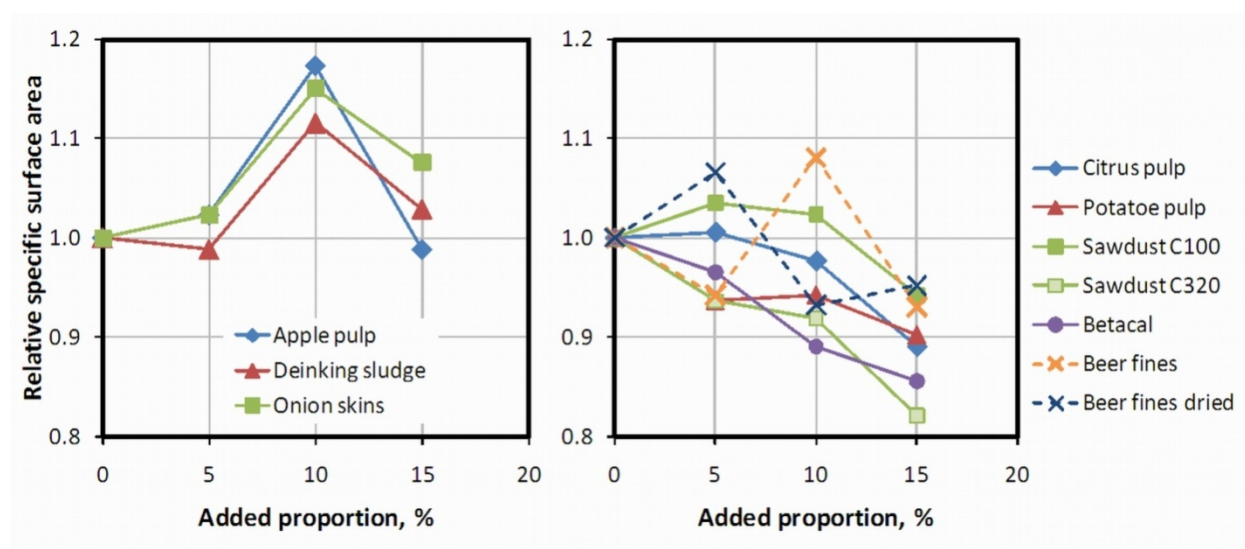
Figure 7. Relative specific surface area versus added proportion of alternative pulp. Alternative additives increasing specific surface area (left), and decreasing specific surface area (right). For relative values, the surface area of the pure reference pulp (1.73 m²/g) was set as 1.

Deviations in pulp behavior compared with the pure reference pulp depend on shape and size of the added particles and their distributions. Wide distributions can cause insignificant changes of the specific surface area.

Apple pulp, deinking sludge and onion pulp increase the hydrodynamic specific surface up to an added proportion of 10%. Further addition (15% alternative pulp) reverses this tendency, but the resulting data are still higher than those of pure reference pulp. Of these alternative materials, only deinking sludge seems to decrease the specific surface area and thus improve dewatering to

certain extent when added in minor proportions (5%) (Figure 7 left). The added alternative materials with tendency to decrease specific surface area and thus increase drainability are assembled in Figure 7 right. Sawdust C100 and citrus pulp improve drainability only at higher added proportions (15% and 10% respectively). Beer fines both dry and wet have the highest data deviation, but with decreasing tendency, too.

From these results, the alternative additives with the best effect considering dewatering (=decreasing specific surface area) are Betacal and sawdust C320. Both are rather granular materials as seen from microscopic images (Figure 8), and they seem to act like mineral fillers.
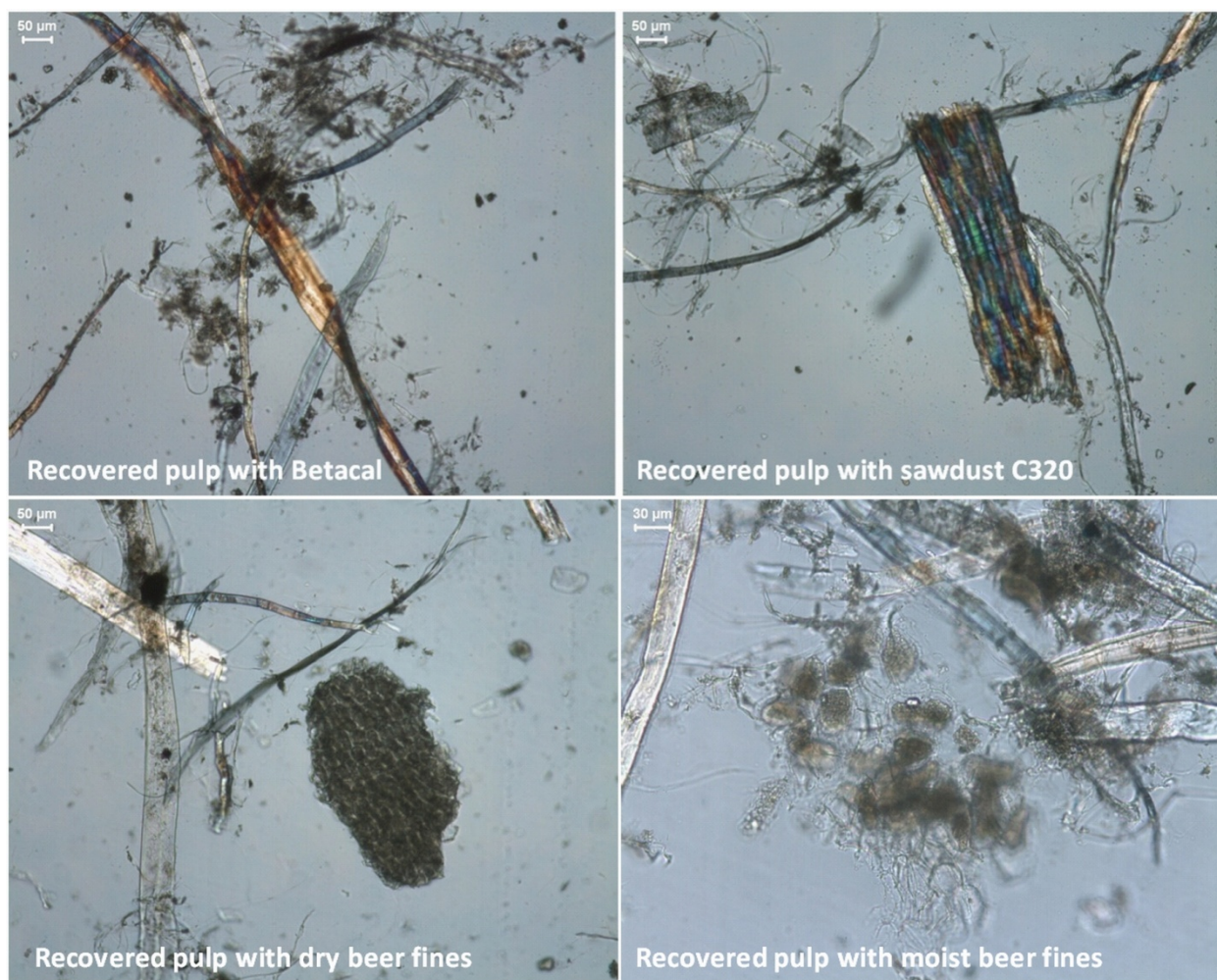
Figure 8. Microscopic images of tested pulps in modified polarized light – Recovered pulp with Betacal (above left), with sawdust C320 (above right), with beer fines dry (below left) and with beer fines moist (below right). Length bar: 50 μm

In the lower part of Figure 8, the high variety of beer fines is visible which causes the very wide deviation of the testing results.

Considering the effect of swelling on dewatering, no clear tendency was seen. For apple pulp (Figure 9 left), swelling seems to decrease the data deviation, however, the swelling of the pulp had no positive effect on drainability. From the tested materials, which decreased specific surface area in dry state, only Betacal and sawdust C320 showed a clear tendency (Figure 9 right) – swelling of Betacal increased specific surface area and was thus detrimental for dewatering improvement, except the high proportion of added material (15%).
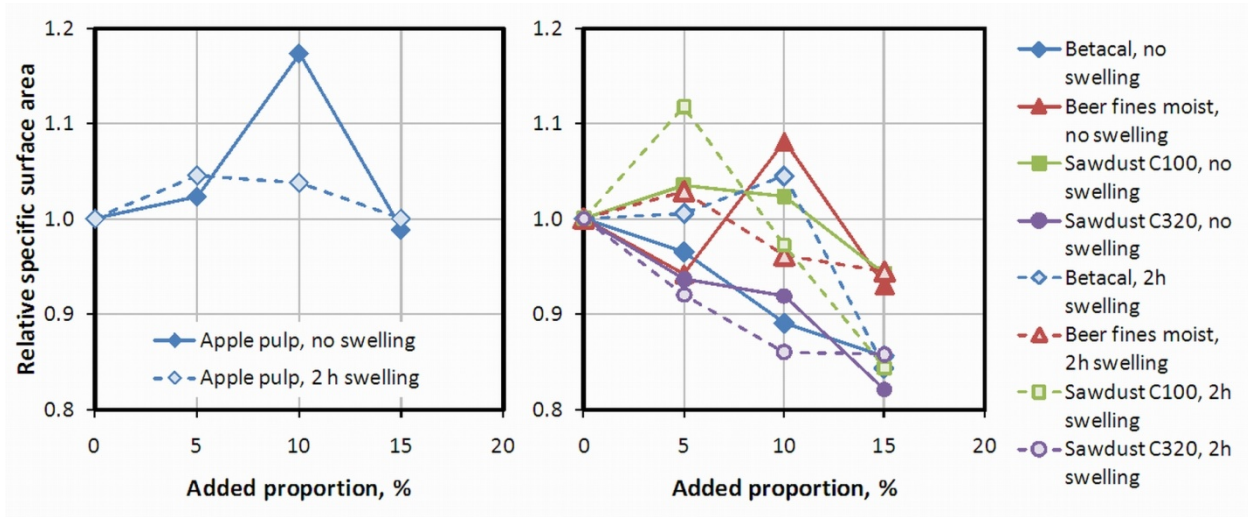
Figure 9. The effect of swelling on drainability depending on the added proportion of alternative pulps. Material increasing specific surface area (left), and material decreasing specific surface area without swelling (right). For relativization, the surface area of the pure reference pulp after 2h swelling (1.79 m²/g) was set as 1.

Swelling of sawdust even improved drainability for the lower added proportions (5%, and 10%). Further swelling of moist beer fines decreased the data deviation with falling tendency, and for sawdust C100, swelling was positive in the sense of dewatering improvement only at higher added proportions.

Due to the wide variation of material character in the pulp mixtures and the resulting high deviation in measuring data, the compression test was modified. Instead of the power function and the parameters m and n, only the compression graphs were interpreted (Figure 10).
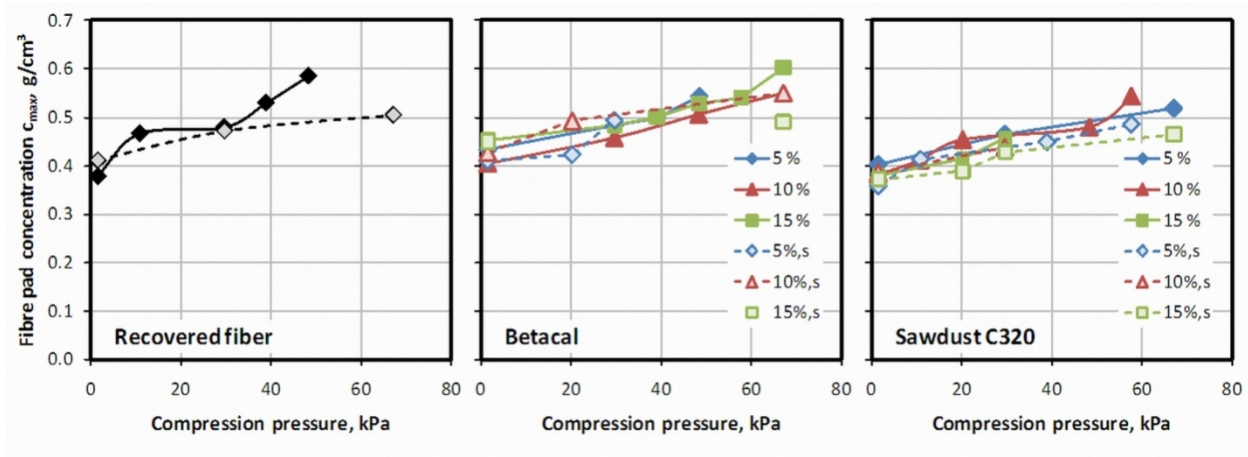
Figure 10. Compressibility behavior of pure recovered fiber (left), Betacal (center), and sawdust C320 (right), for different added proportions and affected by swelling (dotted lines)

The higher the compression pressure the larger is the reachable concentration of the fiber pad. Swelling decreases the compressibility of fibrous material, only smaller fiber pad concentration can be reached with the highest compression pressure. Figure 10 proves this basic knowledge. Besides the pure reference pulp (Figure 10 left), those samples were selected which had the best impact on dewatering. For Betacal (Figure 10 center), no significant difference between non-

swollen (solid lines) and swollen samples (dotted lines) was found. For the coarse sawdust C320 (Figure 10 right), swelling was always detrimental for the compressibility of the pulp mixture.

Conclusions

Permeability tests were found to be suitable laboratory trials to characterize the drainability and dewatering behavior of pulps. Alternative additives from bio-based industries could improve the dewatering to a certain extent. The interactions between the pure reference and the character of the alternative pulps – described by properties such as e.g. dimensions, dimensional distribution, moisture content, and chemical composition – have a high variability. The results show that not always the optimal trial parameters could be applied, but at least some of the alternative materials such as the sugar-based Betacal, the wooden sawdust, but also deinking sludge have a potential to adjust suitable dewatering properties for certain base pulps. Additionally, citrus pulp and probably also potato peelings have a chance for application in this sense.

Acknowledgment

References

Brecht W. and Schanz D. (1957): Attempt to characterize mechanical pulp fines by assessing its specific surface area. Wochenbl. Papierfab. 85(23): 891-898

Campbell N.F. (1965): The surface area of wood pulp. The Papermaker 150(2): 53-57, 61

Cowan W.F. (1970): Wet pulp characterization by means of specific surface, specific volume and compressibility. Pulp Paper Mag. Can. 71(9): 63-66

Das S., Cresson T. and Ramarao B.V. (2001): Pulp characterization using permeability measures: effect of refining. 6th Int. Conf. Pulp Refining, Toronto/ON, Canada. PIRA International, Leatherhead, Surrey, UK

Emerton R.W. (1955): The specific external surface of fibre – Some theoretical considerations. Pulp Paper Mag. Can. 56(2): 65-68

Forgacs O.L. (1963): The characterization of mechanical pulps. Pulp Paper Mag. Can. 64(C): T89-T118

Grén U. (1972): Compressibility and permeability of packed beds of cellulose fibres. Svensk Papperstidning 75(19): 785-793

Grén U. and Hedström B. (1967): Fluid flow and pressure drops in thick beds of cellulose fibres. Svensk Papperstidning 70(10): 339-346

Han S.T. (1969): Compressibility and permeability of fibre mats. Pulp Paper Mag. Can. 70(5): T134-T146

Heinemann S. (1985): Contribution to determine the mass-specific surface area and its effect on strength behavior of pulps. Doctoral Thesis, Dresden University of Technology, Faculty of Engineering

Heinemann S. (2010): Hydrodynamic specific surface area, Lecture material PAPHYS, Part 6.2, Dresden University of Technology/VTT Finland

Ingmanson W.L. (1953): Filtration resistance of compressible materials. Chemical Engineering Progress, 49(11): 577–584

Ingmanson W.L. and Andrews B.D. (1959): The effect of beating on filtration resistance and its components specific surface and specific volume. Tappi J. 42(1): 29-35

Ingmanson W.L. and Andrews B.D. (1963): High-velocity water flow through fiber mats. Tappi J. 46(3): 150-155

Judasz A. (2009): Estimation of impact of alternative papermaking additives on paper web dewatering intensity and paper properties. Master Thesis, Institute of Papermaking and Printing, Lodz/Poland

Judasz A. and Heinemann S. (2009): The effect of alternative additives on the hydrodynamic surface area and volume. STSM-Report within COST Action E54 "Characterization of the fine structure and properties of papermaking fibres using new technologies"

Kozeny J. (1927): About capillary flow of water through soil0 Meeting report of Austrian Academy of Science, IIa, 136, 271-306

Kumar P. and Ramarao B.V. (1995): Characterization of specific surface area, specific volume, compressibility and specific filtration resistance of papermaking pulps. Proc. TAPPI Papermakers' Conf., 465–488

Labreque R.P. (1968): The effect of fiber cross-sectional shape on the resistance to the flow of fluids through fiber mats. Tappi J. 51(1): 8-15

Ljungkvist K. (1983): Pulp characterization by permeability measurements. Doctoral Thesis, Chalmers University of Technology Göteborg, Sweden

Mason S.G. (1950): Specific surface of fibers – Its measurement and application. Tappi J. 33(8): 403-409

Ramarao B.V. (1999): Method and apparatus for determining pulp permeability and compressibility for controlling papermaking process. US Patent 5,954,922. September 21, 1999

Robertson A.A. (1957): A note on the permeability method for determining surface development and swelling during beating and refining. In: Bolam, F. Fundamentals of papermaking fibres, Transactions of the FRC Symposium in Cambridge, UK

Robertson A. and Mason S.G. (1949): Specific surface of cellulose fibres by the liquid permeability method. Pulp Paper Mag. Can. 50(13), 103-110

Schweizer G. (1975): Study about characterization of fibrous material for paper manufacturing by its specific surface area. Das Papier 29(1): 9-15

Thode E.F. (1959): Factors contributing to the strength of paper. Tappi J. 42(1): 74-83

Unger E.-W., Heinemann S. and Strassberger K. (1983) Apparatus to determine specific surface area of coarse disperse material systems. Former GDR Patent 224 941, November 3, 1983

Unger E.-W. and Heinemann S. (1983a): Comparing investigations of different methods for determining the specific surface area of fibers from pulp slurries. Zellstoff und Papier 32(4): 154-157

Unger E.-W. and Heinemann S. (1983b): Contribution to model the paper strength from morphological pulp properties. Zellstoff und Papier 32(2): 50-55

Wang J., Hrymak A.N. and Pelton R.H. (2002): Specific surface and effective volume of water-swollen pulp fibers by a permeability method0J. Pulp Pap. Sci. 28(1): 3–16

Wilder H.D. (1960): The compression creep properties of wet pulp mats. Tappi J. 43(8): 715-720

Yan J.F. and El-Hosseiny F. (1978): Freeness, specific surface and drainage time of pulps. Tappi J. 61(8): 89

BEHAVIOUR OF CELLULOSE FINE STRUCTURES IN PAPERMAKING TESTS

[1]Tiemo Arndt, Gert Meinl, Klaus Erhard

[1]Papiertechische Stiftung, Pirnaer Str. 37, 01809 Heidenau;

E-mail: tiemo.arndt@ptspaper.de

Abstract

In this work the influence of microfibrillated cellulose (MFC) on sheet forming and final paper properties was investigated. In order to reveal more information about the behaviour of these cellulose fine structures a top-down approach from macro-scale to nano-scale was used based on the fibre morphology, dewatering properties and the Page equation. A hydrodynamic specific surface area (SSA) of 182.79 m²/g was calculated for MFC. By addition of 5% MFC to the refined pulp the surface area of the pulp increased from 3.6 m²/g to 12.56 m²/g. Derived from SSA, the retention of MFC was estimated to be 63.5%. In connection with the paper properties measured, it was concluded that behaviour and effectiveness of MFC are not comparable with fines produced during refining because only a minor increase in apparent density was observed due to MFC. However based on the simplified reference fibre network, the bonding strength between fibres was calculated to be 9 MPa for an addition of 5% MFC, which is twice as much as for the pulp starting material.

Introduction

The paper strength is influenced, among other parameters, by the fine structure of pulp fibres. The most frequent method in papermaking to change the fine fibre structure is refining. Fibre fibrillation takes place during refining and increases the surface area of fibres. At the same time different types of fine structures are produced. This influences not only the final paper strength but also optical properties and dewatering properties during sheet forming. The common definition of fines is the fraction that passes through a 200 mesh screen. The largest fines particles are fibre fragments and the smallest are fibrils, whose size can be below 1μm. Depending on the pulp source and treatment the chemical and structural properties of the fines are different. Chemical pulps contain primary fines, which are small particles originally present in the wood, such as, shortened fibres, vessel elements, and secondary fines produced during refining. The content of the primary fines in unrefined pulp is in the range of 2-4%. They have a specific surface area of about 4-6m²/g. The content of secondary fines increases during refining up to 20%. Retulainen et al. (2002) have characterised and analysed secondary fines with BET (Brunauer et al. 1938) and found that the specific surface area of freeze dried bleached softwood kraft fines was in the range of 15-25 m²/g. Also mechanical pulps contain fine particles, which are produced during the mechanical pulping process. These fines particles are lignin containing material peeled out of the middle lamella. Because of their small size and large surface area particularly secondary fines produced in the refining can bind more water and swell more. In this work the influence of micro-fibrillated cellulose (MFC) as a special cellulosic fine material on sheet forming and final paper properties was investigated. This MFC is completely different to common known pulp fines, because of their much smaller size on the connected material properties. MFC was invented in the early 1980-ies by Herrick (1983) and Turbak (1983) by mechanical disintegration of the fibre wall down to the cellulose fibril aggregates as building blocks of the fibre wall. Since that time many patents and applications were introduced based on MFC. However due to the high energy consumption during homogenization of the fibre wall, the preparation of MFC has so far been of limited interest in view of large production costs. In recent years main breakthrough to reduce the energy consumption was made by Lindström and

co-workers (2007) by improvement of the pulp preparation before final homogenization. Today MFC is one of the most interesting nano-materials not only in the papermaking science community, but also in composite materials.

Although MFC is also cellulosic fine material from the fibre wall, this material is completely different compared with primary and secondary fines, because MFC is a fibrillar network of entangled fibrils. The size of the fibrils varies in a broad wide range from 20-30 nm in width, but also larger fibril bundles are present. Alince et al. (2002) compared the behaviour of MFC with fines of high and low specific surface area and microcrystalline cellulose on paper properties. The obtained results indicated that the improvement in strength properties is much higher with MFC. Particularly on bleached kraft pulp a different effectiveness was observed, because the light scattering coefficient was almost unaffected by MFC in contrary to other fines, where an increased light scattering coefficient indicated that a higher relative bonded area (RBA) is responsible for the improvement in strength properties. Due to the nano-scale level and the similarity of MFC to other fines and fibres it is difficult to characterize the effectiveness of MFC in sheet forming. In order to reveal more about the effectiveness and the interaction of MFC with fibres, a top-down approach was used supported by model assumption and calculation methods. The bonding strength was calculated based on the PAGE equation and also the hydrodynamic mass-specific surface area (SSA) of the MFC was calculated.

Materials and methods

Raw materials

A mixture of dried bleached hardwood and softwood pulp (ratio 5:1) where used as pulp source together with 2% suspension of micro-fibrillated cellulose (MFC) delivered by Innventia, Sweden. The MFC was prepared according to Pääkkö et al. (2007). In order to support the retention of fines and MFC, a retention aid based on a high molecular polyethylenimine (PEI) was used.

Technical methods

The dried market pulp was disintegrated 15 minutes in 40°C water at a consistency of 5%. The obtained pulp suspension was refined in a pilot refiner at a consistency of 4% with a specific refining energy of 65 kWh/t and at a specific edge load of 0.1 Ws/m. After refining the fibre dimensions were analyzed with a FiberLab™ 3.0 device. A special method was used to characterize the fibre fraction and dimensions of collapsed and dried fibres in the fibre network according to Meinl and Erhard (2006). Sheets were formed in a Rapid Köthen former according to ISO 5269-2 at a consistency of 0.3%. The MFC used was stirred for 10 minutes at 2 g/l consistency and treated with an ultra-turrax blender for 2 minutes. MFC were added to the stock container of the Rapid Köthen sheet per sheet, to a pulp consistency of 0.3%. When PEI was used as retention agent, it was also added in the stock container after the MFC addition. Before sheet forming the SR value was measured. The dried sheets were characterized according to standard methods for light scattering coefficient S_y, Scott bond z-strength, apparent density, tearing resistance, tensile index, and air permeability.

Mathematical methods

For calculation the mass-specific surface area (SSA) an empirical formula was used based on the SR value.

$$SSA = c_{SSA} \cdot \sqrt{\frac{SR - 4}{100 - SR}} \qquad (1)$$

The factor c_{SSA} is about 6.24 when applying known corresponding values of SR and SSA from Heinemann (1985 and 2001). Equation 2 is only valid if no chemical additives are used which could influence the pulp viscosity. The SSA value is additive. If SSA_{Pulp} / SSA_{MFC}, are the specific surface areas of the pulp / microfibrillated cellulose and w_{MFC} is the mass-weighted MFC share then the specific surface area SSA_{MFC}:

$$SSA_{MFC} = \frac{SSA_{Total} - (100\% - w_{MFC}) \cdot SSA_{Pulp}}{w_{MFC}} \qquad (2)$$

To estimate the relative bonded area (RBA) - a critical value for applying the Page equation - in a given sheet, one can use a regular fibre network reference which is made up of the same fibres and which has the same apparent density like the original fibre network. The RBA was assumed as ratio between bonded area (A_B) and total area (A_T) in accordance with the following equation:

$$RBA = \frac{A_B}{A_T} = \frac{4D^2}{4d \cdot D + 4d \cdot H} \qquad (3)$$

The values D (diameter) and H (height) of the collapsed and dried fibres in the network were calculated by using the fibre morphology data from the FiberLab™ 3.0 according to Meinl and Erhard (2006). We have yet to calculate the distance d (distance of neighbouring fibres in a layer, which equals the length and width of the elementary cell) according to Equation 4. This Equation ensures that the apparent density of the elementary cell equals the apparent density ρ of the sheet.

$$d = \frac{D \cdot \rho_W}{AD} \qquad (4)$$

Bonding strength b can now be calculated via the Page equation (Equation 5, Page 1969) for given values of mean fibre length FL, tensile index T and zero-span tensile index ZI. The cross sectional fibre area A_{CSA} equals $D \cdot H$ and the fibre perimeter P equals $2(D+H)$. For the Zero-span tensile index a value of 150 Nm/g was assumed.

$$\frac{1}{T} = \frac{9}{8ZI} + \frac{12 \cdot A_{CSA} \cdot \rho_W}{b \cdot P \cdot FL \cdot RBA} \qquad (5)$$

Results and Discussion

The sheet properties are listed in Table 1. As expected the dewatering of the pulp mat decreased. The SR dramatically increased from 28 to 86 with 5% MFC. The addition of PEI caused agglomeration of MFC and fines on the fibre surface and helped to reduce the SR. At the same time the strength properties were improved to the same extend. But it is obvious that not all MFC had been retained in the paper sheet, because the PEI containing sheets were always higher in strength properties in comparison with non PEI containing sheets due to better fines and MFC retention. The tensile index increased up to 70% and also the Scott bond z-strength increased up to 170% in comparison with the reference pulp. However one can see that the apparent density

was almost unaffected. That indicates that the strength improvement was not due to a higher RBA as usually expected from common fines. By contrast the light scattering S_y as an indicator for the unbonded area was reduced.

Table 1. Sheet properties of MFC containing papers

MFC	%	0	0	1	3	5	1	3	5
PEI on dry pulp	%	0	0.25	0	0	0	0.25	0.25	0.25
Schopper Riegler		28	28	44	68	86	32	55	77
Density	g/cm³	0.61	0.59	0.60	0.62	0.66	0.62	0.63	0.66
Air permeability	ml/min	1873	1924	603	185	25	1203	214	19
Tensile-Index	Nm/g	36.7	37.9	44.1	49.4	57.0	42.1	50.5	62.3
Internal bond type "Scott Bond" [1]	J/m²	229	305	345	421	453	223	463	551
Tearing resistance	mNm/m	1275	1349	1447	1533	1724	1422	1576	1833
Light-scattering coeff.	m²/kg	40.6	39.1	39.8	37.1	34.3	40.3	36.8	33.6

1) e.g. according to TAPPI standard T569

In order to reveal more about the effectiveness of MFC the SSA was calculated based on the dewatering properties. In Table 2 the results for calculation of the SSA is listed. It is obvious the SSA of the whole pulp had been increased by MFC. With 5% MFC the SSA of the pulp was 12.6 m²/g. This value is in a range usually obtained only by intensive refining. The increase shows that with MFC more OH-groups are available for forming more H-bonds between the pulp fibres. The SSA of the MFC was around 170.7 - 182.8 m²/g. This value is consistent in comparison with other authors working with nanofibrillar cellulose aerogels. Hoepfner et al. (2008) estimated the BET surface area of freeze dried MFC at 160 m²/g and by supercritical drying in the range of 200-220 m²/g.

Table 2. Mass-specific surface area (SSA) of pulp and MFC

W_{MFC}	SR_{Total}	SSA_{Total}	SSA_{MFC}
%		m²/g	m²/g
0	28	3.6	-
1	44	5.3	170.7
3	68	8.8	177.7
5	81	12.6	182.8

Furthermore the influence of MFC on bonding strength b between the fibres was calculated according to (Eq. 5). The bonding strength for the reference pulp was calculated to be 4.76MPa. With 5% MFC the bonding strength increased to 9MPa. As mentioned above PEI as retention agent improved the retention of MFC. This is also obvious in the bonding strength, where the b was calculated to be 10.62. In Figure 1 the calculated bonding strength was plotted against the Scott bond z-strength often used for describing the bonding degree in the paper sheet. It is obvious there is a clear correlation between these two different approaches to estimate the bonding properties. This indicates that the applied method for calculating the bonding strength is useful to describe the bonding behaviour of MFC containing paper sheets. The results suggest that the high surface area and the available OH-groups led to much more H-bonds between the fibres in their contact areas. This can explain why the density and bulk properties were retained by application of MFC.
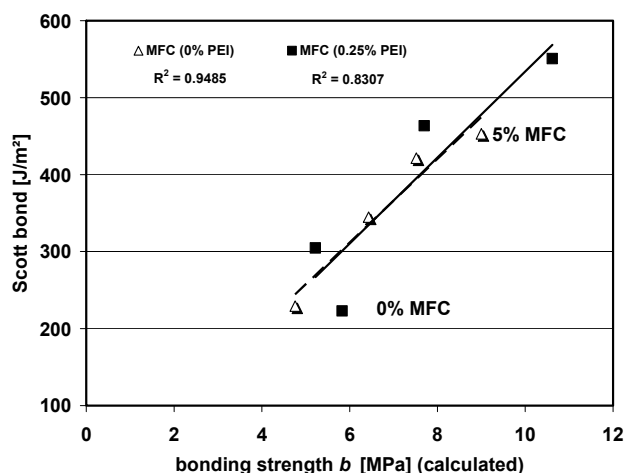
Figure 1.Ccalculated bonding strength in comparison to Scott bond z-strength

Conclusions

The high specific surface area SSA of the MFC led to an improved interaction of fines and fibres. Increased number of H-bonds gave increased bonding strength. It may be concluded that the bonding strength is not only improved, because of a higher bonding area due to a better fines retention, but also by a higher number of H-bonds in the contact areas. However the behavior of MFC is ambiguous and difficult to explain, because the decrease in light scattering properties indicates an increase in RBA, mostly connected to an increase in apparent density. But this was not observed.

Acknowledgement

References

Alince B., Porubská J. and van de Ven T.G.M. (2002): The Science of Papermaking 12th Fund. Res. Symp., Oxford and Cambridge Series. 1343-1355

Brunauer S., Emmett P.H. and Teller E. (1938): Adsorption of gases on multimolecular layers. J. Am. Chem. Soc. 60(2) 309-319

Herrick F.W., Casebier R.L., Hamilton J.K. and Sandberg K.R (1983): Microfibrillated cellulose: morphology and accessibility. *In*: A. Sarko *(Ed.)*. Proc. Ninth Cellulose Conf. Applied Polymer Symp. 37. New York City: Wiley. pp. 797–813. ISBN 0-471-88132-5

Heinemann S. (1985): Contribution to determine the mass-specific surface area and its effect on strength behavior of pulps. Doctoral Thesis, Dresden University of Technology, Faculty of Engineering

Heinemann S. (2001): Evaluation of Specific Surface – History or new opportunity? Int. Mech. Pulping Conf., Helsinki 2001, Finland

Hoepfner S., Ratke L. and Milow B. (2008): Synthesis and characterisation of nanofibrilar cellulose aerogels. Cellulose 15 (1), 121-129

Lindström T., Ankerfors M. and Henriksson G. (2007): Method for the manufacturing of microfibrillated cellulose. Patent Int. Publ. No.WO 2007/091942 A1

Meinl G. and Erhard K. (2006): Use of numerical models for simulation of refining behaviour and resulting paper properties. 9th PIRA Int. Ref. Conf., 22-23 February 2006, Vienna, Austria

Page D.H. (1969): A theory for the tensile strength of paper. Tappi J. 52 (4), 674-681

Pääkkö M., Ankerfors M., Kosonen H., Nykänen A., Ahola S., Österberg M., Ruokolainen J., Laine J., Larsson T., Ikkala O. and Lindström T. (2007): Enzymatic hydrolyis combined with mechanical shearing and high-pressure homogenization for nanoscale cellulose fibrils and strong gels. Biomacromolecules 8 (6), 1934-194

Retulainen E., Luukko K., Fagerholm K., Pere J., Laine J. and Paulapuro, H. (2002): Papermaking quality of fines from different pulps: the effect of size, shape and chemical composition. Appita J. 55 (6), 457-460

Turbak A.F., Snyder F.W. and Sandberg, K.R (1983): Microfibrillated cellulose, a new cellulose product: Properties, uses and commercial potential. J. Appl. Polym. Sci.: Appl. Polym. Symp. 37: 815-827

STRUCTURAL AND MORPHOLOGICAL CHARACTERIZATION OF UNMODIFIED AND GRAFTED UNBLEACHED AND BLEACHED SOFTWOOD KRAFT PULP FIBERS

[1]Carmen-Mihaela Popescu, [1]Marian I. Totolin, [2]Carmen Mihaela Tibirna,

[1]Maria-Cristina Popescu, [3]Paul Ander and [1]Cornelia Vasile

[1] Romanian Academy "P.Poni" Institute of Macromolecular Chemistry, 41A Gr. Ghica Voda Alley, Ro.700487, IASI, Romania

[2] Laval University, Département de Génie Chimique, Faculté des Sciences et de Génie, Sainte-Foy, Québec (Québec) G1V 0A6 Canada.

[3] Department of Forest Products / Wood Science, Swedish University of Agricultural Sciences, Uppsala, Sweden

E-mail: cvasile@icmpp.ro
mihapop@icmpp.ro

Abstract

The processing of wood determines some structural modifications in its components, depending on wood type and on applied procedure. The ATR-FT-IR and XPS results supported the idea that the amount of oxygen atoms was higher on the surface of the bleached kraft pulp fibers than on the unbleached kraft pulp fibers. The decrease in the O/C ratio and the increase in the C_{ox}/C_{unox} suggest the removal of the carbon-containing compounds from the pulp fiber surfaces at bleaching.

The grafting degrees were of about 15 % and 56 % for unbleached kraft pulp grafted with butyric acid and oleic acid, and about 3% and 9 % for bleached kraft pulp grafted with butyric acid and oleic acid, respectively.

The differences between unbleached, bleached and grafted softwood kraft pulp fibers were dependent on the characteristic temperatures and mass losses during various thermogravimetric steps, and to the overall activation energies of decomposition.

Introduction

Pulp is a fibrous material prepared by chemically or mechanically separating fibers from wood, fiber crops or waste paper. Wood pulp is the most common material used to make paper. The pulp produced can be bleached to give a white paper product. The chemicals used to bleach pulp have been a source of environmental concern, and in the early 1990s the pulp industry abandoned chlorine, and are now using chlorine dioxide, oxygen, ozone, hydrogen peroxide (Gellerstedt 2003) and enzymes (Viikari and Lantto 2002) for pulp bleaching. Paper made from bleached kraft or sulfite pulps does not contain significant amounts of lignin and is therefore better suited for books, documents and other applications where high brightness of the paper is essential.

Risen et al. (2004) showed that the surface of softwood and hardwood kraft pulp fibers contain larger lignin and extractive amounts than in the fiber walls. Chemical esterification of cellulose with fatty acids in special solvents, in the presence of acid chlorides, pyridine and trifluoroacetic

acid was developed by Vaca-Garcia et al. (1998). In such cases, the pollution is high, so a physical functionalization of vegetable fiber was recommended by Ludwick et al. (2002). Cold plasma (low temperature and low pressure) technique appears as a useful and suitable technique to: (a) increase wettability of the treated surface; (b) increase surface adhesion of different coating lacquers and binders; (c) render the surface hydrophilic or hydrophobic, e.g. compatibilization of the material with non-polar matrices such as polypropylene; (d) to stabilize wood against weathering; (e) to induce grease barrier properties.

The present paper deals with characterization of the structural, morphological and thermal properties of softwood kraft pulp fibers for elucidating, on a molecular basis, the differences observed after pulp bleaching and grafting.

Materials and methods

The ***unbleached (UBP) and bleached (BP) softwood kraft pulps,*** delivered to the partners of the COST Action E54, were commercial batch cooked pulps, supplied by Södra Cell, Sweden. The spruce (*Picea abies*) to pine (*Pinus sylvestris*) ratio was 79:21. The unbleached pulp was sampled after the oxygen delignification stage. The bleaching sequence was Q-OP-Q + Paa-PO, where Q represents the chelating agent; OP is oxygen + peroxide and Paa is peracetic acid. The kappa numbers were 26.8 for unbleached and 3.2 for bleached pulps. Different working groups involved in COST Action E54 have determined the pulp properties. The average properties of the unbleached and bleached kraft pulps are presented in Table 1.

Table 1. Properties of softwood kraft pulp fibers

Property	Unbleached	Bleached
Wall thickness, μm	8.2	7.8
Intrinsic viscosity, ml/g	1109	728
Kappa number	26.8	3.2
Dry matter content, %	32.3	32.8
Bulk density, cm^3/g	1.9	1.79
Tensile strength, kN/m	1.92	1.74
Stretch, %	2.1	3.4
Tensile energy absorption, J/m^2	30.9	47.3
Tensile stiffness, kN/m	296	241
Modulus of elasticity, N/mm^2	2420	2129

The ***butyric (BA) and oleic (OA) acids*** used for fibers impregnation were purchased from Merck and Aldrich, respectively. The experimental set-up for ***cold plasma fiber grafting*** has been previously presented (Totolin et al. 2008). The ***investigation methods*** applied were both bulk and surface characterization methods. The *bulk methods* of characterization were the following: FT-IR spectroscopy, X-ray diffraction, differential scanning calorimetry and thermogravimetry (see also Popescu et al. 2008; Totolin et al. 2008), while the *surface methods* were: ATR FT-IR spectroscopy, X-ray photoelectron spectroscopy (XPS) and scanning electron microscopy.

Results and Discussion

Bulk characterization of softwood kraft pulp fibers before and after grafting FT-IR spectroscopy

Figure 1 shows the IR spectra and their second derivative in the 3800-2700 cm^{-1} region of unbleached and bleached pulp fiber samples. In this region the bands have lower intensities in the spectrum of the bleached pulp fiber than in the unbleached one. The most significant

absorbance bands in the 3800-2700 cm^{-1} region are those assigned to valence vibrations of the OH groups forming inter- and intramolecular H–bonds in pulp fiber samples and to valence vibration of the C-H groups.
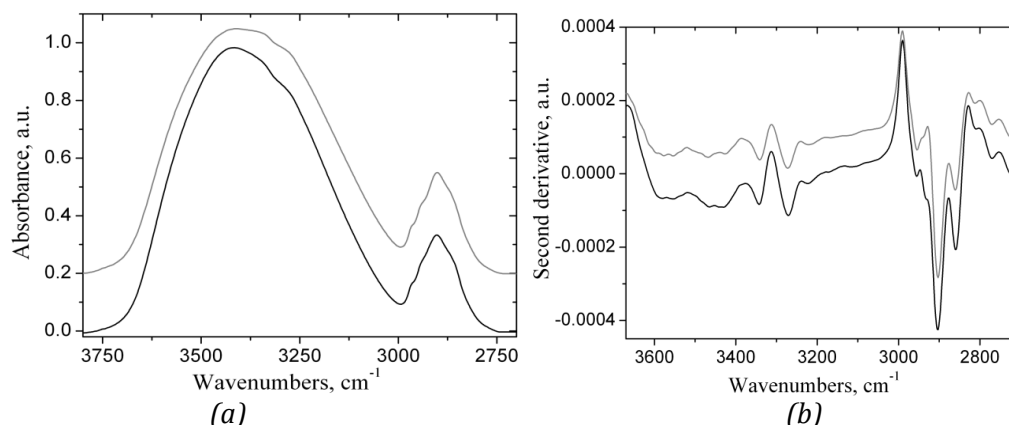

Figure 1. FT-IR spectra (a) and second derivative (b) in the 3800-2700 cm^{-1} of the studied samples: unbleached (black line) and bleached (grey line) kraft pulp fibres

A broad band, with a maximum around 3410 cm^{-1}, was observed in the spectrum of the unbleached pulp sample. The intensity of this band decreased after bleaching. These observations reflect variations in the hydrogen-bond structure of cellulose after bleaching. At least six peaks were identified in the second derivative spectra in the 3700-3000 cm^{-1} region. According to literature data, an intramolecular hydrogen bond vibration, derived from O2–H2···O6, could be expected between 3460 and 3410 cm^{-1}. As the O2–H2···O6 distance is larger than that of the O5–H5···O3 intra-molecular bonded system, this appeared at a higher frequency. A strong band was found in this range, emphasizing that the O5–H5···O3 hydrogen bonds have a smaller influence on load distribution. In kraft pulp fibres, two bands were found in this region, at 3462 and 3431 cm^{-1}. The inter-chain hydrogen bonds, involving the C6 position (primary hydroxyl groups), result in the formation of crystalline regions and contribute to the O-H band at 3430 cm^{-1}. In addition, the fact that the maximum wavenumber for the O-H stretching band was below 3400 cm^{-1} indicates that the crystalline domains in both samples have a type I lattice. These bands shifted to 3469 and 3425 cm^{-1} in the spectrum of the bleached pulp. The frequencies for the O5–H5···O3 intramolecular hydrogen bonds were between 3350 and 3375 cm^{-1}, while in the spectra of kraft pulp fibres, they occurred at 3345 cm^{-1}. A shift to lower frequencies can probably be explained by the stretching of cellulose molecules, parallel to the main fiber direction. Both bands of cellulose I were found at slightly lower frequencies in the pulp fiber spectra, at 3267 cm^{-1} for cellulose Iβ and at 3222 cm^{-1} for cellulose Iα, as shown in Figure 1. The O–H stretching region was deconvoluted into Gaussian profiles, which allows comparing the band positions between spectra, when the band widths and the extent of the overlap differ (Figure 2).

Table 2. Energy of hydrogen bonding for the unbleached and bleached pulp samples

Sample	Energy of the hydrogen bonds (E_H) (kJ/mol)					
	3565 cm^{-1}	3465 cm^{-1}	3430 cm^{-1}	3350 cm^{-1}	3269 cm^{-1}	3222 cm^{-1}
Unbleached	6.08	13.44	15.66	21.74	26.67	30.61
Bleached	6.65	12.94	16.09	21.18	26.60	30.61

After deconvolution as seen in Figure 2, six O–H stretching bands were identified and used to calculate energy (Table 2; Struszczyk 1986) and hydrogen bonding distance. The calculated

energies (Table 2) were higher for both hydrogen bonds of the free OH and O2–H2···O6 intra-molecular H–bonds in cellulose for the bleached pulps. The hydrogen bonding distances values were the same in both samples for all six types of H–bonds from cellulose.
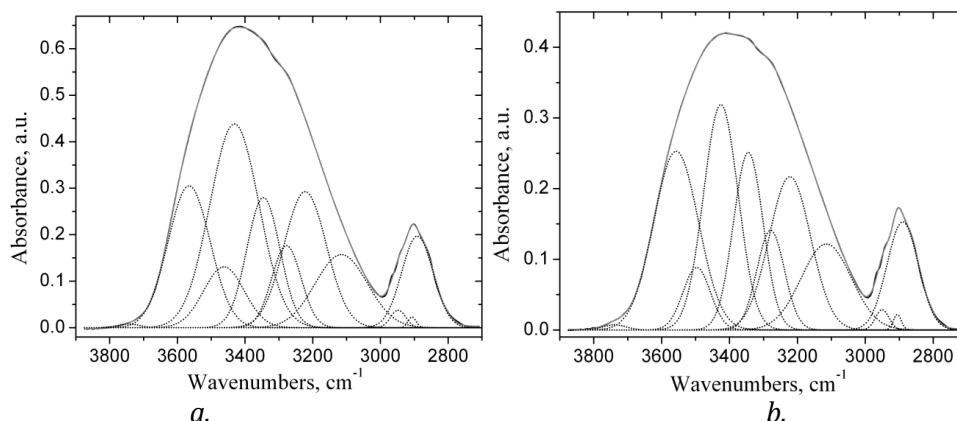

Figure 2. Deconvoluted spectra of the 3800-2800 cm^{-1} regions for unbleached (a) and bleached (b) pulp samples

In the "fingerprint region", the spectra of the pulp samples were very complex, containing many bands assigned to cellulose and to the residues of lignin and hemicelluloses - Figures 3a and b. In normal spectra of kraft pulp fibers, small differences could be observed.

The occurrence of low intensity bands at 1694, 1586, 1512, 1406 and 1259 cm^{-1} is undoubtedly due to the presence of small amounts of lignin in a fiber preparation with complex composition. The band at 1694 cm^{-1} indicates a C=O stretching in unconjugated ketones, carbonyl and ester groups, while the bands at 1586 and 1512 cm^{-1} indicate the aromatic skeleton vibrations in lignin. Also, syringyl and guaiacyl ring and CO stretching appears at 1259 cm^{-1} and CH$_2$ scissoring at 1406 cm^{-1}. All these bands are very small in the spectrum of bleached pulp fibers, indicating a very low amount of lignin in this sample. The absorbancies at 1453, 1373, 1340, 1318, 1282, 1163, 1128, 1113, 1069, 1032 and 1000 cm^{-1}, seen in both spectra, are associated with different stretching vibrations or deformations in cellulose and hemicelluloses. These bands decreased after bleaching, meaning that hemicelluloses were removed during bleaching. A confirmation that both samples have a type I cellulose lattice is supplied by the wavenumber of the CH$_2$ scissoring mode at 1428 cm^{-1}.
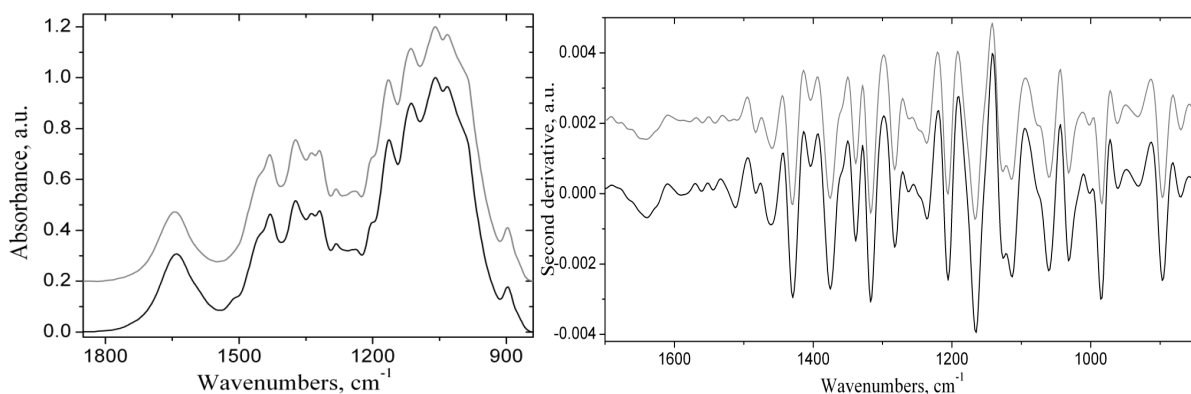

Figure 3. FT-IR spectra (left) and second derivative (right) at 1800-800 cm^{-1} of the studied samples: unbleached (black) and bleached (grey) kraft pulp fibers

The crystallinity values of both samples from FT-IR spectra were estimated by a rapid method, proposed by Hulleman et al. (1994) for cellulose I, based on the observation that the band at 1280 cm^{-1}, assigned to the C–H bending mode, increases with increasing crystallinity, whereas the band assigned to the C–O–C stretching mode of the pyranose ring, at 1200 cm^{-1}, is sensitive to that parameter. The ratio between the absorption intensities of these two bands ($R_{c,h}=I_{1280}/I_{1200}$) was used to determine cellulose crystallinity. This correlation is valid only over the $0.26 \leq x_c \leq 0.75$ range, expressing the limits of cellulose crystallinity used by Hulleman et al. (1994). The values obtained were $56 \pm 1\%$ and $58 \pm 1\%$ for unbleached and bleached pulp fibers, respectively.

In case of pulps grafted with butyric acid the IR spectrum was approximately the same as that for untreated sample. This fact indicates a low amount of butyric acid grafted upon the pulp fiber surfaces. The effect of plasma treatment can be assessed by observing the 1715 and 1610 cm^{-1} bands. The intensities of the two peaks increased after plasma grafting with fatty acids especially in the case of oleic acid. The increase of the grafted amount results in an increase of the intensities of the peaks 1735 and 2855 + 2923 cm^{-1}. The integrated intensities of the peak 1735 cm^{-1} can be used to predict the percentage of grafting. These are 16.13 % for UBP and 13.97 % for BP, increasing up to 17.74 % for UBP+BA, 37.08 % for UBP+OA and 14.44 % for BP+BA, 16.32 % for BP+OA, respectively. Thus, considering the values of these integrated intensities of the bands, the grafting degrees were estimated to be about 15 % and 56 % for UBP+BA and UBP+OA, and at about 3% and 9 % for BP+BA and BP+OA, respectively.

X-Ray diffraction (XRD)

Isogai et al. (1994) established that cellulose I, typically shows peaks at 2θ of 15, 16.5 and 23° due to (101), (10Ī) and (002) reflections, respectively. A shoulder at 2θ of 20° due to (102) reflection was also noted by Rowland (1974) and Kumar (1999) in certain cellulose materials. The X-ray peaks at 2θ of 15° and 2θ of 16.5^o merged into a broad band, which is consistent with literature data.

The unbleached and bleached softwood kraft pulp fibers display typical X-ray pattern of cellulose I - Figure 4. The peak for the (002) plane in the intensity profiles of the bleached pulp fibers became sharper than that of the unbleached one, and the shoulder at around 20° has a tendency to increase in intensity during bleaching. In order to examine the intensities of diffraction bands and to establish the crystalline and the amorphous areas more exactly, the diffractograms were deconvoluted using Gaussian profiles.
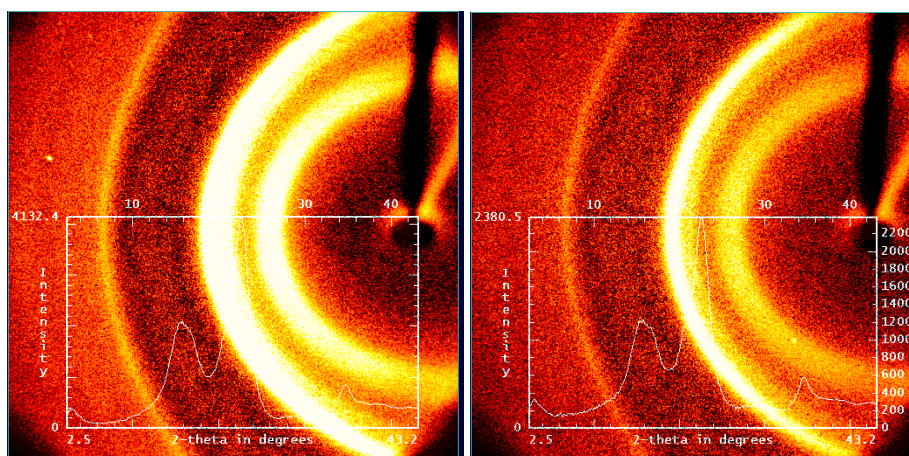

Figure 4. X-ray diffractograms of unbleached (left) and bleached (right) wood pulp samples

After deconvolution, five bands were observed, namely: one around 2θ of 15.2-15.5° reflection assigned by Silva et al. (2008) and other researchers to the (101) crystallographic plane, the 2θ = 16.8-17.0° reflection, assigned to the (10Ī) crystallographic plane, the 2θ = 18.8° reflection, assigned to amorphous phases, the 2θ = 20.6° reflection, assigned to the (102) crystallographic plane, and the 2θ = 22.6° reflection, assigned to the (002) crystallographic plane of cellulose I. The position of the peaks of cellulose crystalline form I, were found to be slightly shifted to higher theta degree in bleached pulp fibers than in unbleached pulp fibers indicating a decrease in d-spacing.

In Table 3 the calculated parameters for the studied samples are presented. The degree of crystallinity (CrI) using both FT-IR spectroscopy and X-ray diffraction was found to increase slightly after bleaching. The more crystalline the cellulose is, the larger the microfibril lateral size is. On the other hand, values determined by SEM were six times higher, even for samples which appear to be single microfibrils, which might suggest that in fact they are composed of several individual microfibrils.

Table 3. The calculated parameters for the studied samples

Parameters	Unbleached	UBP+ OA	Bleached	BP+OA
Cr. I.	60	57	62	59
Cr. I'	56	--	58	--
L101 (nm)	3.26	3.29	3.36	3.39
L10Ī (nm)	5.57	5.96	5.86	5.97
L002 (nm)	4.08	4.76	4.18	4.36
X	0.52	0.57	0.53	0.55
Cellulose fraction	0.86	0.81	0.88	0.84

Cr.I – crystalline index evaluated by XRD, Cr.I' - crystalline index evaluated by FT-IR spectroscopy, L - apparent crystallite size, X - proportion of crystallite interior chains

The observed lower values of the apparent crystallite size for unbleached pulp fibers as compared with bleached pulp fibers may be due to the presence of defects in the crystalline region of the cellulose fiber. Increase in the apparent crystallite size of cellulosic particles after bleaching may indicate that the number of small crystallites decreased, resulting in improvement of the crystallinity of the fiber. The full width at half maximum of the diffraction peaks decreased after bleaching for all deconvoluted bands.

As seen in Table 3, both determination methods show that the degree of crystallinity (CrI) decreased after plasma grafting and was much more important for unbleached pulp fibers grafted with oleic acid affecting also the bulk morphology. For the bleached pulp fibers the effect of grafting was less obvious for the small size alkyl chain such as butyric acid than for oleic acid with C-18 alkyl chain. The comparison of bleached versus unbleached pulp is interesting since the difference in crystallinity of the initial samples can be attributed to the residual lignin (presence as fine particles) which becomes particularly evident when comparing the crystallinity of grafted unbleached and bleached pulp samples.

Thermogravimetry

The mass loss (TG) and derivative (DTG) curves of unbleached, bleached and grafted softwood pulp fibers are shown in Figure 5. The degradation characteristics of pulp fibers can be quantified through several parameters, which are related to the temperature ranges of the different steps of mass loss and residual yield as given in Table 4.

In general, TG/DTG curves have two steps of mass loss, easily observed from DTG curves. The first step seen in Figure 5 corresponds to loss of physically or chemically bound water and certain volatile substances. In Step I, combustion of hemicelluloses and amorphous and crystalline cellulose and also complete combustion of residual compounds and lignin occurs. The first process occurs from 45°C to 150°C with maximum at 76°C for unbleached pulp and 59°C for bleached pulp (Step I in Table 4). The mass loss was about 2.1 wt % for unbleached pulp fibers and larger for bleached ones. As the temperature increased the mass remained constant until 210°C at beginning of the thermal degradation. The main mass loss was obtained in the 210-425°C temperature range for unbleached pulp and at 200-420°C for bleached pulp (Figure 5 and Table 4) as a consequence of cellulose decomposition.
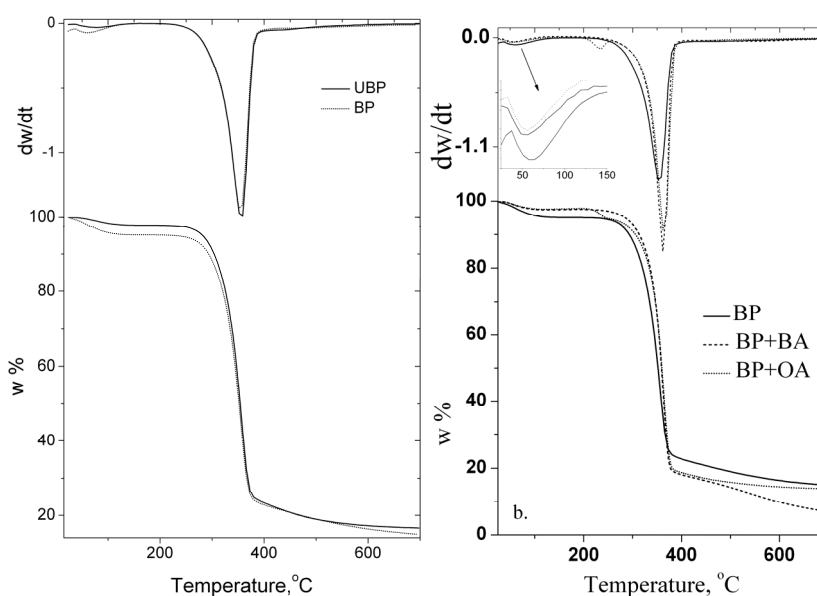
Figure 5. TG/DTG curves for wet unbleached, bleached and plasma grafted kraft pulp fibers

The temperature for the maximum decomposition rate of Step II was approximately the same in both UBP and BP, namely 354 and 356 °C as seen in Table 4. A similar result has also been found by Yang (2006). The mass loss (about 76 mass- %) was higher for unbleached pulp fibers, while for bleached pulp fibers it was about 73.2 mass- % (Table 4). This behavior corroborate with the more compact and more oriented structure of the bleached pulp fibers studied by Carrillo (2004).

In Step II, the initial temperatures for grafted fibers were mostly higher than those for the untreated pulps. The initial temperatures shifted to higher temperatures, indicating an increase in thermal stability. Furthermore, the grafted samples yielded a residual mass which decreased for unbleached pulp fibers treated with butyric acid and were constant for that treated with oleic acid, and increased for both treated bleached pulps fibers.

Although not shown, the residual mass increased from 21.9 mass-% to 32.4 mass-% for butyric acid treated unbleached pulp fibers and decreased by 19.9 mass-% for oleic acid treated unbleached pulp fibers; while for bleached pulp fiber grafted with butyric and oleic acids decreased from 22.5 mass-% to 17.5 mass-% and 17.6 mass-%, respectively. The residual mass was calculated by substracting from 100% the mass losses for the first and second processes which are presented in Table 4.

Table 4. Thermogravimetric data for the studied unbleached and bleached pulps ± BA or OA

Step no.	TG characteristic	UBP	UBP + BA	UBP + OA	BP	BP + BA	BP + OA
Step I	T_i (^{0}C)	36.0	32.0	28.0	36.0	31.8	30.5
	T_m (^{0}C)	75.8	56.0	51.5	59.2	55.4	54.4
	T_f (^{0}C)	152.0	126.7	127.7	153.7	121.4	133.9
	W_i (mass-%)	2.1	1.8	3.4	4.3	2.5	2.3
Step II	T_i (^{0}C)	210.9	193.9	211.3	198.8	203.1	227.1
	T_m (^{0}C)	354.3	351.3	361.9	355.8	361.7	362.4
	T_f (^{0}C)	424.5	407.6	419.1	421.8	417.5	420.9
	W_i (mass-%)	76.0	65.8	76.7	73.2	80.0	80.1

T_i – initial temperature, T_m - temperature corresponding to the maximum rate of mass loss and T_f - end temperature; w - mass loss

The overall kinetic parameters obtained by Coats Redfern, Flynn – Wall and Urbanovici – Segal methods (Popescu et al. 2008), are in accordance with our results in Table 5. The overall activation energy of the first thermogravimetric step was higher for unbleached pulp fibers (52 kJ/mol) than for bleached pulp fibers (43 kJ/mol). The reaction orders (n_{CR} or n_{FW} or n_{US}) gave values around 1.3. It can be supposed that this is a chemical process of elimination of chemically bound water or other low molecular weight compounds (Table 5).

Table 5. Overall kinetic parameters of the thermogravimetric steps for UBP and BP ± OA

Step no.	Kinetic parameters	Unbleached	UBP + OA	Bleached	BP +OA
Step I	E_{CR} kJ/mol	51.86	75.2	42.80	77.1
	n_{CR}	1.30	1.7	1.20	1.7
	E_{FW} kJ/mol	51.51	76.9	46.55	78.7
	n_{FW}	1.20	1.7	1.20	1.8
	E_{US} kJ/mol	44.77	75.9	38.67	78.0
	n_{US}	1.00	1.7	1.00	1.7
Step II	E_{CR} kJ/mol	126.4	156.5	132.1	156.1
	n_{CR}	1.30	1.4	1.40	1.1
	E_{FW} kJ/mol	126.3	158.0	134.7	157.9
	n_{FW}	1.20	1.4	1.40	1.1
	E_{US} kJ/mol	125.0	159.6	130.2	157.2
	n_{US}	1.2	1.4	1.3	1.2

The activation energies of the first thermogravimetric step decreased for plasma grafted sample for both unbleached and bleached pulps. The reaction orders gave values around 1.6-1.7 for pulp fibers grafted with butyric acid and 1.7-1.8 for those grafted with oleic acid, so this can be considered as an order controlled reaction.

The overall activation energy in Table 5 for Step II was 126 kJ/mol for unbleached pulp fibers, and around 132 kJ/mol for the bleached pulp fibers. In this case the reaction order was 1.3 for unbleached and 1.4 for bleached pulp fibers. In the second thermogravimetric step, significant changes in the kinetic parameters were obtained for fibers grafted with oleic acid (OA).

Differential Scanning Calorimetry (DSC) results

In Table 6 are given DSC data for untreated and plasma treated unbleached and bleached pulp fibers.

Table 6. DSC results for UBP and BP untreated and plasma treated samples

Property	UBP	UBP+ OA	BP	BP+OA
T (^{0}C),	158.3	155.3	158.5	159.2
ΔH (J/g)	-123.3	-83.9	-202.5	-83.0
T_{infl} (^{0}C),	144.4	--	136.6	133.2

T is peak temperature and T_{infl} is inflexion temperature

A broad endothermic peak observed in the temperature range of 60–160 ^{o}C in plasma treated pulp fibers corresponds to vaporization heat for water absorbed in the fibers and/or evolution of some volatile compounds. Due to different strength values of water binding in the case of grafted fibers, the characteristic temperatures and the enthalpies vary with the nature of the grafts.

Surface characterization

Attenuated Total Reflectance FT-IR spectroscopy

The ATR FT-IR spectra of the unbleached and bleached pulp fibers and unbleached kraft pulp grafted with oleic acid samples are presented in Figure 6.
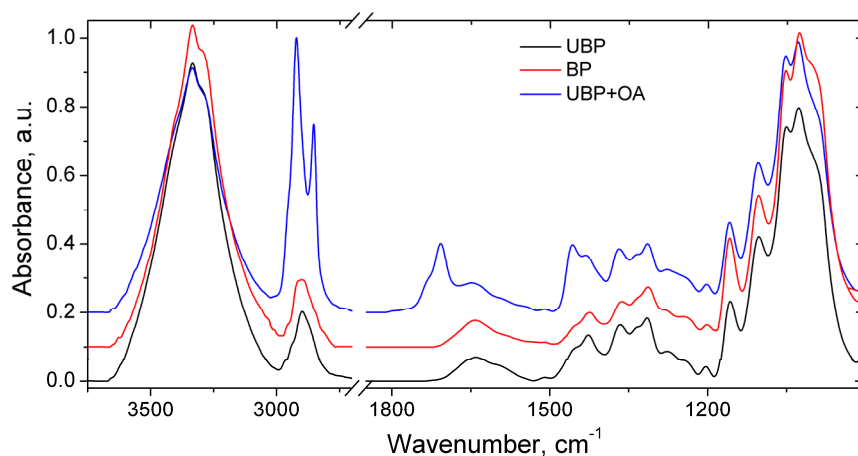
Figure 6. ATR FT-IR spectra for unbleached pulp, bleached pulp and unbleached pulp grafted with oleic acid

IR spectra of grafted fibers with oleic acid showed a shift and splits of the bands found at 2901 cm^{-1} in two bands located at 2850 cm^{-1} and 2923 cm^{-1} assigned to the asymmetric and symmetric CH_2 vibrations. The ester bonds in plasma-grafted samples became obvious at 1715 and 1610 cm^{-1}. The presence of the spectral bands located at 1715, 2850, and 2923 cm^{-1} indicates that the oleic acid was efficiently grafted onto the pulp fiber surface.

X-ray photoelectron spectroscopy (XPS)

XPS analysis of unbleached and bleached softwood pulp fibers revealed the presence of oxygen and carbon from the pulp fibers surface (Figure 7), which give the relative composition of O and C atoms and the calculated oxygen to carbon (O/C) ratio for all species.

Figure 7. XPS spectra unbleached (UBP) and oleic acid grafted (UBP+OA) pulp fibers

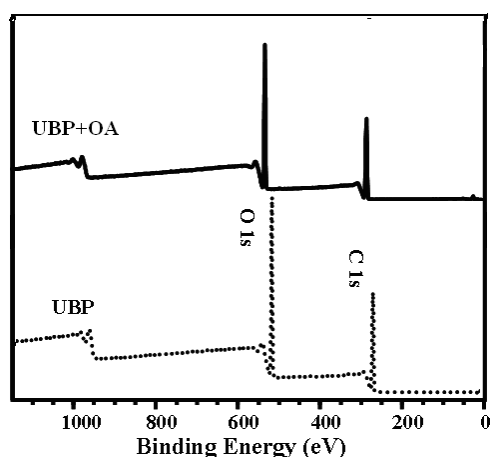The percentage of oxygen detected (Table 7) was higher for bleached pulp (37.5 %) than for unbleached pulp (35.7%), while treatment with oleic acid gave 16.7% and 32.3%, respectively). The percentage of carbon atoms was lower on the surface of the untreated pulp fibers. These changes were more evident in case of unbleached pulp fibers.

The O/C ratio increased from 0.56 to 0.61 after bleaching. The high carbon content in the pulp samples was reported to be an indication of the presence of lignin and extractives on the pulp fiber surfaces. The increase in O/C following bleaching is due to partial removal of carbon-rich extractives such as fatty acids, terpenes, and phenolics. The modification with oleic acid gave rise to a significant change in the O/C ratio, as well as in the amount of non oxygenated C bonds that was significantly higher for unbleached grafted pulp fibers. This confirms successful attachment of oleic acid chains to the cellulose surface.

Table 7. Atomic composition (%) and O/C ratio obtained by XPS analysis of pulp samples

Sample	% C	% O	O/C
UBP	63.2	35.7	0.56
UBP+OA	82.7	16.7	0.20
BP	61.6	37.5	0.61
BP+OA	67.6	32.3	0.48

C1s peaks were deconvoluted into 4 components, C1, C2, C3 and C4. The C1 corresponds to a carbon atom bound only to other carbon atoms and/or hydrogen atoms. It has been established by Kamdem (1991) that this component arises mainly from lignin and wood extractives. The C2 component is due to a carbon bound to a single non-carbonyl oxygen atom, which has been shown to be mainly derived from cellulose. The C3 peak represents a carbon atom bound to a carbonyl oxygen or to two non-carbonyl oxygen atoms. The C4 represents a carbon atom linked to one carbonyl oxygen and one non-carbonyl oxygen.

The signals for the C1-C4 shifted to higher binding energies after bleaching. The height of the C1 peak decreased, while the C2 peak increased during bleaching of the pulp fibers – Table 8. This can be explained by a higher quantity of cellulosic component, after removal of hemicelluloses and lignin. The C3 peak shows a slight increase and the C4 peak was insignificant in both samples (only 1.0 and 0.83%). This is explained by a possible low concentration of carboxylic groups on the pulp fiber surfaces.

Table 8. Integrated area (%) of the C1-C4 peaks obtained by XPS analysis of pulp samples

Sample	C1	C2	C3	C4
UBP	20.93	57.42	20.63	1.00
BP	14.54	54.93	29.70	0.83
BP+OA	26.22	48.07	20.99	4.72

The C1 shape for bleached pulp fibers grafted with oleic acid was similar to ungrafted pulp, but with differences appearing in peak intensities and areas. The areas of C1 and C4 peaks increased, while the areas of C2 and C3 peaks decreased after grafting, see Table 8.

It has been previously shown by Barry (1990) and Hua (1993) that the O1 fraction can be associated with lignin and extractives, the elimination of which decreased the O1 fraction and increased the O1 fraction originating from cellulose and hemicelluloses. The same pattern was observed in our case in the bleached pulps.

The oxygen peaks for the unbleached and bleached pulp fibres treated with oleic acid showed a decrease of the O1 peak. At the same time, the O2 and O3 peaks increased, thus the state of the oxygen containing groups changed after grafting.

Considering the content of hydroxyl groups in the superficial layers of the cellulose fibers (up to ~ 10 nm in depth) – determined to be 57.4 % for unbleached pulp fibers and 54.9 % for bleached pulp fibers respectively – and also the variation of the C2 groups, which decreased after cold plasma treatment with oleic acid, and the increase of the C4 groups for treated samples, a grafting degree of the superficial layers was estimated to be about 55 % for unbleached pulp fibres and 15% for bleached pulp fibres, which is in good accordance with ATR-IR results.

Scanning electron microscopy

The unbleached material was quite heterogeneous and the individual fibers were intact as seen in Figure 8a. As is evident from the micrographs, the bleached softwood pulp fibers had a fibrous structure similar to that of unbleached fibers, but the diameter of the fibers seemed to be smaller after bleaching. Thus, the average diameter of the fibers in the unbleached pulp was 29.9 ± 2.3 μm, while the bleached fibers only were 27.5 ± 1.6 μm in diameter. After grafting (Figures 8c and d) with butyric acid the pulp fibers showed a rough surface, were fragmented and showed formation of pits on the fiber surface, while the pulp fibers grafted with oleic acid had a more pronounced roughness of the surface, a deposition of oleic acid on the fiber surfaces was evident.
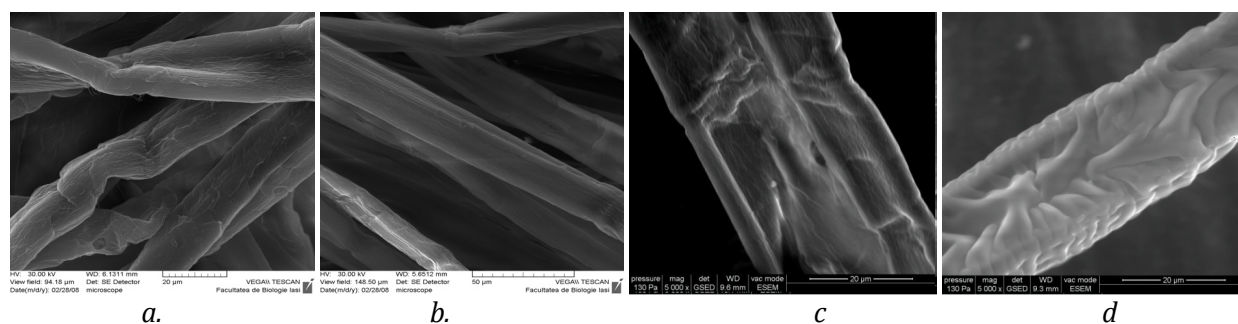

| *a.* | *b.* | *c* | *d* |

Figure 8. SEM micrographs of unbleached (a) bleached (b) and UBP + BA (c), UBP + OA (d) pulp fibers

Conclusions

Unmodified and modified (plasma treated) COST E54 pulp fibers were characterized regarding their structural, morphological and surface characteristics in order to find differences introduced by the different pre- and post-treatment.

The increase in the apparent crystal size and crystallinity index determined by XRD of cellulosic particles after bleaching showed that the number of small crystallites decreased, resulting in improvement of fiber crystallinity, an effect intensified by the removal of the amorphous portion of hemicelluloses and lignin during bleaching.

The differences between unbleached and bleached softwood pulp fibers appeared also in characteristic temperatures, mass losses and overall activation energies. A decrease in O/C ratio and an increase in the C_{ox}/C_{unox} suggests the removal of carbon compounds from the pulp fibers surface during bleaching, giving that more cellulose is exposed on the surface after bleaching. The content of C atoms decreased and the content of O atoms increased after bleaching. The unbleached material was quite heterogeneous and entangled and the individual fibers intact. After bleaching the surface of the individual fibers changed and appeared smooth and the cellulose fibers were oriented in one direction. The diameter of the fibers seemed to become smaller after bleaching.

This work clearly shows that cellulose macromolecules can be grafted successfully by fatty acids using a "green" process (cold plasma). Such treatment can be transferred to practical technologies, particularly in papermaking and textile applications, in which the hydrophobizing of the tissues or paper-based packaging materials is an important issue.

Acknowledgements

References

Barry A. O. and Zoran Z. (1990): Surface analysis by ESCA of sulfite post-treated CTMP. J. Appl. Polym. Sci. 39(1), 31-42

Carrillo F., Colom X., Sunol J. J. and Saurina J. (2004): Structural FTIR analysis and thermal characterisation of lyocell and viscose-type fibres. Eur. Polym. J. 40(9), 2229-2234

Gellerstedt (2007): Chemistry of bleaching. *In:* The Ljungberg Textbook Wood Chemistry and Wood Biotechnology, 3D1058, Ch. 26. Printed by Fibre and Polymer Technology, KTH. ISSN 1652-2443

Hua X., Kaliaguine S., Kokta B. V. and Adnot A. (1993): Surface analysis of explosion pulps by ESCA. Wood Sci. Technol. 28, 1-15

Hulleman S. H. D., van Hazendonk J. M. and van Dam J. E. G. (1994): Determination of crystallinity in native cellulose by Fourier transform infrared spectroscopy. Carbohydr. Res. 261, 163-171

Isogai I. (1994). Allomorphs of cellulose and other polysaccharides, *In* R. D. Gilbert (*Ed*), Cellulosic Polymers, Blends and Composites. Hanser/Garner Publications, Cincinnati, OH, 5-23

Kamdem D. P., Riedl B., Adnot A. and Kaliaguine S. (1991): ESCA spectroscopy of poly(methylmetacrylate) grafted onto wood fibers. J. Appl. Polym. Sci. 43, 1901-1912

Kumar V. and Kothari S. H. (1999). Effect of compressional force on the crystallinity of directly compressible cellulose excipients**.** Int. J. Pharmaceutics. 177, 173-182

Ludwick A.G., Aglan A.H., Abdalla M.A., Badran B., Ashour M., Morcos V., Hassan R. and Mahmoud M. (2002). Chemical and engineering modifications of bagasse for oil absorption. *In*: G.A. Uzochukwu, K. Schimmel, G. Reddy, S.Y. Chang and V. Kabah *(Eds.)*, Proc. 2002 National Conf. Environ. Sci. Technol., Greensboro, North Carolina, USA, September 8 - 10

Popescu C.-M., Tibirna C. M., Raschip I. E., Popescu M. C., Ander P. and Vasile C. (2008): Bulk and surface characterization of unbleached and bleached softwood kraft pulp fibres. Cellulose Chem. Technol. 42(9-10), 525-547

Risen J., Heijnesson-Hultén A. and Paulsson M. (2004): Surface characterization of softwood and hardwood kraft pulp fibers from different stages in a bleaching sequence. J. Wood Chem. Technol. 24(4), 307-321

Rowland P. R. and Roberts E. J. (1974): Availibity of hydroxyl groups for reaction in fibrous cotton cellulose II and hydrocellulose II. J. Polym. Sci. 12, 96-101

Silva M. C., Lopes O. R., Colodette J. L., Porto A. O., Rieumont J., Chaussy D., Belgacem M. N. and Silva G. G. (2008): Characterization of three non-product materials from a bleached eucalyptus kraft pulp mill, in view of valorising them as a source of cellulose fibres. Ind. Crops Prod. 27, 288-295

Struszczyk H. (1986): Modification of lignins. III. Reaction of lignosulfonates with chlorophosphazenes. J. Macromol. Sci. A-23, 973-980

Totolin M. I., Vasile C., Tibirna C. M. and Popescu M.-C. (2008): Grafting of Spanish broom (*Spartium junceum*) fibers with fatty acids under cold plasma conditions. Cellulose Chem. Technol. 42(7-8), 317-333

Vaca-Garcia C., Thiebaud S. and Borredon M. (1998): Cellulose esterification with fatty acids and acetic anhydride in lithium chloride / *N,N* -dimethylacetamide medium. J. American Oil Chemists Society. 75, 315-319

Viikari L. and Lantto R. (2002): BIOTECHNOLOGY IN THE PULP AND PAPER INDUSTRY: 8th ICBPPI MEETING. Progress in Biotechnology 21. Elsevier Science B.V., Amsterdam, pp. 332

Yang H., Yan R., Chen H., Zheng C., Lee D. H. and Liang D. T. (2006): In-depth investigation of biomass pyrolysis based on three major components: hemicellulose, cellulose and lignin. Energy & Fuels 20, 388-393

SWELLING AND ELECTROKINETIC PROPERTIES OF UNBLEACHED/BLEACHED SOFTWOOD KRAFT CELLULOSE FIBERS

Georgeta Cazacu, Anamaria Sdrobis, Manuela Pintilie, Dan Rosu,

Diana Ciolacu, Marian Totolin and Cornelia Vasile

"Petru Poni" Institute of Macromolecular Chemistry, Iasi, Romania

E-mail: gcazacu@icmpp.ro

Abstract

This work presents some results regarding the behavior of cellulose fibers in alkaline solutions. The influence of UV radiation treatments on swelling and electrokinetic properties of the cellulose fibers was also investigated. The assessment of changes in the molecular structures was based by FT-IR spectroscopy, differential scanning calorimetry (DSC), optical microscopy and scanning electronic microscopy (SEM). The electrokinetic properties were analyzed by zeta potential measurements. Based on the obtained results, it can be concluded that the treatments cause certain changes of the fiber properties which are reported.

Introduction

In many applications cellulosic materials require certain pretreatments, which can be based on physical or chemical methods of swelling and activation. The alkaline treatments have been used for many years to modify fiber structure and properties such as swelling degree, crystallinity and orientation of fibrils in cellulosic fibers (Vicker et al. 2001), all having an effect on physico-mechanical properties of the substrates. The interactions taking place between cellulosic fibers and alkaline solutions determine an increase of fiber diameter (swelling) and a decrease of their length (contraction) (Rozmarin (1984; Good and Mueller 1980). The reorganization of cellulose fibers by swelling treatments in alkaline solutions results in numerous structural modifications, causing changes of their accessibility and/or reactivity (Bui et al. 2008). These treatments have a great influence also on the electrokinetic properties of cellulosic materials (Freundenberg et al. 2007). The new properties are important for using cellulose products in biomedical applications (dialysis membranes, wound dressings and skin substitutes and for drug delivery systems), for adsorption of heavy metals (dietary fibers, production of the nanomaterials and colored textile fibers (Freundenberg et al. 2007; Öztürk et al. 2009), and in different chemical reactions of cellulose such as acetylation (Safy El-Din and Abd El-Megeid 1994).

In the present work, the effect of alkaline treatments on kraft pulp fiber characteristics, especially of the swelling degree was investigated. The unbleached/bleached pulps were subjected to the action of various aqueous alkaline solutions at different temperatures and with or without UV irradiation.

Materials and Methods

Pulps

Two types of chemical pulp fibers have been used: the *unbleached* (UBP) and *bleached kraft pulps* (BP) fibers from soft wood (spruce:pine wood ratio=79:21) (supplied by Södra Cell, Sweden). The chemical composition is presented in Table 1, while sugar and lignin content is given by Heinemann and Ander (2011).

Table 1. Lignin and α- and β+γ cellulose content of pulp samples

Sample	Relative humidity (%)	Dry matter content (%)	Intrinsic viscosity (mL/g)	Klason lignin (%)	Kappa number	α-cellulose (%)	β+γ cellulose (%)
Unbleached pulp - UBP	65.1	32.3	1109	3.9	25.9	74.42	7.39
Bleached pulp - BP	65.3	32.8	728	0.75	3.0	86.97	11.17

A. Swelling of the pulp samples wa*s* done in water and alkaline solutions (NaOH and KOH solution) of different concentrations (5, 10 and 40 weight %), for 72 h at room temperature. The treated samples were firstly dried at room temperature.

B. Alkaline activation of pulp: The pulp samples were frozen in 8.5% NaOH solution at minus 30°C during 3 to 71 days (UBP_{1-11} and BP_{1-12}, respectively). The treated pulp was thawed at room temperature, successively washed with 1% NaOH solution, water, dilute acetic acid, water, acetone and ether. The samples were weighed after drying at room temperature. The dried pulps were immersed in water for 24 h to determine swelling degree.

C. UV radiation treatment: The pulp samples were exposed to UV radiation under artificial conditions with different kinds of UV lamps (xenon tube and mercury lamp) as the sources of radiation. The samples, in the form of tablets, were subjected to irradiation on two-faces, using two wavelengths (λ=254 nm and 365 nm, respectively). Changes in the fiber molecular and surface properties were observed after 20 h and 40 h of exposure of each face. The pulp samples were UV irradiated in order to see color development versus irradiation time. To determine the influence of UV treatment on the fiber swelling degree, the samples were immersed in 10% NaOH or KOH solutions at room temperature for 72 h.

Methods of investigation

The structural modifications which appeared during treatments were investigated by: ATR FT-IR spectroscopy (FT-IR Bruker Vertex 70 spectrometer), microscopy (optical microscopy – microscope type LEICA DM 2500M; SEM - scanning electron microscope type VEGA II TESCAN), differential scanning calorimetry (Mettler DSC-12E instrument), ζ potential measurements (SurPASS Electrokinetic Analyzer).

From FT-IR spectra, the following information were obtained: H-bonds energy (Struszczyk 1986); H-bond formation enthalpy (Kadla and Satoshi 2004; Purcell and Drago 1967); H-bounding distance (Pimentel and Sederholm 1956); relative value of optical density (RVDO) (Simionescu et al. 1973); asymmetric index (a/b) (Kotelnikova 1992). The information on the crystalline index (χ_{IR}) of the cellulosic materials was obtained from the absorbance ratio $X_{IR} = A_{1370} / A_{2900}$.

The diameter (D) of swollen fibers was determined by a Leica projection microscope with a magnification of 200x using the relation: $D = [\Sigma\ d_f] / n$, were d_f – swollen fiber diameter (mm) and n – number of fibers measured. Results are expressed as the mean of at least ten measured fibers. The degree of swelling is generally defined as the amount of water or other solvents taken up under specified chemical conditions. Therefore, swelling degree (Q) of the treated samples was determined by weighing and calculated using the relation: $Qmax = [(m – m_0)/ m_0]*100$ (%), where: m_0 **-** dry hydrogels mass (g); m - swollen hydrogel mass (g).

The color changes during the photochemical treatment of the specimens can be described using CIEL*a*b* system, where L* can be thought as a lightness factor, a* is the redness factor and b* is the yellowing index (McLaren 1976). The L*, a* and b* parameters were measured with a color comparison device (Pocket Spec Color QA, SUA). These values were used to calculate the color change ΔE_{ab} as a function of the UV irradiation time, according to the following equation:

$$\Delta E_{ab} = \sqrt{\left(L_2^* - L_1^*\right)^2 + \left(a_2^* - a_1^*\right)^2 + \left(b_2^* - b_1^*\right)^2}$$

Results and Discussion

Swelling of the pulp samples UBP and BP

The interactions between cellulose fibers and alkaline solutions give an increase of fiber diameter due to fibre swelling. These changes were characterized by optical microscopy, FT-IR spectroscopy and swelling degree (Sdrobis et al. 2010). *Optical micrographs* showed the increase of the pulp volume (especially fiber diameter) by immersion of the pulp samples in alkaline solutions for a determined time period (Figure 1). A first observation showed that a larger increase in diameter was observed for UBP samples in all solvents in comparison with BP samples. This can be explained by the presence of more amorphous domains due to lignin and hemicellulose present in UBP, which were removed by the bleaching process. Increase in diameter of the swollen fibers, as seen in optical microscopy images, is given in Table 2.
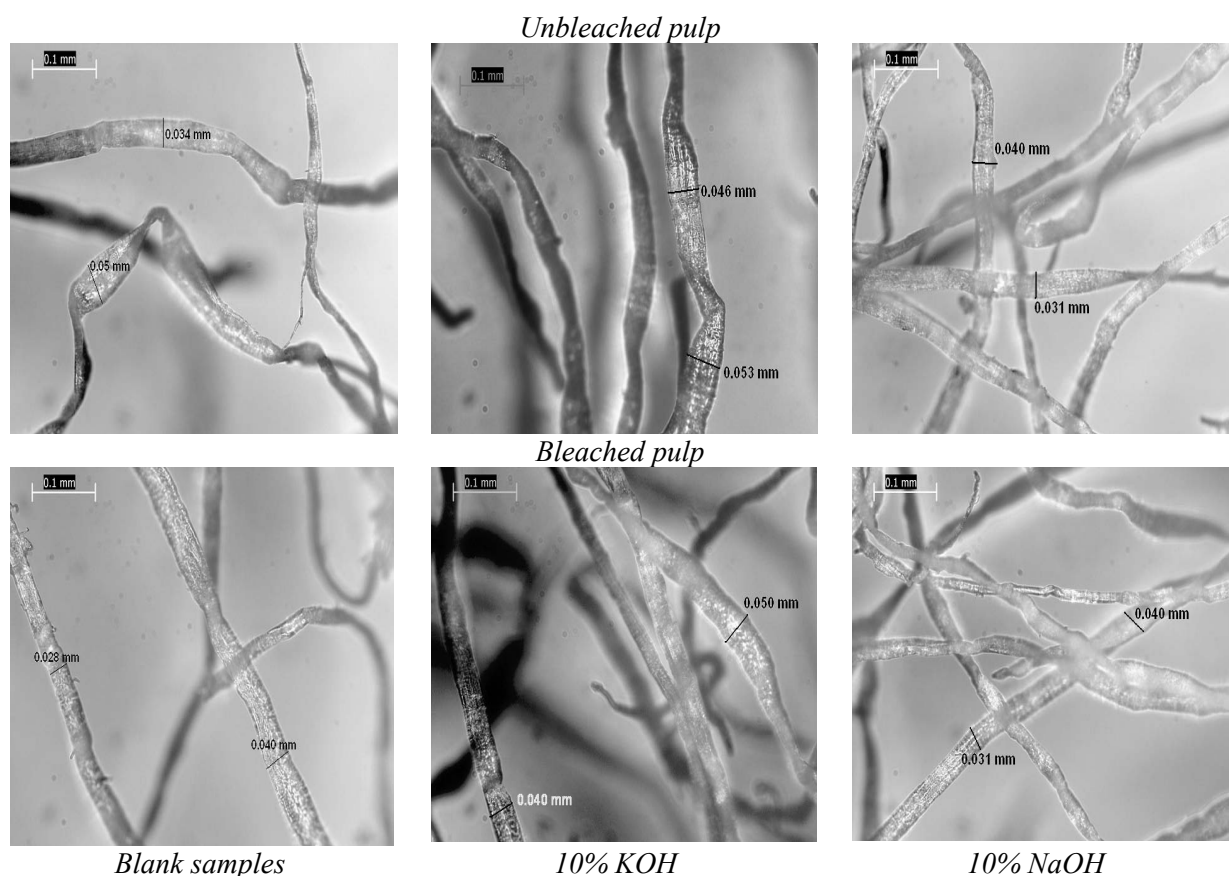
Unbleached pulp

Bleached pulp

| *Blank samples* | *10% KOH* | *10% NaOH* |

Figure 1. Optical microscopy images of swollen samples (200 x)

Table 2. Percent change of kraft pulp fiber diameter in alkaline solutions

Sample	KOH solution			NaOH solution		
	5%	10%	40%	5%	10%	40%
Dry fibers						
UBP	8.82	35.29	19.35	35.29	26.47	35.29
BP	10.71	42.85	32.14	53.57	50.00	64.28
Conditioned fibers						
UBP	100	80.64	61.29	70.96	51.61	80.64
BP	100	78.57	53.57	53.57	42.85	57.14

Both dried and conditioned fibers swelled in KOH solution and showed the highest increase in diameter for the 10% solution, while NaOH gave maximum swelling of the fibers in 5% and 40% solutions. As expected, the increase in fiber diameter was a consequence of the swelling process which is seen by the *swelling degree* presented in Table 3.

Table 3. Maximum swelling degree in alkaline solutions of the kraft pulp fibers

Sample	KOH			NaOH		
	5%	10%	40%	5%	10%	40%
UBP	140.2	146.0	157.1	135.3	140.4	169.2
BP	135.1	139.2	156.0	103.5	132.2	161.8

The *swelling degree* in NaOH and KOH solutions was higher for UBP than for BP (Table 3) in accordance with data obtained by optical microscopy. For samples swollen in 5% and 10% solutions the highest swelling degree was observed for KOH solutions.

The hydration energies are ΔH_{Na+} = -98 kcal/mol and ΔH_{K+} = -77 kcal/mol. As known the hydration energies of ions decrease when increasing ion volume that is why a larger swelling degree was observed for the samples swollen in solutions of 40 mass-% NaOH. Generally, the swelling degree of the fibers increased with increased concentration of alkaline solutions.

Due to the heterogeneous cellulose structure containing both crystalline and amorphous domains and semi-crystalline un-ordered areas, swelling can also be inter- and intracrystalline. Below 20% alkaline solutions, swelling occurs predominantly in amorphous and un-ordered regions, while with higher concentration of alkali, the swelling process gives an intramicelar reaction type with changes of the molecular network as seen by X-ray and FT-IR spectroscopy (Rozmarin 1984).

The *FT-IR spectra* of both unbleached and bleached kraft pulp samples after swelling in alkaline solutions are presented in Figure 2.
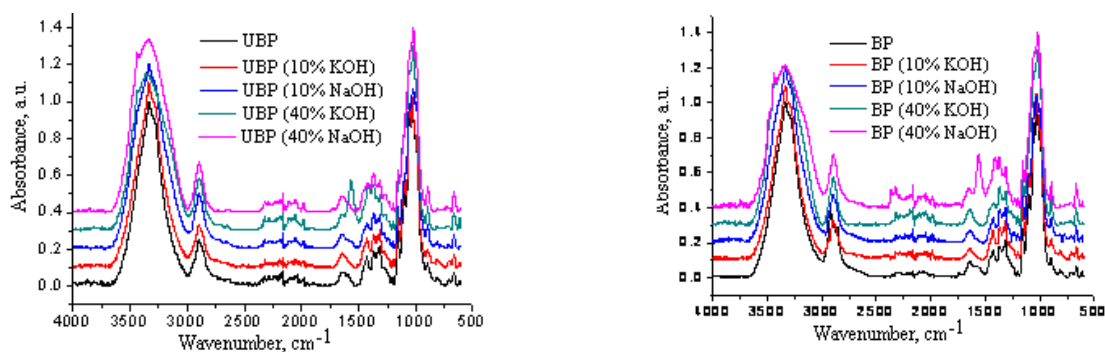

Figure 2. FT-IR spectra for unbleached and bleached samples

A small shift of OH FT-IR bands to higher wave-number values was observed during the cellulose swelling process. The shift increased with increasing solution concentration being more obvious in the case UBP and BP swollen in 40% KOH and NaOH.

The changes which took place in the cellulose structure during alkaline treatment were deduced from the spectral data in Table 4. The modifications recorded could be due to breaking of some inter- and intra-molecular bonds. The decrease of H-bond energy after swelling in alkaline solutions shows that the structural order was disturbed, which was also shown by the increase in hydrogen bonding distances.

Table 4. Spectral characteristics of pulps before and after swelling in alkaline solutions

Sample	OH - band position (cm^{-1})	a/b ratio	E_H (kJ)	ΔH (kJ/mol)	R (Å)
Unbleached pulp					
UBP	3335	1.023	21.575	46.96	2.780
KOH 10%	3336	0.971	21.507	47.92	2.780
NaOH 10%	3338	1.000	21.370	47.67	2.781
KOH 40%	3339	0.754	21.301	48.93	2.781
NaOH 40%	3341	0.920	21.164	48.43	2.782
Bleached pulp					
BP	3335	1.000	21.644	46.91	2.780
KOH 10%	3336	0.958	21.507	47.59	2.780
NaOH 10%	3337	0.969	21.438	47.29	2.781
KOH 40%	3339	0.944	21.301	48.17	2.781
NaOH 40%	3340	0.953	21.233	47.92	2.781

The increased values of hydrogen bonding enthalpy can be due to the increase of crystallinity index (Table 5).

Table 5. The A_{OH}/A_{CH_2} ratio and other relative values of optical density of pulps before and after swelling in alkaline solutions

Sample	χ_{IR} (%)		A_{OH}/A_{CH2} ratio		RVOD
	A_{1370}/A_{2900}	A_{1420}/A_{900}	A_{1315}/A_{1370}	A_{1315}/A_{2900}	A_{1505}/A_{1425}
Unbleached pulp					
UBP	0.656	1.158	0.780	0.634	0.180
KOH 10%	0.760	1.320	0.960	0.696	0.093
NaOH 10%	0.739	1.168	0.813	0.648	0.088
KOH 40%	0.892	1.751	1.147	0.880	0.129
NaOH 40%	0.796	1.500	1.122	0.869	0.097
Bleached pulp					
BP	0.682	0.912	0.810	0.586	0.210
KOH 10%	0.800	1.291	1.052	0.740	0.088
NaOH 10%	0.723	0.965	0.863	0.690	0.075
KOH 40%	0.935	1.633	1.222	0.877	0.161
NaOH 40%	0.853	1.416	1.194	0.758	0.098

The alkaline solutions have two effects on the pulp fibers: one is swelling of the pulp fibers, especially in volume, and the second is lignin removal (amorphous compound). The increase in crystallinity index ($\chi_{IR} \approx A_{1370}/A_{2900}$ or A_{1420}/A_{900}) and of the A_{OH}/A_{CH2} ratio indicates that the

treated samples have an ordered structure due to swelling of the cellulose fibers. The low relative values of optical density indicate that some lignin fragments were removed from the fiber samples during alkaline treatment.

B. Alkaline activation of pulps

Both cellulosic samples (UBP and BP pulps), treated with 8.5% NaOH at -30°C, behaved similar during dissolution (Cazacu et al. 2008). In the first stage, the solubility of the samples in NaOH solution increased achieving a plateau, and then decreased at prolongation of the freezing time (Figure 3). This can be explained by crystallization of water in the samples causing disruption of intermolecular bonds, which made it possible to gradually dissolve the cellulose in the alkaline solution.

The removal of short chains and amorphous fragments, lead to an increase of domains with a high order and large dimensions of cellulose chains (Isogai and Atalla 1998; Kamide et al. 1984; 1992), which determines the decrease of solubility.
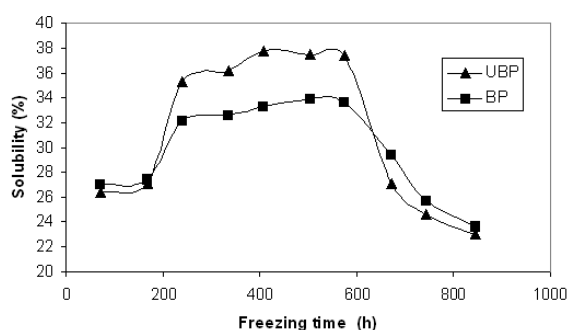

Figure 3. Variation solubility of pulp samples UBP and BP vs. freezing time

FT-IR spectroscopy shows that during alkaline treatments at low temperature structural modifications occur due to breakage of inter- and intra-molecular bonds and to removal of small chains from amorphous domains of the fibers (Cazacu et al. 2008). Thus, after 200 h, a decrease of the E_H was recorded, and simultaneously H-bond energy started to increase, giving breakage of H-bonds in the first stage and then the formation of new H-bonds (Figure 4). A similar behavior of H-bond formation enthalpy was observed (Figure 5).
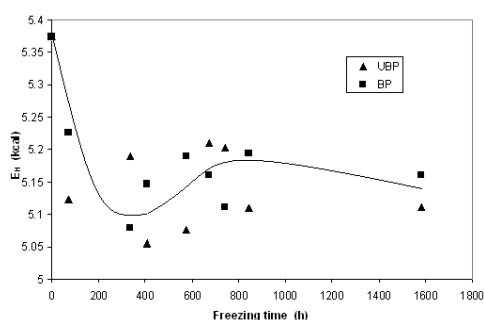

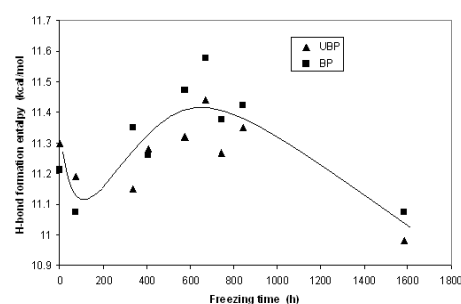*Figure 4. Variation of H-bond energy vs. freezing time*

Figure 5. Variation of H-bond formation enthalpy vs. freezing time

The high values of the hydrogen bond formation enthalpy (UBP=11.15-11.44 kcal/mol and BP=11.07-11.58 kcal/mol) and of the H-bond energy values (UBP=5.055-5.21 kcal and BP=5.08-5.23 kcal) indicate formation of a product with high structural order. This is confirmed by the increase of the crystallinity index values (calculated from A_{1370}/A_{2900} ratio) (Figure 6).

The decrease of the A_{OH}/A_{CH} ratio indicates that during alkaline treatment removal of short fragments of cellulose and lignin occur (Figure 7). The removal of small fragments of lignin from UBP samples was also confirmed by the low relative values of optical density (RVOD=0.13-0.16 in comparison with 0.45 for control UBP sample). The spectral data demonstrate that during alkaline treatment at low temperature structural modifications occur, with new arrangement of molecular chains and establishment of new intra- and intermolecular bonds.
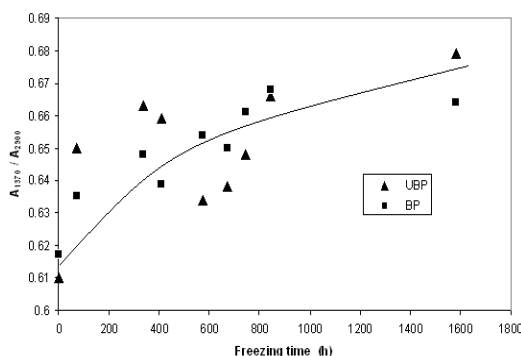

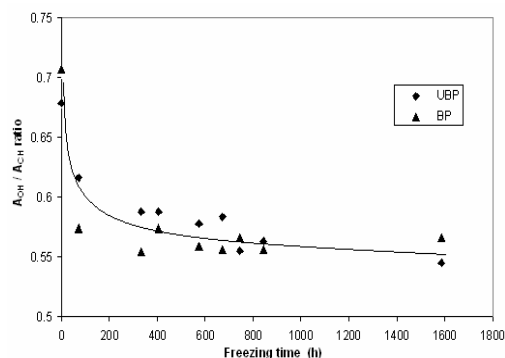*Figure 6. Variation of the χ_{IR} vs crystallinity index vs. freezing time*

Figure 7. Variation of the A_{OH}/A_{CH2} ratio vs. freezing time

The cellulose fibers were analyzed by *scanning electronic microscopy* and it was observed that control fibers (UBP and BP pulps) had an oblate aspect, and in the case of the bleached control fibers, removal of primary wall layers took place by the bleaching (Figure 8a and b).
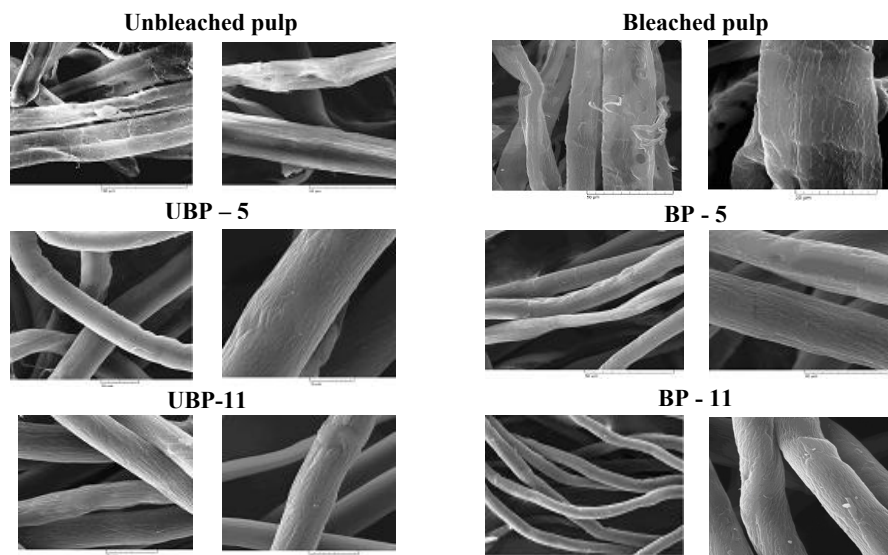

Figure 8a (left) and b (right). SEM images for the pulps treated in alkaline solution at low temperature

After alkaline treatment the fibers were swollen, and the fiber surfaces became smooth and ordered fibrils were observed. The effect of alkaline treatment at low temperature on the cellulosic fibers observed by FT-IR spectroscopy and SEM were confirmed also by differential scanning calorimetry (DSC) data.

In the *DSC diagrams* (Figure 9), the changes of the endothermic peak area at 90-100°C was observed which is attributed to heat of dehydration of bound water. This demonstrates the swelling of fibers during treatment with NaOH at low temperature. Simultaneously, an increase of the decomposition peak was observed probably due to change of cellulose crystallinity, the melting process being overlapped with decomposition. Thermal disruption of cellulose crystalline domains is therefore believed to be the reason for appearance of a high endothermic peak (Pedersoli 2000).
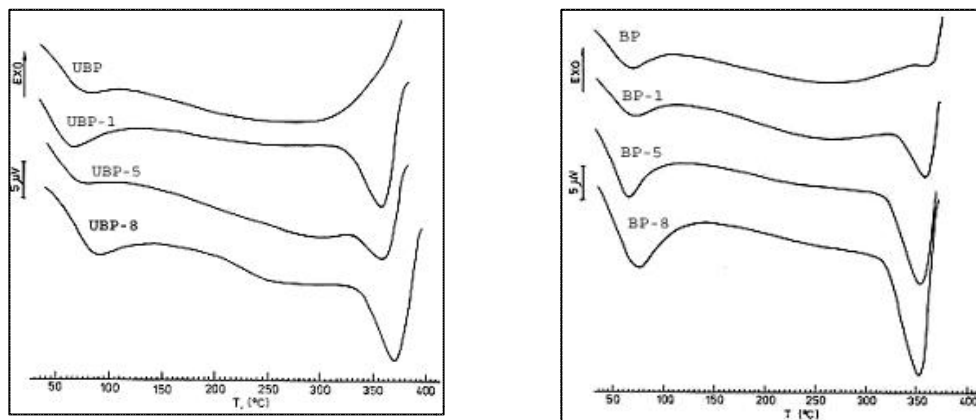

Figure 9. DSC curves of alkaline treated pulp fibers

Generally, the *swelling degree* in water of the dried treated fibers increased with freezing time. From Figure 10 it can be seen that in the first period (until 200h), an increase of swelling degree was recorded followed by a slow decrease. This decrease can be explained by the appearance of new arrangements of the molecular structure and by establishing of new H-bonds.
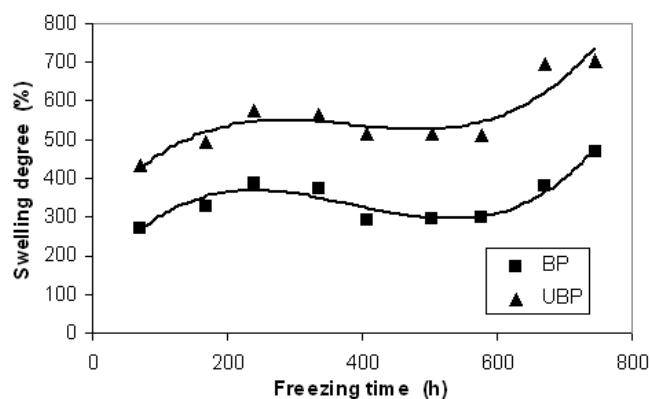

Figure 10. Swelling behavior in water of the treated pulps

The unbleached pulp gave the highest swelling degree, probably due to the presence of many amorphous domains. The alkaline treatment of the bleached pulp destroyed a portion of intra- and inter-molecular bonds leading to dissolution of short chains especially from amorphous domains.

C. UV irradiation treatment

The UV-treated pulp samples were investigated by FT-IR spectroscopy, zeta potential measurements and swelling degree determination in various alkaline solutions (Cazacu et al. (2009). The *IR spectra* with or without UV irradiation were very similar and only a small change

of bands in the range 1800-1500 cm^{-1} was seen in Figure 11. The ratio values of A_{1730}/A_{1050} and A_{1634}/A_{1050} indicate structural modifications during UV irradiation of the pulp fibers (Table 6 in Appendix). In the range of non-conjugated carbonyl groups a broad absorption appeared around 1740 cm^{-1}, as a result of irradiating the samples (*cf.* Alvarez et al. 2006). A decrease in absorbance around 1630 cm^{-1} (conjugated carbonyl groups and adsorbed water in cellulose fibers) was recorded in the spectra for low irradiation wavelength and can be attributed to the loss of water. At higher energies the absorbance increases due to the increase of conjugated carbonyl groups number.

The results indicate that there are several processes in the OH-band region during irradiation in the 3400 - 3500 cm^{-1} range (Appendix Table 6). Thus, the decrease in absorbance band intensity corresponding to -OH indicates the possible transformation of these groups to aldehyde or carboxylic groups and the formation of new intermolecular bonding with the participation of these groups.
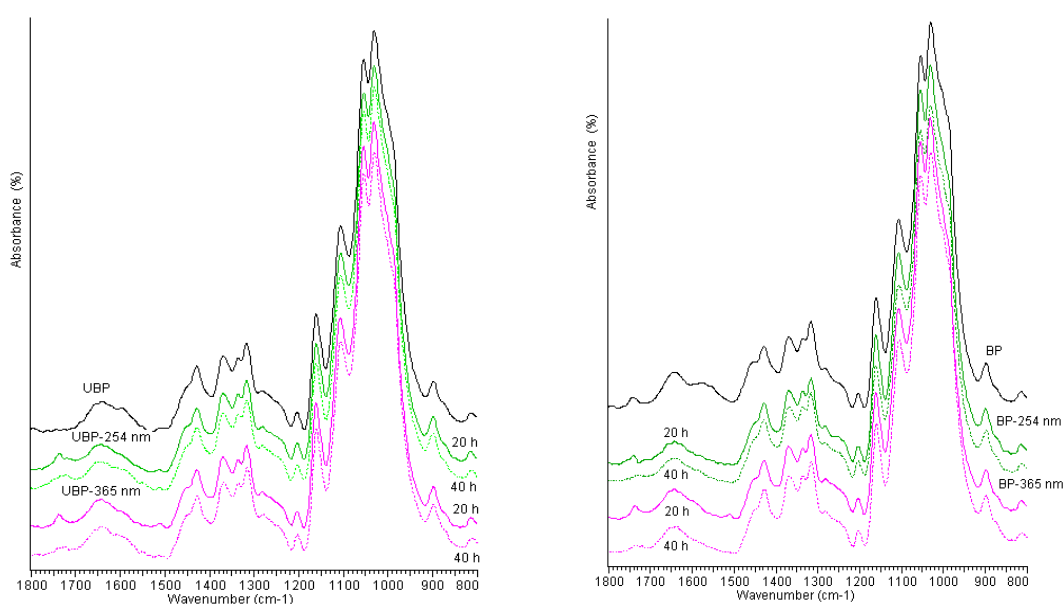

Figure 11. IR spectra of UV irradiated UBP and BP in the 1800-900 cm^{-1} domain

Important *color variations* were observed by UV irradiation for up to 120 h (Figure 12). The overall tendency of the color differences (ΔE^*) was an increase with irradiation time, but each sample had a particular behavior (Figure 12 and Appendix Table 7). For unbleached pulp (UBP) the color differences were greater, with increase of wavelength and exposure time. This can be attributed to the formation and accumulation of chromophore functional groups such as carboxylic acids, quinone-like structures and hydroperoxy radicals due to depolymerization and oxidation of lignin during irradiation. The bleached cellulose (BP) gave a maximum of the ΔE^*. The use of UV radiation at $\lambda=365$ nm lead to lower values for ΔE^*, than for $\lambda=254$ nm, probably due to a more intense photodegradation process of the cellulose material.
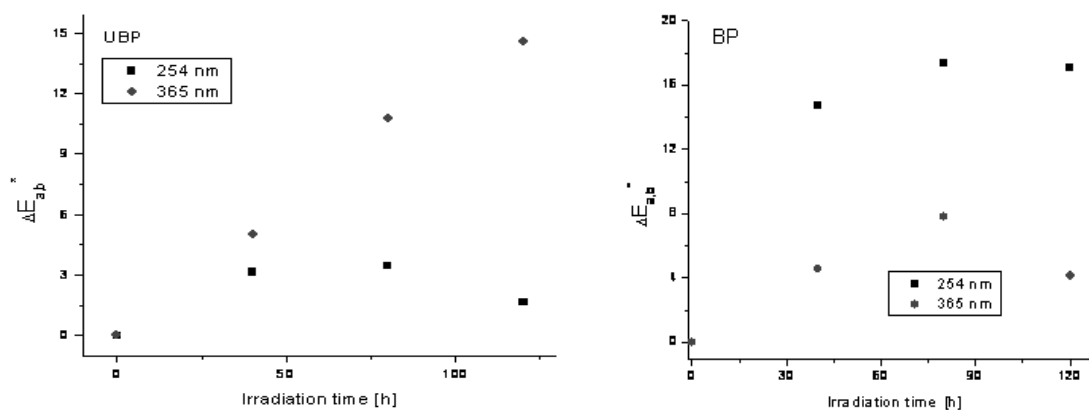
Figure 12. Color variations vs. irradiation time and UV radiation wavelength for UBP and BP

The ΔE* values (Appendix Table 7) were in a large range (1.5-10 for I & II faces), indicating a significant variation in visibility of the color change. Thus, exposure of the BP samples to UV radiation showed a greater accumulation of chromophore groups than the UBP samples.

Variation of different color parameters indicates the accumulation of chromophores on the two faces of the studied samples, and at exposure of BP samples a slight tendency for accumulation of green and yellow chromophores on both surfaces was found. For the UBP samples, UV irradiation caused accumulation of different chromophores with low stability and transforming to other chromophores after prolonged exposure time (λ=254 nm: red - green chromophores, and λ=365 nm: yellow - blue chromophores), probably due to a cellulose pulp degradation process taking place by a complicated mechanism.

The irradiated pulps were swollen in alkaline solutions (NaOH and KOH, 10%) for 72 h. As given in Appendix Table 8, the swelling degree of the irradiated pulp samples were influenced by type of alkaline solution, by UV radiation wavelength and by type of irradiated cellulose pulp. Due to the presence of amorphous lignin and hemicellulose, UBP gave a higher swelling degree than BP. Increase in wavelength and exposure time lead to a decrease of swelling degree, probably due to a crosslinking-coupled degradation process which took place on the cellulose surface during UV irradiation.

KOH gave a larger swelling degree due to a lower hydration energy compared with NaOH solution (ΔH_{Na+} = -98 kcal/mol and ΔH_{K+} = -77 kcal/mol). Also, the presence of carboxyl groups which can be converted to Na^+ salts, may lead to a decrease of the swelling degree (Scallan 1983; Grignon and Scallan 1980).

By the *determination of the zeta potential,* the structural modification which takes place during UV irradiation of the kraft pulps was confirmed. As shown in Figure 13, the evolution of zeta potential with pH shows a plateau in the pH=5-9 range, where the maximal zeta potential for irradiated and control cellulose samples differed. The ζ potential in absolute value for BP increased with UV exposure time and wavelength. For UBP, increase of wavelength and irradiation time decreased the ζ potential in comparison with control pulp fibers. This can be explained by an intense oxidation process of the polymeric support which leads to accumulation of chromophoric structures capable of formation of intermediary colored products. The behavior

of ζ potential at different pHs may also be related to the chemical properties of the fibers. Bleached pulp showed a higher degree of crystallinity (X_{IR}=0.757) and a higher content of α-cellulose (87 %), while UBP exhibited a lower content of crystalline parts (X_{IR}=0.631) and a high content of non-cellulose compounds (L_K=17.55 %).
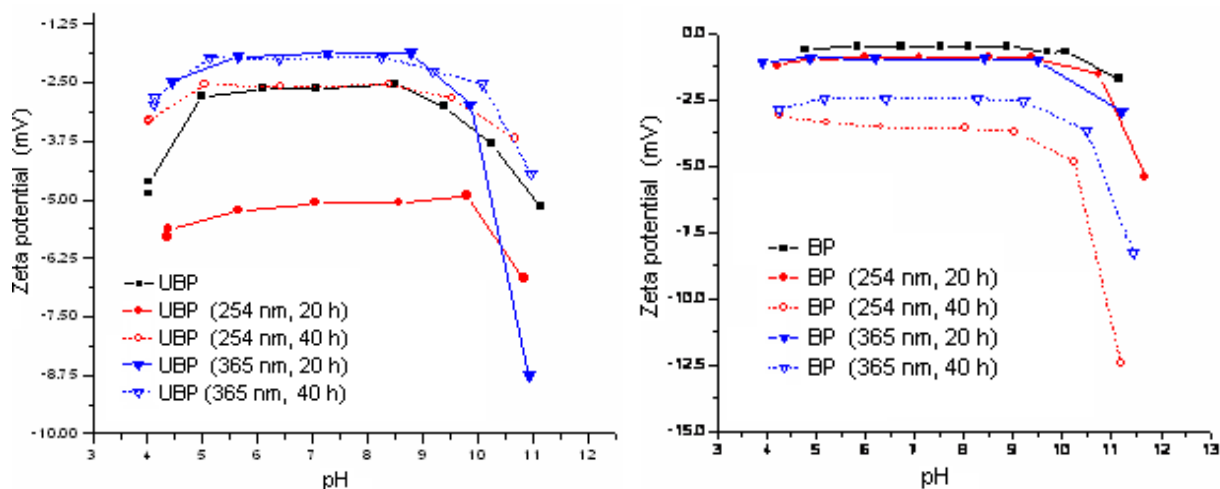

Figure 13. Variation of ζ potential vs. pH in solution for UBP and BP

Conclusions

The behavior of unbleached and bleached kraft pulp fibers during some alkaline treatments including direct treatment with KOH and NaOH solutions, treatment with NaOH at low temperature and treatment with KOH and NaOH after UV irradiation of the pulps was studied. The structural modifications of the treated pulp fibers were demonstrated by FT-IR spectroscopy, while further change in properties were investigated by differential scanning calorimetry, optical and electronic microscopy, zeta potential measurements, and color modifications.

The swelling degree depends on type of pre-treatment, nature of the samples and used alkaline solution. Thus, UV irradiation of the kraft pulps lead to a higher swelling degree in comparison with only NaOH and KOH treatment. The irradiated samples had a higher susceptibility in KOH as compared with NaOH. During alkaline treatment of cellulosic samples (UBP and BP) at low temperature, a swelling and dissolution processes took place.

The results give new insights on the stability of kraft softwood pulp fibers under UV irradiation and in aggressive environments which are useful both in pulp and paper production and for textile industries.

References

Alvarez J., Lipp-Symonowicz B. and Kardas I. (2006): The examination of molecular and supermolecular structure changes of man-made cellulose fibres under the influence of UV radiation. AUTEX Research J. 6(4), 191-195

Bui H.M., Lenninger M., Manian A.P., Abu-Rous M., Schimper C.B., Schuster K. C. and Bechtold T. (2008): Treatment in swelling solutions modifying cellulose fiber reactivity. 2: Accessibility and reactivity. Macromol. Symp. 262, 50–64

Cazacu G., Ciolacu D., Vlad - Bubulac T. and Drobota M. (2008): Swelling kinetics study of E54 pulp samples. COST E54 –5th Meeting Graz, Austria, April 10-11

Cazacu G., Rosu D., Pintilie M., Totolin M., Ciolacu D. and Vasile C. (2009): Electrokinetic properties of COST E54 samples. COST Action E54, Tampere, Finland, 4-6 May

Freundenberg U., Zimmermann R., Schmidt K., Behrens S.H. (2007): Charging and swelling of cellulose films. J. Coll. Interf. Sci. 309, 360-365

Good W.R. and Mueller K.F. (1980): A new family of monolithic hydrogels for controlled release applications. *In:* Controled Release of Bioactive Materials, *Ed.* R. Baker, Academic Press, New York, p. 155

Grignon J. and Scallan A.M. (1980): Effect of pH and neutral salts upon the swelling of cellulose gels. J. Appl. Polym. Sci. 25, 2829-2843

Heinemann S. and Ander P. (2011): Standard pulp and paper tests. *In* COST Action E54 "Characterisation of the fine structure and properties of papermaking fibres using new technologies". *Eds*: Ander P., Bauer W., Heinemann S., Kallio P., Passas R. and Treimanis, A. Swedish University of Agricultural Sciences. p. 211-232. ISBN 978-91-576-9007-4

Isogai A. and Atalla R.H. (1998): Dissolution of cellulose in aqueous NaOH solutions. Cellulose 5, 309-319

Kadla J.F. and Satoshi K. (2004): Lignin-based polymer blends: analysis of intermolecular interactions in lignin–synthetic polymer blends. Composites Part A, 35, 395-400

Kamide K., Okajima K., Kowsaka K. (1992): Dissolution of natural cellulose into aqueous alkali solution: Role of super-molecular structure of cellulose. Polym. J. 24(1), 71-86

Kamide K., Okajima K., Matsui T. and Kowsaka K. (1984): Study on the solubility of cellulose in aqueous alkali solution by deuteration IR and 13C NMR. Polym. J. 16(12), 857-866

Kotelnikova N.I. (1992): *In:* Lignocellulosics, Science, Technology, Development and Use. *Ed.* J.F. Kennedy, G.O. and Phillips, P.A. Williams, Ellis Horwood Limited, p. 597

McLaren K. (1976): The development of the CLE 1976 (L*a*b*) uniform color space and color different formula. J. Soc. Dyers Colors 92, 338-341

Öztürk H.B., Vu-Manh H. and Bechtold T. (2009): Interaction of cellulose with alkali metal ions and complexed heavy metals. Lenzinger Berichte 87, 142-150

Pedersoli J.L. (2000): Effect of cellulose crystallinity on the progress of thermal oxidative degradation of paper. J. Appl. Polym. Sci. 78, 61-66

Pimentel G.C., Sederholm C.H., (1956): Correlation of infrared stretching frequencies and hydrogen bond distances in crystals. J. Chem. Phys. 24, 639-641

Purcell K.F. and Drago R.S. (1967): Theoretical aspects of linear enthalpy wavenumber shift relation for hydrogen-bonded phenols. J. Am. Chem. Soc. 89(12), 2874–2881

Rozmarin G. (1984): Macromolecular basis of wood chemistry. Technical Ed., Bucuresti, Romania, p. 154

Safy El-Din N.M. and Abd El-Megeid F.F. (1994): The effect of cold alkali preatreatment on the reactivity of some cellulosic pulps towards acetylation. Holzforschung, 48, 496-500

Scallan A.M. (1983): The effect of acidic groups on the swelling of pulps: a review. Tappi J. 66 (11), 73-75

Sdrobiş A., Cazacu G., Totolin M. and Vasile C. (2010): Alkaline solution swelling of grafted unbleached and bleached cellulose. Iasi Academic Days "Progress in Organic and Polymer Chemistry". Iasi, Romania. October 8-10

Simionescu C., Grigoras M., Cernatescu-Asandei A. and Rozmarin G. (1973): Wood chemistry from Romania: poplar and willow. Academy Ed., Bucuresti, Romania, p. 118-122

Struszczyk H. (1986): Modification of lignins. III. Reaction of lignosulfonates with chlorophosphazenes. J. Macromol. Sci. A-23 (8), 973-992

Vicker M. E., Briggs N. P., Ibbet R. N., Payne J. J. and Smith S. B. (2001): Small angle X-ray scattering on lyocell cellulosic fibers: the effects of drying, re-wetting and changing coagulation temperature. Polymer, 42, 8241-8248

Appendix

Table 6. Spectral characteristics determined for the irradiated pulp samples

Sample	υOH (cm^{-1})	ΔH (kcal/mole)	E_H (kcal)	A_{1730}/A_{1050}	A_{1634}/A_{1050}	A_{1315}/A_{1050}	$\chi_{IR}=A_{1370}/A_{2900}$
BP	3335	11.246	5.141	0.035	0.104	0.250	0.757
BP (λ=254 nm, 20h)	3335	11.042	5.141	0.032	0.069	0.237	0.754
BP (λ=254 nm, 40 h)	3331	11.314	5.204	0.022	0.071	0.255	0.753
BP (λ=365 nm, 20 h)	3336	11.450	5.125	0.037	0.210	0.226	0.788
BP (λ=365 nm, 40h)	3335	10.974	5.141	0.024	0.171	0.250	0.747
UBP	3335	11.382	5.141	0.012	0.084	0.240	0.631
UBP (λ=254 nm, 20h)	3336	11.246	5.125	0.050	0.075	0.244	0.784
UBP (λ=254 nm, 40 h)	3332	11.518	5.188	0.047	0.078	0.250	0.789
UBP (λ=365 nm, 20 h)	3336	10.497	5.125	0.035	0.097	0.216	0.884
UBP (λ=365 nm, 40h)	3332	11.654	5.188	0.029	0.103	0.236	0.792

*Table 7. Variation of the ΔE^* and L^*, a^* and b^* parameters during UV treatment*

Sample	I Face				II Face			
	ΔE^*	ΔL^*	Δa^*	Δb^*	ΔE^*	ΔL^*	Δa^*	Δb^*
BP (λ=254 nm, 20h)	5,998	-2,179	-0,551	5,561	7,703	-1,440	-2,382	7,183
BP (λ=254 nm, 40h)	7,903	-5,539	-0,896	5,565	7,975	0,468	2,993	7,377
BP (λ=365 nm, 20h)	5,410	0,767	-3,743	3,829	4,635	2,514	-2,334	3,140
BP (λ=365 nm, 40h)	5,634	-0,567	-3,196	4,605	10,815	-0,853	-6,535	8,575
UBP (λ=254 nm, 20h)	6,723	-0,482	5,974	3,046	4,307	-0,703	1,888	3,807
UBP (λ=254 nm, 40h)	2,289	-0,630	0,935	-1,992	1,507	0,043	1,424	0,493
UBP (λ=365 nm, 20h)	2,243	-0,908	-1,992	0,489	1,494	-0,029	1,494	0,014
UBP (λ=365 nm, 40h)	4,967	-4,797	-0,677	-1,098	1,498	-0,897	-0,191	-1,185

Table 8. Influence of the UV irradiation on the swelling degree (Q_{max})

Sample	NaOH, 10%	KOH, 10%
BP (λ=254 nm, 20h)	125.7	140.0
BP (λ=254 nm, 40h)	128.9	147.3
BP (λ=365 nm, 20h)	171.5	186.6
BP (λ=365 nm, 40h)	133.4	159.6
UBP (λ=254 nm, 20h)	137.3	151.6
UBP (λ=254 nm, 40h)	131.4	142.9
UBP (λ=365 nm, 20h)	183.5	196.1
UBP (λ=365 nm, 40h)	141.2	156.5

As shown in Figure 14, the zeta potential tended to have much more electronegative values with increase of conductivity.
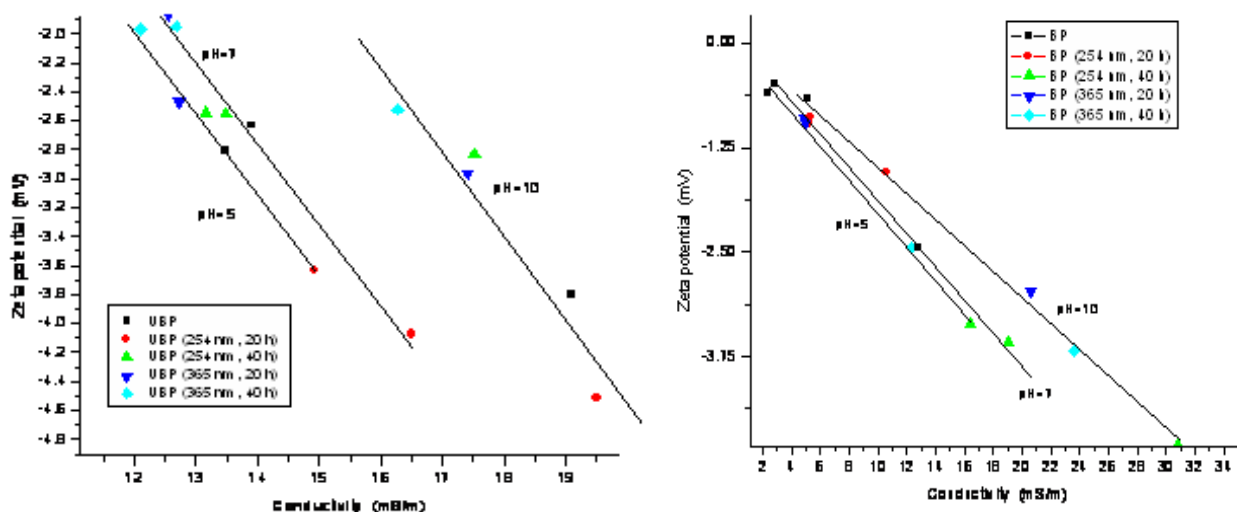
Figure 14. Variation of ζ potential vs conductivity solution

Based on these data, zeta potential decreased at both acidic and basic pH values. This suggests that the ζ potential may be pH-independent at variable conductivity. The effect of conductivity on ζ potential depends on the nature of the pulp and treatment conditions.

Fine Structure of Papermaking Fibres

COST Action E54 "Characterisation of the fine structure and properties of papermaking fibres using new technologies"

The main objective of COST Action E54 was to generate new knowledge on the micro- and nanostructure of papermaking fibres and relevant properties required for the efficient and sustainable use of fibres in traditional, advanced and future products. Action E54 comprised three working groups:

WG1: Structure and chemical composition of papermaking fibres after different types of treatment. The objectives of this WG were to develop methods for the characterisation of pulp fibres, and to generate new data on the fine structure of fibres for papermaking, and other important purposes.

WG2: Treatment and characterisation of individual fibres by microsystem technologies. This WG focused on the development of new instruments, namely, microrobotic platforms, by which individual fibres can be treated and investigated. Using these platforms new possibilities for testing of single fibres have been created.

WG3: The impact of the fine structure of fibres on their papermaking properties and their chemical and enzymatic reactivity. The participants of the WG exchanged their experience with respect to the impact of the fine structure of fibres and their modification on the quality of paper and handsheets. The fibre and paper properties were assessed mainly by strength and optical indices as well as interfibre bonding.

Chapters in this Book are:

Advanced analyses of wood pulp fibres

New and emerging methods such as microrobotics and microscopic techniques

Results of standard pulp and paper tests on Common pulps I and II and other fibre material

The 23 articles in the book written by renown scientists are of interest for chemists, physicists, biologists and technologists working with papermaking fibres. It is also hoped that the book will be useful for undergraduate and graduate students.

Cover photos
Upper left: High resolution image (100 000 x) of the complex branching structure that connects the fractal scaffold with the micro-fibrils in the underlying S1 layer (Turner et al., p. 14)
Upper right: Latewood kraft pulp fibre in polarized light after cleavage by HCl (Ander et al., p. 67)
Lower left: Effect of beating on fibre cross-sections prepared in hand sheets (Kritzinger et al., p. 185)
Lower right: Fibrilar structure of free dried fibre bond from unrefined softwood kraft pulp, 2400 x (courtesy by Bartenwerfer, AMiR Oldenburg/ Germany, and Heinemann, VTT/Finland)